Understanding the microbial ecology of highly radioactive nuclear storage facilities

A thesis submitted to the University of Manchester for the degree of

Doctor of Philosophy in the Faculty of Science and Engineering

2018

Lynn Foster

School of Earth and Environmental Sciences

Contents

List of Figures

Chapter 2: Literature review

Chapter 3: Methodology

Appendix

List of Tables

Supporting information

List of Equations

Chapter 3: Methodology

Word count ……..46,212

List of abbreviations

ATP	adenosine triphosphate
bp	base pair
CCA	complementary chromatic adaptation
Chl-a	chlorophyll-a
C_T	cycle threshold
DEGs	differentially expressed genes
DGGE	denaturing gradient gel electrophoresis
DNA	deoxyribonucleic acid
dNTPs	deoxynucleotide triphosphates
DSB	double strand breaks
dsDNA	double stranded DNA
EDS	energy dispersive X-ray spectroscopy
ESEM	environmental scanning electron microscopy
EXAFS	extended X-ray absorption fine structure
FGMSP	First Generation Magnox Storage Pond
FNU	formazin turbidity unit
FT-IR	Fourier transform infrared
GPX	glutathione peroxidase
Gy	gray
ICP-AES	inductively coupled plasma atomic emission spectroscopy
IR	ionizing radiation
ITS2	internal transcribed spacer region 2
kGy	kilogray
LC	liquid chromatography
LC-MS	liquid chromatography- mass spectrometry
MAA	microsporin-like amino acids
MIC	microbial induced corrosion
NCBI	National Centre for Biotechnology Information
NHEJ	non-homologous end-joining
NNL	National Nuclear Laboratory
OD	optical density
OTU	operational taxonomic unit
PC	principal component
PCA	principal component analysis
PCR	polymerase chain reaction
pH	potential of hydrogen
PolyP	polyphosphate
PPi	pyrophosphate
PRX	peroxiredoxin
QIIME	quantitative insights into microbial ecology
qPCR	quantitative polymerase chain reaction
RDP	ribosomal Database Project
RNA	ribonucleic acid
ROS	reactive oxygen species
rRNA	ribosomal ribonucleic acid

s.d	standard deviation
SC	standard curve
SCGs	single copy genes
SEM	scanning electron microscopy
SNFP	spent nuclear fuel pond
SOD	superoxide dismutase
SSB	single strand breaks
ssDNA	single stranded DNA
TAE	tris-acetic acid-EDTA
TEM	transmission electron microscopy
TEV	total explained variance
TOC	total organic carbon
UoM	University of Manchester
UV	ultra violet
XANES	X-ray absorption near-edge spectroscopy
XAS	X-ray absorption spectroscopy
XRD	X-ray diffraction
µS	micro Siemen

Abstract

The First Generation Magnox Storage Pond (FGMSP) is situated on the Sellafield Ltd. site in the UK, and is an extremely inhospitable environment comprising of significant levels of radioactivity coupled with a high pH of pH 11.4. Despite such extreme conditions, microorganisms are known to colonise the pond and can form dense microbial blooms in the summer months. The blooms can restrict the visibility within the pond which hinders plant operations. The FGMSP is currently undergoing decommissioning and waste retrieval operations, as a priority on site, therefore any plant downtime increases both the cost and timeframe for decommissioning. Here we describe the microbial community that colonises the FGSMP, including during two bloom periods. In addition efforts to determine the adaptive mechanisms that key microorganisms use to colonise the pond and their interactions with Sr are described.

Over the course of the sampling period Proteobacteria were the dominant phylum in the pond, with variations seen at the lower taxonomic levels. In addition, a single cyanobacterium, affiliated with a *Pseudanabaena* species, was identified as the dominant photosynthetic microorganism from samples taken from two bloom periods, comprising up to 30 % of the phylotypes detected. While the FGMSP was dominated by prokaryotes, a hydraulically linked auxiliary pond was more abundant in eukaryotic organisms. Comparisons between the two pond communities suggested that the auxiliary pond was not seeding the FGMSP, as the elevated pH and radiation levels inhibited such colonisation. Data supplied by Sellafield Ltd. showed that the onset of the bloom periods coincided with increases in the residence time of the purge water, used to maintain the elevated pH of the pond. Once the residence time of the purge water was reduced the visibility was restored in the pond, indicating that this was an effective means of removing the bloom-forming microorganisms. Laboratory-cultures of *Pseudanabaena catenata* were used to investigate the adaptive responses to ionizing radiation. The culture was found to consist of 9 other operational taxonomic units, 5 of which were affiliated with genera identified in the FGMSP. Detailed investigations indicated that X-irradiation treatment (95 Gy) had no significant impact on the growth rate of the culture, however there was an increase in polysaccharide production and a reduction in protein and chlorophyll-a production. Increases in polysaccharides could be of importance in the FGMSP as this could influence the fate of radionuclides present in the water. Sr was used to determine whether *P. catenata* could influence the fate of radionuclides. *P. catenata* cells could be seen to accumulate Sr associated with polyphosphate bodies, whilst $SrPO_4$ and calcium containing $SrCO_3$ minerals were formed.

The colonisation of FGMSP by organisms closely related to those studied here, including the cyanobacterium *Pseudanabaena catenata* requires careful consideration. The results presented here suggest that elevated levels of polysaccharides could potentially be generated within the pond as part of an adaptive strategy, and this could have impacts not only on the radionuclide inventory of the pond but could also facilitate the colonisation of the pond by other heterotrophic microorganisms. This project also provides significant first steps into the development of effective control strategies to prevent further bloom events, supporting the hypothesis that purging cycles are able to control bloom formation. Finally the results presented provide an insight into the potential use of organisms identified in such facilities for use in the remediation of contaminated aquatic environments and other engineered facilities.

Declaration

No portion of the work referred in the thesis has been submitted in support of an application for another degree or qualification of this or any other university or other institute of learning.

Copyright Statement

i. The author of this thesis (including any appendices and/or schedules to this thesis) owns certain copyright or related rights in it (the "Copyright") and s/he has given The University of Manchester certain rights to use such Copyright, including for administrative purposes.

ii. Copies of this thesis, either in full or in extracts and whether in hard or electronic copy, may be made **only** in accordance with the Copyright, Designs and Patents Act 1988 (as amended) and regulations issued under it or, where appropriate, in accordance with licensing agreements which the University has from time to time. This page must form part of any such copies made.

iii. The ownership of certain Copyright, patents, designs, trademarks and other intellectual property (the "Intellectual Property") and any reproductions of copyright works in the thesis, for example graphs and tables ("Reproductions"), which may be described in this thesis, may not be owned by the author and may be owned by third parties. Such Intellectual Property and Reproductions cannot and must not be made available for use without the prior written permission of the owner(s) of the relevant Intellectual Property and/or Reproductions.

iv. Further information on the conditions under which disclosure, publication and commercialisation of this thesis, the Copyright and any Intellectual Property and/or Reproductions described in it may take place is available in the University IP Policy (see http://documents.manchester.ac.uk/DocuInfo.aspx?DocID=24420), in any relevant Thesis restriction declarations deposited in the University Library, The University Library's regulations (see http://www.library.manchester.ac.uk/about/regulations/) and in The University's policy on Presentation of Theses.

Acknowledgements

I would like to thank my supervisors Jon Lloyd, Jon Pittman, David Sigee, and Kath Morris for their continued support and advice over the course of this PhD. Their patience and encouragement has allowed me to develop as a scientist and as a person, for which I will always be very grateful. I would also like to thank EPSRC, the University of Manchester and Sellafield Ltd. for providing funding and giving me the opportunity to undertake this research project.

A special thank you must go to Christopher Boothman for all of his help and support with all the many questions and requests that I have had over the 4 years. In addition I would like to thank the following: Heath Bagshaw for his help with the electron microscopes; John Waters for XRD analysis; Paul Lythogoe for all the ICP-AES analysis; Asye Latiff and Kaye Williams for helping out with training and access to the Faxitron machine.

A significant proportion of the work carried out in this thesis was reliant on pond water samples being provided by Sellafield Ltd. and having access to NNL's Central Laboratory to carry out DNA extractions. I would like to thank everyone involved with acquiring the samples, gaining access to site, and carrying out the work. Instrumental to this was Genevieve Boshoff, who kindly acted in the capacity of a supervisor and helped so much in facilitating much of the work that has taken place on site- thank you. A special thank you has to go to Scott Harrison, who has gone above and beyond to help me, for which I am so grateful.

Thank you to the Geomicro group, everyone has always been so helpful and friendly, always ready to help and offer support or advice, I have been very lucky to be part of an amazing research group. Thank you to Naji Bassil for all your help and for putting up with me, maybe one day I will be able to offer more than telling you the benefits of colour coding data. Thanks also to Gina, you helped me so many times with so many things. Adrian, Ellen, and Tom it has been a pleasure to go through my entire PhD with you guys. Thanks also to all you Friday beer folk, those in G.35and squashers.

I would like to thank all my friends for their support, distractions and all the fun things we've done together. I've made some incredible new friends since moving to Manchester (too many people to mention you all), reconnected to others (James) and missed those still at home like mad (Lyndsay and Tom that's you- I guess even you

Mick). Just because I said I would- here is a special thank you to Alex Cooper and Paul Quinn- for your tax contributions that pay my wages…..apparently??? I would also like to thank my sister for just being her.

Finally I have to say the biggest thank you to my parents, who have supported me every step of the way with everything I have done. You are both my rocks, and your unwavering encouragement has allowed me to be brave enough to chase my dreams and do the things I might have otherwise thought to be impossible.

The Author

The author graduated from the University of Leicester in 2014 with a first class BSc honours degree in Biological Sciences, before starting this PhD the same year. Prior to attending university she spent several years working in retail before spending just over 7 months travelling.

Chapter 1

Thesis content and layout

1 Introduction

1.1 Project context

The Sellafield site, situated on the West Coast of Cumbria, is the UKs largest nuclear site and contains several spent nuclear fuel ponds (SNFPs) that are in various stages of decommissioning. One of the older Sellafield SNFPs, the First Generation Mangox Storage Pond (FGMSP), was built in the late 1950s as a storage site for waste fuel from the UK's gas-cooled reactors, also known as Magnox nuclear power stations. The fuel was intended for reprocessing, where the cladding was removed from the fuel rods, however due to extended periods of storage the fuel and particularly the cladding have corroded. The decommissioning and retrieval of waste from older legacy storage facilities, such as the FGMSP, is a priority on the Sellafield Ltd. site.

The FGMSP is an open-aired facility, which means that it is exposed to a variety of environmental factors such as the ingress of carbon, nitrogen, rain water, and seabird guano. In order to minimise further corrosion of the spent fuel in the pond, it is maintained at an alkaline pH of ~pH 11.4. Despite the significant levels of radiation and high pH, the pond is colonised by microorganisms, which are capable of forming microbial blooms. These microbial blooms are thought to be formed by either eukaryotic algae or cyanobacteria since the pond becomes green during these periods. The growth of these organisms has the potential to disrupt waste retrieval operations and decommissioning efforts, since the visibility in the pond is restricted. The implication of the disruption not only has an impact on the timescale of the processes but also results in increased financial costs. Little is known about the microorganisms that inhabit the FGMSP or what organisms are involved in the bloom formations. It is also not known what triggers the bloom events or the adaptive mechanisms these organisms use to colonise the environment. The lack of information about the organisms present in the FGMSP makes it difficult to plan and implement effective control strategies.

This project follows on from a previous PhD project, which made efforts to characterise the microorganisms in a number of other SNFPs on the Sellafield Ltd. site. The focus of this current work is to identify the organisms in the FGMSP and to determine the adaptive mechanisms and radionuclide interactions of key microbial species present in

the blooms. Increased knowledge on the metabolic responses of organisms in the pond is an important step to help develop effective control strategies, and therefore minimise plant downtime. In addition, the work carried out in this project has provided information to support a NNL-based EngD programme focussing on the control of the microbial biomass in the FGMSP. The work carried out in Chapter 5 provided information and material for a further PhD project focused on the biocomplexation of radionuclides in the FGMSP. In addition a clearer and more detailed understanding of the capabilities of the naturally occurring microorganisms could potentially uncover new candidate species that could be used for bioremediation applications in similar facilities and other contaminated sites.

1.2 Aims and objectives

The overall aim of this project was to identify the microorganisms that colonise the FGMSP and more particularly those that formed the microbial blooms. Further to this, the project aimed to understand the adaptive mechanisms that relevant organisms utilise to facilitate the colonisation of the pond. Additionally, the interaction of radionuclides and microorganisms identified in the pond was also to be explored. The project aimed to provide more detailed information that could help inform control strategies that could be employed on site to prevent the unwanted growth of these organisms.

Three main objectives were formulated and investigated using a wide range of techniques including, next generation sequencing platforms, spectroscopy, and light and electron microscopy.

(I) **To determine what microorganisms colonise the FGMSP and what organisms are responsible for the microbial bloom events**. Water samples collected throughout the duration of the project underwent DNA extraction and they were then sequenced using next generation sequencing platforms. The samples were assessed by targeting rRNA gene sequences of prokaryotes and eukaryotes, in addition to the internal spacer region 2 of fungal RNA genes. A variety of data were provided about the FGMSP, which were recorded as part of standard operating procedures by Sellafield Ltd. personnel, including photosynthetic pigment concentrations, pH, temperature, concentrations of NO_3^-, PO_4^{3-}, and SO_4^-. An additional auxiliary

pond, which is allowed to feed into the FGMSP, was also monitored with the aim to determine if this could be a source of microbial contamination.

Hypothesis 1: A mixed community of eukaryotic algae and cyanobacteria will contribute to the microbial blooms in the FGMSP.

(II) **To determine the effect of ionizing radiation on microorganisms that colonise the FGMSP**. By understanding the physiological adaptations that microorganisms use to colonise the FGMSP, a better understanding of their impact pond management, and more specifically the stored inventory could be determined, for example their interactions with radionuclides. Here a laboratory culture of a related cyanobacterium identified in the pond was subjected to doses of ionizing radiation (IR), with the aim of determining the adaptive responses of the organism(s). Spectroscopy and cell counts used to assess the effect of IR on the growth of the culture. The effect on the metabolic state of the culture was determined using Fourier transform infra-red (FT-IR) spectroscopy in conjunction with fluorescent microscopy.

Hypothesis 2: Microorganisms, relevant to the FGMSP will be able to survive high doses of ionizing radiation.

(III) **To determine the fate of Sr in the presence of microorganisms relevant to those colonising the FGMSP**. The FGMSP has an inventory of radionuclides, including fission products mobile in the water. By using a laboratory-culture of a cyanobacterium related to one identified in the pond, specific interactions between the organisms present in the culture and Sr were determined. A range of techniques were used to assess whether Sr had an effect on the growth of the culture, and to identify whether Sr formed any (bio)minerals. Any Sr minerals that were formed were characterised and efforts were made to determine whether these were associated with the microbial cells in the culture.

Hypothesis 3: Microorganisms relevant to the FGMSP will influence the fate of radionuclides such as Sr, for example by forming mineral precipitates.

1.3 Thesis structure

The majority of this thesis is made up of three research papers, which cover the research aims described above. The research chapters are preceded by a general introduction to the scientific knowledge of the research area, including information on the First Generation Magnox Storage Pond (FGMSP), radiation resistance mechanisms, microorganisms in other spent nuclear fuel ponds and the interactions of radionuclides with microorganism. The end of the thesis is made up of a conclusions section and a discussion of future work directions.

Chapter 2: Literature review- provides an introduction to the nuclear fuel cycle and spent nuclear fuel ponds and the microorganisms that have been identified in them. In addition, an overview about algae, microbe and radionuclide interactions and a summary of radiation resistant mechanisms is included.

Chapter 3: Methodology- provides detailed information about the practical and theoretical details of the methods used in this project.

Chapter 4: Research chapter- "The microbial ecology of a spent nuclear fuel pond on the Sellafield site". This paper analyses the microbial community of several samples collected from the FGMSP, including two bloom samples, and an auxiliary pond using next generation sequencing techniques. The sequencing data was supported by a variety of measurements taken in the pond throughout the sampling period. Data were provided by Sellafield Ltd. and included concentrations of the photosynthetic pigments chlorophyll-a and phycocyanin, concentrations of NO_3^-, PO_4^{3-}, and SO_4^{2-}, turbidity, temperature, and pH measurements as well as details about the purge rate during the bloom periods.

Prepared for submission to Microbiome.

Chapter 5: Research chapter- "The effect of X-irradiation on the growth and metabolic status of *Pseudanabaena catenata*". A laboratory culture of *P. catenata* was subjected to a total dose of 95 Gy of X-irradiation over a five consecutive days. Since the culture was not axenic 16S rRNA gene sequencing was carried out to identify what microorganisms were present. The growth of the culture was monitored using direct cell counts, optical density measurements and chlorophyll concentrations. In addition, the

metabolic fingerprint of the culture was assessed by FT-IR spectroscopy, the results of which were supported by total carbohydrate measurements and polysaccharide staining.

Prepared for submission to Nature Communications.

Chapter 6: Research chapter- "The fate of Sr in the presence of *Pseudanabaena catenata*". The impact of *P. catenata* on Sr speciation and solubility was assessed using a range of techniques. Measurements were taken to see if the Sr had any effect on growth. Inductively coupled plasma atomic emission spectroscopy (ICP-AES) measurements were taken to determine the percentage of Sr in solution, whilst transmission electron microscopy (TEM), extended X-ray absorption fine structure (EXAFS) and X-ray diffraction (XRD) were carried out to determine the composition of any minerals formed and if they were associated with the cells in the culture.

Prepared for submission to Applied and Environmental Microbiology

Appendix A1: An outline of the work carried out to date using metagenomic and metatranscriptomic techniques on the *Pseudanabaena catenata* culture. The same laboratory culture of *P. catenata* was subjected to the same ionizing radiation treatment as described in Chapter 5. Metagenomic analysis of the culture was carried out to align the metatranscriptomic data to. The data will be futher analysed for additional publications outside of the scope of the thesis work presented in the main sections. Intended title of research paper: The effect of X-irradiation on the gene expression of *Pseudanabaena catenata*.

1.4 Author contributions

Chapter 4: The microbial ecology of a spent nuclear fuel pond on the Sellafield site

Lynn Foster	Principal author; experimental work; data analysis
Christopher Boothman	DNA sequencing run; manuscript review
Sharon Ruiz-Lopez	qPCR experimental work; methodology
Genevieve Boshoff	Concept development; manuscript review
Peter Jenkinson	Sellafield data collection; manuscript review
David Sigee	Concept development; manuscript review

Jon K Pittman	Concept development; manuscript review
Katherine Morris	Concept development; manuscript review
Jonathan R Lloyd	Concept development; extensive manuscript review

Chapter 5: The effect of X-irradiation on the growth and metabolic status of *Pseudanabaena catenata*

Lynn Foster	Principal author; experimental work; data analysis
Howbeer Muhamadali	Aided with FT-IR data collection and data analysis; manuscript review
Christopher Boothman	DNA sequencing run; manuscript review
David Sigee	Concept development; manuscript review
Jon K Pittman	Concept development; manuscript review
Royston Goodacre	Concept development; manuscript review
Katherine Morris	Concept development; manuscript review
Jonathan R Lloyd	Concept development; extensive manuscript review

Chapter 6: The fate of Sr in the presence of *Pseudanabaena catenata*

Lynn Foster	Principal author; experimental work; data analysis
Adrian Cleary	EXAFS data collection; data analysis; EXAFS write up
Heath Bagshaw	Operation of TEM; manuscript review
David Sigee	Concept development; manuscript review
Jon K Pittman	Concept development; manuscript review
Katherine Morris	Concept development; manuscript review
Kejing Zhang	Carried out trial experiments
Kurt Smith	PHREEQC modelling
Jonathan R Lloyd	Concept development; extensive manuscript review
John Waters	XRD data collection
Paul Lythgoe	ICP-AES data collection

Appendix A1: The effect X-irradiation on the gene expression of *Pseudanabaena catenata*

Lynn Foster	Principal author; experimental work; data analysis
Naji Bassil	Bioinformatics on metatranscriptomic data; data analysis
Sophie Nixon	Metagenomics support
Edwin Gnanaprakasam	Metagenomics support
Robert Danczak	Initial metagenomics data analysis

Chapter 2

Literature review

2 Literature review

2.1 The nuclear fuel cycle

2.1.1 The fuel cycle

The nuclear fuel cycle is a process that generates electricity through the splitting of uranium atoms ("The nuclear fuel cycle," 2018). Electricity generated by nuclear power stations accounts for approximately 10% of the global electricity usage, provided by 430 commercial nuclear reactors (Ewing, 2015). There are several different stages of the cycle, from extracting uranium to the disposal of the waste generated by the process (Figure 2-1).

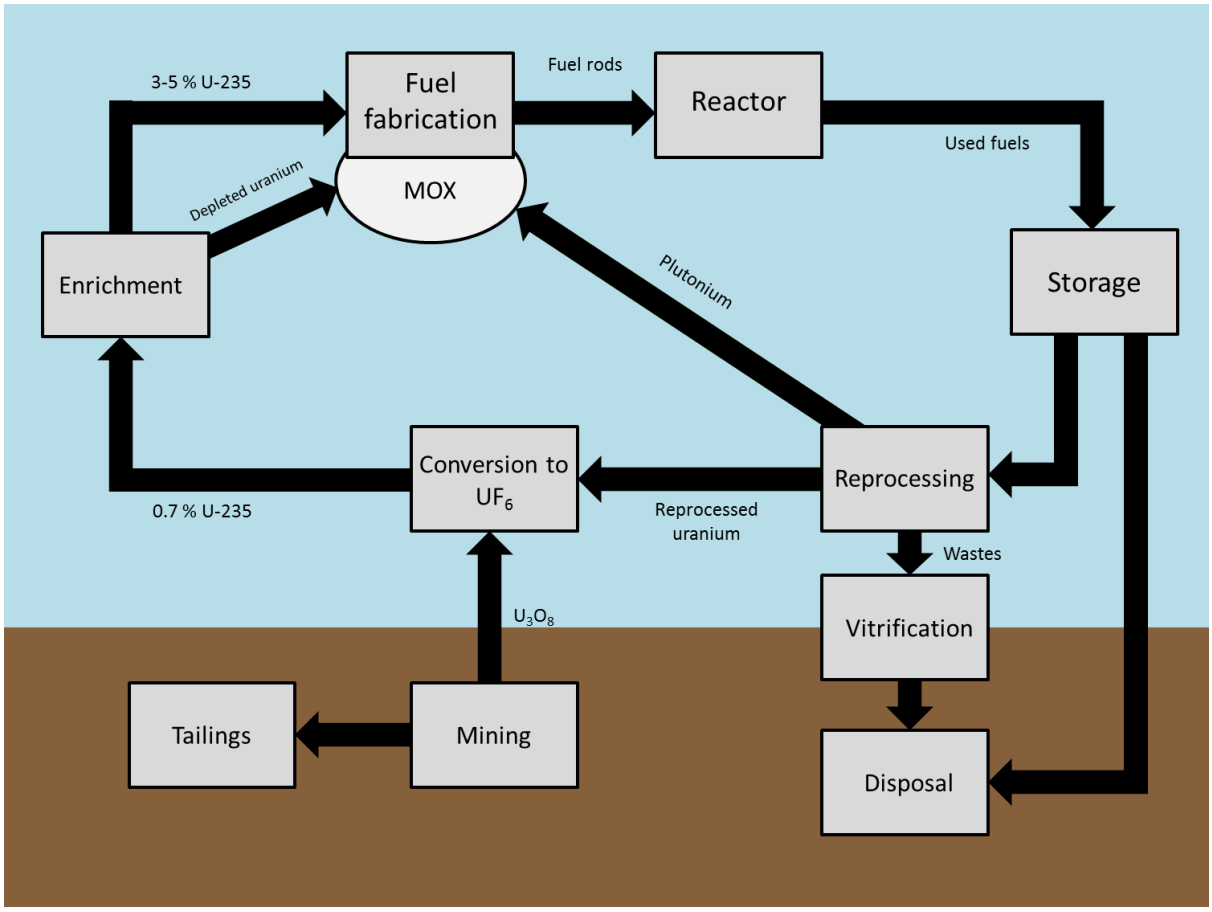

Figure 2-1: A depiction of the nuclear fuel cycle, showing all the stages from uranium mining to disposal (Adapted from "The nuclear fuel cycle," 2018)

U is a relatively abundant element, the highest reserves are found in Australia, Kazakhstan, Russia, Canada and USA, accounting for over 60 % of total U production ("The nuclear fuel cycle," 2018). The first stage in the cycle is mining for uranium. Two methods can be used to extract uranium depending on the depth of the ore and the geology of the rock: 1) Mineralised rock is extracted from the ground, broken down and treated to remove the minerals; or 2) in situ leaching, where the minerals are removed in solution without removing the ore from the ground (Wilson, 1996). Leaching usually involves the use of sulphuric acid to dissolve the uranium oxides due its higher percentage recovery (70-90 %), depending on the geology of the site being mined carbonate can also be used (60-70 % recovery). The minerals are removed once the solution has been transported to the surface (Crossland, 2012; "The nuclear fuel cycle," 2018; Wilson, 1996).

The next stage is milling, the purpose of milling is to generate U_3O_8 concentrate which can then be transported from the mill for the next stages of the nuclear fuel cycle (Crossland, 2012; "The nuclear fuel cycle," 2018; Wilson, 1996). The U_3O_8 is yellowish in colour and is often called yellowcake; the U content of yellowcake is in excess of 80 %. This is a significant concentration especially when compared to the ore from which it was extracted, where the U content can be less than 0.1 % ("The nuclear fuel cycle," 2018). At this stage the main waste is tailings, where the majority of the radioactivity is found. The tailings contain rock and the part of the ore that is not needed. Due to the radioactive nature and heavy metal content of the tailings, they must be disposed of in such a way as they remain isolated from the wider environment ("The nuclear fuel cycle," 2018).

The extracted uranium cannot be used directly as fuel and requires further processing prior to being used. There are a number of different types of nuclear reactor, the majority of which use UO_2 as fuel. Nuclear reactors that use UO_2 as the fuel require the enrichment of fissile ^{235}U, which is used in the nuclear reactor to generate energy, through further processing of U_3O_8 ("The nuclear fuel cycle," 2018; Wilson, 1996). ^{235}U makes up around 0.7 % of the total natural uranium, with the vast majority being composed of the ^{238}U isotope ("The nuclear fuel cycle," 2018; Wilson, 1996). At the end of the enrichment process the ^{235}U content should be between 3.5 and 5 %. The process for enrichment involves converting the U_3O_8 into uranium hexafluoride. Differences in the mass of the uranium isotopes are used to draw off the ^{235}U fraction, leaving behind depleted U. Following the separation UO_2 is regained and can be placed

into fuel rods ("The nuclear fuel cycle," 2018). The fuel rods used by most nuclear reactors consist of a metal outer casing containing ceramic pellets of enriched uranium oxide. The pellets are formed by pressing the uranium oxide and heating it at temperatures in excess of 1400 °C. A chain reaction occurs when ^{235}U splits in the reactor core, this fission generates large amounts of heat ("The nuclear fuel cycle," 2018). Pu is produced by the transmutation of some of the ^{238}U and subsequently contributes to the energy output ("The nuclear fuel cycle," 2018). Electricity is generated by a turbine and an electric generator which are powered by the heat produced by uranium fission. Every 12-18 months the reactor is replenished with fresh fuel and about 1/3 of the fuel is removed (Crossland, 2012; Wilson, 1996).

2.1.2 Spent nuclear fuel storage ponds (SNFPs)

Storage ponds at nuclear power plants have been used for many years. Initially they were intended to be used for a relatively short period of time, approximately 20 years. The length of time that the storage ponds has been extended, in many cases, to around 40 years as it is more convenient to do this (Sarró *et al*., 2005; Tišáková *et al*., 2013). The fuel is stored in stainless steel canisters which are submerged in deionised water. The water acts in two ways, first to shield against radiation. Secondly because the used fuel continues to emit heat, the water absorbs the heat and can be circulated, it is then possible to pass it though a heat exchange system to maintain a stable temperature within the pond (Tišáková *et al*., 2013). Due to the nature of the material being stored in the ponds, efforts must be made to reduce the risk of corrosion and the accumulation of salts. The water undergoes demineralisation treatments in many ponds and is passed through a range of filtration and/or ion exchange systems before release (Chicote *et al*., 2005).

2.1.3 Magnox Reactors and the First Generation Magnox Storage Pond (FGMSP) at Sellafield

Early gas-cooled reactors (Magnox reactors), which form part of the UK's legacy nuclear fleet, were run using fuel consisting of un-enriched U-metal, resulting in different processing requirements (Wilson, 1996). The fuel was produced by heating

pelleted UF_4 that has been mixed with Mg; in addition Al metal coupons were added. The process was carried out in a graphite container sealed in a stainless steel pressure vessel. The reaction generates U-metal, which was cleaned and MgF_2 formed as a by-product, which underwent a leaching process to ensure all the U was removed prior to final disposal (Wilson, 1996). Fuel rods were formed using a casting technique, where the U-metal was heated to in excess of 1500 °C. The rods then underwent beta-quenching, where they were subjected to a further heat treatment to reduce the grain size in the fuel to prevent anisotrophic growth in the U-metal during irradiation (Wilson, 1996). The term Magnox refers to the alloy that provides a non-oxidising cover for the U-metal fuel, which consists of Mg and Al in small quantities.

Spent Magnox fuel is stored in ponds containing deionised water, but this is problematic since the Magnox alloy reacts with water (Jackson *et al*., 2014). The First Generation Magnox Storage Pond (FGMSP) situated on the Sellafield Ltd. site (UK) was constructed to house the spent fuel from Magnox reactors. Sellafield Ltd. shutdown the reprocessing of the FGMSP in the 1970's, therefore fuel was stored for longer periods of time (Jackson *et al*., 2014; Sellafield, 2014). The extended storage of the fuel rods led to their corrosion, as a result of this the radiation levels in the pond are elevated and visibility in the pond is poor (Sellafield, 2014). The FGMSP contains a large quantity of sludge at the bottom of the pond, totalling around 1,500 cubic metres (NDA, 2016). The sludge is made up of "corroded fuel particles, fragments of fuel rod and metal, concrete degradation products, bird guano and animal remains" (Gregson *et al*., 2011a; Jackson *et al*., 2014). When the sludge is disturbed, by movement of the water it reduces the visibility in the pond. Microbial blooms are also known to occur within the pond creating further visibility issues, which impedes the decommissioning operations (Gregson *et al*., 2011a; Jackson *et al*., 2014).

2.2 Microorganisms in nuclear storage facilities

2.2.1 Biofilms, microbial induced corrosion (MIC) and biofouling

Microbes have been observed in many nuclear storage facilities across the world. The conditions in the ponds are extremely inhospitable to life with high levels of radiation present. Additionally the use of highly pure deionized water adds the pressure of osmolarity (Tišáková *et al*., 2013). Despite this there have been a variety of microorganisms identified both as part of both a planktonic and biofilm community (Chicote *et al*., 2005, 2004; Forte Giacobone *et al*., 2011; Masurat *et al*., 2005; Sarró *et al*., 2003; Sarró *et al*., 2005; Sarró *et al*., 2007; Tišáková *et al*., 2013). The formation of biofilms is thought to aid the bacteria in surviving in extreme conditions, such as those found in the SNFPs where the radiation dose is significantly higher than found naturally elsewhere (Masurat *et al*., 2005; Sarró *et al*., 2005). A biofilm is a non-homogenous structure composed of organic polymers, with the microbes existing within the structure (Masurat *et al*., 2005). The conditions within the biofilm are able to be modified when compared to the external environment for example in terms of chemicals present and the temperature, therefore reducing the pressures on the bacteria (Masurat *et al*., 2005; Sarró *et al*., 2003). Links have been made between biofilm formation and microbial induced corrosion (MIC) (Bruhn *et al*., 2009; Chicote *et al*., 2004; Diósi *et al*., 2003; Libert *et al*., 2014; Sarró *et al*., 2003). Identifying the microorganisms that are able to grow within SNFPs would help with efforts to control their growth and provide possible candidates for bioremediation (Chicote *et al*., 2004; Chicote *et al*., 2005).

The accumulation of microorganisms (biofouling) and the potential for MIC are problematic within SNFP as they can/ could hinder the routine running and management of the ponds (Masurat *et al*., 2005). Stainless steel is used for cladding due to its ability to withstand the harsh conditions with minimal corrosion, however MIC has been observed on stainless steel coupons (Chicote *et al*., 2005; Diósi *et al*., 2003; Forte Giacobone *et al*., 2011). Biofilms facilitate MIC although there may be further requirements to cause corrosion (Chicote *et al*., 2004). In addition to the corrosion, the biofilms also accumulate radionuclides, with radioactivity levels reportedly reaching values of around 5,500 Bq cm^{-2} (Chicote *et al*., 2005; Sarró *et al*., 2003). Microorganisms existing free within the water have also been observed (Evans, 2013;

Tišáková *et al*., 2013). Seasonal microbial blooms have been observed within SNFPs, which restrict visibility within the ponds halting work (Evans, 2013).

2.2.2 Techniques used to study microbial communities in SNFPs.

Prior to the development of DNA sequencing, the identification of microorganisms was limited to species that are amenable to culturing, which is roughly 1 % of the total species present, and direct observations using light microscopy that show distinguishing morphologies e.g. algae. Establishing the identity of a microbial community has become much more achievable due to the advances in sequencing techniques. The cost of sequencing DNA has reduced considerably over recent years, which has also allowed molecular identification of microorganisms to be carried out more readily (Hugerth *et al*., 2014). The 16S rRNA gene is commonly used to identify prokaryotic organisms. The region is ubiquitous and contains regions that are unique to particular genera and species as well as conserved regions where primers are able to bind. The 18S rRNA gene is the equivalent for eukaryotic organisms.

Gene targets such as 16S rRNA, are amplified by PCR using oligonucleotide primers that are usually between 18-21 base pairs in length. The amplified gene products can then be subjected to further analysis such as denaturing gradient gel electrophoresis (DGGE). With DGGE the gene products are run on a gel which separates them according to differences in their nucleotide sequence, which confer to different microbial species (Sarró *et al*., 2003). DGGE gives a fingerprint of the community present allowing comparisons between different communities but sequencing is required to identify the organisms present (Díez *et al*., 2007; Lyautey *et al*., 2005). Sequencing the gene and comparing it to reference sequences deposited in databases such as those compiled by NCBI BLAST allows the identity of the microorganisms to be determined (Sarró *et al*., 2003).

Studies assessing the microbial communities that colonise SNFPs have used a range of techniques, based around culturing, microscopy, and DNA analysis. Several studies have visualised and assessed the formation of biofilms and MIC using a variety of microscopy techniques. Epifluorescence was used by Masurat *et al*., (2005), Sarró *et al*., (2003, 2005), and Chicote *et al*., (2005) to inspect the microorganisms in SNFPs and

their ability to potentially corrode steel coupons. Light microscopy, transmission electron microscopy (TEM) and scanning electron microscopy (SEM) have been used to determine the morphology of microorganisms, such as whether they are coccoid, rods, or filamentous (Masurat *et al*., 2005; Santo Domingo *et al*., 1998; Sarró *et al*., 2003; Sarró *et al*., 2005). Masurat *et al*., (2005) were able to identify rod shaped bacteria within a biofilm using TEM, the bacteria were contained within a sheath structure. Several studies have isolated and cultured microorganisms from SNFPs and then subsequently carried out a variety of tests to determine what metabolic capabilities they have. As previously stated, the majority of microorganisms are not amenable to culturing and therefore the true diversity cannot be observed, as was observed by Chicote *et al*., (2005) as epifluorescent observations were significantly more diverse than the results of the culturing suggested. Tests to assess the metabolic capabilities of the microorganisms isolated can provide an insight into how they colonise these inhospitable environments. Galés *et al*., (2004), assessed H_2 metabolism of isolated microorganisms as an energy source (see Table 2-1), by assessing the activity of the hydrogenase enzyme. Diósi *et al*., (2003) tested the ability of cultures, isolated from the Atomic Energy Research Institute (Hungary), to reduce nitrate and sulphate, and sideophore production, in relation to MIC. More general microbiology techniques have also been applied, for example Karley *et al*., (2017) characterised the colonies formed on agar plates according to their size/shape, pigmentation, edge, elevation and the appearance of the surface.

2.2.3 Microbes in SNFPs

Microorganisms have been identified in several SNFPs around the world, and in a water pool containing spent fuel from a research reactor in France (Rivasseau *et al*., 2010). Where the conditions within the SNFPs were recorded, measurements showed a degree of consistency between different facilities, for example: conductivity measurements were ~1 μS cm^{-1}, temperatures ranged from 25- 37 °C, and pH values were between 5 and 7 (Table 2-1). The outdoor open-aired pond studied by MeGraw *et al*., (2018) was the exception, as the temperature of the water showed seasonal variations and a maximum pH of 8 was recorded. Earlier studies investigating the microbial communities within SNFPs utilise culture dependent techniques to isolate and culture

both planktonic and biofilm-forming microorganisms, whilst more recent studies have relied on extracting DNA directly from water samples collected from the ponds.

The microorganisms identified in the most intensively studied site, Confrentes (Spain), that are capable of biofilm formation remain fairly consistent across several studies between 2003 and 2007 (Chicote *et al*., 2004; Chicote *et al*., 2004, Sarró *et al*., 2003; Sarró *et al*., 2005; Sarró *et al*., 2007).The studies identified the presence of Firmicutes and Proteobacteria, which could form biofilms on steel coupons placed in the pond. There was evidence of MIC on the steel coupons, associated with the biofilms. Radionuclides have been seen to accumulate in association with the biofilms on the steel coupons in the Confrentes SNFP (Sarró *et al*., 2003), and also in biofilms produced by microorganisms isolated from an SNFP in India (Karley *et al*., 2017). The ability to accumulate radionuclides (Co^{2+} and Cs^{+}) has been demonstrated in free-living microorganisms isolated from an SNFP on the Sellafield site (Dekker *et al*., 2014) and the green microalgae, *Coccomyxa actinabiotis*, which was isolated from a water pool storing spent fuel from a research reactor in France (Rivasseau *et al*., 2010; Rivasseau *et al*., 2013; Rivasseau *et al*., 2016).

Table 2-1: Summary of microorganisms identified in various spent nuclear fuel ponds

Site	Organism	Method of identification	pH	Temperature	Conductivity	Reference
Savannah River Site, USA	Sulphate-reducing bacteria, and acid producing bacteria	SEM of metal coupons, cell counts	N/A	N/A	N/A	Santo Domingo *et al*., 1998
Unknown	*Ralstonia, Burkholderia, Micrococcus, Staphylococcus, Bacillus, Pseudomonas*	Culture-dependent Planktonic	5.5	30.0 – 37.0	1.0	Galès *et al*., 2004
CLAB, Sweden	*Meiothermus*	Fluorescence microscopy, SEM, TEM Biofilm and planktonic cells	N/A	25 reception basins 36 storage basin	91.4 ± 0.6 85.3 ± 1.3	Masurat *et al*., 2005

Confrentes, Spain	*Bacillus, Actinobacteria, Methylobacterium, Burkholderia, Staphlyococcus, Nocardia, Cellulomonas, Ralstonia, Pseudomonas, Xylophilus, Stenotrophomonas, Gordonia, Aspergillus* (fungi)	Culture-dependent Biofilm	5.0 – 6.5	25.0 – 34.0	0.8 – 1.5	Sarró *et al*., 2003; Sarró *et al.*, 2005; Sarró *et al.*, 2007 & Chicote *et al.*, 2004
Confrentes, Spain	*Pseudomonas, Burkholderia, Sphingomonas, Stenotrophomonas, Methylobacterium, Afipia, Streptococcus, Staphylococcus, Microbacterium, Nocardia*	Culture-dependent Biofilm	5.67	25.0 – 30.0	1.1	Chicote *et al*., 2005
SNFP, Argentina	*Bacillus*	Culture-dependent Planktonic	N/A	N/A	N/A	Forte Giacobane *et al.*, 2011

Interim SNFP (JAVYS inc.) Slovak Republic	*Kocuri; Micrococcus, Ochrobactrum,Pseudomonas, a*	Culture-dependent Planktonic	6.0 ± 0.1	34.8 ± 2.5	1.0 ± 0.4	Tišáková *et al*., 2013
Sellafield, UK	*Tardiphaga, Curvibacter, Serratia, Yersinia*	Culture-dependent Planktonic	N/A	N/A	N/A	Dekker *et al*., 2014
Water pool storing spent fuel, Research nuclear reactor, France	*Coccomyxa actinabiotis* (Green microalgae)	Culture-independent Planktonic	5.3 ± 0.2	25.0 ± 3.0	1.2 ± 0.2	Rivasseau *et al*., 2016
MAPS, India	unidentified	Culture-dependent Biofilm-capabilities	7.0	37.0	< 1.0 μS	Karley *et al*., 2017
Sellafield, UK	*Haematococcus pluvialis* (Green microalgae)	Culture-independent Planktonic	6.4 – 8.0	7.0 – 23.0	3.9 ± 0.6	McGraw *et al*., 2018

Savannah River Site, USA	*Nitrospira,* [*Hyphomicrobiaceae*], *Pedomicrobium, Aquabacterium, Rhodospira, Hyphomicrobium*	Culture-dependent Planktonic	6.1	18.0 – 26.0	1.5	Bagwell *et al*., 2018
Atomic Energy Reseach Institute, Budapest, Hungary	3 aerobic isolates 3 anaerobic isolate	Culture-dependent Biofilm	N/A	N/A	N/A	Diósi *et al*., 2003

2.2.4 Microbial diversity in storage ponds at Sellafield

The FGMSP on the Sellafield site is known to experience algal blooms that disrupt work on site, however very little is known about the organisms causing the blooms (Gregson *et al*., 2011a; Gregson *et al*., 2011b; Jackson *et al*., 2014). The FGMSP is unique in that it is maintained at a high pH which adds an additional pressure for the microorganisms to overcome. A pilot study investigating the microbial community based on the diversity of 16S rRNA genes amplified from DNA extracted from 3 samples collected from the FGMSP was carried out in 2012 (Evans, 2013). The results showed a relatively small level of diversity, as shown in Figure 2-2. The three samples were taken over a short sampling period, where no bloom was present. These data are interesting due to the reports of green algal blooms in the ponds, however no eukaryotic algae were detected based on the PCR results. Additionally cyanobacteria made up only a small proportion of the 16S pyrosequencing data, S01: 0.50 %, S02: 0.70 %, and S03: 2.20 %.

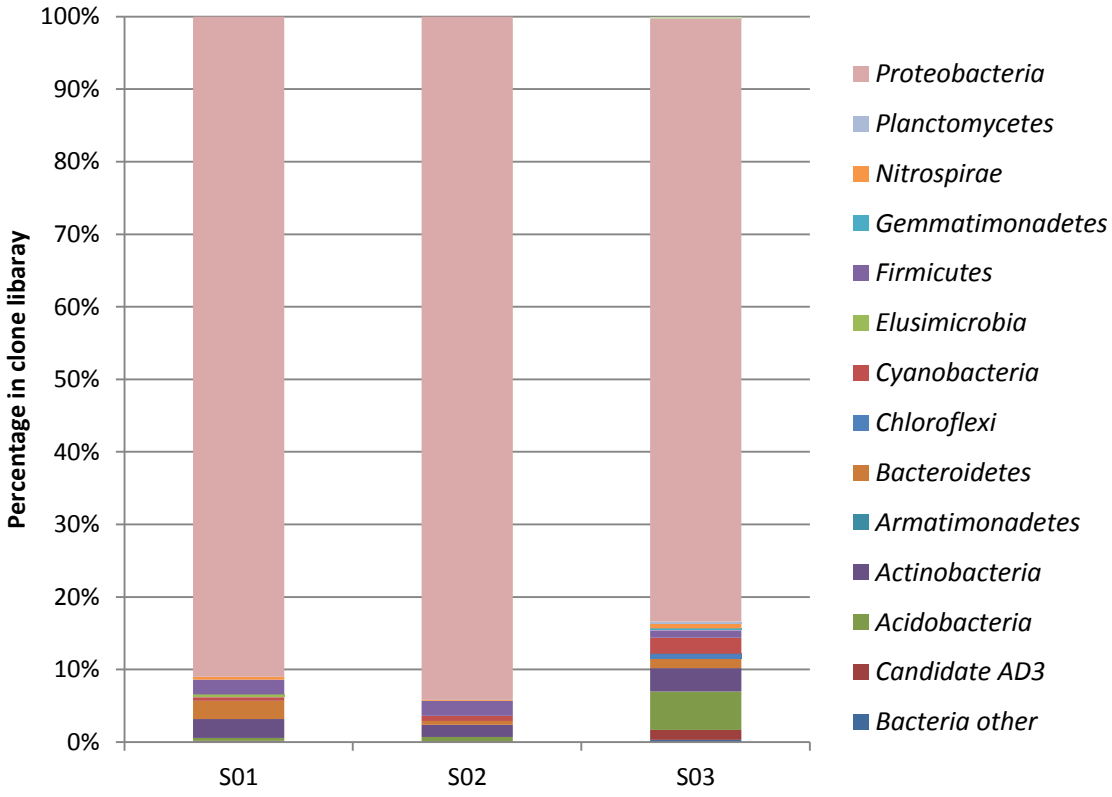

Figure 2-2: Prokaryotic diversity present in the First Generation Magnox Storage Pond, shown as relative abundances at the level of phyla based on next generation pyrosequencing of 16S rDNA (Evans, 2013).

Similarities between the planktonic microorganisms identified in the pond appear to be restricted to species of *Bacillus*, *Pseudomonas*, and *Micrococcus* (Forte Giacobone *et al*., 2011; Galès *et al*., 2004; Tišáková *et al*., 2013). Bagwell *et al*., (2018) are the first to report the presence of microorganisms from the phylum Nitrospirae, which accounted for 12 % of the community they observed, with the majority of the microbial community present affiliated with Proteobacteria (83 %). The majority of studies have only identified prokaryotic microorganisms in SNFPs, however, eukaryotic organisms have been identified in a restricted number of studies. For example, species of *Aspergillus* were found in the biofilms on the steel coupons placed in the Confrentes pond, interestingly this is the only report of fungi across all sites studied so far in an indoor pool (Chicote *et al*., 2004). An outdoor SNFP on the Sellafield site at circumneutral-pH displayed a diverse microbial community of both prokaryotic and eukaryotic organisms (MeGraw *et al*., 2018). The eukaryotic community was dominated by a green microalga that was most closely related to *Haematococcus pluvialis*, with several other members of the Chlorophyta family identified and to a lesser extent some fungi (MeGraw *et al*., 2018). Assessments of the microbial community have thus far been limited. To better understand the full extent of the microbial diversity in SNFPs, more frequent sampling and in depth sequencing efforts are required. The availability of such samples, coupled with radiological risks will place restrictions on such investigations.

2.3 Cyanobacteria and eukaryotic algae

2.3.1 Introduction to cyanobacteria

Cyanobacteria are prokaryotic organisms that are capable of synthesising complex carbon compounds using CO_2 and light energy through photosynthesis. They are often described as simple organisms since they lack organelles (Bellinger & Sigee, 2010). The size and shape of cyanobacteria varies considerable, they are capable of living as single cells or as branched or unbranched filaments (linear colonies of cells). Cyanobacteria can be either be planktonic or benthic (Bellinger and Sigee, 2010).

Table 2-2: A description of the 4 morphotypes of cyanobacteria (Bellinger and Sigee, 2010).

Cyanobacterial morphotype	Description
Chroococcales	Simplest- unicellular, no filaments, usually have a thin layer of mucilage
Oscillatoriales	Filamentous, lack cell differentiation, relatively simple
Nostocales	Filamentous, form heterocysts and akinetes, no true branching
Stigonematales	Filamentous, heterocysts and akinetes, show true branching, structurally most complex

Cyanobacteria are a large phylum of bacteria and are found in a wide variety of environments. It is largely believed that cyanobacteria were responsible for the great oxygenation event which occurred approximately 2.4 billion years ago (Schirrmeister *et al*., 2013).. Cyanobacteria produce the photosynthetic pigments that are associated with they thylakoid membranes, these are chlorophyll-a and the phycobilin pigments phycocyanin and phycoerythrin (Bellinger and Sigee, 2010; Madigan and Brock, 2011). Some species are capable of regulating their buoyancy within the water column due to gas vesicles. They are known to be capable of inhabiting extreme environments including; high temperature, low temperature, consistent exposure to direct sunlight, desiccation and radiation- with ultra violet (UV) or ionizing (Madigan and Brock, 2011). Cyanobacteria exist as a variety of morphotypes and are commonly divided into 4 groups on the basis of this, described in Table 2-2. Cells lack true organelles, but do contain granular inclusions such as phosphate bodies and carboxysomes (Bellinger and Sigee, 2010). Some species of cyanobacteria are capable of complementary chromatic adaptation (CCA) (Figure 2-3), which is a process whereby the organism restructures the phycobilisomes to optimise the transfer of light energy to the photosystem II reaction centres in response to different light conditions (Kehoe and Gutu, 2006). The

ability to carry out CCA, provides the organisms with a competitive advantage against other photosynthetic microorganisms under varying light conditions.

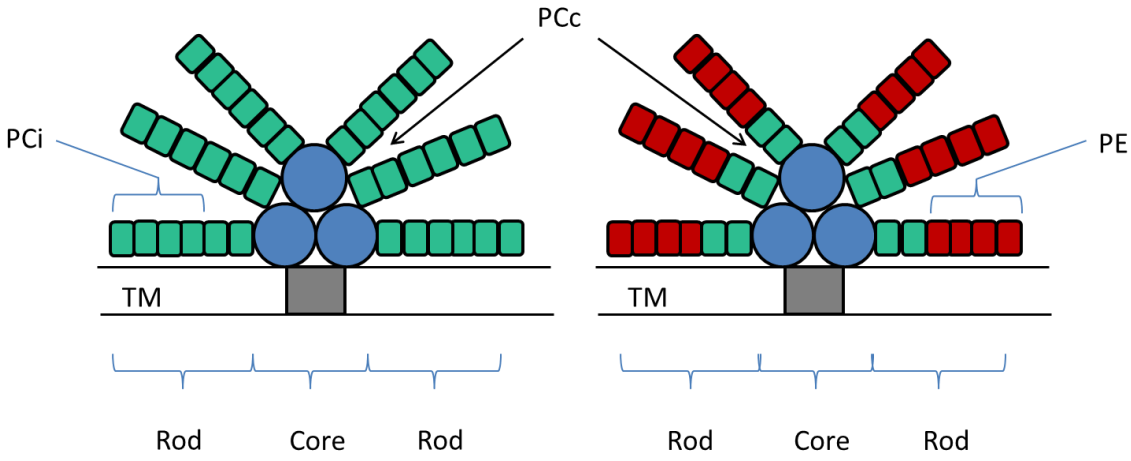

Figure 2-3: A schematic of complementary chromatic adaptation (CCA) of the phycobilisomes of cyanobacteria (adapted from Stowe-Evans & Kehoe, 2004). Blue circles indicate the allophycocyanin core molecules, with the antenna comprised of either phycocyanin (PC) or phycoerythrin (PE). The antenna consist of a PC core, if the organism is capable of CCA, the composition of the antenna can change. Under red light PC is favoured, whilst green light PE is favoured (Kehoe and Gutu, 2006; Stowe-Evans and Kehoe, 2004).

2.3.2 Introduction to eukaryotic algae

Eukaryotic algae include several different groups which include: Glaucophyta; Rhodophyta; Chlorophyta; Charophyta; Haptophyta; Crytophyta; Ochrophyta; Cercozoa-Chlorarachniophyceae; and Euglenozoa-Euglenophyceae (Barsanti & Gualtieri, 2014). Efforts to estimate the number of extant species of eukaryotic algae vary between 30,000 and 1 million.

As with cyanobacteria, eukaryotic algae inhabit a wide range of environments including, freshwater, marine, soil, rocks, ice and snow (Anderson, 1992). Different algal species inhabit environments with very different light intensities, they therefore produce an array of secondary pigments that either absorb light at different wavelengths (i.e. in water at depths where red light cannot penetrate) or to protect them from photo-damage caused by reactive oxygen species such as singlet oxygen. The range of

pigments gives rise to the common names given to different groups of algae including; green, red, brown, and golden (Barsanti & Gualtieri, 2014).

Eukaryotic algae can vary dramatically in their morphology and size, ranging from picoplankton (0.2-2.0 μm) to much larger kelps (Barsanti & Gualtieri, 2014). Algal cells are enclosed by a plasma membrane and a cell wall, and a wide range of extracellular materials such as sheaths and mucilages can also be observed (Barsanti & Gualtieri, 2014). Whilst the majority of algal species use photosynthesis to generate complex carbon molecules for respiration from sunlight and CO_2, some algal species are heterotrophic. These heterotrophic algae obtain the organic carbon molecules either by engulfing bacteria and other cells, or by taking up dissolved substances. In addition there are many species that are capable of switching between photoautotrophic and heterotrophic metabolism (Barsanti & Gualtieri, 2014). Reproduction in algae also shows a great deal of variation including both asexual and sexual reproduction.

For more information on the information described in this section see Algae: anatomy, biochemistry, and biotechnology text book (Barsanti & Gualtieri, 2014).

2.3.3 Bloom formation and collapse

2.3.3.1 Cyanobacteria and algal blooms

Cyanobacteria and eukaryotic algae inhabit a wide range of aquatic environments from freshwater to marine. The population dynamics of algal communities fluctuate, with increases in population numbers being described as an algal bloom (Carstensen *et al*., 2004). Interest in determining the cause of bloom events has largely been due to the negative impacts associated with their occurrence, such as the production of toxins by cyanobacteria. The organisms responsible for the blooms have been identified using morphological characteristics and molecular analysis. Blooms can be dominated by an individual species, which can be replaced by different species and referred to as a succession event. An example of succession can be seen in a study by Davis *et al*., (2009), the group identified an initial dominance of *Anabaena* during a bloom in Lake Agawam, later *Microcystis* was seen to be dominant. Fine scale analyses of the organisms in a bloom have also shown that different strains are capable of showing similar shifts in dominance (Rodriguez-Brito *et al*., 2010).

Triggers for bloom formation are not completely understood, the timing and intensity of blooms being somewhat inconsistent from year to year (Kahru *et al*., 2000). Roelke & Buyukates (2001) suggest that a combination of different conditions trigger blooms of cyanobacteria, and that these are species specific. Blooms are frequently associated with water that is nutrient rich (Azad and Borchardt, 1970; Davis *et al*., 2009). Factors affecting algal growth include: light availability; light-dark cycles; temperature; pH; nutrient availability such as phosphorus, nitrogen, iron etc. (Azad and Borchardt, 1970; Dubinsky and Berman-Frank, 2001; Finden *et al*., 1984; Jiang *et al*., 2008). Links between reduced nitrogen and phosphorus ratios, increases in the amount of phosphorus and temperature with the initiation of blooms (Davis *et al*., 2009; Jia *et al*., 2013; Jin *et al*., 2005; Kahru *et al*., 2000; Kononen *et al*., 1996; O'Neil *et al*., 2012; Stal *et al*., 2003). Increases to the phosphorus levels in natural water systems have been attributed to human activity and upwelling from sediments- particularly when oxic sediments become anoxic (Kahru *et al*., 2000; O'Neil *et al*., 2012).

Conditions within the water body determine what organisms are present. Elevated pH levels in water are known to favour the growth of cyanobacteria over green algae (Jin *et al*., 2005; López-Archilla *et al*., 2004). In addition the pH of water increases as cyanobacteria growth continues, due to the depletion of CO_2 caused by increased photosynthesis. Cyanobacteria are capable of thriving at pH levels between 10 and 11 (López-Archilla *et al*., 2004; Summerfield and Sherman, 2008), while there is evidence of cyanobacteria at even higher pH levels in excess of 12 (Pikuta *et al*., 2007). Water that is stratified in terms of nutrients favour cyanobacteria, particularly those containing gas vesicles as they can move through the water column to access the required nutrients (Kahru *et al*., 2000).

Phytoplankton have the ability to store nutrients such as phosphorus, which is referred to as luxury nutrient uptake, this prolongs their growth when the stored nutrients become limiting (Azad and Borchardt, 1970; Cade-Menun and Paytan, 2010; Dubinsky and Berman-Frank, 2001). The occurrence of *Aphanizomenon* species, which are dominant in Baltic Sea blooms, is almost entirely due to luxury uptake of phosphorus prior to the initiation of the bloom (Lilover and Stips, 2008; Raateoja *et al*., 2011). Since many cyanobacteria are capable of fixing atmospheric nitrogen, phosphorus becomes one of the key limiting nutrients (Jin *et al*., 2005; Kahru *et al*., 2000; Lilover and Stips, 2008; O'Neil *et al*., 2012). Affects associated with phosphorus starvation include increases to stored lipids, elevated carbohydrate: protein ratios, light and

temperature stress responses are potentially altered as a result of P-deficiency (Cade-Menun and Paytan, 2010; Gao *et al*., 2015; Jin *et al*., 2005). Links have been reported between phosphorus availability and the uptake of nitrate by cyanobacteria due to the effects on ATP and so enzyme activity (Hu *et al*., 1990; Jiang *et al*., 2008).

Phytoplankton species have developed mechanisms for concentrating inorganic carbon dissolved in water to provide the carbon source for photosynthesis. O'Neil *et al*., (2012) noted that knowledge about the effect on cyanobacterial growth with high CO_2 concentrations is limited, however they acknowledge that certain cyanobacterial genera can bloom at low CO_2 concentrations. Carbon can be available in different forms, with different species having different preferences and requirements. Differences in dissolved inorganic uptake was determined in two species of *Chlorophyceae*, *Nannochloropsis gaditana* Lubia´n could utilise bicarbonate (HCO_3^-) whilst *Nannochloris maculate* Butcher preferentially utilised CO_2 (Huertas, 2000).

Many links have been made with the formation of bloom events coinciding with seasonal increases in water temperatures. Yu *et al*, (2007) measured levels of chlorophyll-*a* as an indicator of biomass. Increases in biomass were seen to occur with increases in the water temperature, suggesting that higher temperatures stimulated the growth of the cyanobacteria (Yu *et al*., 2007). In natural systems such as lakes, temperature increases have been linked with algal recruitment from the sediments (Jia *et al*., 2013). Studies such as those by Jiang *et al* (2008) highlight the growth promoting effect that increased temperatures have on algae. There is an upward movement of nutrients through the water column at higher temperatures. Cyanobacteria that can regulate their buoyancy using gas vesicles gain advantage as they can gain access to the nutrients, so outcompeting non buoyant organisms (O'Neil *et al*., 2012; Paerl and Otten, 2013).

2.3.3.2 Bloom Collapse

Phytoplankton often store excess organic carbon generated by photosynthesis, elevated excretion of this has been linked to limited nutrients and a reduction in growth rates and cell death (Dubinsky and Berman-Frank, 2001; Paerl and Otten, 2013). Light intensity has a limiting effect on both cyanobacterial and eukaryotic algal growth, once it goes above a threshold it has a damaging effect on the photosynthetic apparatus. Viral lysis

and predation by grazing are considered to be influential in the end of a bloom period. When the cells are lysed following infection by viruses there is a release of nutrients into the water body (Paerl and Otten, 2013). In large natural water bodies changes in the mixing of the water can disperse the bloom, resulting in their end (Paerl and Otten, 2013).

2.3.3.3 Sellafield bloom events and methods to control cyanobacterial and eukaryotic algal populations

Seasonal blooms of photosynthetic organisms (cyanobacteria or eukaryotic algae) have been reported to occur in the FGMSP at Sellafield, causing disruption to routine maintenance and plant operations (Gregson *et al*., 2011a; Jackson *et al*., 2014). Little is known about the organisms responsible for these bloom events and the triggers for the bloom formation. Work undertaken by Evans (2013) highlighted some organisms present in the FGMSP but the samples were not taken when the pond was experiencing a bloom (see 2.2.4). Another outdoor SNFP, which is circumneutral pH, was dominated by the eukaryotic green algae *H. pluvialis* (MeGraw *et al*., 2018), which is capable of accumulating a red ketocarotenoid pigment with strong antioxidant properties called astaxanthin (Boussiba and Vonshak, 1991). Production of the astaxanthin pigments and the formation of red cysts (aplanospores) is triggered by oxidative stress conditions (Wang *et al*., 2004). Secondary pigments such as astaxanthin are thought to have a protective role, different mechanisms have been proposed to explain this, such as a physicochemical barrier against free radicals, and as antioxidant against reactive oxygen species (ROS) (Wang *et al*., 2003). In addition astaxanthin acts as a carbon sink (Dubinsky and Berman-Frank, 2001).

The blooms in the SNFPs are unwanted as they limit the visibility in the ponds and work has to be stopped. The water in the SNFPs is filtered, deionised/demineralised, however despite this and the high radiation levels, microorganisms are still able to colonise these environments (Chicote *et al*., 2005). There are various treatment methods that are possible to reduce/stop the growth of the microorganisms in the ponds as summarised in Table 2-3 (for more detailed summary of the treatment methods see Konovalovaite, 2017). Roelke & Buyukates (Roelke and Buyukates, 2001) suggest that a single treatment method is unlikely to be sufficient to control photosynthetic blooms

since the conditions in which they occur vary. Careful consideration is required due to the radiation within the ponds and to ensure that the treatments do not have any negative impacts to the conditions necessary for safety.

Table 2-3: Summary of treatment methods to prevent algal and microbial growth, taken from Konovalovaite, 2017.

Treatment	Organisms targeted	Advantages	Disadvantages	Effects of pH
Sonication/ Jet cavitation	Low frequencies: cyanobacteria High frequencies: green algae	No residue Wide range of organisms targeted	Low depth penetration High efficiency requires large power inputs Long treatment times May only redistribute species in the mix. Cyanobacteria lacking gas vacuoles not targeted	No reported effects due to pH
Photocatalysts	Most algal species and bacteria	Can be used without additional light source Works on numerous organisms Can reduce bacterial cultures as well	Catalyst loss Have to be on water surface Have to be immobilised to improve efficiency	

UV light	Most algal species and bacteria	No chemicals required No residue Can be used to remove bacterial cultures Works on numerous organisms	Additional lighting source on large area High power input required Long treatment times Several treatments required Lighting frequency dependent Some organisms may have defence mechanisms	
Biocides	Most algal species and may work on some species of bacteria	Can target specific organisms May require only one treatment	Species specific Residual concentration Required concentration can be very high to be effective Long biodegradation times	pH sensitive, depends on biocide
Oxidation	Most algal species	Very low residual concentration Effective on broad spectrum of organisms Can be used to reduce bacterial cultures	Oxidative compounds can react with metals in the pond Unstable in high pH Varied efficiency depending on compound used Safety hazard, special holding conditions	pH sensitive

Halogenation	Most algal species	Effective on broad spectrum of organisms Can be used on bacterial cultures	Possibility of reaction with metals Can leave halogenated compounds post algal removal Safety hazard, special holding conditions	pH sensitive
Coagulation	Most algal species	Can be species specific, but will remove part of the culture Easily available Does not damage cell membrane leading to increased nutrient availability Can remove some nutrients from the water	Large quantities of non-soluble residue Large doses required Routine treatment required Algae still viable and can be resuspended Requires collection mechanism Waste disposal	pH sensitive, depends on coagulant

Filtration	Algae and bacteria- filter parameters determine which	Efficiency depends on cell size and shape, easy to adapt to suit a mixture of organisms If sizing of the membrane is right , can remove bacteria as well	Can foul easily Some of the fouling is irreversible Efficiency decreases with use Washing required periodically	pH sensitive, effects depend on water chemistry and membrane used
Nutrient removal	Algae and bacteria	Will reduce growth on several species Is a preventative rather than a treatment method Would have an effect on other microorganisms than algae	May require several technologies May only lead to redistribution of organisms Periodic treatment may be required May require additional equipment	pH sensitive

Electrochemical	Most algal species	No chemical required, but can be used to enhance the treatment Works on several species	High power input required Efficiency depends on electrodes used Generates oxidising compounds	pH sensitive
Barley straw	Some algae-potentially growth promoting	Easily obtainable material Can be used as preventative measure	Long lag period Additional pre-treatment required to reduce lag phase Growth phase dependant Can have promotional effects on some species May require periodic treatment	

Flushing	Most cultures	Works on several species No chemicals used No residuals	Increased energy requirement Can have a limited effect May cause sludge resuspension due to increased water movement Water quality can deteriorate if discontinued

2.4 Radiation resistance

2.4.1 Ionizing radiation

Ionizing radiation (IR) can either be particulate or electromagnetic. Particulate IR, such as α and β particles, generates ions by collision events. The particles have a short range and their energy is deposited after entering matter (Cox and Battista, 2005). Gamma (γ) radiation is part of the electromagnetic spectrum and is able to penetrate into cells (Bagwell *et al*., 2008). Gamma-rays use energy absorption to generate ions e.g. the Compton effect; here following collision with matter, the wavelength of the electromagnetic radiation increases (Cox and Battista, 2005). Radiation can have both a direct and an indirect effect on cellular components, both affecting DNA, proteins and lipids (Bagwell *et al*., 2008; Kottemann *et al*., 2005). The direct effects are from the radiation itself and account for approximately 20 % of the total damage to cells (Kottemann *et al*., 2005). Indirect effects are associated with the production of radicals and reactive oxygen species (ROS), irradiation in aqueous environments results in the radiolysis of water resulting high levels of ROS (Kottemann *et al*., 2005). This indirect effect of radiation is responsible for the remaining 80 % damage to DNA (Kottemann *et al*., 2005).

2.4.2 Reactive oxygen species

Microorganisms readily generate ROS as a by-product of metabolic processes, (Kaur *et al*., 2010; Liu *et al*., 2000; Priya *et al*., 2010; Zelko *et al*., 2002). The ROS that are generated include singlet oxygen ($^1O_1$), hydrogen peroxide (H_2O_2), superoxide ($O_2^{\bullet -}$) and the hydroxide radical (•OH) (Banerjee *et al*., 2013; Hakkila *et al*., 2014; Robinson *et al*., 2011). These have a damaging effect to the cells, affecting DNA, proteins and lipids (Banerjee *et al*., 2013; Campbell and Laudenbach, 1995; Priya *et al*., 2010). The $^1O_1$ molecule is more reactive than $O_2^{\bullet -}$and H_2O_2, however the latter two are known to be involved in the production of the highly reactive •OH radical. Enzymatic removal of $O_2^{\bullet -}$ produces H_2O_2, which can react with ferrous iron in the Fenton reaction shown here:

$$Fe^{2+} + H_2O_2 \rightarrow Fe^{3+} + OH^- + \bullet OH$$

The •OH is highly reactive and is known to cause the production of other free radicals, which damage molecules in cells (Aguirre and Culotta, 2012; Banerjee *et al*., 2012; Hakkila *et al*., 2014; Lemire *et al*., 2013). The combination of the reactions of $O_2^{\bullet -}$ and the Fenton reaction is referred to as the Harber-Weiss reaction (Lemire *et al*., 2013). A schematic of the ROS generated and some of the reactions that take place are shown in Figure 2-4.

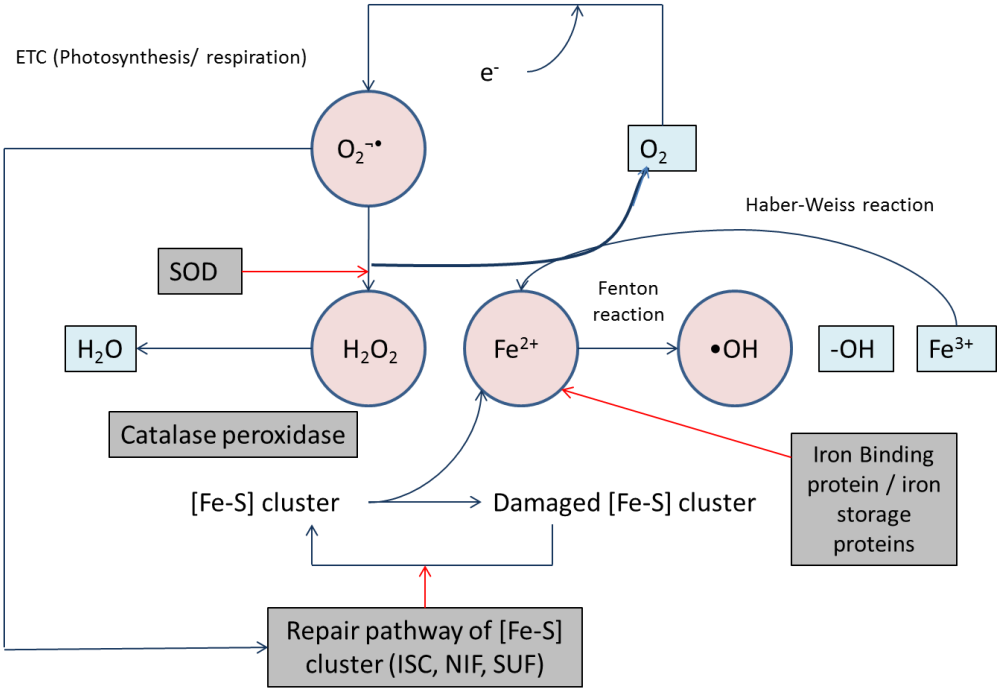

Figure 2-4: Generation of ROS by photosynthetic bacteria and some of the detoxification mechanisms. Circles are toxic species or free radicals; squares are non-toxic; grey boxes are detoxifying or repair enzymes (Banerjee *et al*., 2013).

2.4.2.1 DNA damage

Ionizing radiation is capable of causing a variety of damage to DNA as shown in Figure 2-5**,** including double stand breaks (DSB) and single strand breaks (SSB), base modifications, structural modifications and cross-links (Cox and Battista, 2005; Mrázek, 2002). The most common lesion in DNA is the 7,8-dihydro-8-oxoguanine, this occurs due to the low-redox potential of guanine, which is subject to the majority of the oxidative attack (Vieira *et al*., 2014). The ROS can also modify DNA bases, for example 8-hydroxy-2'-deoxyguanosine is well known and is associated with the formation of DSBs following efforts to remove the modified base (Kottemann *et al*., 2005).

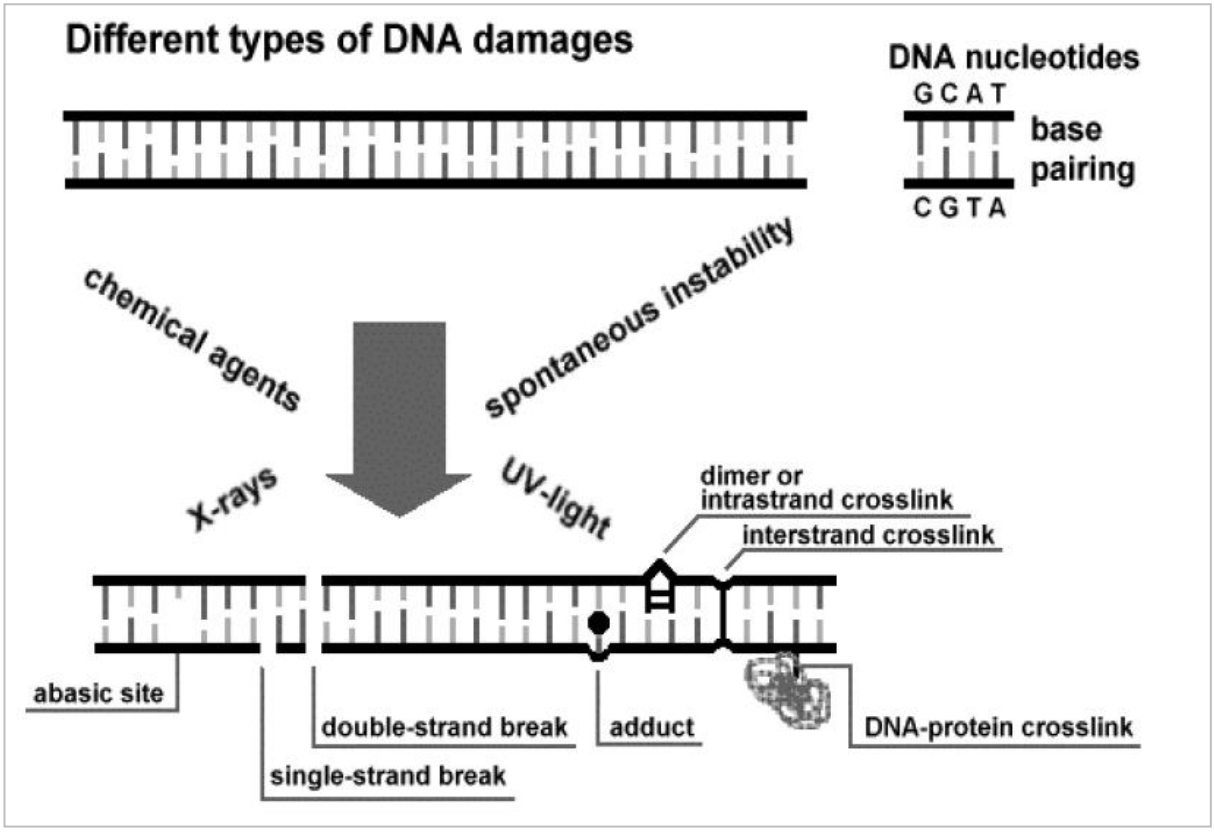

Figure 2-5: Different types of DNA damage induced by ionizing radiation (Horneck *et al*., 2002).

Organisms have developed a variety of repair mechanisms to repair DNA damage as summarised in Table 2-4. Breaks in DNA result from DNA-damaging agents and can occur in replication, these are potentially lethal and so must be repaired. Bacteria repair breaks in their DNA via two mechanisms these are non-homologous end-joining (NHEJ) and homologous recombination (Wigley, 2013). In NHEJ is the main repair mechanism of double stranded breaks in eukaryotic organisms (Shuman and Glickman, 2007). The process involves the modification of the two ends of DNA, allowing them to be ligated together. This method of repair is simple but potentially will introduce mutations since the process has low fidelity. All organisms utilise homologous recombination, simply this process requires a second copy of the genome to act as a template (Wigley, 2013) Recombinase (RecA) in bacteria is involved in locating and paring of the homologous sequences (Shuman and Glickman, 2007).

Deinococcus radiodurans can withstand doses of 5,000 Gy with no perceived loss of viability, surviving around 100 DSBs per genome at 10,000 Gy (Cox and Battista, 2005; Daly *et al*., 2007). This is in contrast to radiation sensitive organisms such as

Shewanella oneidensis that is unable to survive 70 Gy (Daly *et al*., 2007). The amount of double-strand and single-strand DNA breaks has been shown to be 2-3 orders of magnitude higher when the DNA is in the aqueous state (Daly, 2012).

Table 2-4: The repair mechanisms used for different types of DNA lesion and the causative agent for the lesions (Horneck *et al*., 2002).

DNA lesion	Cause	Repair mechanism
Base mismatches, loops and bubble structure	Replication errors and recombination	Base excision and general mismatch repair
Deamination (the removal of an amine group from a molecule)	Heat	Base excision
Depurination (loss of a purine; adenine or guanine from the DNA backbone)		
Oxidative damage	Oxidative metabolism, anoxia/hypoxia and ionizing radiation	Base excision
Alkylation/alkyl adducts (nonbulky/bulky adducts; non-native chemical bonds that do not fit in the standard double helix)	Nitrogen mustard polyaromatic compounds (alkylating agents - attaches an alkyl group to DNA)	Direct repair and base excision
Intrastrand crosslinks (Bulky adducts)	UV or cisplatin (alkylating-like agent)	Direct repair and nucleotide excision
Interstrand crosslinks	Psoralen or melphalan (alkylating agents)	Nucleotide excision and recombination
Single-strand break	Ionizing radiation and oxidative stress	Ligation
Double-strand break	Ionizing radiation	Ligation and recombination

2.4.2.2 Protein damage

The level of DNA damage caused by IR was thought to be the critical factor in determining if an organism was sensitive or resistant (Daly, 2009). Recent studies have shown that it is in fact the level and severity of protein damage as a result of ROS that is the critical factor determining survival following irradiation (Daly, 2012). Comparative studies looking into the effect of IR, different cellular components highlighted that resistant organisms experience much less oxidative damage to their proteins than IR sensitive organisms (Banerjee *et al*., 2014; Daly, 2012). Daly (2012) notes that some hypersensitive bacteria can encounter 100 times more oxidation of proteins as a result of IR when compared to resistance species. Damage to proteins includes carbonylation of amino acid residues, cross links and oxidation of the backbone of the protein. Iron-sulphur and haem group containing proteins are more prone to this damage (Robinson *et al*., 2011; Webb and Diruggiero, 2012). In protecting proteins, organisms enable repair mechanisms to be implemented thus enabling damage to DNA to be corrected. The damage incurred by DNA due to IR has been found to be comparable between resistant and sensitive organisms (Banerjee *et al*., 2014; Daly, 2012).

Amino acid residues of radiation-resistant organisms have been shown to be less susceptible to oxidation than those of radiation sensitive species (Sghaier *et al*., 2013). Analysis of the amino acids present in radiation resistant organisms found that there were fewer amino acids that contained aromatic rings, whilst there was an increase in the abundance of small amino acids (Sghaier *et al*., 2013; Vieira *et al*., 2014). The amino acid side chains that are most susceptible to attack by OH• are those containing sulphur, aromatic rings and those which only contain carbon and hydrogen (Sghaier *et al*., 2013; Webb and Diruggiero, 2012). The amount of oxidative damage seen in radiation sensitive organisms can be as much as 100 times greater than that observed in resistant organisms. The reduction of damage in radiation resistant organisms has been linked to the antioxidant status of the cell as well as substitutions of amino acid residues for those that are less likely to suffer from oxidative damage (Sghaier *et al*., 2013). Aromatic amino acid residues are maintained at active sites to maintain the function of the enzyme. Sghaier *et al*., (2010) compared the sequence of RecA proteins from *E.coli* and *D. radiodurans* and found the phenylalanine had been substituted for another aromatic amino acid tyrosine in *D. radiodurans*.

2.4.2.3 Impacts on lipids

Singh *et al*., (2002) highlight the importance of maintaining membrane integrity in response to environmental stress, particularly desiccation. The composition of lipids confers to how likely they are to be targeted by ROS, with unsaturated bonds being more prone to attack. The rates of these reactions can be unlimited as they are not governed by enzymes, additionally they can result in highly reactive products that damage other macromolecules in the cell. ROS attack on lipids and fatty acids has consequences for cellular membranes in terms of fluidity, permeability and metabolic functions in the cell (Cabiscol *et al*., 2000; Singh *et al*., 2002). Changes in membrane fluidity are known to be triggered by a variety of stress conditions and therefore can be an unspecific response to the environment the microorganism is in (Ramos *et al*., 2001). However, Cabiscol *et al*., (2000) stated that the oxidative attack of lipids can result in their degradation, which can lead to the formation of damaging compounds such as aldehydes.

2.4.3 Radiation and microorganisms

Organisms have been identified that are able to survive continuous exposure to radiation at doses of 1,500 kilorads. Studies estimating the levels of radiation present throughout the Earth's history do not indicate that such doses have occurred naturally; the highest is estimated to be 400 mGy/year raising questions about the adaptation of these organisms (Cox and Battista, 2005; Pikuta *et al*., 2007; Singh *et al*., 2010). It is thought that the ability of these organisms to withstand exposure to IR is due to their ability to survive other stresses that result in similar cellular damage (Billi, 2009; Daly, 2012; Pikuta *et al*., 2007).

Table 2-5 shows the percentage survival of a number of microorganisms at different doses of radiation measured in kilogray (kGy). The physical unit, gray is the absorption of 1 joule of radiation energy per 1 kilogram of matter, however different forms of radiation affect biological molecules to different degrees (Horneck *et al*., 2002).

Table 2-5: The percentage survival of different microorganisms at different doses of radiation kGy.

Organism	Dose of radiation (kGy)	% survival (if known)	Reference
***Chroococcidiopsis* sp.**	2.5 15.0 20.0	30-80 0	Billi *et al*., 2000
***Synechococcus* sp.**	2.5	0	
Escherichia coli	1.0	0	
***Halobacterium* sp.**	5.0	10	Robinson *et al*., 2011
***Kineococcus* sp.**	20	-	Bagwell *et al*., 2008
***Anabaena* sp.**	5.0	Comparable to other more resistant species	Singh *et al*., 2010
A. torulosa	11.0	37	
***Anabaena* L-31**	11.0	52	
***Anabaena* 7120**	3.0 5.0 12.0	80 50 10	Singh *et al*., 2013
***Chlororphyceae Coccomyxa actinabiotis* (eukaryote)**	6.0 6.0 10.0 20.0	50 ~100 50 15	Rivasseau *et al*., 2013
Deinococcus radiodurans	10.0 20.0	50	

2.4.4 Desiccation tolerance linked to radiation tolerance

Links have been made between organisms that have the ability to survive periods of desiccation and resistance to IR, for example in the case of *Chroococcidiopsis* sp. and *D. radiodurans* (Billi, 2009; Cox and Battista, 2005; Daly, 2012; Singh *et al*., 2010). *Chroococcidiopsis* can survive for extended periods in a dehydrated state, additionally

members of this genus can survive doses of IR up to 15 kGy (Billi, 2009). Desiccation tolerance is not fully understood, however there have been links to the ability to form spores and with extracellular polysaccharide production (Billi *et al*., 2000). Organisms that are able to survive periods of desiccation are known to protect their proteins against oxidative damage (Daly, 2012). Other species of cyanobacteria such as *Nostoc commune* and strains of *Anabaena* have also been shown to be able to survive high doses of IR and periods of desiccation (Shirkey *et al*., 2003; Singh *et al*., 2010).

DNA of *N. commune* is known to undergo modifications, which are repaired upon rehydration but there is little evidence of degradation or oxidative damage to the DNA (Shirkey *et al*., 2003). Billi (2009) was able to show that following a period of desiccation the genome of *Chroococcidiopsis* showed little fragmentation, which is in contrast to observations made when the genome of *D. radiodurans* was inspected after an irradiation treatment. This suggests that organisms use different mechanisms to protect against the damage sustained by desiccation and therefore ionizing radiation e.g. *N. commune* accumulates trehalose when in the desiccated state, this is a nonreducing disaccharide. Trehalose is thought to replace water and also to act as a type of cyropreservant (Wada *et al*., 2013). Organisms can either protect against the damage and/or repair any damage they sustain (Billi, 2009). The damage is incurred by oxidative stress, for example during dessication, affects lipids, proteins and nucleic acids (Billi *et al*., 2000).

2.4.5 Enzymes involved in ROS response

Microorganisms have developed various mechanisms to combat ROS stress; these include the production of enzymes which act to remove these species or repair the damage caused and photoprotective compounds (Singh *et al*., 2002). Enzymes linked to combating oxidative damage include superoxide dismutases (SOD), catalases and peroxidases (Singh *et al*., 2002).

2.4.5.1 Superoxide dismutases

An important first line defence against ROS are superoxide dismutases (SODs); these are a family of enzymes that are found in all organisms that act on $O_2^{\bullet -}$ (Zelko *et al*.,

2002). SODs are categorised by the metal co-factor that they contain which include Fe, Mn, Cu/Zn or Ni (Adhikary and Klug, 2007; Priya *et al*., 2007). The specificity of Fe- and Mn-SOD for the metal co-factor has been shown to be interchangeable, with Mn-SOD having been shown to incorporate Fe instead of Mn. All the SODs carry out the same dismutation reaction, however they have been shown to have different structures (Aguirre and Culotta, 2012; Liu *et al*., 2000; Zelko *et al*., 2002). These antioxidant enzymes catalyse the following dismutation reaction (Priya *et al*., 2010)

$$O_2^- + 2H + \rightarrow O_2 + H_2O_2$$

This dismutation reaction is a key factor in the elevated H_2O_2 levels in cells (Banerjee *et al*., 2013).

Oxidative stress is particularly prominent in cyanobacteria due to their photosynthetic capabilities which generate oxygen (Priya *et al*., 2010). It is thought that the chlorophylls and phycobilins could increase the level of oxidative stress cyanobacteria encounter when irradiated. $O_2^{\bullet -}$ is thought to be largely produced by the photosystem I (PSI) complex, in a process known as the Mehler reaction (Badger *et al*., 2000; Priya *et al*., 2010). Cyanobacteria are found in some very harsh conditions such as arid deserts, hot springs and water pockets in Antarctic, therefore they have built up a variety of tolerance mechanisms for stress (Banerjee *et al*., 2013). Banerjee *et al*., (2013) were able to show that the heterocyst forming cyanobacteria *Anabaena* produced a Mn-SOD in the heterocysts to protect against ROS. Heterocysts are specialised cells where nitrogenase fixes N_2, this is a highly sensitive enzyme to oxygen, so therefore requires protection, both enzymatic and non (Banerjee *et al*., 2013; Liu *et al*., 2000). Elevated levels of SodF (a superoxide dismutase) have been found in *N. commune*, which is thought to provide a protective role against oxidative damage when cells are rehydrated (Ramos *et al*., 2001).

2.4.5.2 Catalases and peroxidases

There are two classes of enzymes that detoxify H_2O_2; catalases and peroxidases. Peroxidases can be divided into peroxiredoxins (PRXs), which are ubiquitous and glutathione peroxidases (GPXs). There are four types of PRXs, they function by

reducing H_2O_2 to water, but can also act on peroxinitrite and alkyl hydroperoxides (Banerjee *et al*., 2013; Cui *et al*., 2012; Dayer *et al*., 2008). Catalases can be divided into 3 groups; 1) monofunctional; 2) bifunctional; or 3) binuclear Mn-catalase (Bernroitner *et al*., 2009). They function by detoxifying H_2O_2 via a dismutation reaction, generating O_2 and water (Banerjee *et al*., 2012).

Cyanobacteria are known to generate high levels of ROS species due to their metabolic processes, surprisingly catalases are rare in these organisms. Cui *et al*., (2012) analysed nearly 40 cyanobacterial genomes and found that the majority of genomes lacked genes with homology to catalases, however, the bifunctional catalase peroxidase KatG is known to be present in a large number of cyanobacteria (Banerjee *et al*., 2012; Dayer *et al*., 2008). Despite not being as efficient as other H_2O_2 scavenging enzymes, PRXs are considered to be important for the detoxification of peroxide in cyanobacteria (Cui *et al*., 2012). The synthesis of 2-Cys-PRX, a peroxiredoxin that contains a catalytic cysteine residue, is upregulated in cyanobacteria exposed to oxidative stress (Banerjee *et al*., 2012).

2.4.5.3 Manganese complexes

There are several microorganisms that are known to be able to survive oxidative stress despite a lack of enzymes associated with acting on ROS. *Lactobacillus planetarium* is deficient in SOD enzymes, whilst *D. radiodurans* and *Halobacterium salinarium* retain resistance to IR when SOD enzymes are knocked out (Sharma *et al*., 2013; Webb *et al*., 2013). This demonstrates other mechanisms are important in the ability to survive irradiation (Sharma *et al*., 2013).

Studies on *D. radiodurans* have shown that high cytosolic levels of Mn(II) play an important role in the radiation resistance of these organisms (Daly, 2009; Ghosal *et al*., 2005). The Mn(II) forms complexes with metabolites, such as orthophosphate, in the cytosol that act as ROS scavengers, reducing the level of damage the cells experience both during and after irradiation (Daly, 2012; Daly *et al*., 2010; Daly *et al*., 2004; Sghaier *et al*., 2013). Mn^{2+} forms complexes with inorganic phosphorus (P_i), which acts on $O_2^{\bullet -}$ via a disproportionation mechanism that is completely different to that utilised by SOD enzymes (Barnese *et al*., 2008; Sghaier *et al*., 2013). In addition the Mn(II) can replace Fe as the cofactor in some enzymes, which helps to prevent damage to the active

site (Aguirre and Culotta, 2012; Daly, 2012). Several studies have highlighted that increased Mn/Fe ratios can be correlated to increased radiation tolerance (Aguirre and Culotta, 2012; Daly, 2009; Kottemann *et al*., 2005; Omelchenko *et al*., 2005). Levels of Mn^{2+} have been found to increase by up to 300 times whilst the Fe(II) levels can decline by 3 times (Vieira *et al*., 2014). Ghosal *et al*., (2005) demonstrated that *D. radiodurans* accumulated high levels of Mn(II) and had low levels of Fe^{2+}; Mn^{2+} is said to have an antioxidant role in the cell. In contrast *Shewanella oneidensis* was found have the high Fe(II) and low Mn(II) levels and is very sensitive to IR (Ghosal *et al*., 2005). Cyanobacteria have been shown to complex Mn^{2+} with trehalose as a mechanism of protecting against oxidative damage associated with desiccation (Aguirre and Culotta, 2012; Robinson *et al*., 2011; Shirkey *et al*., 2003; Webb *et al*., 2013). Mn(II) in bicarbonate solutions at physiological pH can also disproportionate H_2O_2, further reducing the damaging effects of ROS (Aguirre and Culotta, 2012). Daly *et al*., (2010) demonstrated that protein-free cell extracts from *D. radiodurans* are capable of protecting against oxidative damage to proteins at very high doses of IR. The ultrafiltrate contained high levels of Mn(II), phosphates, nucleosides, bases and peptides. The group exposed the proteins in the ultrafiltrate to doses up to 50,000 Gy, and were able to show 50 % of the dodecameric enzyme glutamine synthetase retained its activity. *Escherichia coli* and human Jurkat T cells were protected against extreme damage by IR when they were in the *D. radiodurans* protein-free cell extract (Daly *et al*., 2010).

2.4.6 Non- enzymatic protection against ROS- carotenoids, melanin and micosporin-like amino acids (MAAs)

The black pigment melanin has been linked to the ability of some species of fungi to tolerate and thrive in highly radioactive environments. Melanin is believed to have a variety of roles in the cell, for example metabolically linked electron transfer (Dighton *et al*., 2008). The pigment is known to absorb all types of electromagnetic radiation, additionally Dadachova *et al*., (2007) showed it can scatter or trap electrons or photons. Melanin may enable organisms such as fungi to utilise radiation as a source of energy for metabolism, in a similar way to other energy harvesting pigments e.g. chlorophylls (Dadachova *et al*., 2007; Dadachova and Casadevall, 2008).

Carotenoids are produced by a wide variety of organisms, they function as both an accessory pigment in photosynthesis for capturing light and they also protect against ROS (Asker *et al*., 2007; Glaeser and Klug, 2005; Wada *et al*., 2013). The two main environmental factors that are linked with the increased production of carotenoids are illumination and irradiation. Asker *et al*., (2007) studied the diversity of carotenoids that a variety of bacteria produced in the naturally radioactive site of the Misasa spa region in Japan. The authors concluded that there was a clear correlation between carotenoid synthesis and an increase in radiation tolerance. *H. salinarium* and *D. radiodurans* both produce red pigment, the carotenoid bacteriorubrin, associated with their membrane proteins. Bacteriorubrin has been shown to reduce the effects of gamma irradiation by scavenging ROS such as hydroxyl radicals (Kottemann *et al*., 2005). *D. radiodurans* produces other carotenoids that are known to have antioxidant properties such as deinoxanthin (Tian *et al*., 2009).

H. pluvialis is a species of green algae that is known for its ability to produce large quantities of the ketocarotenoid astaxanthin (Sandesh Kamath *et al*., 2008). Astaxanthin production is associated with stress conditions such as high irradiance, with cells changing from green vegetative cells to red cysts (aplanospores) due to the accumulation of the pigment in lipid bodies with the membrane (Kottemann *et al*., 2005; Li *et al*., 2008; Wang *et al*., 2003; Wang *et al*., 2004). Wang *et al.,* (2003) demonstrated the role of astaxanthin in light absorption and linked this with a photo-protective role against oxidative stress in the cell. *H. pluvialis* upregulates the synthesis of astaxanthin when exposed to stress conditions, however proteomic data has indicated that the initial protection to the cell against oxidative damage is due to enzymes (Wang *et al*., 2004). The group predict that the build-up of astaxanthin replaces the enzymatic response as the cells become aplanospores, with the pigment having an antioxidant role (Sandesh Kamath *et al*., 2008; Wang *et al*., 2004). Li *et al*., (2008) demonstrated that the production of astaxanthin uses large quantities of oxygen, which reduces the amount of subcellular molecular oxygen substrates and therefore reduce the level of oxidative damage. In addition astaxanthin has been demonstrated to react much faster with ROS, such as superoxide, than the associated enzymes, supporting its protective role in cells (Li *et al*., 2008). *H. pluvialis* has recently been identified growing in an outdoor SNFP at Sellafield forming dense algal blooms with a characteristic red colour (MeGraw *et al*., 2018). Cultures of the algae were subjected to periodic doses of X-ray treatment,

which showed increases in the production of astaxanthin suggesting a role in protecting the organism against the effects of ionizing radiation (MeGraw *et al*., 2018).

Cyanobacterial species such as *Anabaena doliolum* have also been shown to use non-enzymatic molecules such as carotenoids and α-tocopherol to combat the adverse effects of oxidative stress, particularly that of singlet oxygen (Banerjee *et al*., 2013; Hakkila *et al*., 2014). In addition the presence of microsporin-like amino acids (MAAs), which are small hydrophilic secondary metabolites, has been linked with stress resistance associated with high levels of UV-irradiation in particular UV-B (Oren and Gunde-Cimerman, 2007; Rath and Adhikary, 2007). Rath & Adhikary (2007) demonstrated that the cyanobacterium *Lyngbya aestuarii* up regulated the expression of MAAs and carotenoids when exposed to high levels of UV-B radiation. Some MAAs have been shown to have antioxidant properties and have been shown to scavenge ROS, particularly those containing an aminocyclohexenone structure (Oren and Gunde-Cimerman, 2007; Wada *et al*., 2013). The presence of high levels of MAAs in freshwater cyanobacteria is not common, with the notable exception of *Microcystis*, instead accumulation is thought to aid organisms surviving in highly saline environments and desiccation (Oren and Gunde-Cimerman, 2007). Wada *et al*., (2013) noted that there have been several studies that have demonstrated that oxidative stress, induced by light or heat, triggers MAAs production.

2.5 Interactions of microorganisms and radionuclides

Public concern about radiation and the release of radionuclides into the environment has brought about extensive research into their fate (Lloyd and Gadd, 2011; Lloyd and Renshaw, 2005). Accidental release of radionuclides has occurred, for example at the Chernobyl (Ukraine) and Fukushima (Japan) sites, despite efforts to prevent such events (Fukuda *et al*., 2014; Krejci *et al*., 2011). Effective remediation strategies need to be employed in such instances to minimize the transport of the released radionuclides and therefore limit their harmful effects. There is much interest in the potential application of microorganisms for the remediation of contaminated environments, since they are ubiquitous in the environment and have a diverse range of metabolic capabilities (Blanco-Rivero *et al*., 2005; Gadd, 2004; Pikuta *et al*., 2007). Microbes have been shown to influence the speciation and mobility of metal species, and play a role in the

removal of toxic metals (Gadd, 2004, 1996; Simonoff *et al*., 2007; White *et al*., 1995). A diverse range of microorganisms, including bacteria, fungi, and algae (eukaryotic and cyanobacteria) have been shown to influence the fate of radionuclides using both metabolism-dependent and –independent techniques, summarised in Figure 2-6 (Gadd, 1990; Macaskie and Lloyd, 2002).

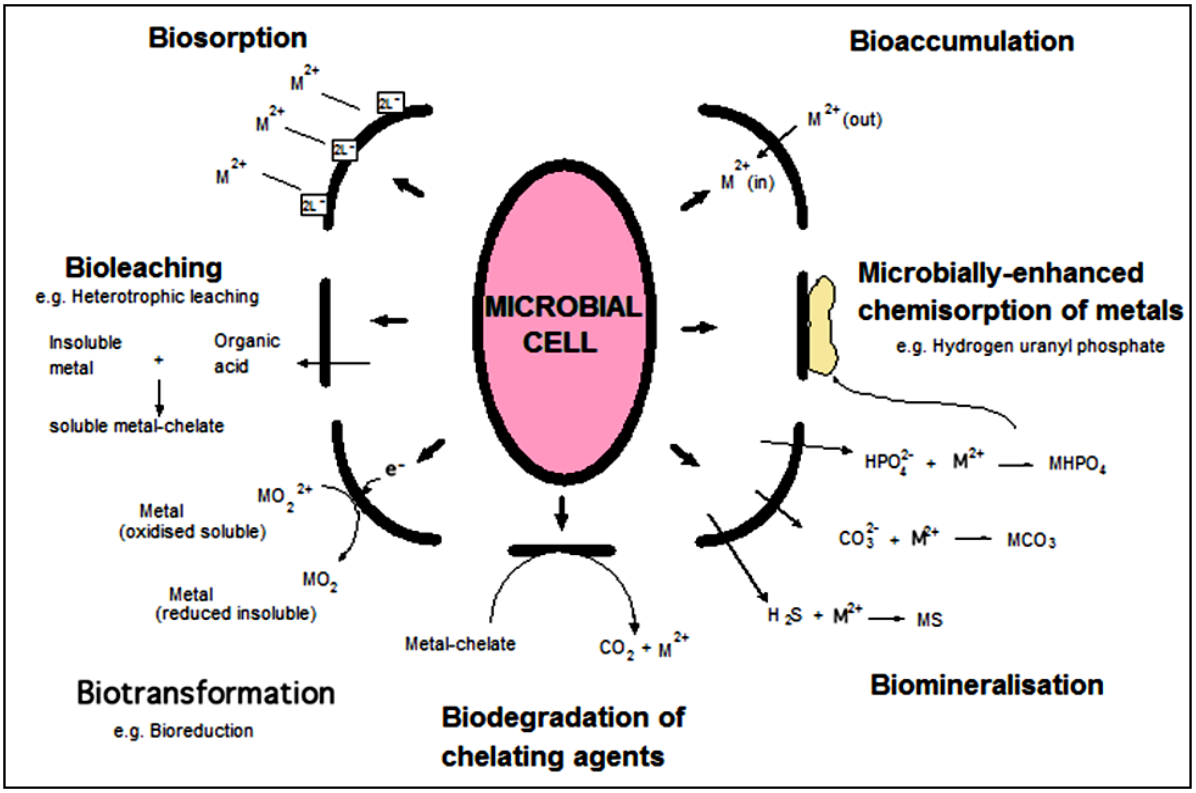

Figure 2-6: Interactions between microbial cells and radionuclides and metals (Macaskie and Lloyd, 2002).

Biosorption is energy independent and the radionuclide can either be absorbed or adsorbed. Experiments have shown that biosorption can occur with both live and dead biomass, with dead cells of *Saccharomyces cerevisiae* sorbing 40 % more than live cells (Brady and Duncan, 1994; Volesky and May-Phillips, 1995; White *et al*., 1995). Biosorption is influenced by the environment in which it is taking place, there is a decline in the biosorption capacity of heavy metals when the pH is less than 6 (Nakajima and Tsuruta, 2004; Yan and Viraraghavan, 2003). Cell walls contain regions of negative charge; this is where the adsorption of cations occurs (Gadd, 1996; Valentine *et al*., 1996). In bacteria the carboxyl groups in the peptidoglycan layer are where biosorption occurs, in fungal cell walls it is chitin (Gadd, 1996; White *et al*.,

1995). It can also occur on extracellular components such as lipopolysaccharides, glycoproteins and polysaccharides (Renshaw *et al*., 2007).

Bioaccumulation is an energy-depended process in which microorganisms take up metals (Macaskie and Lloyd, 2002). When the radionuclides are inside the cells they can be bound, precipitated, or contained within intracellular structures (Gadd, 1996).

The oxidation state of toxic metals and metalloids can be altered by microorganisms, where transformations are a result of the direct catalytic action of the microbes enzymes, for example by enzymes from *Desulfovibrio* species (Lloyd and Renshaw, 2005; Macaskie and Lloyd, 2002). This bioreduction can result in the metals being less mobile in the environment, for example U(VI) reduction to the less soluble U(VI) form in anaerobic conditions (Lloyd and Gadd, 2011; Lovley, 1993). In addition to direct interactions, microorganisms can produce reducing compounds that interact with the metals and result in changes in their oxidation state or complex with the ions (Renshaw *et al*., 2007; Simonoff *et al*., 2007). More detail of these processes see (Behrends *et al*., 2012; Lloyd and Gadd, 2011; Macaskie and Lloyd, 2002; Renshaw *et al*., 2007).

The radioactive isotope ^{137}Cs is not a naturally occurring radionuclide and results from the fission of uranium (Idaho National Engineering Laboratory, 1996). It has a half-life of ~30 years and decays by beta emission to ^{137}Ba (Macaskie and Lloyd, 2002). Most microorganisms are able to accumulate Cs^+ into their cells despite there being no known biological role (Avery and Tobin, 1992). Uptake is usually through K^+ transport systems as Cs^+ is chemically similar to K^+ and is an active process (Gadd, 1996; Tišáková *et al*., 2013). Different bacterial species vary in their ability to accumulate Cs^+, for example when *Pseudomonas fluorescens* was grown in the presence of Cs^+, no uptake of Cs^+ was detected, whereas *Rhodococcus* species under the same conditions accumulated large quantities (Avery, 1995). Avery *et al*., (1991) demonstrated that high concentrations of Cs^+ inhibited the growth of cyanobacteria. It was suggested that the cells stopped growing due to a lack of K^+, which is important in photosynthesis and respiration (Avery *et al*., 1991).

2.5.1 Interaction between microbes from SNFPs and radionuclides

As discussed in section 1.1, microorganisms have been identified colonising several SNFPs in a variety of different locations. Amongst these studies several have reported interactions between the members of native microbial community and a variety of radionuclides. Microorganisms such as *Bacillus* sp. were identified in the Confrentes SNFP that were capable of forming biofilms, which when analysed were shown to accumulate radionuclides (Chicote *et al*., 2004; Chicote *et al*., 2005; Sarró *et al*., 2003; Sarró *et al*., 2005; Sarró *et al*., 2007). The accumulation of radionuclides to biofilms occurs due to the negative charge associated with the largely polysaccharide composition (Sarró *et al*., 2003). Processes such as biosorption and bioaccumulation are responsible for the accumulation of radionuclides within biofilms (Sarró *et al*., 2003; Tišáková *et al*., 2013). MeGraw *et al*., (2018) were able to show that both ^{90}Sr and ^{137}Cs were retained on filter papers containing microorganisms from a near neutral SNFP on the Sellafield site, indicating that that these fission products were associated with the biomass.

In addition to the extracellular accumulation of radionuclides, there have been several studies showing intracellular accumulation of a variety of radionuclides in microorganisms that colonise SNFPs. Tišáková *et al*., (2013), isolated four pure cultures of bacteria from an SNFP and tested their ability to accumulate ^{137}Cs and ^{60}Co. The different microbial isolates showed varying levels of accumulation of the radionuclides, with the maximum ^{60}Co accumulated 86.6 ± 12.2 μmol g^{-1} in *Micrococcus luteus* and for 20.1 ± 2.2 μmol g^{-1} in *Kocuria palustris* (Tišáková *et al*., 2013). The interaction of Cs^+ ions with the microbes was suggested to have occurred by a rapid metabolic-independent interaction with negatively charged functional groups on the cell surface. The bioaccumulation resulted in the transport of Cs^+ ions, through K^+ transport systems (Dekker *et al*., 2014) inside the cells where it was compartmentalised and finally they observed a gradual release of the intracellular Cs^+. ^{60}Co also showed interactions with cell surfaces and accumulation intracellularly, however it exhibited a toxic effect on cells. The toxicity of ^{60}Co, resulted in the lysis of cells and thus release of Co back into solution. The eukaryotic microalga *Coccomyxa actinabiotis*, which as previously mentioned has been isolated from a research facility in France (Rivasseau *et al*., 2010; Rivasseau *et al*., 2016), has been shown to be able to accumulate a wide range of radionuclides in various concentrations (Rivasseau *et al*., 2013). *C. actinabiotis* was

capable of accumulating the following radionuclides; ^{238}U; ^{137}Cs; ^{110m}Ag; ^{60}Co; ^{54}Mn; ^{65}Zn and ^{14}C, in relatively high concentrations (Rivasseau *et al*., 2013). There is limited information about the interaction of microorganisms found in such facilities, for example their metabolic capabilities and interactions with radionuclides. Further work is required to determine the extent to which the native microbial communities of SNFPs are able to influence the fate of radionuclides, since they could provide cost-effective and efficient remediation strategies in contaminated areas.

2.5.2 Sr interactions

Sr exists as a divalent cation that is analogous to Ca^{2+} and therefore is of biological interest since it can be taken up through the same transport routes as Ca, despite it having no known essential biological function (Avery *et al*., 1999; Avery and Tobin, 1992; Krejci *et al*., 2011). Radioactive strontium (^{90}Sr) is generated as part of the fission reactions of nuclear industry, the isotope has a half-life of ~29 years and can be highly mobile in the environment (Avery *et al*., 1999). Sr is present as part of inventory of radionuclides in SNFPs, although the fate of Sr with microorganisms within these engineered systems has not been studied.

Sr^{2+} can be adsorbed onto cell surfaces and in some cases this has been seen to occur with the release of Mg^{2+} and Ca^{2+} , for example with the alga *Vaucheria* species (Crist *et al*., 1990). Studies have shown that Sr can be accumulated by microorganisms, such as *Saccharomyces cerevisiae*, which transports the Sr into its vacuoles (Avery and Tobin, 1992). Anderson & Appanna (1994) demonstrated that the growth of *Pseudomonas fluorescens* was not inhibited by the presence of Sr. *P. flourescens* was shown to be involved in the production of $SrCO_3$ crystal precipitates, it is thought that this allows their continued growth in Sr-rich environments (Anderson and Appanna, 1994). There has been much interest in the ability of microorganisms and the formation of $CaCO_3$ minerals, largely from a geological perspective. Other divalent cations have been shown to be incorporated into carbonate minerals including Sr, and can be seen at different ratios with Ca (Mitchell and Ferris, 2005; Rivasseau *et al*., 2013). Extracellular carbonate mineral formation has been associated with the bacterial hydrolysis of urea, with Sr co-precipitating into calcite minerals (Mitchell and Ferris, 2005; Mitchell and Ferris 2006). Cyanobacteria are known to form carbonate minerals, a process that has

largely been viewed as an extracellular process (Cam *et al*., 2015) driven by increases in the external pH by photosynthetic activity. The incorporation of Sr into carbonate minerals poses a potential remediation strategy in aquatic environments.

Recently there have been several studies that have identified the ability of some species of cyanobacteria (Benzerara *et al*., 2014; Cam *et al*., 2015; Cam *et al*., 2016; Cam *et al*., 2018; Couradeau *et al*., 2012) and a eukaryotic green desmid alga species (Krejci *et al*., 2011) to form intracellular carbonate minerals. The majority of this work has centred around $CaCO_3$ minerals although Sr and Ba have been shown to be incorporated (Benzerara *et al*., 2014; Cam *et al*., 2015; Cam *et al*., 2016; Cam *et al*., 2018; Couradeau *et al*., 2012). At present it is not known how widespread intracellular carbonate synthesis is in microorganisms. Traditional sample preparation techniques for investigating the ultrastructure of cells and other features within the cells such as these biominerals has been shown to distort or result in their complete removal (Li *et al*., 2016). The cyanobacteria that have been shown to form intracellular carbonates, so far, are deep branching species, which suggests this is an ability that evolved early on. At present it is not known whether this capability was lost in some species or has evolved separately several times (Benzerara *et al*., 2014). Benzerara *et al*., (2014) suggest that the formation of carbonate minerals might be inhibited by polyphosphate, which are a common feature in all organisms.

Polyphosphate (polyP) bodies can be found in many organisms, and are composed of orthophosphate residues linked by phosphanhydride bonds (Achbergerová and Nahálka, 2011; Albi and Serrano, 2016). PolyP bodies have a variety of functions, such as being a phosphate store for when it becomes limited, they are also thought to play a role in stress responses and metal detoxification (Albi and Serrano, 2016; Keasling, 1997). There has been a lot of research which has shown metal binding to polyP, particularly Ca, Cd, and Pb, which reduces the concentrations that are free in the cytoplasm (Albi and Serrano, 2016; Baxter and Jensen, 1980; Jensen *et al*., 1982). In addition, research has shown that enzymatic activity can cleave the metals bound to polyP as phosphate minerals and export them out of the cell, via the Pit transport system, thus reducing their toxic effect (Albi and Serrano, 2016; van Veen *et al*., 1994). Interestingly there is virtually no information about the association of Sr with polyP, Baxter and Jensen (1980) report intracellular Sr in the cyanobacterium *Plectonema boryanum*, however this is not consistent and P is not always present.

2.6 References

Achbergerová, L., Nahálka, J., 2011. Polyphosphate - an ancient energy source and active metabolic regulator. Microb. Cell Fact. 10, 1–14. https://doi.org/10.1186/1475-2859-10-63

Adhikary, S.P., Klug, G., 2007. Detection of a gene for iron containing superoxide dismutase in the terrestrial cyanobacterium *Tolypothrix byssoidea*. Indian J. Biotechnol. 6, 118–120.

Aguirre, J.D., Culotta, V.C., 2012. Battles with iron: Manganese in oxidative stress protection. J. Biol. Chem. 287, 13541–13548. https://doi.org/10.1074/jbc.R111.312181

Albi, T., Serrano, A., 2016. Inorganic polyphosphate in the microbial world. Emerging roles for a multifaceted biopolymer. World J. Microbiol. Biotechnol. 32, 1–12. https://doi.org/10.1007/s11274-015-1983-2

Anderson, S., Appanna, V.D., 1994. Microbial formation of crystalline strontium carbonate. FEMS Microbiol. Lett. 116, 43–48. https://doi.org/10.1111/j.1574-6968.1994.tb06673.x

Asker, D., Beppu, T., Ueda, K., 2007. Unique diversity of carotenoid-producing bacteria isolated from Misasa, a radioactive site in Japan. Appl. Microbiol. Biotechnol. 77, 383–392. https://doi.org/10.1007/s00253-007-1157-8

Avery, S. V., 1995. Caesium accumulation by microorganisms: uptake mechanisms, cation competition, compartmentalization and toxicity. J. Ind. Microbiol. 14, 76–84. https://doi.org/10.1007/BF01569888

Avery, S. V., Codd, G.A., Gadd, G.M., 1991. Caesium accumulation and interactions with other monovalent cations in the cyanobacterium *Synechocystis* PCC 6803. J. Gen. Microbiol. 137, 405–413. https://doi.org/10.1099/00221287-137-2-405

Avery, S. V., Smith, S.L., Ghazi, A.M., Hoptroff, M.J., 1999. Stimulation of strontium accumulation in linoleate-enriched *Saccharomyces cerevisiae* is a result of reduced Sr2+ efflux. Appl. Environ. Microbiol. 65, 1191–1197.

Avery, S. V., Tobin, J.M., 1992. Mechanisms of strontium uptake by laboratory and brewing strains of *Saccharomyces cerevisiae*. Appl. Environ. Microbiol. 58, 3883–3889.

Azad, H.S., Borchardt, J.A., 1970. Variations in phosphorus uptake by algae. Environ. Sci. Technol. 4, 737–743. https://doi.org/Doi 10.1021/Es60044a008

Badger, M.R., Von Caemmerer, S., Ruuska, S., Nakano, H., Laisk, A., Allen, J.F., Asada, K., Matthijs, H.C.P., Griffiths, H., 2000. Electron flow to oxygen in higher plants and algae: Rates and control of direct photoreduction (Mehler reaction) and rubisco oxygenase. Philos. Trans. R. Soc. B Biol. Sci. 355, 1433–1446. https://doi.org/10.1098/rstb.2000.0704

Bagwell, C.E., Bhat, S., Hawkins, G.M., Smith, B.W., Biswas, T., Hoover, T.R., Saunders, E., Han, C.S., Tsodikov, O. V., Shimkets, L.J., 2008. Survival in nuclear

waste, extreme resistance, and potential applications gleaned from the genome sequence of *Kineococcus radiotolerans* SRS30216. PLoS One 3. https://doi.org/10.1371/journal.pone.0003878

Bagwell, C.E., Noble, P.A., Milliken, C.E., Li, D., Kaplan, D.I., 2018. Amplicon sequencing reveals microbiological signatures in spent nuclear fuel storage basins. Front. Microbiol. 9, 1–12. https://doi.org/10.3389/fmicb.2018.00377

Banerjee, M., Ballal, A., Apte, S.K., 2012. Mn-catalase (Alr0998) protects the photosynthetic, nitrogen-fixing cyanobacterium *Anabaena* PCC7120 from oxidative stress. Environ. Microbiol. 14, 2891–2900. https://doi.org/10.1111/j.1462-2920.2012.02847.x

Banerjee, M., Raghavan, P.S., Ballal, A., Rajaram, H., Apte, S.K., 2013. Oxidative stress management in the filamentous, heterocystous, diazotrophic cyanobacterium, *Anabaena* PCC7120. Photosynth. Res. 118, 59–70. https://doi.org/10.1007/s11120-013-9929-8

Banerjee, R., Roy, A., Mukhopadhyay, S., 2014. Genomic and proteomic signatures of radiation and thermophilic adaptation in the *Deinococcus-Thermus* genomes. Int. J. Pharm. Pharm. Sci. 6, 287–300.

Barnese, K., Gralla, E.B., Cabelli, D.E., Valentine, J.S., 2008. Manganous phosphate acts as a superoxide dismutase. J. Am. Chem. Soc. 130, 4604–4606. https://doi.org/10.1021/ja710162n

Baxter, M., Jensen, T., 1980. Uptake of magnesium, strontium, barium, and manganese by *Plectonema boryanum* (*Cyanophyceae*) with special reference to polyphosphate bodies. Protoplasma 104, 81–89. https://doi.org/10.1007/BF01279371

Behrends, T., Krawczyk-Bärsch, E., Arnold, T., 2012. Implementation of microbial processes in the performance assessment of spent nuclear fuel repositories. Appl. Geochemistry 27, 453–462. https://doi.org/10.1016/j.apgeochem.2011.09.014

Bellinger, E.G., Sigee, D.C., 2010. Freshwater algae: Identification and use as bioindicators, 2010th ed. John Wiley & Sons, Ltd.

Benzerara, K., Skouri-Panet, F., Li, J., Férard, C., Gugger, M., Laurent, T., Couradeau, E., Ragon, M., Cosmidis, J., Menguy, N., Margaret-Oliver, I., Tavera, R., López-García, P., Moreira, D., 2014. Intracellular Ca-carbonate biomineralization is widespread in cyanobacteria. Proc. Natl. Acad. Sci. 1–6. https://doi.org/10.1073/pnas.1403510111

Bernroitner, M., Zamocky, M., Furtmüller, P.G., Peschek, G.A., Obinger, C., 2009. Occurrence, phylogeny, structure, and function of catalases and peroxidases in cyanobacteria. J. Exp. Bot. 60, 423–440. https://doi.org/10.1093/jxb/ern309

Billi, D., 2009. Subcellular integrities in *Chroococcidiopsis* sp. CCMEE 029 survivors after prolonged desiccation revealed by molecular probes and genome stability assays. Extremophiles 13, 49–57. https://doi.org/10.1007/s00792-008-0196-0

Billi, D., Friedmann, E.I., Hofer, K.G., Caiola, M.G., Ocampo-Friedmann, R., 2000. Ionizing-radiation resistance in the desiccation-tolerant cyanobacterium *Chroococcidiopsis*. Appl. Environ. Microbiol. 66, 1489–1492.

Blanco-Rivero, A., Leganés, F., Fernández-Valiente, E., Calle, P., Fernández-Piñas, F., 2005. *mrpA*, a gene with roles in resistance to Na+ and adaptation to alkaline pH in the cyanobacterium *Anabaena* sp. PCC7120. Microbiology 151, 1671–1682. https://doi.org/10.1099/mic.0.27848-0

Boussiba, S., Vonshak, A., 1991. Astaxanthin accumulation in the green alga *Haematococcus pluvialis*. Plant Cell Physiol. 32, 1077–1082. https://doi.org/10.1093/oxfordjournals.pcp.a078171

Brady, D., Duncan, J.R., 1994. Binding of heavy metals by the cell.pdf 16, 633–638.

Bruhn, D.F., Frank, S.M., Roberto, F.F., Pinhero, P.J., Johnson, S.G., 2009. Microbial biofilm growth on irradiated, spent nuclear fuel cladding. J. Nucl. Mater. 384, 140–145. https://doi.org/10.1016/j.jnucmat.2008.11.008

Cabiscol, E., Tamarit, J., Ros, J., 2000. Oxidative stress in bacteria and protein damage by reactive oxygen species. Int. Microbiol. 3, 3–8. https://doi.org/10.2436/im.v3i1.9235

Cade-Menun, B.J., Paytan, A., 2010. Nutrient temperature and light stress alter phosphorus and carbon forms in culture-grown algae. Mar. Chem. 121, 27–36. https://doi.org/10.1016/j.marchem.2010.03.002

Cam, N., Benzerara, K., Georgelin, T., Jaber, M., Lambert, J.F., Poinsot, M., Skouri-Panet, F., Cordier, L., 2016. Selective uptake of alkaline earth metals by cyanobacteria forming intracellular carbonates. Environ. Sci. Technol. 50, 11654–11662. https://doi.org/10.1021/acs.est.6b02872

Cam, N., Benzerara, K., Georgelin, T., Jaber, M., Lambert, J.F., Poinsot, M., Skouri-Panet, F., Moreira, D., López-García, P., Raimbault, E., Cordier, L., Jézéquel, D., 2018. Cyanobacterial formation of intracellular Ca-carbonates in undersaturated solutions. Geobiology 16, 49–61. https://doi.org/10.1111/gbi.12261

Cam, N., Georgelin, T., Jaber, M., Lambert, J.F., Benzerara, K., 2015. In vitro synthesis of amorphous Mg-, Ca-, Sr- and Ba-carbonates: What do we learn about intracellular calcification by cyanobacteria? Geochim. Cosmochim. Acta 161, 36–49. https://doi.org/10.1016/j.gca.2015.04.003

Campbell, W.S., Laudenbach, D.E., 1995. Characterization of four superoxide dismutase genes from a filamentous cyanobacterium. J. Bacteriol. 177, 964–972.

Carstensen, J., Conley, D.J., Henriksen, P., 2004. Frequency, composition, and causes of summer phytoplankton blooms in a shallow coastal ecosystem, the Kattegat. Limnol. Oceanogr. 49, 191–201. https://doi.org/10.4319/lo.2004.49.1.0191

Chicote, E., García, A.M., Moreno, D.A., Sarró, M.I., Lorenzo, P.I., Montero, F., 2005. Isolation and identification of bacteria from spent nuclear fuel pools. J. Ind. Microbiol. Biotechnol. 32, 155–162. https://doi.org/10.1007/s10295-005-0216-3

Chicote, E., Moreno, D. a, García, A.M., Sarró, M.I., Lorenzo, P.I., Montero, F., 2004. Biofouling on the walls of a spent nuclear fuel pool with radioactive ultrapure water. Biofouling 20, 35–42. https://doi.org/10.1080/08927010410001662670

Couradeau, E., Benzerara, K., Gérard, E., Moreira, D., Bernard, S., Brown, G.E., López-García, P., 2012. An early-branching microbialite cyanobacterium forms

intracellular carbonates. Science (80-.). 336, 459–462. https://doi.org/10.1126/science.1216171

Cox, M.M., Battista, J.R., 2005. *Deinococcus radiodurans* - the consummate survivor. Nat. Rev. Microbiol. 3, 882–92. https://doi.org/10.1038/nrmicro1264

Crist, R.H., Martin, J.R., Guptill, P.W., Eslinger, J.M., Crist, D.L.R., 1990. Interaction of metals and protons with algae. 2. Ion exchange in adsorption and metal displacement by protons. Environ. Sci. Technol. 24, 337–342. https://doi.org/10.1021/es00073a008

Crossland, I., 2012. Nuclear fuel cycle science and engineering, 1st ed. Woodhead Publishing, Philadelphia.

Cui, H., Wang, Y., Wang, Y., Qin, S., 2012. Genome-wide analysis of putative peroxiredoxin in unicellular and filamentous cyanobacteria. BMC Evol. Biol. 12, 220–235. https://doi.org/10.1155/2012/164690

Dadachova, E., Bryan, R.A., Huang, X., Moadel, T., Schweitzer, A.D., Aisen, P., Nosanchuk, J.D., Casadevall, A., 2007. Ionizing radiation changes the electronic properties of melanin and enhances the growth of melanized fungi. PLoS One 2. https://doi.org/10.1371/journal.pone.0000457

Dadachova, E., Casadevall, A., 2008. Ionizing radiation: how fungi cope, adapt, and exploit with the help of melanin. Curr. Opin. Microbiol. 11, 525–531. https://doi.org/10.1016/j.mib.2008.09.013.Ionizing

Daly, M.J., 2012. Death by protein damage in irradiated cells. DNA Repair (Amst). 11, 12–21. https://doi.org/10.1016/j.dnarep.2011.10.024

Daly, M.J., 2009. A new perspective on radiation resistance based on *Deinococcus radiodurans*. Nat. Rev. Microbiol. 7, 237–245. https://doi.org/10.1038/nrmicro2073

Daly, M.J., Gaidamakova, E.K., Matrosova, V.Y., Kiang, J.G., Fukumoto, R., Lee, D.Y., Wehr, N.B., Viteri, G.A., Berlett, B.S., Levine, R.L., 2010. Small-molecule antioxidant proteome-shields in *Deinococcus radiodurans*. PLoS One 5, 10–15. https://doi.org/10.1371/journal.pone.0012570

Daly, M.J., Gaidamakova, E.K., Matrosova, V.Y., Vasilenko, A., Zhai, M., Leapman, R.D., Lai, B., Ravel, B., Li, S.M.W., Kemner, K.M., Fredrickson, J.K., 2007. Protein oxidation implicated as the primary determinant of bacterial radioresistance. PLoS Biol. 5, 769–779. https://doi.org/10.1371/journal.pbio.0050092

Daly, M.J., Gaidamakova, E.K., Matrosova, V.Y., Vasilenko, A., Zhai, M., Venkateswaran, A., Hess, M., Omelchenko, M. V, Kostandarithes, H.M., Makarova, K.S., Wackett, L.P., Friedrickson, J.K., Ghosal, R., 2004. Accumulation of Mn (II) in *Deinococcus radiodurans* facilitates gamma-radiation resistance. Science 306, 1025–28. https://doi.org/10.1126/science.1103185

Davis, T.W., Berry, D.L., Boyer, G.L., Gobler, C.J., 2009. The effects of temperature and nutrients on the growth and dynamics of toxic and non-toxic strains of *Microcystis* during cyanobacteria blooms. Harmful Algae 8, 715–725. https://doi.org/10.1016/j.hal.2009.02.004

Dayer, R., Fischer, B.B., Eggen, R.I.L., Lemaire, S.D., 2008. The peroxiredoxin and glutathione peroxidase families in *Chlamydomonas reinhardtii*. Genetics 179, 41–57. https://doi.org/10.1534/genetics.107.086041

Dekker, L., Osborne, T.H., Santini, J.M., 2014. Isolation and identification of cobalt- and caesium-resistant bacteria from a nuclear fuel storage pond. FEMS Microbiol. Lett. 359, 81–84. https://doi.org/10.1111/1574-6968.12562

Díez, B., Bauer, K., Bergman, B., 2007. Epilithic cyanobacterial communities of a marine tropical beach rock (Heron Island, Great Barrier Reef): Diversity and diazotrophy. Appl. Environ. Microbiol. 73, 3656–3668. https://doi.org/10.1128/AEM.02067-06

Dighton, J., Tugay, T., Zhdanova, N., 2008. Fungi and ionizing radiation from radionuclides. FEMS Microbiol. Lett. 281, 109–120. https://doi.org/10.1111/j.1574-6968.2008.01076.x

Diósi, G., Telegdi, J., Farkas, G., Gazsó, L.G., Bokori, E., 2003. Corrosion influenced by biofilms during wet nuclear waste storage. Int. Biodeterior. Biodegrad. 51, 151–156. https://doi.org/10.1016/S0964-8305(02)00138-5

Dubinsky, Z., Berman-Frank, I., 2001. Uncoupling primary production from population growth in photosynthesizing organisms in aquatic ecosystems. Aquat. Sci. 63, 4–17. https://doi.org/10.1007/PL00001343

Evans, V.E., 2013. The microbial ecology and biogeochemistry of nuclear waste storage facilities in the UK. University of Manchester.

Ewing, R.C., 2015. Long-term storage of spent nuclear fuel. Nat Mater 14, 252–257. https://doi.org/10.1038/nmat4226

Finden, D. a. S., Tipping, E., Jaworski, G.H.M., Reynolds, C.S., 1984. Light-induced reduction of natural iron(III) oxide and its relevance to phytoplankton. Nature 309, 783–784. https://doi.org/10.1038/309783a0

Forte Giacobone, A.F., Rodriguez, S.A., Burkart, A.L., Pizarro, R.A., 2011. Microbiological induced corrosion of AA 6061 nuclear alloy in highly diluted media by *Bacillus cereus* RE 10. Int. Biodeterior. Biodegrad. 65, 1161–1168. https://doi.org/10.1016/j.ibiod.2011.08.012

Fukuda, S. ya, Iwamoto, K., Atsumi, M., Yokoyama, A., Nakayama, T., Ishida, K. ichiro, Inouye, I., Shiraiwa, Y., 2014. Global searches for microalgae and aquatic plants that can eliminate radioactive cesium, iodine and strontium from the radio-polluted aquatic environment: A bioremediation strategy. J. Plant Res. 127, 79–89. https://doi.org/10.1007/s10265-013-0596-9

Gadd, G.M., 2004. Microbial influence on metal mobility and application for bioremediation. Geoderma 122, 109–119. https://doi.org/10.1016/j.geoderma.2004.01.002

Gadd, G.M., 1996. Influence of microorganisms on the environmental fate of radionuclides. Endeavour 20, 150–155. https://doi.org/10.1016/S0160-9327(96)10021-1

Gadd, G.M., 1990. Heavy metal accumulation by bacteria and other microorganisms.

Experientia 46, 834–840. https://doi.org/10.1007/BF01935534

Galès, G., Libert, M.F., Sellier, R., Cournac, L., Chapon, V., Heulin, T., 2004. Molecular hydrogen from water radiolysis as an energy source for bacterial growth in a basin containing irradiating waste. FEMS Microbiol. Lett. 240, 155–162. https://doi.org/10.1016/j.femsle.2004.09.025

Gao, L., Pan, X., Zhang, D., Mu, S., Lee, D.J., Halik, U., 2015. Extracellular polymeric substances buffer against the biocidal effect of H2O2 on the bloom-forming cyanobacterium *Microcystis aeruginosa*. Water Res. 69, 51–58. https://doi.org/10.1016/j.watres.2014.10.060

Ghosal, D., Omelchenko, M. V., Gaidamakova, E.K., Matrosova, V.Y., Vasilenko, A., Venkateswaran, A., Zhai, M., Kostandarithes, H.M., Brim, H., Makarova, K.S., Wackett, L.P., Fredrickson, J.K., Daly, M.J., 2005. How radiation kills cells: Survival of *Deinococcus radiodurans* and *Shewanella oneidensis* under oxidative stress. FEMS Microbiol. Rev. 29, 361–375. https://doi.org/10.1016/j.femsre.2004.12.007

Glaeser, J., Klug, G., 2005. Photo-oxidative stress in *Rhodobacter sphaeroides*: Protective role of carotenoids and expression of selected genes. Microbiology 151, 1927–1938. https://doi.org/10.1099/mic.0.027789-0

Gregson, C.R., Goddard, D.T., Sarsfield, M.J., Taylor, R.J., 2011a. Combined electron microscopy and vibrational spectroscopy study of corroded Magnox sludge from a legacy spent nuclear fuel storage pond. J. Nucl. Mater. 412, 145–156. https://doi.org/10.1016/j.jnucmat.2011.02.046

Gregson, C.R., Hastings, J.J., Sims, H.E., Steele, H.M., Taylor, R.J., 2011b. Characterisation of plutonium species in alkaline liquors sampled from a UK legacy nuclear fuel storage pond. Anal. Methods 3, 1957. https://doi.org/10.1039/c1ay05313b

Hakkila, K., Antal, T., Rehman, A.U., Kurkela, J., Wada, H., Vass, I., Tyystjärvi, E., Tyystjärvi, T., 2014. Oxidative stress and photoinhibition can be separated in the cyanobacterium *Synechocystis* sp. PCC 6803. Biochim. Biophys. Acta - Bioenerg. 1837, 217–225. https://doi.org/10.1016/j.bbabio.2013.11.011

Horneck, G., Baumstark-Khan, C., Facius, R., 2002. Life under conditions of ionizing radiation, Astrobiolo. ed. Springer Berlin Heidelberg, New York.

Hu, T., Yang, S., Mao, Y., 1990. The effects of γ-irradiation on *Spirulina plantesis*. Acta Agric. Nucleatae Sin. 4, 120–124.

Huertas, E., 2000. Effects of dissolved inorganic carbon availability on growth, nutrient uptake and chlorophyll fluorescence of two species of marine microalgae. Aquac. Eng. 22, 181–197. https://doi.org/10.1016/S0144-8609(99)00038-2

Hugerth, L.W., Muller, E.E.L., Hu, Y.O.O., Lebrun, L.A.M., Roume, H., Lundin, D., Wilmes, P., Andersson, A.F., 2014. Systematic design of 18S rRNA gene primers for determining eukaryotic diversity in microbial consortia. PLoS One 9. https://doi.org/10.1371/journal.pone.0095567

Idaho National Engineering Laboratory, I., 1996. Selected radionuclides important to low-level radioactive waste management. Idaho Falls, Idaho.

Jackson, S.F., Monk, S.D., Riaz, Z., 2014. An investigation towards real time dose rate monitoring, and fuel rod detection in a First Generation Magnox Storage Pond (FGMSP). Appl. Radiat. Isot. 94, 254–259. https://doi.org/10.1016/j.apradiso.2014.08.019

Jensen, T.E., Baxter, M., Rachlin, J.W., Jani, V., 1982. Uptake of heavy metals by *Plectonema boryanum* (Cyanophyceae) into cellular components, especially polyphosphate bodies: An X-ray energy dispersive study 27, 119–127.

Jia, Y., Dan, J., Zhang, M., Kong, F., 2013. Growth characteristics of algae during early stages of phytoplankton bloom in Lake Taihu, China. J. Environ. Sci. (China) 25, 254–261. https://doi.org/10.1016/S1001-0742(12)60058-8

Jiang, Y., Ji, B., Wong, R.N.S., Wong, M.H., 2008. Statistical study on the effects of environmental factors on the growth and microcystins production of bloom-forming cyanobacterium-*Microcystis aeruginosa*. Harmful Algae 7, 127–136. https://doi.org/10.1016/j.hal.2007.05.012

Jin, X., Chu, Z., Yi, W., Hu, X., 2005. Influence of phosphorus on *Microcystis* growth and the changes of other environmental factors. J. Environ. Sci. 17, 937–941.

Kahru, M., Leppänen, J.M., Rud, O., Savchuk, O.P., 2000. Cyanobacteria blooms in the Gulf of Finland triggered by saltwater inflow into the Baltic Sea. Mar. Ecol. Prog. Ser. 207, 13–18. https://doi.org/10.3354/meps207013

Karley, D., Shukla, S.K., Rao, T.S., 2017. Isolation and characterization of culturable bacteria present in the spent nuclear fuel pool water. Environ. Sci. Pollut. Res. 1–9. https://doi.org/10.1007/s11356-017-0376-5

Kaur, A., Van, P.T., Busch, C.R., Robinson, C.K., Pan, M., Pang, W.L., Reiss, D.J., Diruggiero, J., Baliga, N.S., 2010. Coordination of frontline defense mechanisms under severe oxidative stress. Mol. Syst. Biol. 6, 1–16. https://doi.org/10.1038/msb.2010.50

Keasling, J.D., 1997. Regulation of intracellular toxic metals and other cations by hydrolysis of polyphosphate. Ann. N. Y. Acad. Sci. 829, 242–249. https://doi.org/10.1111/j.1749-6632.1997.tb48579.x

Kehoe, D.M., Gutu, A., 2006. Responding to color: the regulation of complementary chromatic adaptation. Annu. Rev. Plant Biol. 57, 127–150. https://doi.org/10.1146/annurev.arplant.57.032905.105215

Kononen, K., Kuparinen, J., Mäkelä, K., Laanemets, J., Pavelson, J., Nömmann, S., 1996. Initiation of cyanobacterial blooms in a frontal region at the entrance to the Gulf of Finland, Baltic Sea. Limnol. Oceanogr. 41, 98–112. https://doi.org/10.4319/lo.1996.41.1.0098

Konovalovaite, J., 2017. Control of algae in fuel storage ponds. University of Manchester.

Kottemann, M., Kish, A., Iloanusi, C., Bjork, S., DiRuggiero, J., 2005. Physiological responses of the halophilic archaeon *Halobacterium* sp. strain NRC1 to desiccation and gamma irradiation. Extremophiles 9, 219–227. https://doi.org/10.1007/s00792-005-0437-4

Krejci, M.R., Finney, L., Vogt, S., Joester, D., 2011. Selective sequestration of strontium in desmid green algae by biogenic co-precipitation with barite. ChemSusChem 4, 470–473. https://doi.org/10.1002/cssc.201000448

Lemire, J.A., Harrison, J.J., Turner, R.J., 2013. Antimicrobial activity of metals: Mechanisms, molecular targets and applications. Nat. Rev. Microbiol. 11, 371–384. https://doi.org/10.1038/nrmicro3028

Li, J., Margaret Oliver, I., Cam, N., Boudier, T., Blondeau, M., Leroy, E., Cosmidis, J., Skouri-Panet, F., Guigner, J.-M., Férard, C., Poinsot, M., Moreira, D., Lopez-Garcia, P., Cassier-Chauvat, C., Chauvat, F., Benzerara, K., 2016. Biomineralization patterns of intracellular carbonatogenesis in cyanobacteria: Molecular hypotheses. Minerals 6, 10. https://doi.org/10.3390/min6010010

Li, Y., Sommerfeld, M., Chen, F., Hu, Q., 2008. Consumption of oxygen by astaxanthin biosynthesis: A protective mechanism against oxidative stress in *Haematococcus pluvialis* (Chlorophyceae). J. Plant Physiol. 165, 1783–1797. https://doi.org/10.1016/j.jplph.2007.12.007

Libert, M., Schütz, M.K., Esnault, L., Féron, D., Bildstein, O., 2014. Impact of microbial activity on the radioactive waste disposal: Long term prediction of biocorrosion processes. Bioelectrochemistry 97, 162–168. https://doi.org/10.1016/j.bioelechem.2013.10.001

Lilover, M.J., Stips, A., 2008. The variability of parameters controlling the cyanobacteria bloom biomass in the Baltic Sea. J. Mar. Syst. 74, 108–115. https://doi.org/10.1016/j.jmarsys.2008.03.029

Liu, Y., Zhou, R., Zhao, J., 2000. Molecular cloning and sequencing of the sodB gene from a heterocystous cyanobacterium *Anabaena* PCC 7120. Biochim. Biophys. Acta 1491, 248–252.

Lloyd, J.R., Gadd, G.M., 2011. The Geomicrobiology of Radionuclides. Geomicrobiol. J. 28, 383–386. https://doi.org/10.1080/01490451.2010.547551

Lloyd, J.R., Renshaw, J.C., 2005. Bioremediation of radioactive waste: Radionuclide-microbe interactions in laboratory and field-scale studies. Curr. Opin. Biotechnol. 16, 254–260. https://doi.org/10.1016/j.copbio.2005.04.012

López-Archilla, A.I., Moreira, D., López-García, P., Guerrero, C., 2004. Phytoplankton diversity and cyanobacterial dominance in a hypereutrophic shallow lake with biologically produced alkaline pH. Extremophiles 8, 109–115. https://doi.org/10.1007/s00792-003-0369-9

Lovley, D.R., 1993. Dissimilatory Metal Reduction. Annu. Rev. Microbiol. 47, 263–290. https://doi.org/10.1146/annurev.mi.47.100193.001403

Lyautey, E., Lacoste, B., Ten-Hage, L., Rols, J.L., Garabetian, F., 2005. Analysis of bacterial diversity in river biofilms using 16 S rDNA PCR-DGGE: Methodological settings and fingerprints interpretation. Water Res. 39, 380–388. https://doi.org/10.1016/j.watres.2004.09.025

Macaskie, L.E., Lloyd, J.R., 2002. Microbial interactions with radioactive wastes and potential applications, in: Livens, F.R., Keith-Roach, M. (Eds.), Microbiology and Radioactivity. Elsevier Science Ltd, London.

Madigan, M.T., Brock, T.D., 2011. Brock biology of microorganims, 13th, Inte ed. Pearson Education, Harlow.

Masurat, P., Fru, E.C., Pedersen, K., 2005. Identification of *Meiothermus* as the dominant genus in a storage system for spent nuclear fuel. J. Appl. Microbiol. 98, 727–740. https://doi.org/10.1111/j.1365-2672.2004.02519.x

MeGraw, V.E., Brown, A.R., Boothman, C., Goodacre, R., Morris, K., Sigee, D., Anderson, L., Lloyd, J.R., 2018. A novel adaptation mechanism underpinning algal colonization of a nuclear fuel storage pond. MBio 9, 1–15. https://doi.org/10.1128/mBio.02395-17

Mitchell, A.C., Ferris, F.G., 2006. Effect of strontium contaminants upon the size and solubility of calcite crystals precipitated by the bacterial hydrolysis of urea. Environ. Sci. Technol. 40, 1008–1014. https://doi.org/10.1021/es050929p

Mitchell, A.C., Ferris, F.G., 2005. The coprecipitation of Sr into calcite precipitates induced by bacterial ureolysis in artificial groundwater: Temperature and kinetic dependence. Geochim. Cosmochim. Acta 69, 4199–4210. https://doi.org/10.1016/j.gca.2005.03.014

Mrázek, J., 2002. New technology may reveal mechanisms of radiation resistance in *Deinococcus radiodurans*. Proc. Natl. Acad. Sci. U. S. A. 99, 10943–10944. https://doi.org/10.1073/pnas.182429699

Nakajima, A., Tsuruta, T., 2004. Competitive biosorption of thorium and uranium by *Micrococcus luteus*. J. Radioanal. Nucl. Chem. 260, 13–18. https://doi.org/10.1023/B:JRNC.0000027055.16768.1e

NDA, 2016. Nuclear Decommissioning Authority: Business plan 2017 to 2020 [WWW Document]. Gov.uk. URL https://www.gov.uk/government/consultations/nuclear-decommissioning-authority-business-plan-2017-to-2020 (accessed 5.4.18).

O'Neil, J.M., Davis, T.W., Burford, M.A., Gobler, C.J., 2012. The rise of harmful cyanobacteria blooms: The potential roles of eutrophication and climate change. Harmful Algae 14, 313–334. https://doi.org/10.1016/j.hal.2011.10.027

Omelchenko, M. V, Wolf, Y.I., Gaidamakova, E.K., Matrosova, V.Y., Vasilenko, A., Zhai, M., Daly, M.J., Koonin, E. V, Makarova, K.S., 2005. Comparative genomics of *Thermus thermophilus* and *Deinococcus radiodurans*: divergent routes of adaptation to thermophily and radiation resistance. BMC Evol. Biol. 5, 57. https://doi.org/10.1186/1471-2148-5-57

Oren, A., Gunde-Cimerman, N., 2007. Mycosporines and mycosporine-like amino acids: UV protectants or multipurpose secondary metabolites? FEMS Microbiol. Lett. 269, 1–10. https://doi.org/10.1111/j.1574-6968.2007.00650.x

Paerl, H.W., Otten, T.G., 2013. Harmful cyanobacterial blooms: Causes, consequences, and controls. Microb. Ecol. 65, 995–1010. https://doi.org/10.1007/s00248-012-0159-y

Pikuta, E. V., Hoover, R.B., Tang, J., 2007. Microbial extremophiles at the limits of life. Crit. Rev. Microbiol. 33, 183–209. https://doi.org/10.1080/10408410701451948

Priya, B., Premanandh, J., Dhanalakshmi, R.T., Seethalakshmi, T., Uma, L.,

Prabaharan, D., Subramanian, G., 2007. Comparative analysis of cyanobacterial superoxide dismutases to discriminate canonical forms. BMC Genomics 8, 435. https://doi.org/10.1186/1471-2164-8-435

Priya, B., Sivaprasanth, R.K., Jensi, V.D., Uma, L., Subramanian, G., Prabaharan, D., 2010. Characterization of manganese superoxide dismutase from a marine cyanobacterium *Leptolyngbya valderiana* BDU20041 1–10.

Raateoja, M., Kuosa, H., Hällfors, S., 2011. Fate of excess phosphorus in the Baltic Sea: A real driving force for cyanobacterial blooms? J. Sea Res. 65, 315–321. https://doi.org/10.1016/j.seares.2011.01.004

Ramos, J.L., Gallegos, M.T., Marqués, S., Ramos-González, M.I., Espinosa-Urgel, M., Segura, A., 2001. Responses of gram-negative bacteria to certain environmental stressors. Curr. Opin. Microbiol. 4, 166–171. https://doi.org/10.1016/S1369-5274(00)00183-1

Rath, J., Adhikary, S.P., 2007. Response of the estuarine cyanobacterium <i>Lyngbya aestuarii</i< to UV-B radiation. J. Appl. Phycol. 19, 529–536. https://doi.org/10.1007/s10811-007-9166-7

Renshaw, J.C., Lloyd, J.R., Livens, F.R., 2007. Microbial interactions with actinides and long-lived fission products. Comptes Rendus Chim. 10, 1067–1077. https://doi.org/10.1016/j.crci.2007.02.013

Rivasseau, C., Farhi, E., Atteia, A., Couté, A., Gromova, M., de Gouvion Saint Cyr, D., Boisson, A.-M.M., Féret, A.-S., Compagnon, E., Bligny, R., 2013. An extremely radioresistant green eukaryote for radionuclide bio-decontamination in the nuclear industry. Energy Environ. Sci. 6, 1230–1239. https://doi.org/Doi 10.1039/C2ee23129h

Rivasseau, C., Farhi, E., Compagnon, E., de Gouvion Saint Cyr, D., van Lis, R., Falconet, D., Kuntz, M., Atteia, A., Couté, A., 2016. *Coccomyxa actinabiotis* sp. nov. (Trebouxiophyceae, Chlorophyta), a new green microalga living in the spent fuel cooling pool of a nuclear reactor. J. Phycol. 52, 689–703. https://doi.org/10.1111/jpy.12442

Rivasseau, C., Farhi, E., Gromova, M., Ollivier, J., Bligny, R., 2010. Resistance to irradiation of micro-algae growing in the storage pools of a nuclear reactor investigated by NMR and neutron spectroscopies. Spectroscopy 24, 381–385. https://doi.org/10.3233/SPE-2010-0459

Robinson, C.K., Webb, K., Kaur, A., Jaruga, P., Dizdaroglu, M., Baliga, N.S., Place, A., DiRuggiero, J., 2011. A major role for nonenzymatic antioxidant processes in the radioresistance of *Halobacterium salinarum*. J. Bacteriol. 193, 1653–1662. https://doi.org/10.1128/JB.01310-10

Rodriguez-Brito, B., Li, L., Wegley, L., Furlan, M., Angly, F., Breitbart, M., Buchanan, J., Desnues, C., Dinsdale, E., Edwards, R., Felts, B., Haynes, M., Liu, H., Lipson, D., Mahaffy, J., Martin-Cuadrado, A.B., Mira, A., Nulton, J., Pašić, L., Rayhawk, S., Rodriguez-Mueller, J., Rodriguez-Valera, F., Salamon, P., Srinagesh, S., Thingstad, T.F., Tran, T., Thurber, R.V., Willner, D., Youle, M., Rohwer, F., 2010. Viral and microbial community dynamics in four aquatic environments. ISME J. 4, 739–751. https://doi.org/10.1038/ismej.2010.1

Roelke, D., Buyukates, Y., 2001. The diversity of harmful algal bloom-triggering mechanisms and the complexity of bloom initiation. Hum. Ecol. Risk Assess. An Int. J. 7, 1347–1362. https://doi.org/10.1080/20018091095041

Sandesh Kamath, B., Vidhyavathi, R., Sarada, R., Ravishankar, G.A., 2008. Enhancement of carotenoids by mutation and stress induced carotenogenic genes in *Haematococcus pluvialis* mutants. Bioresour. Technol. 99, 8667–8673. https://doi.org/10.1016/j.biortech.2008.04.013

Santo Domingo, J.W., Berry, C.J., Summer, M., Fliermans, C.B., 1998. Microbiology of spent nuclear fuel storage basins. Curr. Microbiol. 37, 387–394. https://doi.org/10.1007/s002849900398

Sarró, M.I., García, A.M., Moreno, D.A., 2005. Biofilm formation in spent nuclear fuel pools and bioremediation of radioactive water. Int. Microbiol. 8, 223–230. https://doi.org/im2305032 [pii]

Sarró, M.I., García, A.M., Moreno, D.A., Montero, F., 2007. Development and characterization of biofilms on stainless steel and titanium in spent nuclear fuel pools. J. Ind. Microbiol. Biotechnol. 34, 433–441. https://doi.org/10.1007/s10295-007-0215-7

Sarró, M.I., Moreno, D.A., Chicote, E., Lorenzo, P.I., García, A.M., Montero, F., 2003. Biofouling on austenitic stainless steels in spent nuclear fuel pools. Mater. Corros. Und Korrosion 54, 535–540. https://doi.org/DOI 10.1002/maco.200390117

Schirrmeister, B.E., de Vos, J.M., Antonelli, A., Bagheri, H.C., 2013. Evolution of multicellularity coincided with increased diversification of cyanobacteria and the Great Oxidation Event. Proc. Natl. Acad. Sci. 110, 1791–1796. https://doi.org/10.1073/pnas.1209927110

Sellafield, 2014. Sellafield magazine [WWW Document]. URL https://www.gov.uk/government/publications/sellafield-magazine-issue-4 (accessed 5.30.18).

Sghaier, H., Satoh, K., Ohba, H., Narumi, I., 2010. Assessing the role of RecA protein in the radioresistant bacterium *Deinococcus geothermalis*. African J. Biochem. Res. 4, 111–118.

Sghaier, H., Thorvaldsen, S., Saied, N.M., 2013. There are more small amino acids and fewer aromatic rings in proteins of ionizing radiation-resistant bacteria. Ann. Microbiol. 63, 1483–1491. https://doi.org/10.1007/s13213-013-0612-2

Sharma, A., Gaidamakova, E.K., Matrosova, V.Y., Bennett, B., Daly, M.J., Hoffman, B.M., 2013. Responses of Mn2+ speciation in *Deinococcus radiodurans* and *Escherichia coli* to γ-radiation by advanced paramagnetic resonance methods. Proc. Natl. Acad. Sci. 110, 5945–5950. https://doi.org/10.1073/pnas.1303376110

Shirkey, B., McMaster, N.J., Smith, S.C., Wright, D.J., Rodriguez, H., Jaruga, P., Birincioglu, M., Helm, R.F., Potts, M., 2003. Genomic DNA of *Nostoc commune* (Cyanobacteria) becomes covalently modified during long-term (decades) desiccation but is protected from oxidative damage and degradation. Nucleic Acids Res. 31, 2995–3005. https://doi.org/10.1093/nar/gkg404

Shuman, S., Glickman, M.S., 2007. Bacterial DNA repair by non-homologous end

joining. Nat. Rev. Microbiol. 5, 852–861. https://doi.org/10.1038/nrmicro1768

Simonoff, M., Sergeant, C., Poulain, S., Pravikoff, M.S., 2007. Microorganisms and migration of radionuclides in environment. Comptes Rendus Chim. 10, 1092–1107. https://doi.org/10.1016/j.crci.2007.02.010

Singh, H., Anurag, K., Apte, S.K., 2013. High radiation and desiccation tolerance of nitrogen-fixing cultures of the cyanobacterium *Anabaena* sp. strain PCC 7120 emanates from genome/proteome repair capabilities. Photosynth. Res. 118, 71–81. https://doi.org/10.1007/s11120-013-9936-9

Singh, H., Fernandes, T., Apte, S.K., 2010. Unusual radioresistance of nitrogen-fixing cultures of *Anabaena* strains. J. Biosci. 35, 427–434. https://doi.org/10.1007/s12038-010-0048-9

Singh, S.C., Sinha, R.P., Hader, D.P., 2002. Role of lipids and fatty acids in stress tolerance in cyanobacteria. Acta Protozool. 41, 297–308. https://doi.org/citeulike-article-id:3906403

Stal, L.J., Albertano, P., Bergman, B., Von Bröckel, K., Gallon, J.R., Hayes, P.K., Sivonen, K., Walsby, A.E., 2003. BASIC: Baltic Sea cyanobacteria. An investigation of the structure and dynamics of water blooms of cyanobacteria in the Baltic Sea - Responses to a changing environment. Cont. Shelf Res. 23, 1695–1714. https://doi.org/10.1016/j.csr.2003.06.001

Stowe-Evans, E.L., Kehoe, D.M., 2004. Signal transduction during light-quality acclimation in cyanobacteria: A model system for understanding phytochrome-response pathways in prokaryotes. Photochem. Photobiol. Sci. 3, 495–502. https://doi.org/10.1039/b316952a

Summerfield, T.C., Sherman, L.A., 2008. Global transcriptional response of the alkali-tolerant cyanobacterium *Synechocystis* sp. strain PCC 6803 to a pH 10 environment. Appl. Environ. Microbiol. 74, 5276–5284. https://doi.org/10.1128/AEM.00883-08

The nuclear fuel cycle [WWW Document], 2018. . World Nucl. Assoc. URL http://www.world-nuclear.org/information-library/nuclear-fuel-cycle/introduction/nuclear-fuel-cycle-overview.aspx (accessed 2.6.18).

Tian, B., Sun, Z., Shen, S., Wang, H., Jiao, J., Wang, L., Hu, Y., Hua, Y., 2009. Effects of carotenoids from *Deinococcus radiodurans* on protein oxidation. Lett. Appl. Microbiol. 49, 689–694. https://doi.org/10.1111/j.1472-765X.2009.02727.x

Tišáková, L., Pipíška, M., Godány, A., Horník, M., Vidová, B., Augustín, J., 2013. Bioaccumulation of 137Cs and 60Co by bacteria isolated from spent nuclear fuel pools. J. Radioanal. Nucl. Chem. 295, 737–748. https://doi.org/10.1007/s10967-012-1932-6

Valentine, N.B., Bolton, H., Kingsley, M.T., Drake, G.R., Balkwill, D.L., Plymale, A.E., 1996. Biosorption of cadmium, cobalt, nickel, and strontium by a *Bacillus simplex* strain isolated from the vadose zone. J. Ind. Microbiol. 16, 189–196. https://doi.org/10.1007/BF01570003

van Veen, H.W., Abee, T., Kortstee, G.J.J., Konings, W.N., Zehnder, A.J.B., 1994. Translocation of metal phosphate via the phosphate inorganic transport system of

Escherichia coli. Biochemistry 33, 1766–1770. https://doi.org/10.1021/bi00173a020

Vieira, H.G.S., Grynberg, P., Bitar, M., Da Fonseca Pires, S., Hilário, H.O., Macedo, A.M., Machado, C.R., De Andrade, H.M., Franco, G.R., 2014. Proteomic analysis of *Trypanosoma cruzi* response to ionizing radiation stress. PLoS One 9. https://doi.org/10.1371/journal.pone.0097526

Volesky, B., May-Phillips, H.A., 1995. Biosorption of heavy metals by *Saccharomyces cerevisiae*. Appl. Microbiol. Biotechnol. 42, 797–806. https://doi.org/10.1007/s002530050333

Wada, N., Sakamoto, T., Matsugo, S., 2013. Multiple roles of photosynthetic and sunscreen pigments in cyanobacteria focusing on the oxidative stress. Metabolites 3, 463–483. https://doi.org/10.3390/metabo3020463

Wang, B., Zarka, A., Trebst, A., Boussiba, S., 2003. Astaxanthin accumulation in *Haematococcus pluvialis* (Chlorophyceae) as an active photoprotective process under high irradiance. J. Phycol. 39, 1116–1124. https://doi.org/10.1111/j.0022-3646.2003.03-043.x

Wang, S.-B., Chen, F., Sommerfeld, M., Hu, Q., 2004. Proteomic analysis of molecular response to oxidative stress by the green alga *Haematococcus pluvialis* (Chlorophyceae). Planta 220, 17–29. https://doi.org/10.1007/s00425-004-1323-5

Webb, K.M., Diruggiero, J., 2012. Role of Mn2+ and compatible solutes in the radiation resistance of thermophilic bacteria and archaea. Archaea 2012. https://doi.org/10.1155/2012/845756

Webb, K.M., Yu, J., Robinson, C.K., Noboru, T., Lee, Y.C., DiRuggiero, J., 2013. Effects of intracellular Mn on the radiation resistance of the halophilic archaeon *Halobacterium salinarum*. Extremophiles 17, 485–497. https://doi.org/10.1007/s00792-013-0533-9

White, C., Wilkinson, S.C., Gadd, G.M., 1995. The role of microorganisms in biosorption of toxic metals and radionuclides. Int. Biodeterior. Biodegrad. 35, 17–40. https://doi.org/10.1016/0964-8305(95)00036-5

Wigley, D.B., 2013. Bacterial DNA repair: Recent insights into the mechanism of RecBCD, AddAB and AdnAB. Nat. Rev. Microbiol. 11, 9–13. https://doi.org/10.1038/nrmicro2917

Wilson, P.D., 1996. The nuclear fuel cycle from ore to waste. Oxford University Press, Oxford.

Yan, G., Viraraghavan, T., 2003. Heavy-metal removal from aqueous solution by fungus *Mucor rouxii*. Water Res. 37, 4486–4496. https://doi.org/10.1016/S0043-1354(03)00409-3

Yu, J., Tang, D., Wang, S., Lian, J., Wang, Y., 2007. Changes of water temperature and harmful algal bloom in the Daya Bay in the northern south China sea. Mar. Sci. Bull. 9, 25–33.

Zelko, I.N., Mariani, T.J., Folz, R.J., 2002. Superoxide dismutase multigene family: A comparison of the CuZn-SOD (SOD1), Mn-SOD (SOD2), and EC-SOD (SOD3)

gene structures, evolution, and expression. Free Radic. Biol. Med. 33, 337–349. https://doi.org/10.1016/S0891-5849(02)00905-X

Chapter 3

Methodology

3 Methodology

3.1 Pond water sample collection, procedures and safety

Samples of pond water were collected from two facilities on the Sellafield site, namely the FGMSP and the auxiliary pond, by Sellafield Ltd. staff. The samples were collected from a depth of approximately 1 m, using a hose dispensed into the pond. Water was drawn through the hose into a collection bottle, prior to being sent to the National Nuclear Laboratory's (NNL) Central Laboratory. At the Central Laboratory radioactivity monitoring was conducted and the samples were then stored at 4 ˚C prior to further handling. The samples were monitored before DNA extractions were carried out (see 3.2), the resulting DNA samples were stored at 4˚C. Strict radiological monitoring procedures are in place to facilitate the movement of the samples from this nuclear licensed site to the University of Manchester (UoM). Upon arrival at the UoM, samples were monitored again before being stored at -20 ˚C, to await PCR checks, qPCR and sequencing.

Additional pond data was collected by Sellafield Ltd. staff as part of routine operations on site, for details (see Chapter 4).

3.2 Molecular biology- DNA extraction, amplification, quantitative amplification and visualisation

3.2.1 DNA extraction

All DNA extractions were carried out using the MoBio PowerWater DNA isolation kit (MoBio Laboratories, Inc., Carlsbad, CA, USA). The FGMSP and auxiliary pond samples were not a consistent volume, records were kept of the volume of water used for the extractions at Central Laboratory. DNA extractions carried out at the Central Laboratory were performed in a UV hood, which had the UV lamp on for 15 min before samples were handled. Where *P. catenata* cultures were sampled for DNA extraction a 1 mL volume was used, the extractions were carried out in the designated "clean" molecular laboratory at the University of Manchester.

All samples were passed through a sterile 0.2 μm filter using a vacuum filtration technique. The DNA extraction protocol set out in the in-kit manual was followed for all the samples (Figure 3-1). The first step after the filtrations chemically lysed the cells, the filter papers were placed into bead beading tubes and 1 mL of the PW1 reagent (heated to 55 °C to dissolve any precipitates) was added before the samples were vortexed at maximum speed for 5 min (Qiagen, 2018). The samples were then centrifuged for 2 min at 4000 *g*. A volume of 650 μL was then transferred to a fresh collection tube and centrifuged at 14,000 *g* for 1 min. The supernatant was transferred to a fresh Eppendorf collection tube where 200 μL of PW2 reagent was added, the samples were vortexed to mix and then incubated at 4 °C for 5 min. PW2 reagent removes unwanted inorganic and organic materials from the samples, excluding DNA, e.g. cell debris and proteins which would otherwise inhibit further analysis of the DNA (Qiagen, 2018). Following the incubation at 4 °C, the samples were centrifuged at 14,000 *g* for 1 min, and the supernatant was transferred to a fresh collection tube. A high concentration salt solution, PW3, was added (650 μL) to the samples to allow the binding of DNA to the spin filters, whilst any remaining organic and inorganic material will pass through (Qiagen, 2018). Aliquots of 650 μL of the samples were loaded onto the spin filters and centrifuged at 14,000 *g* for 1 min, this process was repeated until all of the sample is used, the flow through was discarded. The spin filter was placed into a fresh collection tube, and 650 μL of PW4 was added, this is an alcohol based wash that is used to wash the samples further (Qiagen, 2018). The samples were centrifuged at 14,000 *g* for 1 min, the flow through was discarded, before 650 μL of PW5 was added, which is a wash solution that removes PW4 from the samples. The samples were then centrifuged twice at 14,000 *g* the first time for 2 min and the second for 1 min, discarding the supernatant each time, this ensures that all of the wash solution is removed prior to eluting the DNA (Qiagen, 2018). The final step removes the DNA from the silica spin filter membrane, using 100 μL of PW6 (a sterile elution buffer). Once PW6 was added the samples are centrifuged for a final time (in a fresh collection tube) at 14,000 *g* for 1 min. The samples could be analysed immediately or stored at -20 °C to await future analysis (Qiagen, 2018).

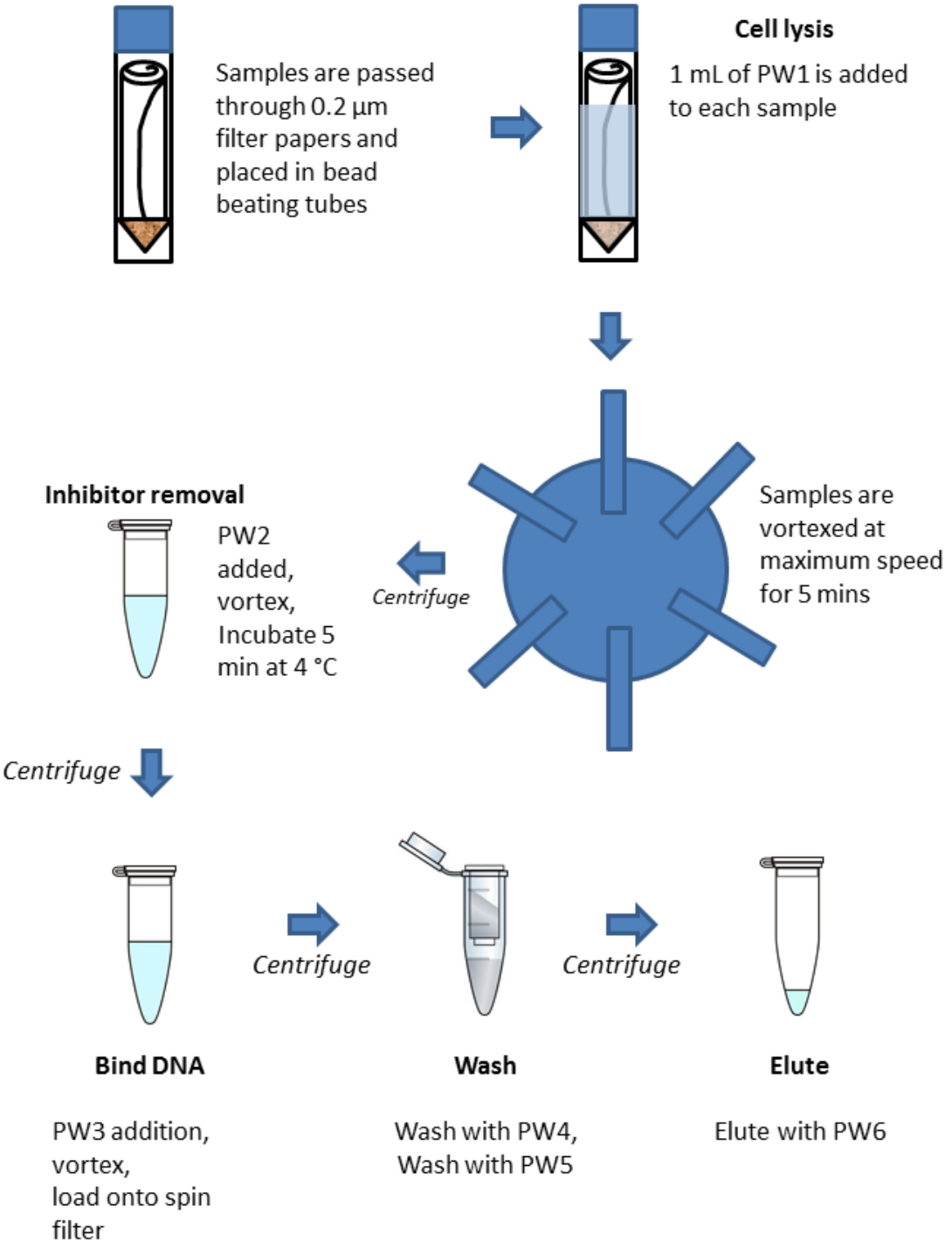

Figure 3-1: Schematic of the protocol for DNA extraction using the MoBio PowerWater DNA isolation kit (MoBio Laboratories, Inc., Carlsbad, CA, USA) [adapted from Qiagen, 2018].

3.2.2 Polymerase Chain Reaction (PCR)

Polymerase chain reaction (PCR) is a technique that is used to amplify regions of DNA to concentrations that can then be used for other techniques and processes (Saiki *et al*., 1988). The requirements for PCR include; template double stranded DNA, forward and reverse primers; a thermo-stable polymerase enzyme (Taq), and deoxynucleotide triphosphates (dNTPS). The primers ideally are 18-24 bases in length and must bind to sequences upstream and downstream to the region of interest (Devereux *et al*., 2004). The enzyme used in a PCR was isolated from *Thermus aquaticus*, which is a thermophilic bacterium and can therefore withstand the elevated temperatures used without being denatured (Chien *et al*., 1976). The reaction takes place in the presence of a buffer and a known concentration of $MgCl_2$ solution, this alters the specificity of the primers binding.

The first stage of the PCR reaction involves heating the DNA at 94-95 °C to separate the two strands of the double helix. Following from this 30-39 cycles of different temperatures are used to copy the DNA, resulting in hundreds of billions of copies of the target DNA (Saiki *et al*., 1988). The cycles include strand separation or denaturation at 94-95 °C, followed by a reduction in temperature (usually between 50-60 °C) to allow the primers to anneal to the template DNA. The temperature is then raised to ~72 °C to allow the polymerase to copy the DNA. There is a final extension step at ~72 °C once the cycles have been completed. The stages of PCR are shown in Figure 3-2. Control samples are run alongside the samples of interest, these include a negative control (PCR grade water), to check for contamination, which should show no signs of amplification. A positive control is also included, which is a sample of DNA that is known to contain the target DNA sequence that is being amplified in the reaction. The controls allow for contamination of the reagents to be detected (negative control) and to check that the PCR has run correctly; that the reagents were correctly added; and that the correct primers and cycling conditions were used.

PCR runs were carried out on the DNA extracted from the pond samples and the *P. catenata* cultures to screen for the presence of prokaryotes, eukaryotes and archaea. Ribsomal RNA (rRNA) genes are present in all living organisms, since they encode ribosomes that are involved in protein synthesis, the genes have been conserved. Prokaryotes and archaea ribosomes are encoded by the 16S and 23S rRNA genes, these code for the small and large subunits of the ribosomes, respectively. In eukaryotes the

genes are the 18S and the 28S rRNA molecules, respectively. The 16S and 18S rRNA genes have 9 hypervariable regions that are different in different species, therefore making these genes ideal candidates for phylogenetic analysis (Case *et al*., 2007; Ishaq and Wright, 2014; Weisburg *et al*., 1991). The presence of prokaryotes, archaea and eukaryotes can be identified by the amplification and visualisation of the 16S and 18S rRNA genes, and the identification of the organisms can be determined by sequencing the genes and the subsequent analysis.

The preparation of the PCR mixes took place in a UV-hood. Empty 200 µL thin walled PCR tubes, 1.5 mL Eppendorf tubes, reagents for the PCR (except the polymerase and DNA), pipettes and tips were subjected to UV light for a 5-10 min. A master mix was prepared for each primer set, of which 48 µL was then transferred to each 200 µL PCR tube. The reactions were made up to 50 µL with the addition of 2 µL of purified DNA. A negative control for all PCR reactions was ran with 2 µL of sterile Roche PCR Grade water (Sigma-Aldrich, Dorset, UK) instead of DNA to check for contamination. Where possible a suitable positive control was used to check the PCR was working correctly. Cycling conditions were optimised for each primer set. The tubes were then transferred to a thermal cycling machine where the DNA underwent cycles of denaturation, annealing, and extension. The product of the reaction were stored until required at -20 °C or visualised by running the samples on a 1 % agarose gel in 1x TAE (Tris- acetic acid- EDTA) buffer. The samples were stained using Syber safe DNA stain (Invitrogen, Carlsbad, CA, USA), this binds to the DNA and fluoresces in UV light. DNA was viewed using a BioRad Geldoc 2000 system (BioRad, Hemel Hempstead, Herts, UK) under short-wave UV light. The reaction mixtures used for PCR reactions were as follows (quantities per reaction- scaled up for the number of samples):

TaKaRa Ex Taq polymerase (Clonetech, UK): 36.7 µL sterile purified water (Roche PCR Grade); 5 µL 10x Ex Buffer; 4 µL dNTP mixture (2.5 mM Each nucleotide); 1 µL 25 µM forward primer; 1 µL 25 µM reverse primer; and 0.3 µL Ex Takara Taq.

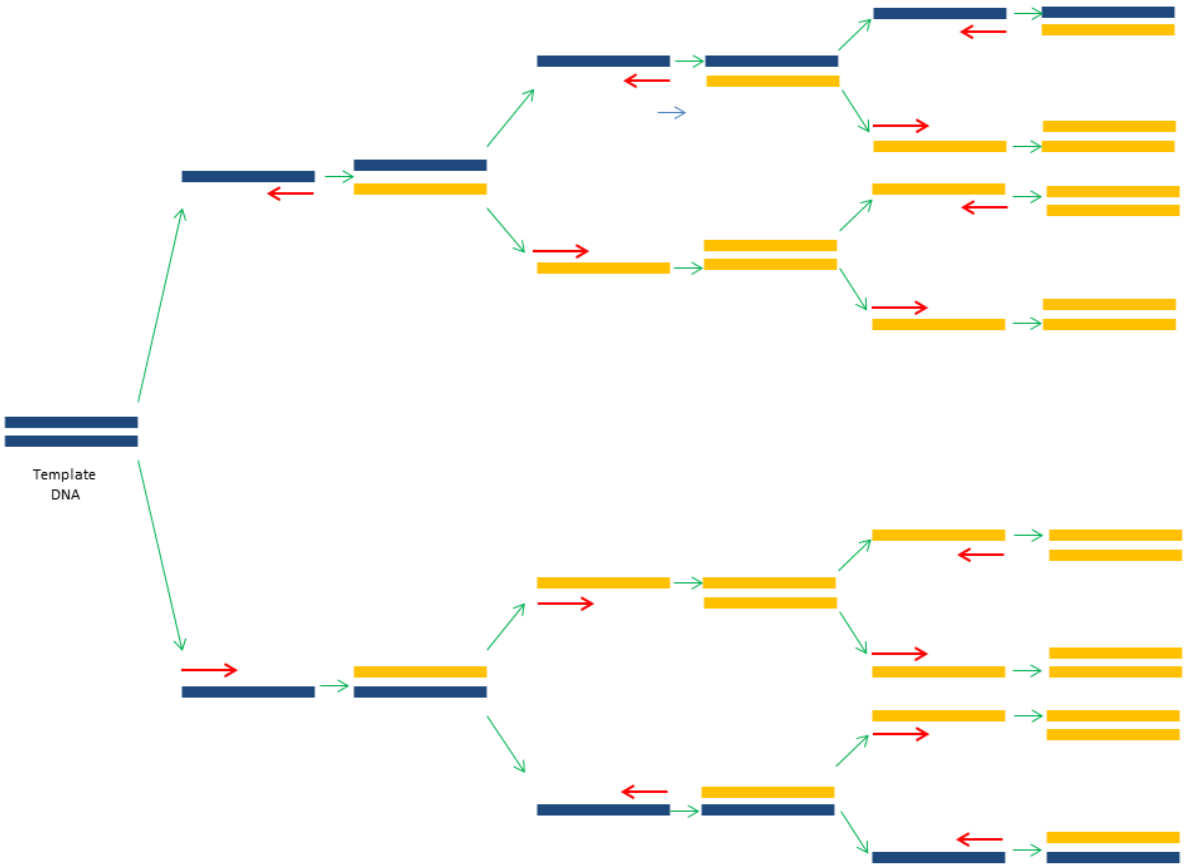

Figure 3-2: The stages of a PCR, where a target sequence on DNA undergoes multiple rounds of thermal cycling. The initial step is denaturation, where the double stranded DNA is separated this usually takes place at ~95 °C. The temperature is reduced to allow the primers to bind to the single strands of DNA (50-60 °C). The polymerase enzyme then adds individual nucleotides that are complementary to the template DNA, working from the 5' end to the 3' end. This process is repeated for 30+ cycles (adapted from Purves *et al.*, 2004).

3.2.3 Quantitative polymerase chain reaction (qPCR)

Quantitative polymerase chain reaction (qPCR) is a technique which is based on the standard PCR (described above) and run on a real-time PCR instrument. During a qPCR run the amplification of the target DNA (e.g. a region of the 16S rRNA gene) can be quantified in real time. In order to track the amplification of the template DNA, a fluorescent dye is added to the reaction (e.g. SYBR Green, Invitrogen, Carlsbad, CA, USA), which binds to the major groove of double stranded DNA (dsDNA) and emits a fluorescent signal. When the dye is free in solution, for example when the dsDNA is denatured, the fluorescent signal is very weak. Each PCR cycle results in double the number of copies of DNA, as a result more of the fluorescent dye can bind with the

dsDNA and therefore a stronger fluorescent signal is emitted. Each qPCR run includes a set of standards, run in triplicate, that contain known concentrations of DNA extracted from a pure culture. The fluorescent signals recorded for the standards are used to generate a standard curve, which are used to quantify the concentration of the DNA in the samples being tested. The standard curve is used to set the cycle threshold. In order to quantify the concentration of DNA in a given sample, the level of fluorescence detected over the course of the qPCR run must reach a cycle threshold level. Where higher initial concentrations of DNA are present in a sample, the cycle threshold will be reached with fewer PCR cycles. The data collected from a qPCR run can then be used to calculate an estimate of the copy number of the target gene amplified in the sample (Equation 3-1).

$$\text{Ctarget} = n\text{target x } \frac{cDNA\ x\ N_a}{l\text{DNA x Mbp}}$$

Equation 3-1: Calculation of target concentration where: Ctarget is copies μL^{-1}; *n*target is the number of targets per DNA fragment; cDNA is the concentration of DNA (ng μL^{-1}); N_a is Avagadro's constant (6.022 X 10^{23} bp mol^{-1}); *l*DNA is the length of the DNA fragment (bp); Mbp is the average weight of a double stranded base pair (660 g mol^{-1} = 6.6 x 10^{11} ng mol^{-1}) (Brankatschk *et al*., 2012).

3.2.4 Agarose gel electrophoresis

DNA or RNA can be separated and visualised using agarose gel electrophoresis. A polymeric matrix is formed by dissolving agarose (0.8-2.0 % wt/vol) in an electrolyte-containing solution (usually tris-acetic acid-EDTA) by boiling, the matrix allows DNA (or RNA) to be separated according to the fragment length. A loading dye is mixed with the DNA prior to being loaded in the wells of the gel, this allows the DNA to sink to the bottom of the well. Once loaded in the agarose gel, which is covered in the electrolyte buffer, an electric current is applied, which carried the DNA fragments towards the cathode (Figure 3-3), due to the negative charge of the phosphate molecules in the backbone of DNA. The smaller fragments of DNA travel further through the matrix during the run, therefore allowing for size separation. A DNA ladder is added to a run, this contains known lengths of DNA fragments, to allow the size of samples to be qualitatively determined. The gels in these studies were stained with SyberSafe (Invitrogen, Carlsbad, CA, USA), which binds to the DNA molecule and allows the DNA to be visualised under UV light.

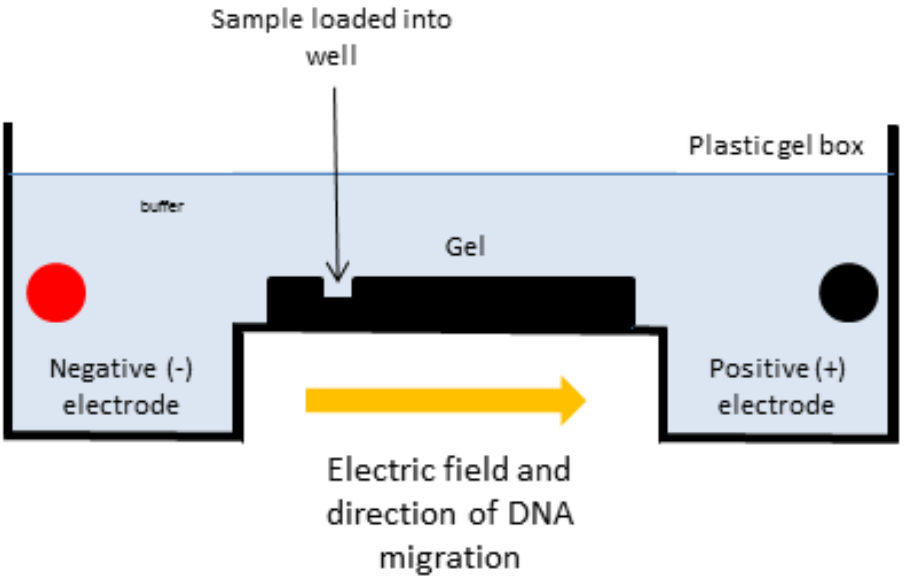

Figure 3-3: A schematic of the set-up of an agarose gel electrophoresis run, side view (adapted from Biotech, 2018).

3.3 Pyrosequencing

Pyrosequencing is a method of sequencing DNA or RNA (Figure 3-4) that does not require the generation of clone libraries (Hamady *et al*., 2008). It is a flexible process that can generate several hundred thousand reads (>100,000 sequences per run) and relatively long sequence lengths of ~900 bp. During pyrosequencing nucleotides are detected and identified as they are added to the growing DNA strand (real time detection), this is achieved through chemiluminescence detected by a charged coupled device (CCD) camera (Ronaghi *et al*., 1996). The requirements for pyrosequencing include: single stranded DNA (ssDNA); primers, DNA polymerase; primers; and dNTPs. The sequencing method also needs the following enzymes ATP sulfurylase; luciferase and apyrase, in addition luciferin and adenosine 5' phosphosulphate substrates are required. During a pyrosequencing run, dNTPs are added one at a time in a sequential order to the samples, where the dNTP is complementary to the template DNA. The polymerase enzyme forms a phosphodiester bond between the nucleotide and the last nucleotide of growing DNA chain, resulting in the release of pyrophosphate (PPi). The PPi reacts with adenosine 5' phosphosulphate (APS) in the presence of the APT sulfurylase enzyme, resulting in the production of SO_4^{2-} and adenosine triphosphate (ATP). Light is generated by the luciferase enzyme, which utilises the ATP

as the energy source to oxidise luciferin. Free nucleotides and any remaining ATP are degraded at the end of each reaction by the addition of Apyrase. The process is repeated with the next nucleotide in the sequence, resulting in the full sequence of the DNA being determined (Ronaghi, 2001; Ronaghi *et al*., 1996). Longer length sequences generated by this process are advantageous for downstream analysis, however due to its extended use, the DNA polymerase might introduce errors whilst copying the DNA template (Ronaghi and Nyrén, 1998).

The work carried out in Chapter 4 was carried out using 454-pyrosequencing, this is an array based technology that allows multiple samples to be run in parallel. The sequences produced during 454-pyrosequencing can be assigned to individual samples by adding a specific 454 Life Systems adapter to the template DNA (Hamady *et al*., 2008). Streptavidin-coated beads covered in complementary sequences for the adapters (one adapter sequence per bead). The template DNA binds to a bead with the corresponding adapter, resulting in each bead being specific for a single sample. Microreactors are created for each bead by adding a droplet of oil and water over the bead, and an emulsion PCR can then be carried out resulting in millions of copies of each DNA fragment on a single bead. A picotitre plate is used for the pyrosequencing run, the plate contains in excess of 1 million wells that are designed to allow only a single bead per well. At this stage the substrates and enzymes mentioned earlier are added and the plate can then be placed into the sequencer and sequencing can begin (Bassil, 2015).

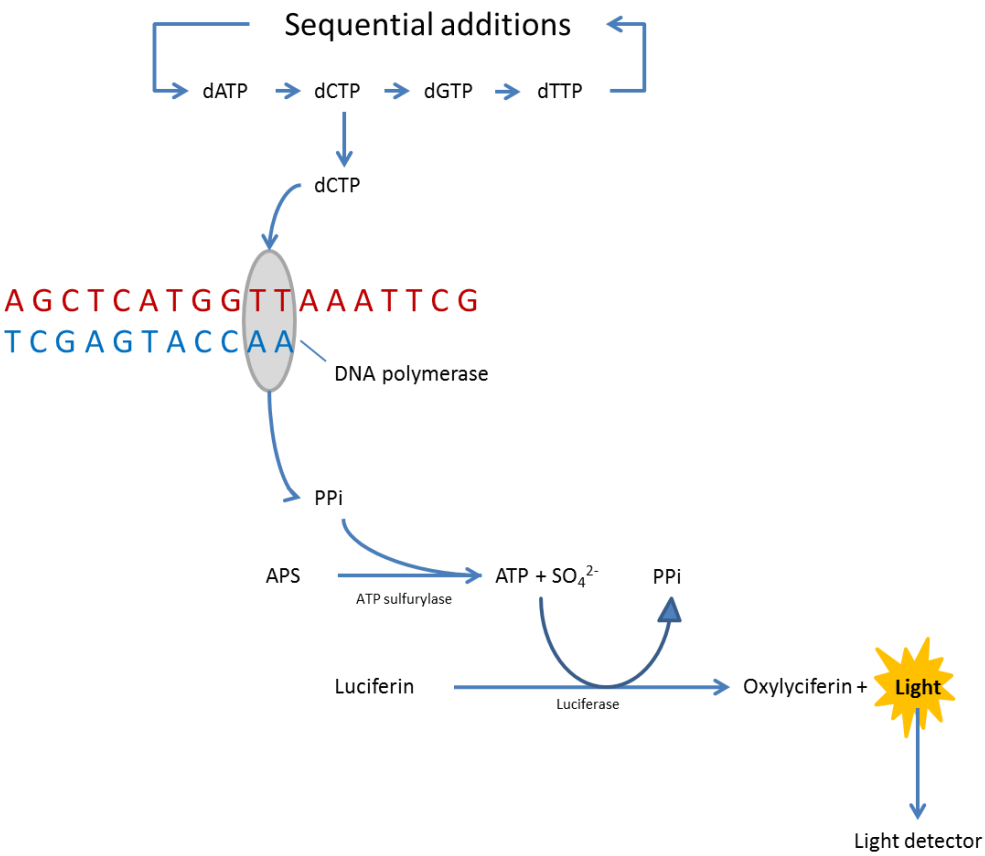

Figure 3-4: Schematic of the chemical reactions that occur during a pyrosequencing run (adapted from Owen-Hughes and Engeholm, 2007; Sarwat & Yamdagni, 2016; Fakrauddin *et al*., 2012). dNTPs are added sequentially, if they are complementary to the template DNA sequence they are incorporated into the growing nucleic acid chain by DNA polymerase. A pyrophosphate (PPi) molecule is releases, which reacts with adenosine 5' phosphosulphate (APS) in the presence of the ATP sulfurylase enzyme which results in the production of ATP and SO_4^{2-}. The ATP is used as the energy source for the enzymatic conversion by luciferase of luciferin to oxylyciferin. In addition visible light is produced which is then detected.

The pyrosequencing PCR was carried out using the FastStart High Fidelity PCR system (Roche, Basel, Switzerland). The tagged fussion universal primers 27F (Lane, 1991) and 907R (Muyzer *et al*., 1995) were used to amplify the V1-V5 hypervariable regions of the 16S rRNA, the primers were synthesized by IDTdna (Integrated DNA Technologies, BVBA, Leuven, Belgium). The fusion forward primer

(5'- CCA TCT CAT CCC TGC GTG TCT CCG ACT CAG NNNNNNNNNN AG AGT TTG ATC MTG GCT CAG-3') contained the 454 Life Sciences "Lib-L Primer A", a 4 base "key" sequence (TCAG), a unique ten-base barcode "MID" sequence for each sample, and bacterial primer 27F. The reverse fusion primer (5'- CCT ATC CCC

TGT GTG CCT TGG CAG TCT CAG CCG TCA ATT CMT TTR AGT TT -3') contained the 454 Life Sciences "Lib-L Primer B", a 4 base "key" sequence (TCAG), and bacterial primer 907R (MeGraw *et al*., 2018). The reactions were set up using the following reagents and quantities per reaction: 40 µL Sterile Purified Water (Roche PCR Grade); 5 µL Reaction Buffer; 1 µL Nucleotide Mix; 0.8 µL (25 µM) 907R Primer; 0.4 µL High Fidelity Enzyme Blend. The reactions are made up to 50 µL with the addition of 2 µL of DNA template and 0.8 µL of different MID labelled forward primer (25 µM). The amplification of each sample was carried out in triplicate to ensure sufficient DNA for sequencing. The thermal cycling conditions for the reaction were as follows: initial denaturation step at 94 ˚C for 4 min; 35-39 cycles of: 94˚C for 30 s; 58˚C for 30 s; 72˚C for 1 min; followed by a final extension step at 72˚C for 5 min.

The entire product of each PCR was subsequently run on a 2 % Tris-Acetate-EDTA/agarose gel and bands at 900 bp were exercised from the gel. The QIAquick Gel Extraction Kit (Qiagen, Limburg, The Netherlands) was used to extract the DNA from the gel and clean it, following the manufacturers protocol. The concentration of the DNA was measured using an Agilent 2100 Bioanalyzer (Agilent Technologies, Inc., Santa Clara, CA, USA), which was then diluted to achieve a final concentration of 10 ng μL^{-1}. Prior to the emulsion PCR, the DNA samples were stored at 4 °C, the University of Manchester's 454 GS Junior pyrosequencing system (Roche) was used to carry out the sequencing (Bassil, 2015).

The Quantitative Insights Into Microbial Ecology (QIIME) 1.8.0. release pipeline (Caporaso *et al*., 2010) was used to analyse the raw data from the pyrosequencing runs. The barcode sequences were used to group the samples, the sequences were size selected and the reverse primer was removed (Bassil, 2015). The Usearch 6.1 programme (Edgar, 2010) was used to detect chimeras, which were then removed, and to pick operational taxonomic units (OTUs) that were compared to the greengenes OTU reference (at 97% sequence similarity). Taxonomic classification of the reads was carried out in Qiime, using the Ribosomal Database Project (RDP) at 90 % confidence threshold (Cole *et al*., 2009), while the closest GenBank match for the OTUs that contained the highest number of reads (the representative sequence for each OTU was used) was identified by Blastn nucleotide search. In addition, QIIME was used to show the rarefaction curves.

3.4 MiSeq, Illumina next generation sequencing

The Illumina MiSeq is a sequencing platform, which like pyrosequencing is based on sequencing by synthesis, multiple samples can be analysed in parallel generating millions of reads per sample. During MiSeq sequencing, the addition of nucleotides to the query DNA template is detected through chemiluminescence, with each nucleotide emitting a characteristic wavelength. In contrast to pyrosequencing (see Section 3.3), sequencing is carried out on a flow cell where clusters of identical DNA templates are created, which ensures the level of light emitted as a nucleotide is incorporated into the growing nucleotide chain can be detected.

3.4.1 Sample preparation

The first step to prepare a set of samples is to amplify the DNA in a PCR run with appropriately tagged primers designed for the MiSeq platform (for example the V4 region of the 16S gene). The final DNA fragments generate contain; an adapter region that is complementary to oligonucleotides that are tethered to the flow cell used for sequencing; an index region which allows the reads generated during the sequencing to be assigned to a sample; and regions for the binding of primers for sequencing.

Following the PCR the concentration of DNA is quantified using a Qubit 3.0 Fluorometer (Thermo Fisher Scientific, Waltham, MA, USA). Briefly a fluorescent dye that binds nucleic acids is added to the samples. UV excitation results in the fluorescence of the dye that is intercalated between the bases in DNA, the intensity of fluorescence is directly proportional to the concentration of the DNA in the sample. Known concentrations are used to calibrate the Qubit 3.0 fluorometer (Thermo Fisher Scientific, Waltham, MA, USA) prior to running the samples. For Qubit analysis 2 μL of DNA is added to a solution containing 198 μL of working stock solution (10x reactions is made with 1990 μL buffer and 10 μL of fluorescent dye). For the standards 190 μL of the working stock solution is added to 10 μL of the standards. All samples are mixed thoroughly by vortexing and incubated at room temperature for 2 min, prior to analysis.

The samples are then purified and normalised, this was carried out using the SequalPrep^{TM} normalisation kit (Thermo Fisher Scientific, Waltham, MA, USA) in this

thesis, following the in kit manual. The kit works by adjusting the pH of the samples, which causes nucleic acid binding. Contaminants and proteins that are not bound can then be washed away. A further quantification of the DNA concentrations was then carried out on the Qubit 3.0 Fluorometer (Thermo Fisher Scientific, Waltham, MA, USA) as previously described. The samples were then assessed using a 2100 Bioanalyzer (Agilent, Santa Clara, CA, USA) to check the sequence lengths are the correct size. The bioanlyzer works on the combined principles of fluorometry (excitation and emission) and gel-electrophoresis (charge to mass ratios). The samples are separated by electrophoresis and fluorescent signals are then used to detect the components.

The Illumina MiSeq library preparation protocol was followed to create the final DNA library for MiSeq sequencing (Illumina, San Diego, CA, USA). The steps involved include adding equimolar concentrations of the samples to create a pooled library (4 nM), which is then denatured to form single stranded DNA and diluted to a 4 pM library. In addition a PhiX control is prepared, denatured and diluted to the same concentration as the pooled library, to which it is added to give a final concentration of 10 % (Kozich *et al*., 2013). The 600 µL of the pooled library is then added the MiSeq reagent cartridge, that has been fully defrosted and the reagents mixed.

3.4.2 Cluster generation

Sequencing on the MiSeq platform is carried out on a flow cell, which is a glass slide with lanes on it; the lanes are channels where the clusters that will be sequenced are formed. The surface of the channels is covered with two different oligonucleotide sequences, complementary to the adapters on the DNA fragments (Figure 3-5). The ssDNA fragments are introduced to and they hybridize with the oligonucleotides on the channel surface (Illumina, 2012). The template DNA is copied using a DNA polymerase, once the copy is completed the strands are separated through denaturation to separate the bases of the double stranded molecule and the template DNA is washed off. This ssDNA fragment then folds over and hybridizes to the second oligonucleotide sequence forming a bridge. DNA polymerase creates a copy of the DNA fragment in a process called bridge amplification. Once the complementary strand has been made, the double stranded bridge is denatured to linearize the DNA forming both forward and

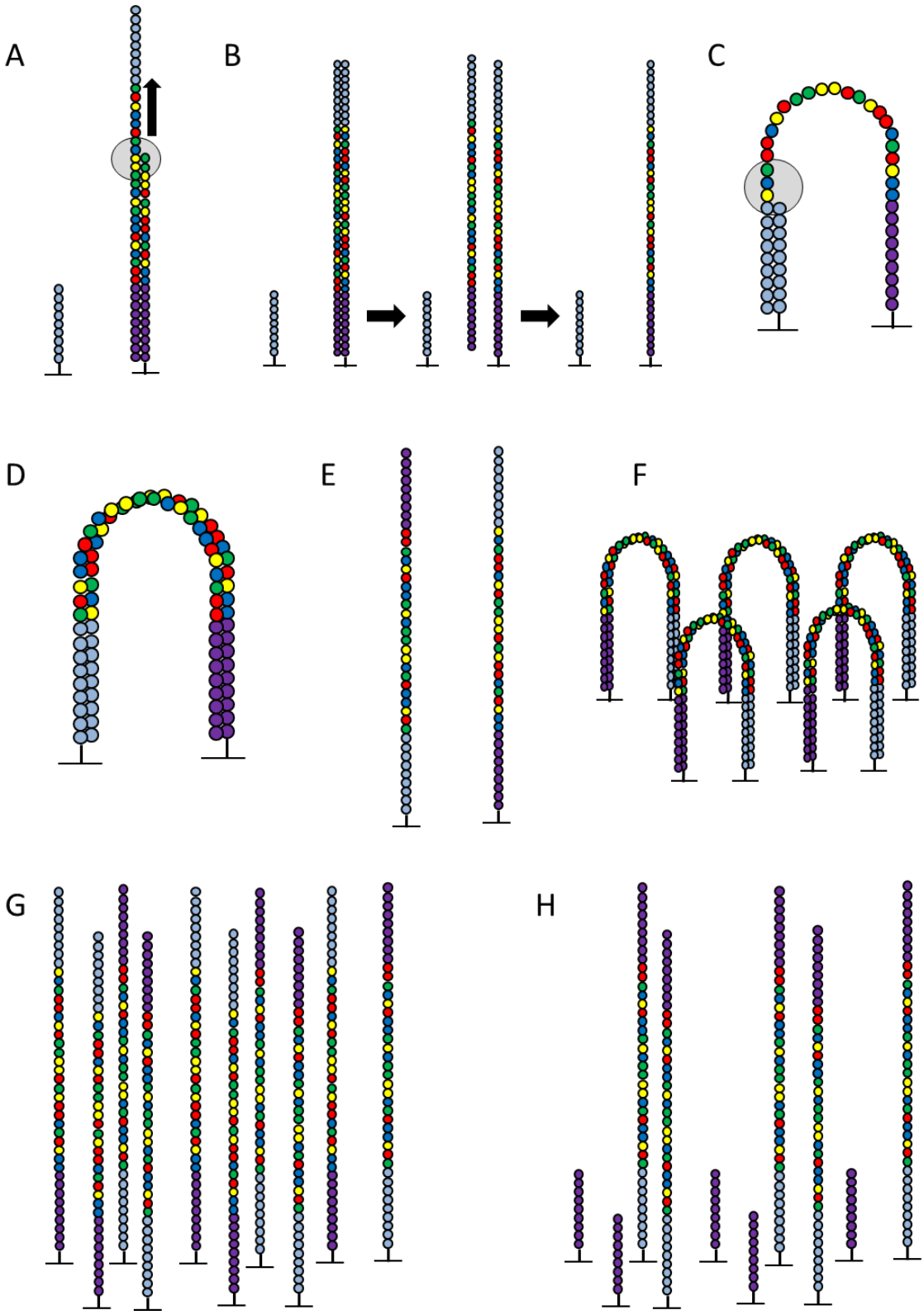

Figure 3-5: Cluster generation: a) MiSeq flow cell channels contains a lawn of two different types of oligonucleotide (light blue and purple circles) attached to the surface. The single stranded fragment DNA hybridizes with one of the oligonucleotides on the flow cell. DNA polymerase then creates a complementary strand of nucleotides to the

fragmented strand. b) once the DNA polymerase (large grey circle) has created a copy, the strands are denatured, the original DNA is released and washed away, leaving the copied tethered strand; c) colonial amplification of the DNA strand attached to the flow cell occurs by bridge amplification. Here the DNA strand bends over and is hybridized to the 2nd type of oligonucleotide on the flow cell; d) A double stranded bridge is formed through the action of DNA polymerase which generates a complementary strand; e) two separate copies of DNA are generated by the denaturation of the double stranded bridge; f) processes (a-e) are repeated multiple times over the whole of the flow cell; g) clusters of the same forward and reverse sequences of single-stranded DNA fragments tethered to the flow cell are generated as a result of repeated bridge amplification; and h) the reverse strands are cleaved off at the oligonucleotides and the 3' ends are blocked, thus preventing unwanted priming events from occurring (Adapted from Illumina MiSeq vision, Illumina, 2012).

reverse ssDNA fragments that are tethered to the flow cell (Illumina, 2012). This process is repeated multiple times to generate a cluster of identical linear ssDNA fragments. Millions of clusters are generated across the channels, which can then be sequenced in parallel. The reverse strand of DNA is cleaved and removed, the 3' ends of the DNA are blocked to prevent any unwanted priming, the first round of sequencing can then begin (Illumina, 2012).

3.4.3 Sequencing

Sequencing of the forward strand is carried out first and then followed by the reverse strand (Figure 3-6). The process begins with the addition of the first primer to the channels, which binds to the DNA strand. The DNA strand is copied by DNA polymerase which adds a fluorescently labelled nucleotide to the growing chain one at a time (Illumina, 2012). After the addition of each nucleotide the clusters are excited by a light source, which results in the incorporated nucleotide emitting a fluorescent signal. The four different nucleotides each emit a characteristic wavelength of light which in addition to the signal intensity, can be used to determine what base was added (Illumina, 2012). Following the excitation of the cluster, the fluorescent tag is cleaved and the cycle can be repeated. The number of cycles is dependent on the desired read length, once this has been achieved the read sequence is removed from the tethered DNA template and washed away (Illumina, 2012). An index read is generated by in a similar way to the forward read, using index 1 primer. The index read is removed and the 3' ends are unblocked, which allows the ssDNA to fold over and hybridize with an oligonucleotide sequence on the surface of the channel. A second index read is carried

out (index 2) in the same manner as before using the index 2 primer (Illumina, 2012). A double stranded bridge is generated by DNA polymerase, which is subsequently denatured resulting in ssDNA molecules of both the forward and reverse sequences. The forward sequence is cleaved and washed away, 3’ ends are once again blocked, thus allowing for the reverse read to be sequenced. The second primer is then introduced and the process of nucleotide addition and the recording of the fluorescence emissions are repeated as with the forward run (Illumina, 2012).

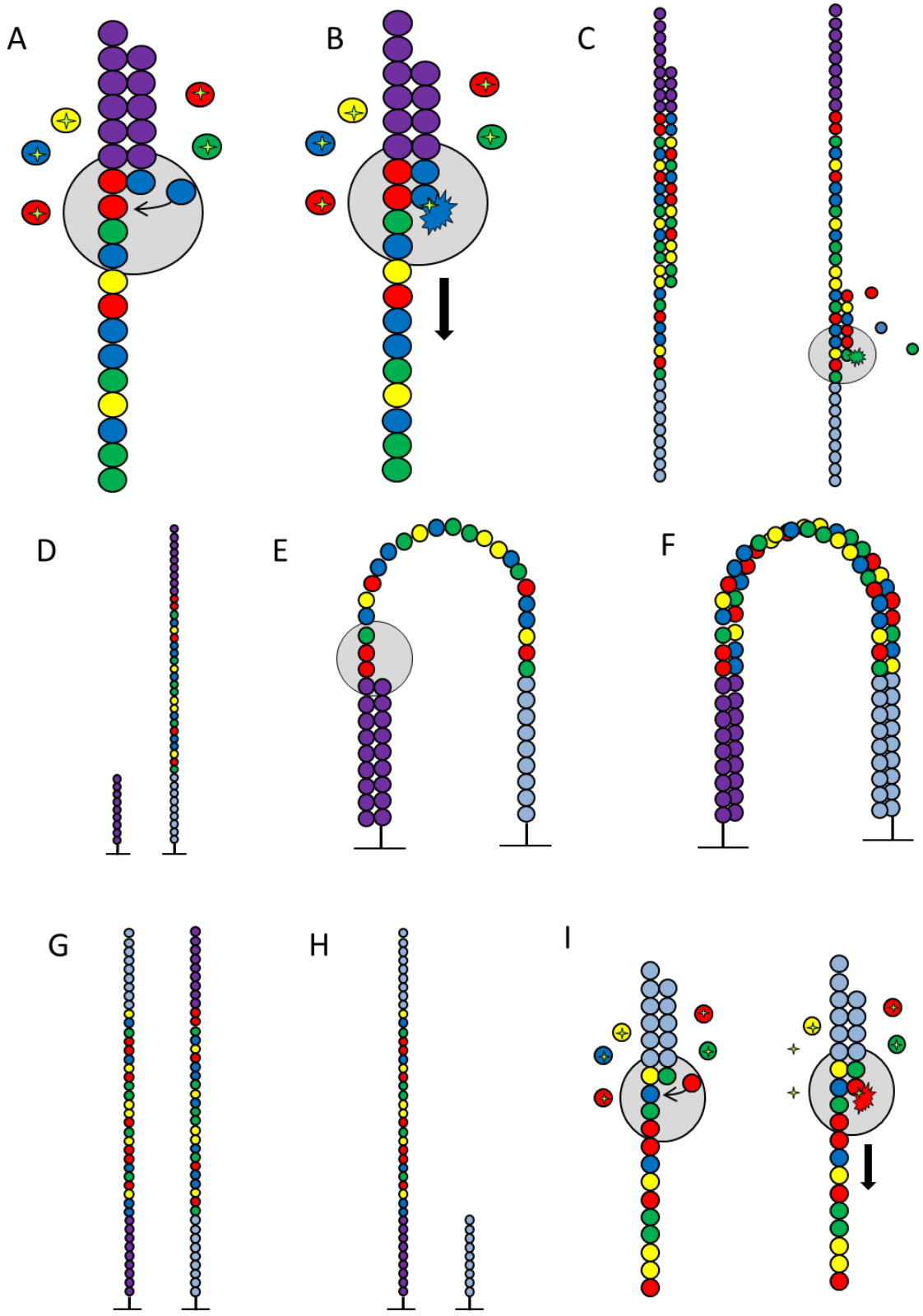

Figure 3-6: DNA sequencing of the forward stand on the MiSeq sequencing platform; a) the first sequencing primer anneals to the tethered DNA strand, where DNA polymerase creates a copy of t by the addition of a complementary nucleotide; b) each nucleotide is fluorescently tagged, after the addition of each individual nucleotide, a light source excites each cluster, which generates a characteristic fluorescent signal. The fluorescent tag is

then cleaved; c) after the desired number of reads has been achieved the read product and the tethered strand are denatured and the read product is washed away. The index 1 read primer is added and hybridizes to the template DNA. A read is generated in a similar way as described in a and b; d) the index read product is washed off and the 3'-block is removed to facilitate sequencing of the reverse strand; e) the forward strand bends over and hybridizes with the complementary oligonucleotide on the flow cell. Index 2 is read in the same way as index 1, and DNA polymerase then copies the forward strand of DNA; f) A double stranded bridge is formed containing the forward and reverse sequences; g) the double stranded bridge is linearized by denaturing the DNA; h) the forward strand is cleaved and washed away, the 3' ends are blocked to prevent unwanted priming; i) the read 2 primer is added and the reverse read is sequenced as described in a) (adapted from Illumina MiSeq vision, Illumina, 2012).

3.4.4 Data analysis

Millions of reads are generated during the sequencing process, and require further handling to ensure the quality of the sequencing is sufficiently high and that the data are usable. The unique indices introduced, where multiple samples are sequenced in parallel, allow for the sequences to be sorted into samples. The raw data from a sequencing run are checked for quality and assigned a Phred score, which ranges from 0-40. The Phread score assigned to the sequencing run gives an indication of the how accurately the base call was during the run. A quality score of above 30 is required to ensure that the accuracy is above 99.9 %. The data set then undergoes quality control steps, which include trimming the sequences and filtering them. The end of the sequences usually require trimming since the quality score usually drops at the end of the sequence. Trimming scripts remove sequences that are below the quality threshold, in addition the adapters are also removed from the sequences. The forward and reverse sequences (read 1 and read 2) are aligned to create full length sequences, therefore improving the quality and the length of the reads. The sequences are then checked for the presence of chimeras, which are hybrid products that have formed from two or more parent sequences. These could be mistakenly identified as a novel sequence and therefore give a false indication of the diversity in a sample (Haas *et al*., 2011). Chimeric sequences once detected are removed from the sequencing data, using chimera detection tools for example ChimeraSlayer (Haas *et al*., 2011) and UCHIME (Edgar *et al*., 2011). The sequences are assessed to determine how similar they are to one another; sequences that are highly similar (97 %) are then grouped together to form an operational taxonomic unit (OTU). Rarefaction analysis is then carried out on the data, this assesses the species richness, providing an indication of the number of species

present in a sample. Rarefaction curves can be generated where the number of species is plotted against the number of sequences, if the sequencing depth has been sufficient the curve should reach a plateau (Figure 3-7). Plots where the curve has not levelled out, indicate that the depth of sequencing was insufficient to detect all the diversity within a sample. Taxonomic classification of the sequences is then determined, this process involves aligning the sequencing data to known DNA sequences that have been deposited in reference databases. For the tools used to carry out these analyses in this thesis for 16S and 18S rRNA genes and the fungal internal transcribed spacer region 2 (ITS2) sequencing data see Chapter 4.

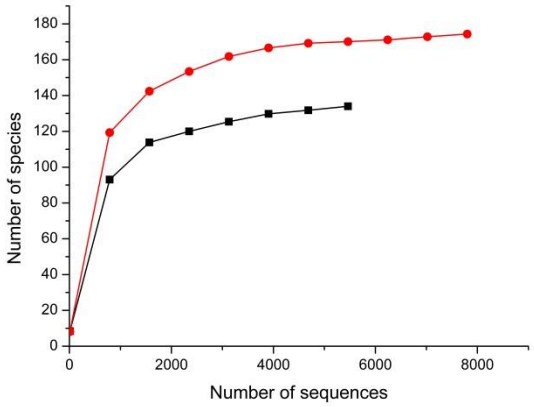

Figure 3-7: An example of an alpha-rarefaction curve, showing the sequencing depth is sufficient to identify all species within the samples.

3.5 Measurement of *Pseudanabaena catenata* growth

Isolation and cultivation of microbial cultures from pond water samples was not possible during the course of this project. A culture of *P. catenata* (NIVA-CYA 152), which is a close relative of the *Pseudanabaena* species identified in the FGMSP, was acquired from the NIVA culture collection of algae, Norway. An axenic culture of *P. catenata* was not available, therefore the culture used throughout this thesis was a mixed community, which later 16S rRNA gene sequencing would reveal contained several of the key genera that were present in the FGMSP samples, and was therefore highly representative of the microbial community in the pond. All cultures were grown in unmodified BG11 media (see Appendix A2), and grown in a Sanyo/Panasonic MLR-352-PE growth cabinet set to 25 ± 1 °C, a photon flux density of 150 μmol m^{-2} s^{-1}, and

a 16:8 h light–dark cycle, cultures were shaken at 100 rpm. Cultures were set up in triplicate for all experimental work and included appropriate sets of controls. The growth of the *P. catenata* cultures were measured in three ways, the optical density at 600 nm (OD_{600nm}), the concentration of chlorophyll-a (Chl-a), and direct cell counts of *P. catenata*.

The OD_{600nm} and Chl-a concentration measurements were carried out using a Jenway 6700 UV/Vis spectrophotometer (Bibby Scientific Limited, Staffordshire,UK). Spectrophotometers measure the absorbance or the transmission of a material as a function of wavelength. Spectrophotometers can either be single of dual (split) beamed (Figure 3-8). Absorbance values were recorded for both OD_{600nm} and Chl-a measurements. Monochromatic light at specific wavelengths was passed through samples which were placed in low absorbance disposable plastic microcuvettes (1 mL). A blank measurement at each wavelength was made prior to assessment of the samples, blanks were typically BG11 medium or 70 % ethanol, which allowed for the collection of quantitative data.

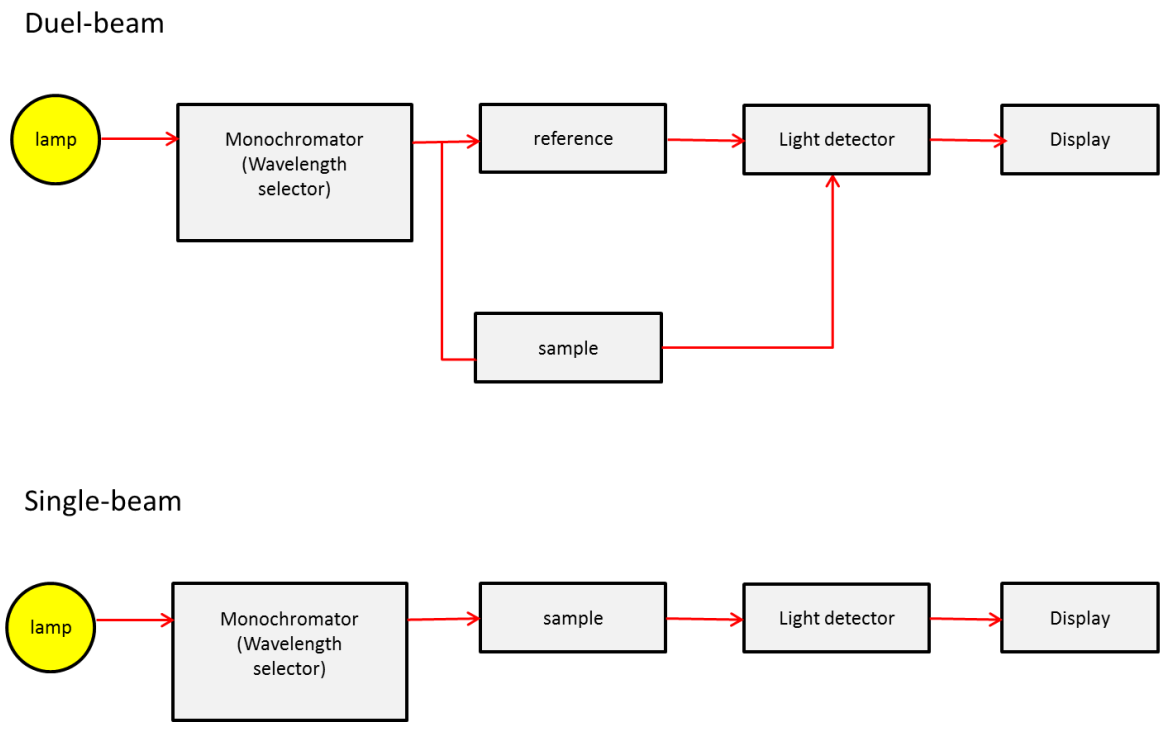

Figure 3-8: Schematic of duel and single beam spectrophotometers (adapted from Aduroka, 2017)

3.5.1 Chl-a concentration analysis

1 mL samples of *P. catenata* were centrifuged at 14,000 *g* for 10 min to pellet the cells. The supernatant was discarded and the cells re-suspended in 1 mL of 70 % ethanol and incubated at room temperature for 2 h. The samples were then centrifuged at 14,000 *g* for 10 min, the supernatant was then removed and analysed using the Jenway 6700 UV/Vis spectrophotometer (Bibby Scientific Limited, Staffordshire, UK). The absorbance was measured at 665 nm (Chl-a) and at 750 nm to correct for turbidity (Bellinger and Sigee, 2010). The concentration of Chl-a was then calculated using the formula of Jespersen and Christoffersen, (Jespersen and Christoffersen, 1987)(Equation 3-2).

$$Chl - a\ (\mu g\ L^{-1}) = \frac{V_e\ x\ f\ x\ A}{V_s\ x\ l}$$

Equation 3-2: Equation to determine the concentration of Chl-a (Jespersen and Christoffersen, 1987). Where: V_e = total volume of solvent (ml), A = Absorbance at 665nm - Absorbance at 750nm, V_s= Total volume of sample filtered (litres), L = Cell path length (cm), f= (1/specific extraction coefficient)*1000, where the specific extinction coefficient for Chl-a in 96% (v/v) ethanol is 83.41 g^{-1} cm^{-1} (Wintermans and De Mots, 1965).

3.6 X-irradiation of *P. catenata*

A Faxitron CP-160 cabinet X-radiator (Faxitron; Arizona, USA) was used to generate the X-radiation used to irradiate cultures of *P. catenata* in Chapter 5. Briefly the machine generates electrons from a source (cathode), an applied voltage is applied which accelerates the electrons that then collide with the anode, a metal target (tungsten). Core electrons are then ejected from the target atoms, as a consequence of the collision of the electrons. The electron vacancy is filled as an outer orbital electron drops down, releasing an X photon. Triplicate cultures of *P. catenata* was inoculated into 20 mL fresh sterile BG11 medium to a starting OD_{600nm} of 0.2 and subjected to total dose of 95 Gy (1 Gy min^{-1}) administered over five consecutive days.

3.7 Microscopy

All light microscopy was carried out using a Zeiss Imager A1 microscope (Carl Zeiss International) fitted with an Axiocam 506 mono camera using Zen2 imaging software.

3.7.1 Cell counts

A visual assessment of the cultures was carried out to directly quantify the number of *P. catenata* cells per mL of culture. All cell counts were carried out using a Sedgewick rafter cell counting chamber (Figure 3-9). The Sedgewick rafter holds 1 mL of liquid and the chamber is divided into 1000 squares that are 1 mm^2. The cultures were assessed at X10 magnification using a Zeiss Imager A1 microscope (Carl Zeiss International). Random squares were selected and photographed using an attached camera for analysis using ImageJ (NIH, 2018).

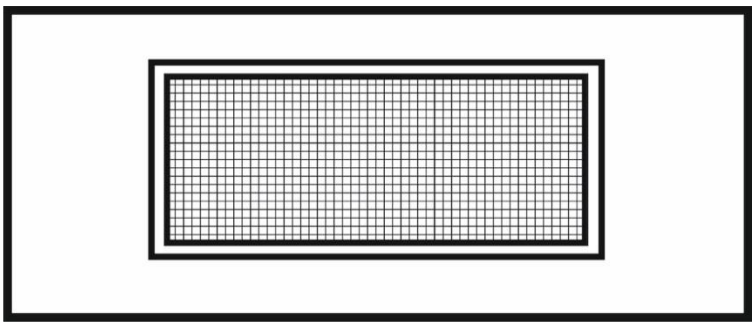

Figure 3-9: Diagram of a Sedgewick rafter counting chamber, showing the central chamber which holds 1 mL of sample, the bottom of the chamber is scored with 1 mm squares. Volume of the chamber is 50 mm x 20 mm x 1 mm.

The length of *P. catenata* filaments were measured using ImageJ. All filaments touching the top and left sides of a square were included in the measurements, whilst those in contact with the right and bottom sides were discounted. Individual cell lengths were then determined of 100 cells and the average cell length was calculated. The total filament length was then divided by the average cell length to give the number of cells, Equation 3-3 shows the calculation used to determine the number of cells per mL.

$$Cells\ mL^{-1} = \left(\frac{total\ filament\ length\ of\ 10\ squares}{average\ cell\ length}\right)\ x\ 100\ x\ dilution\ factor$$

Equation 3-3: calculation used to determine the number of *P. catenata* cells per mL

3.7.2 Calcofluor white cell staining

Calcofluor white cell stain (Sigma-Aldrich, Dorset, UK) was used to determine whether there were any differences in the polysaccharide content of samples of irradiated and non-irradiated cells in *P. catenata* cultures. There are a variety of stains that can be used to bind to different polysaccharides, in this project calcofluor white was utilised as it binds to a broad range of β-1,4-linked polysaccharides, including chitin, which is a component of fungal cell walls (Anderson *et al*., 2010; Dunker *et al*., 2017).

Samples were prepared using the same method as used for the Fourier-transform infrared (FT-IR) Spectroscopy to allow for comparisons to be drawn between the results. Sterile normal saline solution (9 g L^{-1} NaCl) was used to wash 500 µL samples of irradiated and non-irradiated *P. catenata* cultures, samples were washed twice. An equal volume of calcofluor white stain (5 µL) was added to cells on a glass slide, mixed, a cover slide was placed over the sample, which was then left in the dark for 10 min prior to being analysed. Samples were analysed at X100 magnification under oil-emersion. Calcofluor white stain is a fluorescent dye, excitation occurs at 355 nm, whilst the emission range is between 300-440 nm. The Zeiss filter set #49 was used to assess the fluorescence of calcofluor white (335-383 nm excitation and 420-470 nm emission). In addition to the auto-fluorescence of *P. catenata* cells was also monitored, this was carried out using the Zeiss filter set #00 (530-585 nm excitation and 615-4095 nm emission).

3.7.3 Electron microscopy

Samples collected from the Sr-containing cultures (Chapter 6) were visualised using electron microscopy, since it has much higher resolution than light microscopy. Identification of the elements present within the samples was determined using energy dispersive X-ray spectroscopy (EDS). EDS analysis detects secondary X-rays, specific

to each element, that are generated when the sample becomes excited from the electron beam used to generate images.

3.7.3.1 Transmission electron microscopy (TEM)

Transmission electron microscopy (TEM) was used to identify the biomineral precipitates formed when Sr was added to cultures of *P. catenata* (Chapter 6). TEM samples were prepared by washing a 1 mL sample twice in sterile deionised water before loading 2 μL of sample onto a copper TEM grid with a carbon film (Agar Scientific, Essex, UK). The dried samples were placed in the TEM where an electron beam (under vacuum), focussed by electromagnetic lenses, was passed through the sample and onto the detector (Figure 3-10). Since the image is generated from the electrons that pass through the sample there is a requirement that the sample should be very thin to facilitate this process. A FEI Tecnai T20 LaB6 Transmission Electron Microscope that was equipped with an Oxford XMax EDS detector.

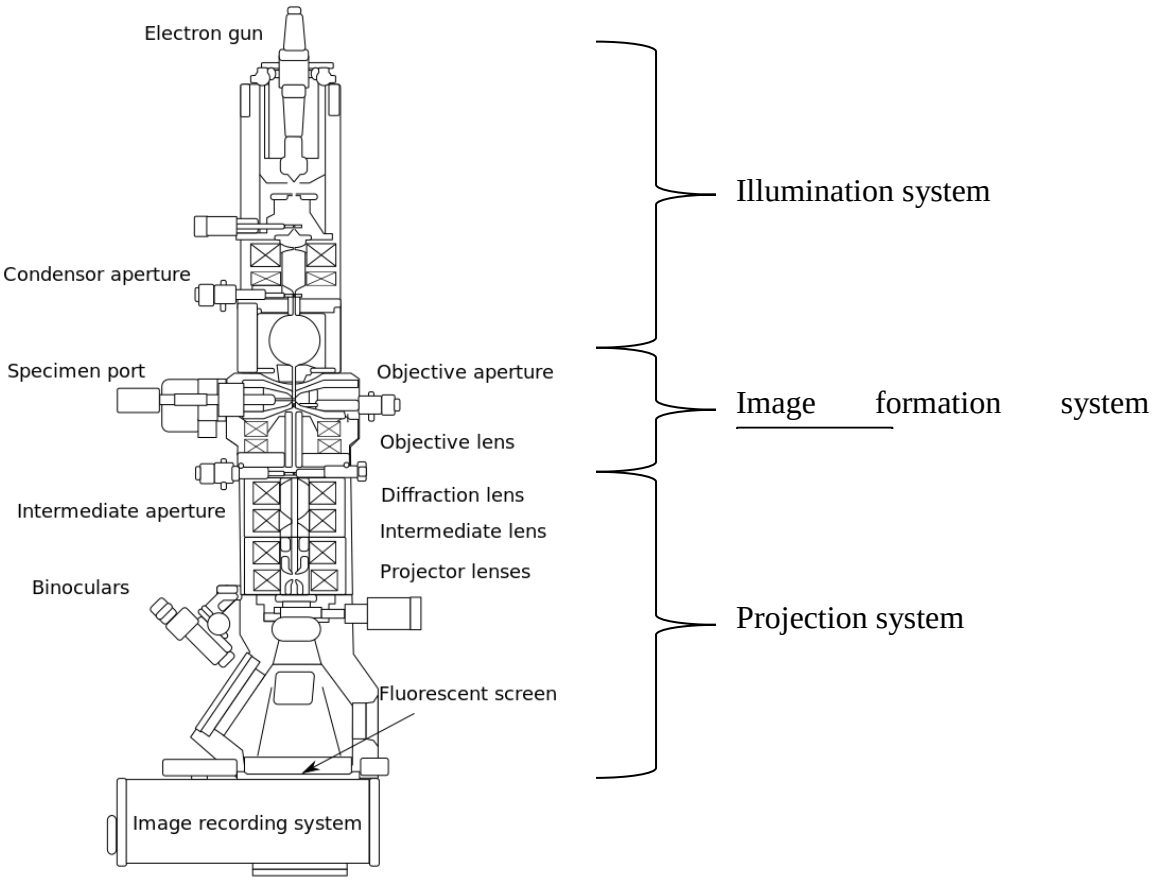

Figure 3-10: Image showing the main features of a transmission electron microscope (TEM), electrons are fired from the electron gun at the top of the TEM and focussed on to the specimen, which they pass through (Karlsson, 2007).

3.7.3.2 Environmental scanning electron microscopy (ESEM)

An environmental scanning electron microscope was used to gather images Sr-biominerals formed when Sr was added to cultures of *P. catenata*. This technique passes a beam of electrons through an atmosphere of water vapour prior to the beam hitting the sample (Figure 3-11). There are two ways in which an image can be generated using the ESEM. In secondary electron mode a high resolution topographical image can be generates as the low energy electrons are emitted from the sample surface. The second mode of the ESEM is backscattered electron mode, here the electron beam collides with atomic nuclei resulting in high energy electrons coming off the sample which are picked up by a detector. Elements with higher atomic numbers generate higher degrees of backscattering, which results in heavier elements appearing brighter in the resulting images. The work carried out in this thesis was carried out on a FEI Quantia 650 FEG SEM operating at 20 kV, EDS data was collected using a Bruker Quantax system with

Bruker XFlash EDS detector. Bruker Espirt V2.1 software was used to carry out the EDS analysis.

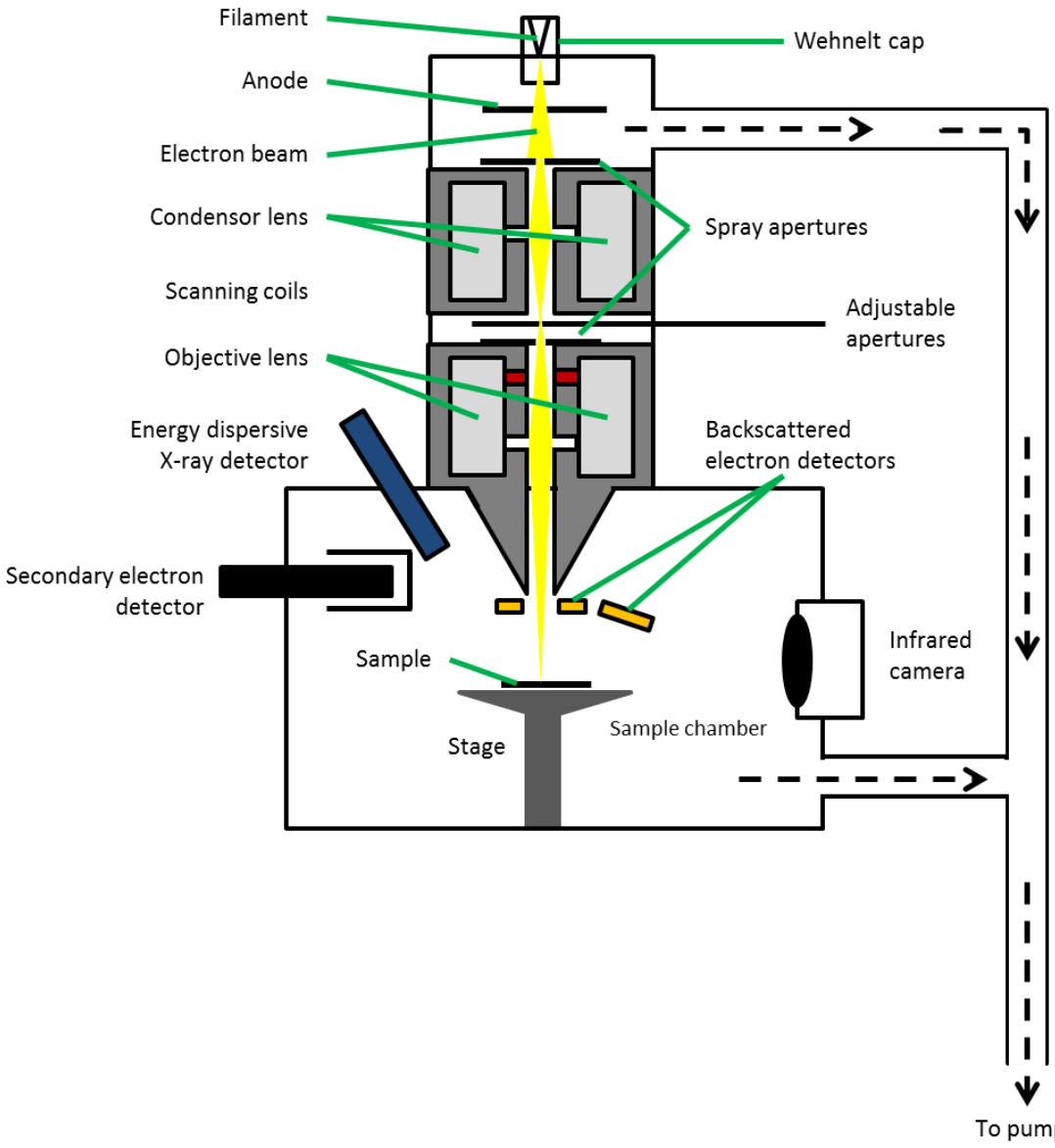

Figure 3-11: Schematic of an ESEM, an electron beam is fired from the top of the microscope and focused onto the sample which is supported on a stage. The electrons which come off the sample can be detected by the backscattered electron detector or the secondary electron detector, depending on which settings are used. In addition the identification of the elements in the sample can be determined using the energy dispersive X-ray detector (adapted from Electron microanalysis core facility, (University of Arizona, 2018)

3.8 Fourier-transform infrared (FT-IR) spectroscopy

The metabolic profile of microorganisms can be determined by Fourier-transform infrared (FT-IR) spectroscopy. The technique allows for rapid, quantitative sample analysis with minimum sample preparations (Brown, 2013; Goodacre *et al*., 2004; Wang *et al*., 2010). Samples are subjected to a beam of infrared radiation, for such analysis the mid-infrared (4000-600 cm^{-1}) region. This region is used since it is information rich and targets regions of biological interest, namely; 3050-2800 cm^{-1} (CH_2 and CH_3 vibrations of fatty acids); 1750-1500 cm^{-1} (C-N, C=O, and N-H from proteins and peptides); and 1200-900 cm^{-1} (C-O, C-O-C from polypeptides) . Functional groups in the sample absorb the radiation, which results in characteristic vibrations that correlate with (bio)chemical species (Table 3-1), further assignments can be found in Ellis *et al*., (2003) and Wang *et al*., (2010).

Table 3-1: Assignment of specific wavenumber(s) to biochemical bands identified using FT-IR spectroscopy (adopted from Ellis *et al*., 2003)

Region	Wavenumber / cm^{-1}	Assignment
	3400	OH
	2956	CH_3 asymmetric stretch
Fatty acid	2920	CH_3 asymmetric stretch
	2870	CH_3 asymmetric stretch
	2850	CH_3 asymmetric stretch
	1745/1735	C=O stretch (fatty acid esters)
Amide	1705	C=O stretch (esters, carboxylic
	1652-1648	groups
	1550-1548	Amide I, (C=O) different
	1460-1454	conformation
		Amide II (NH, C-N)
		CH_2 bend
Mixed	1400-1398	C-O bend (carboxylate ions)
	1310-1240	Amide III (C-N)
	1240	P=O (phosphate)

	1222	P=O
	1114	C-O-P, P-O-P
Polysaccharide	1085	Sugar ring vibrations
	1052	C-O, C-O-C (polysaccharide)

FT-IR is a form of spectroscopy that quantifies the light absorption of the sample at each wavelength over a given range. Infrared spectra can be collected simultaneously over a range of wavelengths using FT-IR due to the incorporation of an interferometer and the application of the Fourier transform algorithm to generate the signal output (a coherent spectrum). A FT-IR adapted interferometer is designed to split a beam of light generated by an infrared source, the two beams are then reflected on two mirrors, one static, one motorised. As the non-static mirror moves, it generates waves of different path lengths, resulting in a beam containing a different spectrum at each moment. The split beams are reflected back to the beam splitter, some of this light is passed to the sample, where it is focussed. Baseline measurements are recorded with no sample present, absorption peaks are then measured when a sample is analysed.

Samples of *P. catenata* (1 mL) were collected at 4 time points (day 4, 8, 12, and 16). Samples were washed twice in sterile normal saline (0.9 % wt/vol NaCl) discarding the supernatant. The cell pellet was flash frozen in liquid nitrogen and stored at -80 °C until further analyses. The frozen samples were then re-suspended in sterile normal saline solution, the OD_{600nm} was normalised to 15. Following normalisation 3 x 20 µL of each sample was plated out onto a pre-washed Bruker 96-well silicon plate (Bruker Ltd, Coventry, UK). Each sample was randomly assigned a well using the randomising function in Excel. A standing oven was then used to heat the samples to dryness for 30 min at 55 °C. A Bruker Equinox 55 infrared spectrometer was used to carry out the FT-IR analysis of the samples. Further details of the FT-IR run can be found in Chapter 5.

MATLAB version 9 (The MathWorks Inc., Natick, MA) was used to analyse the collected FT-IR spectra. The extended multiplicative signal correction (EMSC) method (Martens *et al*., 2003) was used to scale the spectra generated from the FT-IR run, the CO_2 bands (2400-2275 cm^{-1}) were removed and replaced with a linear trend. Principal component analysis (PCA) is a way of simplifying complicated data sets with multiple variants, such as the FT-IR spectral data. The unsupervised method of PCA, was

applied to the spectral data in this thesis to reduce its dimensionality and to determine the variations between groups.

3.9 Inductively-coupled plasma atomic emission spectroscopy (ICP-AES)

The total concentration of strontium in solution was measured using inductively-coupled plasma atomic emission spectroscopy (ICP-AES). Analysis was carried out on cell free samples of BG11 medium where Sr had been added to the culture at the start of the experiment. The cell-free samples were diluted in 2 % nitric acid to give a final concentration between 0.1-10 mg L^{-1}. The technique generates an aerosol mist from the sample using a nebuliser. The aerosol is then passed through an argon plasma, which ionizes the sample. The concentration of a specific element by ICP-AES relies on the emission of a photon of light which is produced when an outer shell electron is excited and subsequently relaxes. Each element has characteristic wavelengths of light that are generated, therefore facilitating their identification, the concentration of the element within a sample is determined by the intensity of the light generated using a calibration curve.

3.10 X-ray absorption spectroscopy

X-ray absorption spectroscopy (XAS) is a non-destructive technique that can be used across a range of samples such as solids (amorphous or crystalline) and solutions, to generate detailed information about a specific element's local coordination environment and speciation. A synchrotron (or storage ring) is used to accelerate a high-energy electron beam. X-rays are generated when the trajectory of an electron beam is bent as it passes through electromagnets, the X-rays are then passed through the sample (Penner-Hahn, 2004). Inner electrons (K or L shell) absorb the X-rays and the absorption increases at the absorption edge, when the binding energy and the X-ray energy are equal. The atom is left in an unstable excited state due to the ejection of an electron. The hole that has been left is filled with an electron from the L or M shell, resulting in the release of energy as a secondary fluorescent X-ray. The energy of incident X-rays that result in the ejection of an electron is specific for each element. If an element is redox

active the absorption edge will change position dependent on the oxidation state of the element, however this is not relevant for Sr^{2+} since it is not redox active. Information can also be gathered from observing the interaction of the secondary X-ray with surrounding atoms. XAS can be split into two different regions (Figure 3-12) these being the X-ray absorption near-edge spectroscopy (XANES) and the extended X-ray absorption fine-structure spectroscopy (EXAFS). XANES includes a region ~ 50 eV above the absorption edge and provides information about the absorbing atoms oxidation state and coordination chemistry (e.g. tetrahedral coordination) (Newville, 2014). EXAFS is the area of the spectra more than ~ 50 keV from the absorption edge, oscillations in this region are the result of a spherical wave generated when the electron is ejected from the central absorber that is scattered by the surrounding atoms. EXAFS data are commonly presented as a function of the wave vector, k and in order to enhance the signal at higher energies are weighted as k^3. In addition, a Fourier transform can be applied to provide a pseudo-radial distribution function.

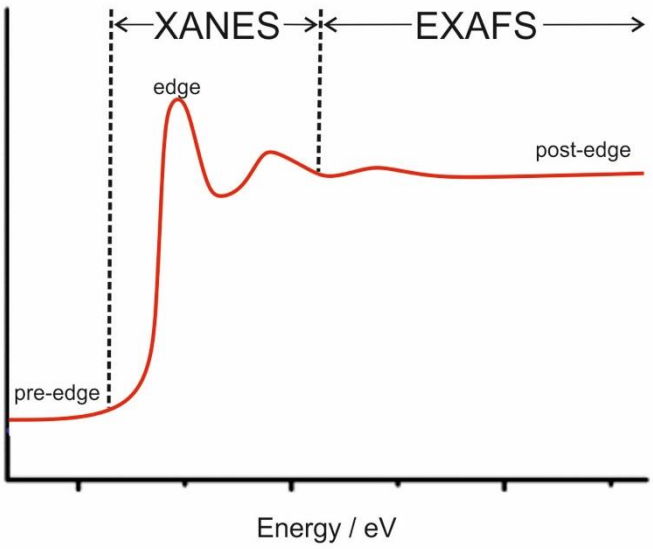

Figure 3-12: Schematic of a normalised spectrum indicating the different XAS regions

XAS was used to determine the speciation and coordination environment of Sr in the biominerals formed when Sr was added to cultures of *P. catenata*. The solid phase was removed from solution by vacuum filtration and a pellet containing a ~1 % Sr loading was prepared by diluting in cellulose. The sample was analysed at the Diamond Light Source, Harwell, UK on the beamline B18 using a liquid nitrogen cooled cryostat in transmission mode, where Sr K-edge spectra (16115.26 keV) were collected. ATHENA

(Ravel and Newville, 2005) was used to average, calibrate, background subtract and normalise multiple scans. The coordination of Sr in the solid phase was determined by using ARTEMIS to fit EXAFS spectra (Ravel and Newville, 2005). The F-test was used to determine whether shells made statistical improvements to the model fit, only those that were statistically significant were included (Downward *et al*., 2007). Preparation of the sample for XAS analysis, running on the beamline and data analysis were carried out by Adrian Cleary.

3.11 X-ray diffraction

The crystallographic structure of precipitated minerals was analysed using X-ray diffraction (XRD). Samples are subjected to X-rays which are subsequently diffracted by the planes of a mineral lattice. In order for the X-rays to provide constructive interference, Bragg's Law must be satisfied (Equation 3-4). A range of diffraction angles (between 5 ° and 70 °) and lattice spacings are generated since the X-ray tube and detector are rotated around the sample (360 °). Where the mineral assessed consists of a highly ordered crystal structure, at concentrations in excess of 5 % by mass, the mineral can be identified by using standard reference materials to compare with the lattice d-spacings generated by the technique (Cullity, 1978).

$$n\lambda = 2d\ sin\theta$$

Equation 3-4: Bragg's Law, where; n is a positive integer; λ is the wavelength of the incident X-ray; d is the lattice spacing; θ is the diffraction angle

3.12 References

Aduroja, O., 2017. No Title [WWW Document]. Appl. Anal. Syst. LTD. URL http://aasnig.com/category/standard/ (accessed 6.29.18).

Anderson, C.T., Carroll, A., Akhmetova, L., Somerville, C., 2010. Real-Time Imaging of Cellulose Reorientation during Cell Wall Expansion in Arabidopsis Roots. Plant Physiol. 152, 787–796. https://doi.org/10.1104/pp.109.150128

Bassil, N.M., 2015. Cellulose degradation under alkali conditions, representative of cemetitious radioactive waste disposal sites. University of Manchester.

Bellinger, E.G., Sigee, D.C., 2010. Freshwater algae: Identification and use as bioindicators, 2010th ed. John Wiley & Sons, Ltd.

Biotech, O., 2018. Agraose gel electrophoresis for DNA samples [WWW Document]. URL http://orbitbiotech.com/agarose-gel-electrophoresis-for-dna-samples-gel-electrophoresis-macro-molecules-edta-tris-glacial-acetic-acid-gel-loading-agarose-dye-buffer-gel-case-tae-glycerol-etbr/ (accessed 8.10.18).

Brankatschk, R., Bodenhausen, N., Zeyer, J., Burgmann, H., 2012. Simple absolute quantification method correcting for quantitative PCR efficiency variations for microbial community samples. Appl. Environ. Microbiol. 78, 4481–4489. https://doi.org/10.1128/AEM.07878-11

Brown, A.R., 2013. The impact of ionizing radiation on microbial cells pertinent to the storage, disposal and remediation of radioactive waste. University of Manchester.

Caporaso, J.G., Kuczynski, J., Stombaugh, J., Bittinger, K., Bushman, F.D., Costello, E.K., Fierer, N., Peña, A.G., Goodrich, J.K., Gordon, J.I., Huttley, G. a, Kelley, S.T., Knights, D., Koenig, J.E., Ley, R.E., Lozupone, C. a, Mcdonald, D., Muegge, B.D., Pirrung, M., Reeder, J., Sevinsky, J.R., Turnbaugh, P.J., Walters, W. a, Widmann, J., Yatsunenko, T., Zaneveld, J., Knight, R., 2010. correspondence QIIME allows analysis of high- throughput community sequencing data Intensity normalization improves color calling in SOLiD sequencing. Nat. Publ. Gr. 7, 335–336. https://doi.org/10.1038/nmeth0510-335

Case, R.J., Boucher, Y., Dahllöf, I., Holmström, C., Doolittle, W.F., Kjelleberg, S., 2007. Use of 16S rRNA and rpoB genes as molecular markers for microbial ecology studies. Appl. Environ. Microbiol. 73, 278–288. https://doi.org/10.1128/AEM.01177-06

Chien, A., Edgar, D.B., Trela, J.M., 1976. Deoxyribonucleic acid polymerase from the extreme thermophile *Thermus aquaticus* 127, 1550–1557.

Cole, J.R., Wang, Q., Cardenas, E., Fish, J., Chai, B., Farris, R.J., Kulam-Syed-Mohideen, A.S., McGarrell, D.M., Marsh, T., Garrity, G.M., Tiedje, J.M., 2009. The Ribosomal Database Project: Improved alignments and new tools for rRNA analysis. Nucleic Acids Res. 37, 141–145. https://doi.org/10.1093/nar/gkn879

Cullity, B.D., 1978. Elements of X-ray diffraction, 2nd ed. Addison-Wesley Publishing Company Inc., Reading MA, Menlo Park CA, London, Amsterdam, Don Mills, Ontario- Sydney.

Devereux, R., Devereux, R., Wilkinson, S.S., Wilkinson, S.S., 2004. Amplification of ribosomal RNA sequences. Mol. Microb. Ecol. Man. 3, 509–522. https://doi.org/10.1007/978-94-011-0351-0

Downward, L., Booth, C.H., Lukens, W.W., Bridges, F., 2007. A variation of the F-test for determining statistical relevance of particular parameters in EXAFS fits. AIP Conf. Proc. 882, 129–131. https://doi.org/10.1063/1.2644450

Dunker, S., Althammer, J., Pohnert, G., Wilhelm, C., 2017. A fateful meeting of two phytoplankton species—chemical vs. cell-cell-interactions in co-cultures of the green algae *Oocystis marsonii* and the cyanobacterium *Microcystis aeruginosa*. Microb. Ecol. 74, 22–32. https://doi.org/10.1007/s00248-016-0927-1

Edgar, R.C., Haas, B.J., Clemente, J.C., Quince, C., Knight, R., 2011. UCHIME improves sensitivity and speed of chimera detection. Bioinformatics 27, 2194–2200. https://doi.org/10.1093/bioinformatics/btr381

Ellis, D.I., Harrigan, G.G., Goodacre, R., 2003. Metabolic fingerprinting with Fourier transform infrared spectroscopy, in: Harrigan, G.G., Goodacre, R. (Eds.), Metabolic Profiling: Its Role in Biomarker Discovery and Gene Function Analysis. Kluwer Academic, Boston, MA; London.

Fakruddin, M., Chowdhury, A., Hossain, M.N., Mannan, K.S. Bin, Mazumdar, R.M., 2012. Pyrosequencing-Principles and Applications. Int. J. Life Sci. Pharma Res. 2, L65-76.

Goodacre, R., Vaidyanathan, S., Dunn, W.B., Harrigan, G.G., Kell, D.B., 2004. Metabolomics by numbers: Acquiring and understanding global metabolite data. Trends Biotechnol. 22, 245–252. https://doi.org/10.1016/j.tibtech.2004.03.007

Haas, B.J., Gevers, D., Earl, A.M., Feldgarden, M., Ward, D. V, Giannoukos, G., Ciulla, D., Tabbaa, D., Highlander, S.K., Sodergren, E., Methé, B., DeSantis, T.Z., The Human Microbiome Consortium, Petrosino, J.F., Knight, R., Birren, B.W., 2011. Chimeric 16S rRNA Sequence Formation and Detection in Sanger and 454-Pyrosequenced PCR Amplicons. Genome Res. 21, 494–504. https://doi.org/10.1101/gr.112730.110.Freely

Hamady, M., Walker, J.J., Harris, J.K., Gold, N.J., Knight, R., 2008. Error-correcting barcoded primers for pyrosequencing hundreds of samples in multiplex. Nat. Methods 5, 235–237. https://doi.org/10.1038/nmeth.1184

Illumina, 2012. Illumina MiSeq vision [WWW Document]. URL https://www.youtube.com/watch?v=t0akxx8Dwsk (accessed 8.10.18).

Ishaq, S.L., Wright, A.D.G., 2014. Design and validation of four new primers for next-generation sequencing to target the 18S rRNA genes of gastrointestinal ciliate protozoa. Appl. Environ. Microbiol. 80, 5515–5521. https://doi.org/10.1128/AEM.01644-14

Jespersen, A.-M., Christoffersen, K., 1987. Measurements of chlorophyll-a from phytoplankton using ethanol as extraction solvent. Arch. Hydrobiol. 109, 445–454.

Karlsson, L.S., 2007. Transmission Electron Microscopy of III-V Nanowires and Nanotrees. Lund University.

Kozich, J.J., Westcott, S.L., Baxter, N.T., Highlander, S.K., Schloss, P.D., 2013.

Development of a dual-index sequencing strategy and curation pipeline for analyzing amplicon sequence data on the miseq illumina sequencing platform. Appl. Environ. Microbiol. 79, 5112–5120. https://doi.org/10.1128/AEM.01043-13

Lane, D.J., 1991. Nucleic acid techniques in bacterial systematics. John Wiley & Sons, Ltd, New York.

Martens, H., Nielsen, J.P., Engelsen, S.B., 2003. Light scattering and light absorbance separated by extended multiplicative signal correction. Application to near-infrared transmission analysis of powder mixtures. Anal. Chem. 75, 394–404. https://doi.org/10.1021/ac020194w

MeGraw, V.E., Brown, A.R., Boothman, C., Goodacre, R., Morris, K., Sigee, D., Anderson, L., Lloyd, J.R., 2018. A novel adaptation mechanism underpinning algal colonization of a nuclear fuel storage pond. MBio 9, 1–15. https://doi.org/10.1128/mBio.02395-17

Muyzer, G., Teske, A., Wirsen, C.O., Jannasch, H.W., 1995. Phylogenetic relationships of *Thiomicrospira* species and their identification in deep-sea hydrothermal vent samples by denaturing gradient gel-electrophoresis of 16S rDNA fragments. Arch. Microbiol. 164, 165–172. https://doi.org/10.1007/bf02529967

Newville, M., 2014. Fundamentals of XAFS. Rev. Mineral. Geochemistry 78, 33–74. https://doi.org/10.2138/rmg.2014.78.2

NIH, 2018. ImageJ [WWW Document]. URL https://imagej.nih.gov/ij/ (accessed 8.10.18).

Owen-Hughes, T., Engeholm, M., 2007. Pyrosequencing positions nucleosomes precisely. Genome Biol. 8, 10–13. https://doi.org/10.1186/gb-2007-8-6-217

Penner-Hahn, J.E., 2004. X-ray absorption spectroscopy, 2nd Edition. Comprehenisve coordination chemistry, 2nd ed. Elsevier, Ann Arbor. https://doi.org/10.1038/npg.els.0002984

Purves, W.K., Sadava, D., Orians, G.H., C, H.H., 2004. Life: The science of biology, 7th ed. Sinauer Associates, Sunderland, MA.

Qiagen, 2018. MO BIO's PowerWater DNA isolation kit handbook [WWW Document]. MoBio Lab. Inc. URL https://www.qiagen.com/us/resources/resourcedetail?id=0b5d47e0-e312-413d-bfd8-563fec8fcc9f&lang=en (accessed 8.10.18).

Ravel, B., Newville, M., 2005. *ATHENA, ARTEMIS, HEPHAESTUS*: Data analysis for X-ray absorption spectroscopy using *IFEFFIT*. J. Synchrotron Radiat. 12, 537–541. https://doi.org/10.1107/S0909049505012719

Ronaghi, M., 2001. Pyrosequencing Sheds Light on DNA Sequencing Pyrosequencing Sheds Light on DNA Sequencing. Genome 11, 3–11. https://doi.org/10.1101/gr.150601

Ronaghi, M., Karamohamed, S., Pettersson, B., Uhlén, M., Nyrén, P., 1996. Real-time DNA sequencing using detection of pyrophosphate release. Anal. Biochem. 242, 84–89. https://doi.org/10.1006/abio.1996.0432

Ronaghi, M., Nyrén, P., 1998. A sequencing method based on real-time

phyrophosphate. Science (80-.). 281, 363–365.

Saiki, R.K., Gelfand, D.H., Stoffel, S., Scharf, S.J., Higuchi, R., Horn, G.T., Mullis, K.B., Erlich, H.A., 1988. Primer directed enzymatic amplification of DNA with a thermostable DNA polymerase. Science 239, 487–491. https://doi.org/10.1126/science.2448875

Sarwat, M., Yamdagni, M.M., 2016. DNA barcoding, microarrays and next generation sequencing: Recent tools for genetic diversity estimation and authentication of medicinal plants. Crit. Rev. Biotechnol. 36, 191–203. https://doi.org/10.3109/07388551.2014.947563

University of Arizona, 2018. Electron microanalysis core facility [WWW Document]. URL https://nau.edu/cefns/labs/electron-microprobe/glg-510-class-notes/instrumentation (accessed 8.10.18).

Wang, H., Law, N., Pearson, G., Van Dongen, B.E., Jarvis, R.M., Goodacre, R., Lloyd, J.R., 2010. Impact of silver(I) on the metabolism of *Shewanella oneidensis*. J. Bacteriol. 192, 1143–1150. https://doi.org/10.1128/JB.01277-09

Weisburg, W. G., Barns, S. M., Pelletier, D. A., Lane, D.J., 1991. 16S ribosomal DNA amplification for phylogenetic study. J. Bacteriol. 173, 697–703. https://doi.org/n.a.

Wintermans, J.F.G.M., De Mots, A., 1965. Spectrophotometric characteristics of chlorophylls a and b and their phenophytins in ethanol. BBA - Biophys. Incl. Photosynth. 109, 448–453. https://doi.org/10.1016/0926-6585(65)90170-6

Chapter 4

Research chapter 4: Understanding the microbial ecology of a high pH spent nuclear fuel pond on the Sellafield site

4 Research chapter 4: The microbial ecology of a high pH spent nuclear fuel pond on the Sellafield site

Lynn Foster[1], Christopher Boothman[1], Sharon Ruiz-Lopez[1], Genevieve Boshoff[2], Peter Jenkinson[3], David Sigee[1], Jon K Pittman[1], Katherine Morris[1], and Jonathan R Lloyd[1*]

[1] Research Centre for Radwaste Disposal and Williamson Research Centre for Molecular Environmental Science, School of Earth and Environmental Sciences, The University of Manchester, Oxford Road, Manchester M13 9PL, U.K.

[2] National Nuclear Laboratory, Chadwick House, Birchwood, Warrington WA3 6AE, UK

[3] Sellafield Ltd, Seascale, Cumbria CA20 1DW, UK

Key words: *Pseudanabaena,* cyanobacteria, Spent nuclear fuel pond, high pH, Sellafield

4.1 Abstract

The First Generation Magnox Storage Pond (FGMSP) is a high pH spent nuclear fuel pond (SNFP) situated on the Sellafield Ltd. site, Cumbria, UK. Despite the inhospitable conditions associated with the pond, microorganisms have been noted to cause "blooms" within the facility, the nature of which has previously been unknown. Using high throughput next generation sequencing techniques, the identity of the microbial community colonising the pond, including during two microbial bloom periods, in 2014 and 2016, has been determined. Probe data collected from the pond indicated a cyanobacterial bloom event, quantitative polymerase chain reaction (qPCR) quantification of 16S rRNA and 18S rRNA genes indicated that prokaryotic organisms were most abundant in the pond, particularly during the 2016 bloom. Analysis of the 16S rRNA gene revealed that a single cyanobacterial genus was dominant during the blooms, which was most closely related to *Pseudanabaena*. In addition, comparisons between the microbial community of FGMSP and an additional SFNP, that is occasionally purged into the FGMSP showed distinct community profiles. Pond data show that the onset of the microbial blooms occurred when the purge rate was reduced, but can be managed by re-establishing a high purge rate. In addition to supporting the targeted development of microbial control procedures, the identification of members of the *Pseudanabaena* genus that can colonise the pond and dominate during the bloom period is of interest, since *Pseudanabaena* species have received little attention for their roles in cyanobacterial blooms. This work could also be relevant to bioremediation

efforts to treat waters contaminated with radionuclides, which could benefit from the use of cyanobacteria able to tolerate the extreme environment of the FGMSP.

4.2 Introduction

Microorganisms are ubiquitous in the environment and are known to exhibit a broad range of adaptive and metabolic capabilities (Billi and Potts, 2002; Blanco-Rivero *et al*., 2005; Pikuta *et al*., 2007). With the development of culture independent profiling techniques increasingly hostile environments have been shown to support microbial colonisation, including radioactive contaminated land and nuclear facilities (Ashworth *et al*., 2018; Karley *et al*., 2017; MeGraw *et al*., 2018; Rivasseau *et al*., 2013). The ability of microorganisms to withstand high doses of radiation have been widely studied, with the most intensively studied organism, *Deinococcus radiodurans* recording the highest tolerance, and able to withstand acute doses in excess of 10 kGy (Daly *et al*., 2004; Daly, 2009; Rivasseau *et al*., 2013). Several other organisms have been shown to display high levels of radiation resistance, for example species of cyanobacteria that belong to the genera *Anabaena* (Singh *et al*., 2013), *Arthrospira* (Badri *et al*., 2015; El-Fatah Abomohra *et al*., 2016) and *Chroococcidiopsis* (Billi *et al*., 2000). Natural radiation levels have not been recorded at such high doses, therefore it has been suggested that the ability to withstand such doses and colonise significantly radioactive environments is a consequence of adaptations to other extreme environments that generate high levels of reactive oxygen species (Billi *et al*., 2000; Billi and Potts, 2002; Jolivet *et al*., 2003).

Microorganisms have been detected in many nuclear facilities across the world, including ponds used to store spent fuels, and there has been much interest in applying state of the art DNA characterisation techniques to understand the microbial communities of such systems (Bagwell *et al*., 2018; Chicote *et al*., 2005; Dekker *et al*., 2014; MeGraw *et al*., 2018; Sarró *et al*., 2007). Microbial growth in nuclear facilities causes concern for several reasons e.g biofouling (Gadd, 1990) and reduced visibility (MeGraw *et al*., 2018), interactions with redox sensitive radionuclides and other fission products (Avery *et al*., 1992; Avery *et al*., 1992; Gadd, 2004; Rivasseau *et al*., 2013), and the potential for microbial induced corrosion (MIC) (Bruhn *et al*., 2009). Studies have shown that microorganisms capable of biofilm formation and MIC of steel

coupons are present in the Confretes spent nuclear fuel pond (SNFP) (Valencia, Spain) (Chicote *et al*., 2005; Sarró *et al*., 2003; Sarró *et al*., 2005, Sarró *et al*., 2007). In other SNFPs the presence of microorganisms is problematic due to their ability to form microbial blooms, for example as shown with the eukaryotic microalgae *Haematococcus pluvialis* in another SNFP (MeGraw *et al*., 2018). Dense microbial growth restricts visibility in the pond, which is disruptive to plant operations such as waste retrieval (Ashworth *et al*., 2018.; MeGraw *et al*., 2018).

Part of the UK's legacy nuclear fleet included gas-cooled reactors, more commonly referred to as Magnox reactors due to the nature of the cladding used for the fuel rods (Crossland, 2012; Wilson, 1996). The fuel rods utilised in the Magnox reactors were composed of unenriched uranium metal encased in a magnesium non-oxide (Magnox) cladding (Gregson *et al*., 2011a; Gregson *et al*., 2011b; Jensen and Nønbel, 1999). Once the fuel rods are no longer efficient at producing energy they are usually stored in large engineered ponds containing demineralised water. The water provides thermal cooling and shields against radiation, since the rods continue to generate heat and radiation after power generation (Wilson, 1996). Currently in the UK, the spent Magnox fuel is stored in the FGMSP on the Sellafield Ltd. site (Cumbria, UK) (Jackson *et al*., 2014). The FGMSP contains a stock of historic (legacy) fuel that is unsuitable for reprocessing, which has been stored for a significantly longer period of time than anticipated. The Magnox fuel rods are chemically unstable in water, resulting in corrosion of the fuel and cladding (Gregson *et al*., 2011a; Gregson *et al*., 2011b; NDA, 2016). The extended storage period of the fuel rods has resulted in the build-up of significant levels of radioactive sludge as a result of the corrosion (Chen, 2011; Sellafield, 2014). In order to prevent further corrosion of the fuel cladding and fuel, the pond is continuously purged with water dosed to a pH of 11.4 using NaOH. In addition, since the pond is open-aired, it is subject to an influx of environmental debris, providing carbon and nitrogen (Gregson *et al*., 2011a; Gregson *et al*., 2011b).

The FGMSP is currently undergoing decommissioning which involves waste retrieval operations and sludge removal (Sellafield, 2014). Visibility in the pond is important to allow efficient and safe plant operations to be carried out. The microbial community in the pond is known to undergo seasonal microbial growth which increases the turbidity in the pond and considerably restricts the visibility in the waters (Sellafield, 2014). When the visibility is reduced plant operations are halted, which results in both an

increased timeframe for decommissioning and increased financial cost. The microbial blooms are thought to occur when the purge into the pond is disrupted.

Whilst the presence of microorganisms is well known within the pond (Gregson *et al*., 2011a), including indications that the bloom is of algal origin, nothing is known about the identity of the organisms present. The purpose of this study is to determine the composition of the microbial community, particularly during a bloom period. Here water samples were collected, and extracted DNA samples were sequenced and analysed to characterise the prokaryotic and eukaryotic community over a three-year period. In addition, samples were collected from a hydraulically isolated auxiliary pond, which is allowed to overflow into the main pond, to determine if this could be a potential source of bloom forming microbial inocula. Identifying the microbial community in the pond is the first step in determining the potential metabolic functions that they are utilising to colonise the pond, and will also help inform bloom control strategies, for example the use of purge strategies, application of biocides or employment of sonication systems.

4.3 Materials and Methods

4.3.1 Pond samples, sampling and pond description

The FGMSP is a legacy pond situated on the Sellafield site (Cumbria,UK) and is the primary storage pond for legacy Magnox spent fuel. The pond is continuously purged with caustic dosed demineralised water at a pH of 11.4, and contains an outflow point, where water is removed from the pond. There are two further feeds into the pond, the first contains caustic dosed water (pH ~11.4) from another fuel handling pond facility on site. The second inlet comes from an auxiliary settling tank (auxiliary pond). Water from the auxiliary pond is allowed to flow into the FGMSP when its water levels are sufficiently high.

A total of 7 samples were taken from two sites from the FGMSP between 2014 and 2017 (Table 4-1). All samples, approximately 200 mL, were collected from a depth of 1 m, using a hose and syringe to withdraw the water and decant into sample bottles. A

further 6 samples were taken from the auxiliary pond, and were collected using the same method.

Table 4-1: Details of the date, location and names of all samples collected from the FGMSP and auxiliary ponds between August 2014 and September 2017

Sample date	Sampling location	Sample name
13/08/14 (Bloom sample)	FGMSP main pond	Main_Aug_14_1 Main_Aug_14_2
04/08/16 (Bloom sample)	FGMSP main pond	Main_Aug_16
24/09/16 (Background water sample)	FGMSP main pond	Main_Sept_16_1 Main_Sept_16_2
26/06/17 (Background water sample)	FGMSP main pond	Main_Jun_17
24/09/17 (Background water sample)	FGMSP main pond	Main_Sept_17
12/08/14	Auxiliary pond	Aux_Aug_14_1 Aux_Aug_14_2
24/05/16	Auxiliary pond	Aux_May_16

05/08/16	Auxiliary pond	Aux_Aug_16
26/06/17	Auxiliary pond	Aux_Jun_17
24/09/17	Auxiliary pond	Aux_Sept_17

Data about the pond conditions between 2014 and 2016 were provided by Sellafield Ltd as part of standard pond operations. The sampling depth for all measurements was approximately 1 m, which is the same depth at which water samples were collected for DNA extraction. The data collected covers the pond conditions during two microbial blooms in the facility, which were reported to start 29th July 2014 and 28th July 2016 and lasted 6 and 4 weeks respectively. Estimations of the abundance of photosynthetic microorganisms in the pond were made using an Exo total algae sensor (WTW Wissenschaftlich-Technische Werkstätten, Germany), which is a dual-channel fluorescence sensor designed to measure chlorophyll and phycocyanin pigments. The sensor emits a blue excitation beam (470 ± 15 nm) which, quantifies the chlorophyll-a molecule found in all photosynthetic algae. Additionally an orange excitation beam (590 ± 15 nm) is emitted that quantifies the phycocyanin molecule found in cyanobacteria. Measurements were also taken routinely by Sellafield Ltd throughout the sampling period for the following; turbidity (Formazin turbidity unit, FNU), SO_4 (µg mL^{-1}), NO_3 (µg mL^{-1}), PO_4 (µg mL^{-1}), plus total organic carbon measurements (TOC, ppm), temperature (°C) and pH.

4.3.2 DNA extraction and 16S rRNA gene sequencing

Samples were stored at 4 °C in the dark at the National Nuclear Laboratory's Central Laboratory facility situated on the Sellafield site (Cumbria, UK) to await DNA extraction due to the significant levels of radioactivity associated with the water. All DNA extractions were carried out in a UV hood, and each sample was passed through a

sterile 0.2 μm filter using a vacuum filtration technique. DNA was then extracted using the MoBio PowerWater DNA isolation kit (MoBio Laboratories, Inc., Carlsbad, CA, USA). All samples were eluted into 100 μL volumes and frozen prior to storage and eventual transfer to the University of Manchester.

4.3.2.1 454-pyrosequencing

The DNA extracted from samples taken in 2014 were analysed using 454-pyrsosequencing of the 16S rRNA gene. The tagged fusion universal bacterial primers 27F (Lane, 1991) and 907R (Muyzer *et al*., 1995), synthesised by IDTdna (Integrated DNA Technologies, BVBA, Leuven, Belgium), were used to perform PCR amplification of the V1-V5 hypervariable regions of the 16S rRNA gene. The fusion forward primer

(5'-AGAGTTTGATCMTGGCTCAGNNNNNNNNNNAGAGTTGATCMTGGCTCA G-3') contained the 454 Life Sciences "Lib-L Primer A", a 4 base "key" sequence (TCAG), a unique ten-base barcode "MID" sequence for each sample, and bacterial primer 27F. The reverse fusion primer (5'- CCGTCAATTCMTTTRAGTTT -3') contained the 454 Life Sciences "Lib-L Primer B", a 4 base "key" sequence (TCAG), and bacterial primer 907R.

The pyrosequencing run was done at the University of Manchester sequencing facility, using a Roche 454 Life Sciences GS Junior system. Qiime 1.8.0 release (Caporaso et al., 2010) was used to analyse the 454-pyrosequencing reads, and during OTU picking (at 97% sequence similarity) with usearch (Edgar, 2010), QIIME performed de-noising and chimera removal. QIIME was used to perform the taxonomic classification of the reads, using the Ribosomal Database Project (RDP) at 90 % confidence threshold (Cole et al., 2009), while the closest GenBank match for the OTUs that contained the highest number of reads (the representative sequence for each OTU was used) was identified by Blastn nucleotide search. In addition, Qiime was used to generate the rarefaction curves.

4.3.2.2 Illumina MiSeq sequencing

The pyrosequencing platform was discontinued in 2015, therefore the Illumina MiSeq sequencing platform was used to sequence samples collected after this time. Samples taken between 2016 and 2017 were analysed to identify the microbial community present in the FGMSP and auxiliary pond by sequencing the 16S rRNA and 18S (Amaral-Zettler *et al*., 2009) rRNA genes, and also the fungal internal transcribed spacer region 2 (ITS2) region (Taylor *et al*., 2016). Sequencing of each set of PCR amplicons from each set of primers (see Supplementary Table 4-1) was conducted with the Illumina MiSeq platform (Illumina, San Diego, CA, USA). All PCR amplifications were carried out in 50 μL reactions, utilising the Roche FastStart High Fidelity PCR system (Roche Diagnostics Ltd, Burgess Hill, UK), using conditions specific for the primer sets used (Supplementary Table 4-1). The SequalPrep Normalization Kit (Fisher Scientific, Loughborough, UK) was used to purify and normalise the PCR products to ~20 ng each. The PCR amplicons from all samples were pooled in equimolar ratios. The run was performed using a 4 pM sample library spiked with 4 pM PhiX to a final concentration of 10 % following the method of Schloss and Kozich (2013).

For the 16S and 18S rRNA gene sequencing runs a sequencing pipeline was used to divide the raw sequences into samples by barcodes (up to one mismatch was permitted). Cutadapt (Martin, 2011), FastQC (Andrews, 2018), and Sickle (Joshi and Fass, 2011) were used to perform quality control and trimming, whilst SPADes (Nurk *et al*., 2013) was used to carry out MiSeq error corrections. Forward and reverse reads were incorporated into full-length sequences with Pandaseq (Masella *et al*., 2012). ChimeraSlayer (Haas *et al*., 2011) was utilised to remove chimeras. The 16S rRNA OTU's generated UPARSE (Edgar, 2013) were classified by Usearch (Edgar, 2010) at the 97 % similarity level, and singletons were removed. VSEARCH (Rognes *et al*., 2016) was used to generate and classify the 18S rRNA OTUs. Rarefaction analysis was conducted using the original detected OTUs in QIIME (Caporaso *et al*., 2010). The RDP classifier, version 2.2 (Wang *et al*., 2007) was used to perform the taxonomic assignment of the 16S rRNA gene data. 18S rRNA gene taxonomic assignment was performed by UCLUST using the Silva119 database (Quast *et al*., 2013)

The fungal ITS2 region data was analysed using the PIPITS automated pipeline (Gweon *et al*., 2015). Reference based chimera detection UCHIME (Edgar *et al*., 2011) in

conjunction with the UNITE UCHIME reference data set was utilised to remove chimeras. The UNITE fungal ITS reference data set and the RDP classifier (Wang *et al*., 2007) were used to perform taxonomic assignment.

4.3.3 qPCR analysis of DNA extracts to determine approximate total microbial numbers

Quantitative PCR (qPCR) of target genes was performed in polypropylene 96-well plates on a Mx3000P qPCR Stratagene System (Agilent Genomics, Headquarters, Santa Clara, CA, United States). The qPCR master mix contained 0.4 µL forward primer 25 µM, 0.4 µL reverse primer 25 µM, 0.4 µL of 1 in 500 diluted ROX reference dye (Agilent Genomics, Headquarters, Santa Clara, CA, United States), 12.5 µL of 2x Brilliant II SYBR green master mix (Agilent Genomics, Headquarters, Santa Clara, CA, United States) and PCR grade water (Roche Diagnostics, Mannheim, Germany) to make up a final volume of 23 µL. Universal primers 1391F and EukBr were used to target the V9 region of 18S rRNA gene (Tanaka *et al*., 2014), and primers 8F and 519R to target the V1-V3 region of 16S rRNA gene (Lane, 1991). Finally 2 µL of the DNA samples was added. A standard curve for qPCR reaction was created by plotting the C_T (cycle threshold) values on serial known dilutions of template DNA. The thermal profile was as follows: Initial denaturing step at 94 ^{0}C for 10 min, followed by 35 cycles of 94 °C for 30 s, 50 °C for 30 s, and 72 °C for 45 s. After 35 cycles a dissociation curve was made for all qPCR products by increasing from 50 °C to 94 °C at a ramp rate of 0.01 °C per second. Each plate included triplicate reactions per DNA sample and the appropriate number of standards. In order to quantify the concentration of target genes, the absolute quantification by the standard-curve (SC) method was used (Brankatschk *et al*., 2012). Baseline and threshold calculations were done by the MxPro–Mx3000P software (Version 3.00, Stratagene, USA).

4.4 Results

4.4.1 General FGMSP pond conditions over study period

Throughout the sampling period, the pH of the pond was maintained at an average pH of 11.4 ± 0.1 (Supplementary Figure 4-1), by continuous purging with caustic dosed demineralised water, which minimises any further corrosion of the fuel and cladding. The temperature of the pond typically shows seasonal variations, with maximum temperatures of ~19 °C recorded during the summer months monitored in this study, whilst the pond temperature dropped to ~8 °C in the winter (Supplementary Figure 4-2). TOC were typically between 6-8 ppm (Supplementary Figure 4-3a), which is consistent with an oligotrophic environment (Bagwell *et al*., 2018). The TOC levels increased 19 ± 15 ppm in late September 2014, three weeks after the end of the bloom, which is most likely to be a result of ingress external organic inputs from the environment or disturbed organics from the pond floor, from pond operations and retrievals. The concentrations of NO_3^-, PO_4^{3-}, and SO_4^{2-} were monitored between July 2014 and December 2016 (Supplementary Figure 4-3). In general, the concentration of NO_3^- remained fairly consistent, with 3 elevated readings recorded, the largest of which was 0.80 μg mL^{-1} on 27th August 2014 during the bloom period, compared to an average NO_3^- concentration of 0.05 μg mL^{-1} (Supplementary Figure 4-3b). The concentrations of PO_4^{3-} showed small-scale fluctuations over the sampling period, with the majority of measurements recorded being below detection limits (<0.00 μg mL^{-1}). Spikes in PO_4^{3-} concentrations can be seen regularly between 2014 and 2016, two of which coincided with the two bloom periods (Supplementary Figure 4-3c). The concentration of SO_4^{2-} also showed consistent low background levels throughout the sampling period, with some spikes in the concentrations observed, particularly during the 2016 bloom period where concentrations reached a maximum of 4.00 μg mL^{-1} (Supplementary Figure 4-3d).

Limited data (not shown) were available for the hydraulically-linked auxiliary pond, since it is a redundant settling tank it is less frequently monitored. In general, the information provided by Sellafield Ltd. indicated that the pH of the pond ranged from pH 9.8-10.9. The concentration of NO_3^- in the pond was higher than observed in the FGMSP, with concentrations ranging from 1.10 to 2.00 μg mL^{-1} between 2016 and 2017. The data collected for the concentrations of PO_4^{3-} were all below the limit of

detection (<0.00 μg mL^{-1}), whilst the SO_4^{2-} concentrations were consistently high, in excess of 5.8 μg mL^{-1}.

4.4.2 Photosynthetic pigment, residence time, and turbidity in the FGMSP during the microbial blooms

The pond is continuously monitored using probes designed to detect the photosynthetic pigments chlorophyll-a (Chl-a) and phycocyanin, which are representative of a broad spectrum of photosynthetic organisms and cyanobacteria, respectively. Background measurements from both the Chl-a and phycocyanin probes showed low levels of fluorescence, suggesting that the abundance of photosynthetic microorganisms and cyanobacteria was low.

In 2014 the average phycocyanin concentration between mid-February and the end of July, prior to the bloom was 0.30 μg L^{-1}, whilst the average Chl-a concentration was 0.30 μg L^{-1} (Supplementary Figure 4-4). The bloom period was deemed to have started by pond operators on the 29th July, with visibility in the pond restored after a six week period. The phycocyanin and Chl-a concentrations increased rapidly over seven-day period (initiated on 29th July) reaching concentrations of 0.56 μg L^{-1} and 0.53 μg L^{-1}, respectively. These concentrations remained stable for a week, with moderate fluctuations during the week of the 5th August, but was followed by a drop in the concentration of both pigments, returning to an average of 0.34 μg L^{-1} phycocyanin and 0.35 μg L^{-1} Chl-a after 6 weeks. During normal plant operations the residence time in the pond is approximately 2 weeks, however during the week of 29th July the purge rate was significantly reduced, resulting in an increase in residence time to approximately 27 weeks (Figure 4-1a). The increase in the phycocyanin and Chl-a pigments occurred a week after the drop in the purge rate. The increased residence time also coincided with an increase in the PO_4^{3-} and NO_3^- concentrations, at 0.03 μg mL^{-1} and 0.17 μg mL^{-1}, respectively, recorded on the 6th August 2014. The temperature of the pond at the start of the bloom was 19.8 °C and gradually fell over the next six weeks to 15.3 °C. Turbidity measurements over the course of the bloom period showed an increase in line with chlorophyll concentrations (Figure 4-2).

The second bloom, which occurred in 2016 was reported to have begun on the 28th July and took four weeks for pond visibility to be restored. Phycocyanin concentrations

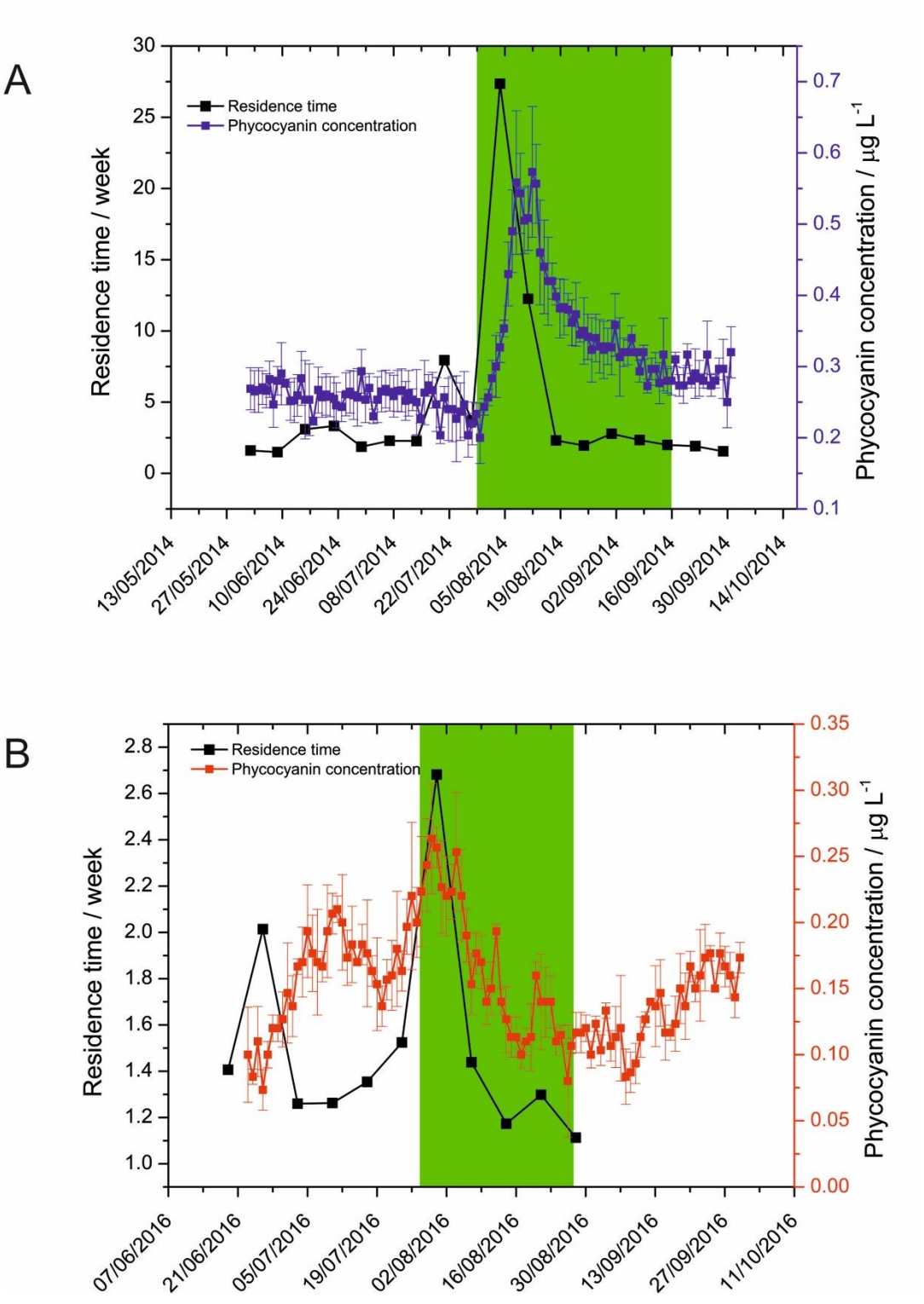

Figure 4-1: Residence time of the purge water plotted against the average phycocyanin concentration (µg L^{-1}) for the FGMSP. A) data collected from 2014; B) data collected from 2016. Error bars denote standard deviation of measurements collected on the day (3+ replicates). Green panel indicates when the microbial blooms were reported.

were consistently lower in 2016 than 2014, with background levels at approximately 0.10 µg L^{-1} (Figure 4-1b). The concentration of phycocyanin increased from the end of

June and then returned to close to background levels by the end of July. From the 19th July a second increase in phycocyanin concentrations could be observed, which reached a maximum of 0.26 μg L^{-1}, and remained at approximately 0.22 μg L^{-1} for six days before gradually returning to background levels. The purge water residence time in the pond was 2 weeks at the point where there was an increase in the phycocyanin concentrations at the end of June. The purge rate was increased for 3 weeks resulting in a residence time of approximately 1.2 weeks, which coincides with the drop in phycocyanin concentration (Figure 4-1b). The purge water residence time increased over the first week of the bloom to 2.7 weeks, with the phycocyanin concentration following the same trend. This suggests that cyanobacteria in the pond were potentially in the early stages of forming a bloom at the end of June, but the increased purge rates limited their impact on pond visibility. Interestingly the PO_4^{3-} and NO_3^- concentrations did not appear to follow the same trend as seen in 2014, as peaks in their concentration were observed as the bloom was declining, according to the phycocyanin concentrations. The temperature during this bloom period was 17.2 °C and remained relatively consistent throughout the 4 weeks the bloom was evident (Supplementary Figure 4-2). The turbidity in the pond during the 2016 bloom period increased in line with the increase in phycocyanin concentration from 28th July onwards (Supplementary Figure 4-5). A reduction in the turbidity was observed over the next two weeks, however there is more variation in the turbidity towards the end of the bloom period, which could be a result of other non-biological particulates which became suspended in the water column, due to pond operations and retrievals.

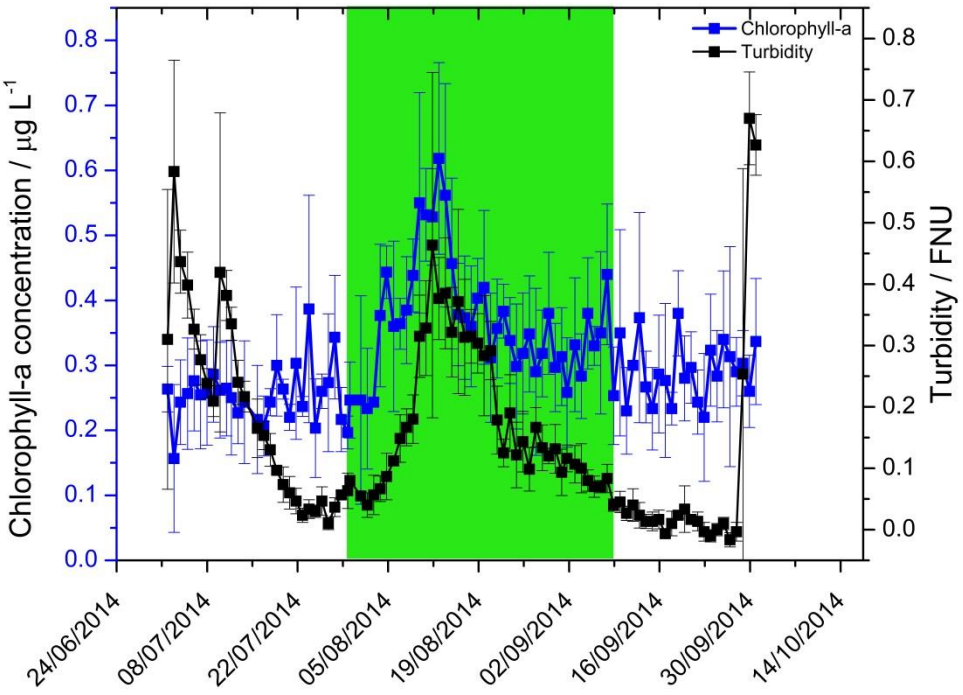

Figure 4-2: Turbidity (black points) and chlorophyll-a (blue points) concentrations measured in the FGMSP from 1st July- 30th September 2014, including a microbial bloom period indicated by the green panel. Error bars denote the standard deviation of 3+ measurements collected each day.

4.4.3 Quantitative polymerase chain reaction (qPCR)

In order to quantify the relative abundance of the prokaryotic and eukaryotic communities, qPCR was run targeting the 16S and 18S rRNA genes (Figure 4-3). The qPCR results showed that in the two samples collected in August 2014 the copy numbers of 16S rRNA genes per mL were 5.36 x 10^6 and 6.61 x 10^6. During the August 2016 bloom the copy number mL^{-1} was higher at 3.37 x 10^7, which is not surprising since this sample was taken earlier on during the bloom period than the 2014 samples were taken (Figure 4-3a). The remaining samples were collected when no loss in visibility was recorded. The September 2016 and June 2017 samples showed a significantly lower copy number of 16S rRNA genes mL^{-1}, at 8.46 x 10^4, 2.63 x 10^5, and 1.53 x10^6. Interestingly the final sample taken in September 2017 indicated that the abundance of prokaryotic organisms was in line with the level seen during the 2016 bloom. There was no obvious turbidity in the water sample that the DNA was extracted from. The 18S rRNA qPCR showed that across all the samples that the abundance of eukaryotic organisms was low, with all readings lower than the prokaryotic copy

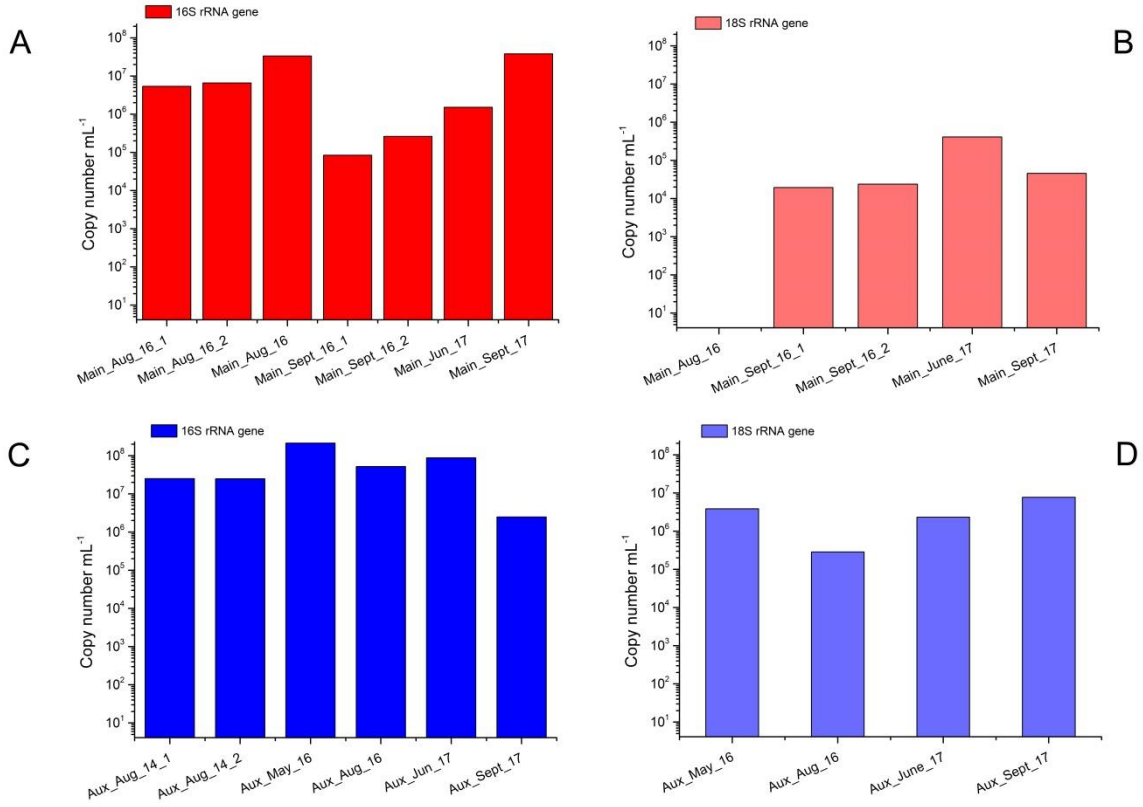

Figure 4-3: qPCR quantification of the copy number of a) 16S rRNA gene from samples collected from the FGMSP; b) 18S rRNA gene from samples collected from the FGMSP; c) 16S rRNA gene from samples collected from the auxiliary pond; and d) 18S rRNA from samples collected from the auxiliary pond.

numbers for the same samples (Figure 4-3b). The maximum copy number of 18S rRNA genes mL^{-1} recorded was in the June 2017 sample at 4.12 x 10^5, which is an order of magnitude less than the corresponding prokaryotic copy number. An estimation of the copy number mL^{-1} was unavailable for the sample from the August 2016 bloom, since the concentration of the DNA was too low, this suggests that the microbial bloom in 2016 was predominantly prokaryotic in nature.

The overall copy number mL^{-1} of prokaryotic and eukaryotic rRNA genes was higher in the auxiliary pond than in the FGMSP (Figure 4-3c). The sample collected in May 2016 had the highest prokaryotic 16S rRNA gene copy number mL^{-1}, 2.14 x 10^8, while the abundance of prokaryotic organisms estimated in the remaining samples were lower. Interestingly the sample collected in September 2017, showed the lowest copy number mL^{-1} for the 16S rRNA gene but the highest estimation for the 18S rRNA gene, 2.50 x 10^6 and 7.75 x 10^6, respectively. The lowest eukaryotic copy number mL^{-1} was recorded in the August 2016 sample, at 2.88 x 10^5 (Figure 4-3d).

4.4.4 Microbial community analysis of 16S rRNA gene of the FGMSP

Guided by the qPCR data, the numerically dominant prokaryotic microbial community composition of 7 samples, collected between August 2014 and September 2017, was determined by amplifying and sequencing the 16S rRNA genes within the samples (Figure 4-4). Three samples were collected when the pond was experiencing microbial blooms and the visibility in the pond was significantly reduced, whilst the remaining "background" samples were taken when no loss in visibility was recorded. The total number of operational taxonomic units (OTUs) present in each of the samples varied and ranged from 43, seen in the sample taken during the 2016 bloom, to 79, taken in June 2017. Rarefaction curves show that the sequencing depth was sufficient for all the samples analysed (Supplementary Figure 4-6).

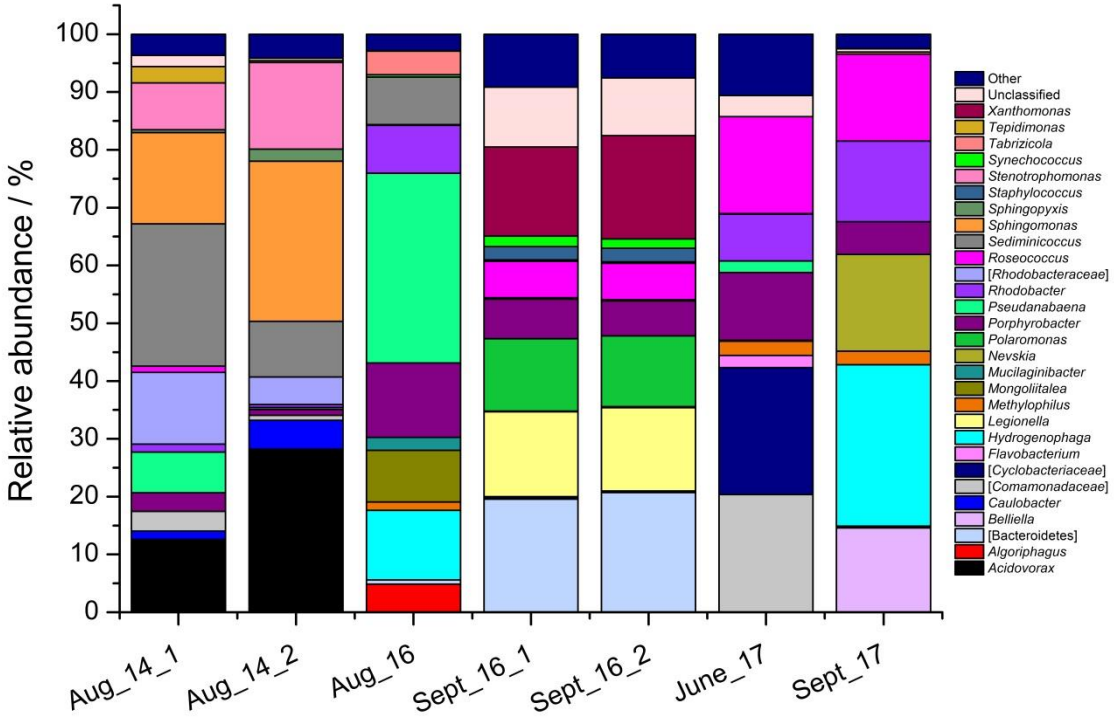

Figure 4-4: Genus-level microbial community comparison of FGMSP samples collected between August 2014 and September 2017, based of 16S rRNA gene sequences. Genera that accounted for 1 % or less of the combined abundance were omitted. Parentheses indicate the last matched taxonomic level of identification, where sequences could not be resolved to genus-level.

Duplicate samples were collected in August 2014 two weeks after the onset of the bloom. The community profile of the two samples showed the same genera present in each sample, however there were differences observed in the relative abundances between the samples. Proteobacteria was the dominant phylum in both samples (88.89 %; 46 OTUs and 97.20 %; 43 OTUs). The most abundant OTUs were affiliated with the following genera; *Acidovorax* (12.58 % and 28.23 %; 3 OTUs); *Sediminicoccus* (24.63 % and 9.66 %; 3 OTUs); *Sphingomonoas* (15.77 % and 27.70 %; 3 OTUs); *Stenotrophomonas* (8.13 % and 14.99 %; 3 OTUs). Additionally, 8 OTUs affiliated with members of the *Rhodobacteriaceae* family accounted for 13.78 % and 5.27 % in the samples. The samples showed significantly different levels in the abundance of OTUs affiliated with cyanobacteria, only one genus of cyanobacteria was detected, namely *Pseudanabaena* (7.02 % and 0.32 %; 2 OTUs).

The August 2016 sample was collected one week after the onset of the microbial bloom. This sample showed the lowest relative abundance of Proteobacteria, at 49.2 % (28 OTUs), whilst Bacteroidetes became more abundant at 16.79 % (7 OTUs). Three OTUs were affiliated with Cyanobacteria and accounted for 33.94 % of the sequences, the most abundant OTU (32.83%) was again most closely affiliated with a member of the *Pseudanabaena* genus, as seen in the 2014 samples. The genera of the remaining OTUs were affiliated with *Synechocystis* (0.40 %) and *Nodosilinea* (0.71 %). Approximately 50% of the community could be described by 8 OTUs that were affiliated with the following genera; *Porphyrobacter* (12.88%, 2 OTUs); *Hydrogenophaga* (12.05 %; 2 OTUs); *Mongoliitalea* (8.94 %; 1 OTUs); *Rhodobacter* (8.29 %; 2 OTUs); and *Sediminicoccus* (8.22 %; 1 OTUs).

Two samples were collected one month after the end of the bloom in 2016; the samples were taken from two different locations in the pond, and showed surprising levels of similarity. Proteobacteria remained the most abundant phylum in both samples accounting for 60.16 % and 61.14 % (36 and 38 OTUs). There were 8 OTUs affiliated with the phylum Bacteroidetes which made up 20.12 % and 21.16 % of the reads. The most abundant OTU could not be identified past the phylum level and accounted for 19.30 % and 20.45 % of the overall community. Firmicutes were present at 2.31 % and 2.38 % (1 OTU), whilst there was also 1 OTU at 4.29 % and 2.99 % that was affiliated with Planctomycetes. Both samples contained the greatest diversity of OTUs that were affiliated with Cyanobacteria (2.67 % and 2.30 %; 8 OTUs). The most abundant OTUs were most closely associated with members of the *Synechococcus* genus (1.82 % and

1.61 %; 2 OTUs). The genus *Pseudanabaena* was once again detected albeit at trace levels (0.05 % and 0.07%; 1 OTU), whilst the remaining OTUs that could be classified down to genus-level belonged to *Leptolyngbya* (0.10 % and 0.07 %; 2 OTUs) and *Geitlerinema* (0.06 % and 0.4 %; 1 OTU). Approximately 50% of the microbial community within the samples could be described by 7 OTUs that were affiliated with 4 genera namely; *Xanthamonas* (15.42 % and 17.87 %, 1 OTU); *Legionella* (14.69 % and 14.40 %, 4 OTUs); *Polaromonas* (12.53 % and 12.27 %, 1 OTU); and *Porphyrobacter* (6.84 % and 6.04 %, 1 OTU).

The background sample collected in June 2017 had a very similar profile at the phylum-level, with Proteobacteria dominating (64.69 %; 37 OTUs); Bacteroidetes accounted for 26.15 % (18 OTUs); Firmicutes were present at 2.72 % (2 OTUs). Cyanobacteria were detected at low levels in the sample (2.21 %; 3 OTUs), with the most abundant OTU again affiliated with the *Pseudanabaena* genus (2.00 % of sample). The most abundant OTU, which made up 20.32 % of the total reads in the sample could only be categorised to the family level, namely *Comamonadaceae*. A further two OTUs affiliated to the *Cyclobacteriaceae* family represented 21.95 % of the sample. A further 36.71 % of the diversity in the sample was accounted for by 5 OTUs, affiliated to 3 genera, which included; *Roseococcus* (16.76 %; 2 OTUs); *Porphyrobacter* (11.74 %; 1 OTU); and *Rhodobacter* (8.21 %; 2 OTUs).

The final sample analysed, which was collected in September 2017, consisted almost entirely of Proteobacteria (83.86%; 32 OTUs) and Bacteroidetes (15.37 %; 13 OTUs). Approximately 94 % of the diversity in the sample was linked to 8 OTUs which were affiliated with 6 genera. The most abundant OTU could be identified as a member of the *Hydrogenophaga* genus (27.90 %). Three of the genera detected had been identified in previous samples taken from the pond, namely; *Roseococcus* (15.06 %, 2 OTUs); *Rhodobacter* (13.93 %; 1 OTU); and *Porphyrobacter* (5.67 %). There were two genera identified in the sample at high abundance that had previously not been observed, these were *Nevskia* (16.72 %; 2 OTUs) and *Belliella* (14.56 %; 1 OTU).

4.4.5 Microbial community analysis of 16S rRNA gene of the auxiliary pond

A total of 6 samples were analysed by the amplification and sequencing of the 16S rRNA gene, to determine the prokaryotic community present in the pond. All samples

were dominated by Proteobacteria, with the duplicate samples taken in August 2014 showing the highest abundance at approximately 91 % in both samples. The samples analysed from 2016 onwards showed more variation at the phylum level with Bacteroidetes comprising a significant fraction of the samples, the highest abundance seen was 40.10 % in May 2016, whilst the abundance was 11.44 % in September 2017. Members of the Verrucomicrobia phylum were present in the samples taken after 2016. The samples collected in August 2014 were similar in their community profile, with dominant genera including; *Acidovorax* (16.67 % and 6.67 %); *Rhodobacter* (18.54 % and 27.74 %); *Sphingomonas* (14.59 % and 8.67 %); and *Stenotrophomonas* (10.20 % and 2.89 %). The samples taken in May and August 2016 showed some similarities with some genera common between the two samples such as *Algoriphagus*; *Porphyrobacter*; and *Prosthecobacter*. The August 2016 sample contained a single OTU that was affiliated with the cyanobacterial genus *Synechococcus* abundant at 2.00 %, whilst the presence of 2 OTUs affiliated with the genus *Legionella* could be observed at 5.20 %. The sample collected in June 2017 contained a large proportion of OTUs that could not be identified at the genus-level (32.22 %), of the OTUs that could be ascribed to a genus the most abundant were; *Flavobacterium* (18.76 %); *Limnohabitans* (9.74 %); and *Polynucleobacter* (7.87 %). The September 2017 sample contained a high percentage of OTUs that could not be identified at the genus-level (28.15 %), and members of the *Polynucleobacter* genus remained in high abundance (15.85 %). OTUs affiliated with members of the Cyanobacteria phylum were largely absent across the samples from the auxiliary pond, with the exception of the September 2017 sample. Here a single OTU accounted for 21.01 % of the sample and was affiliated with the genus *Cyanobium*, whilst a further 4.33 % belonged to other unidentified cyanobacterial groups. Rarefaction curves show that the sequencing depth was sufficient for all the samples analysed (Supplementary Figure 4-6)

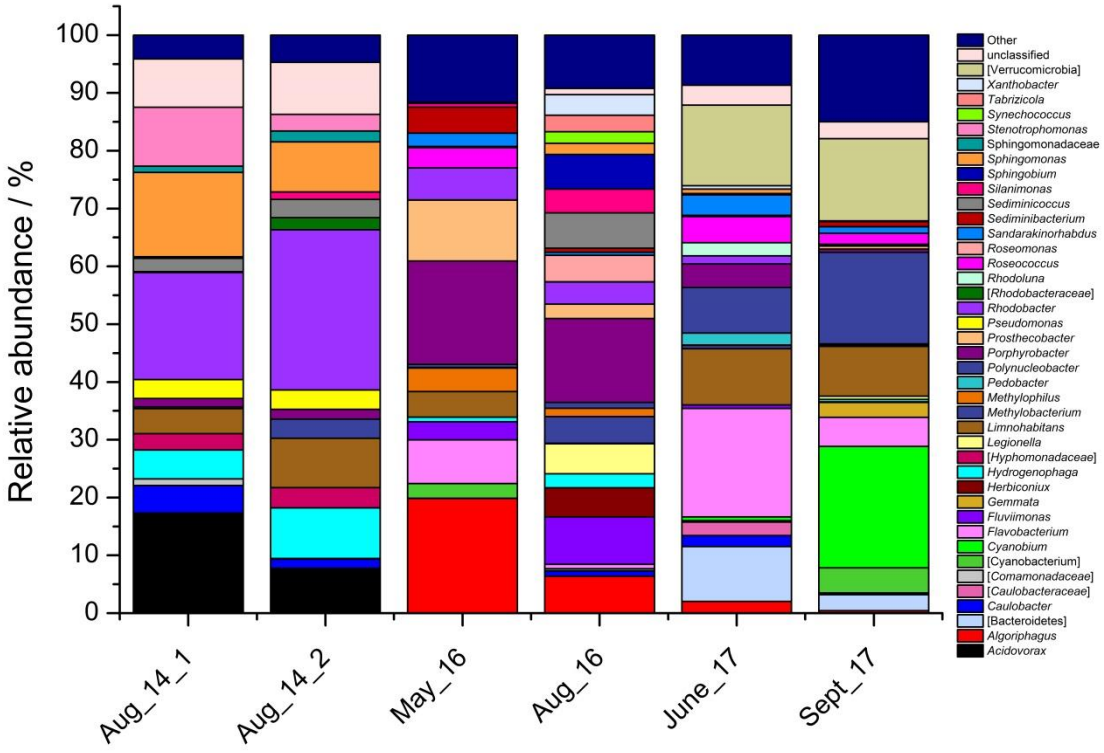

Figure 4-5: Genus-level microbial community comparison of auxiliary pond samples collected between August 2014 and September 2017, based of 16S rRNA gene sequences. Genera that accounted for 1.5 % or less of the combined abundance were omitted. Parentheses indicate the last matched taxonomic level of identification, where sequences could not be resolved to genus-level.

4.4.6 Microbial community analysis of 18S rRNA gene and fungal ITS2-region

In order to characterise the eukaryotic and fungal community profiles of the pond, the 18S rRNA gene and the fungal ITS2 region were amplified and sequenced. Eukaryotes, including fungi, did not appear to be major contributors to the microbial community profile, since the copy number of the 18S rRNA gene was significantly lower in the FGMSP compared to the copy number of the 16S rRNA gene, particularly in regards to the August 2016 bloom sample. Analysis of the sequencing data from both the fungal ITS2 region and the 18S rRNA gene are provided in the supplementary material (Supplementary Figure 4-8 toSupplementary Figure 4-9Supplementary Figure 4-10Supplementary figure 4-11). Rarefaction curves show that the sequencing depth was sufficient for all the samples analysed (Supplementary Figure 4-7)

4.5 Discussion

The First Generation Magnox Storage pond (FGMSP) situated on the Sellafield site is an inhospitable environment, with significant levels of radioactivity and high pH. Despite these conditions the pond is colonised by microorganisms, which are known to form microbial blooms. Here we describe for the first time the composition of the microbial community present in the pond, including fluctuations in the community structure over a 3-year period between 2014 and 2017. This time period included two samples collected during two separate bloom events. In addition, further samples were collected from an auxiliary pond, from which water is occasionally purged into the FGMSP. Analysis of the auxiliary pond's microbial community was used to determine whether the microorganisms inhabiting the pond could be responsible for the colonisation and subsequent blooms observed in the FGMSP.

Collectively the sequencing data and the information regarding the pond conditions throughout the sampling period indicate that the planktonic microbial community colonising the FGMSP is predominantly prokaryotic. The ponds ecosystem is diverse and includes primary photosynthetic colonisers and heterotrophs, including fungi. Interestingly the concentrations of the photosynthetic pigments phycocyanin and Chl-a were consistent with one another in 2014, which suggests that cyanobacteria were the dominant organisms causing the bloom, since elevated levels of eukaryotic algae would result in significantly higher concentrations of Chl-a. Whilst no Chl-a data were available for the August 2016 bloom, qPCR data and phycocyanin concentrations indicate a cyanobacterial-dominated bloom. A single cyanobacterium was identified in the 2014 samples, which were collected in the latter stages of the bloom period, and belonged to the genus *Pseudanabaena*. A member of this genus was the dominant OTU in the August 2016 sample, and could be observed at low levels in the samples collected in September 2016 and June 2017. The results suggest that *Pseudanabaena* is a persistent organism in the pond, and contributes to the cyanobacterial blooms observed. Low levels (<0.8 %) of two other cyanobacterial genera were observed in the 2016 bloom, the extent to which these cyanobacteria contributed to the bloom cannot be fully determined from a single sample. Correlations between the concentration of PO_4^{3-} and phycocyanin are apparent in the 2014 data, however such trends are not apparent in the 2016 data, which suggests that PO_4^{3-} concentrations were not controlling biomass levels. The phycocyanin concentrations increased prior to the onset of the July 2016

bloom, indicating cyanobacterial growth, which could have limited the accumulation of PO_4^{3-} in the water. The residence time in the pond shows strong correlations to the concentration of phycocyanin, providing evidence that continuous purging is effective at keeping the cyanobacterial population low. The data show that the cyanobacteria present in the pond are able to respond quickly to reductions in the purge rate, forming blooms that are sufficient to restrict visibility.

There were 3 proteobacterial genera that were present in all of the FGMSP samples analysed, namely *Porphyrobacter*, *Rhodobacter* and *Roseococcus*, suggesting species of these genera are persistent in the pond. These bacteria are pigmented and contain bacteriochlorophyll-a and a variety of carotenoids (Boldareva *et al*., 2009; Glaeser and Klug, 2005; Hanada *et al*., 1997; Hiraishi *et al*., 2002; Willett *et al*., 2007; Yurkov *et al*., 1994), which have antioxidant properties and could facilitate their persistence in the pond. Differences in the microbial community were observed between the samples collected at different time points, which implies that the background microbial community is dynamic and subject to seasonal variations. In contrast the microbial community profile appears to be more diverse in the auxiliary pond in comparison to the FGMSP and also contains a more consistent background prokaryotic community, with 10 genera being present in all four samples. The lack of consistency in the microbial community in the FGMSP could be a result of the continuous purging, which restricts the long-term colonisation of pelagic microorganisms. The persistence of the *Pseudanabaena* genus in the FGMSP could be explained by the formation of cyanobacterial biofilms or mats which are established in more static regions or to surfaces within the pond. With the exception of the high levels of *Cyanobium* present in the September 2017 sample, the auxiliary pond appeared to be largely devoid of cyanobacteria, with no OTUs ascribed to the *Pseudanabaena* genus. The lack of abundant cyanobacterial OTUs in the auxiliary pond suggests that the source of the bloom forming cyanobacteria in the FGMSP is unlikely to be a result in the transfer of water between these ponds. Similarities between the prokaryotic community profiles of the two ponds can be observed for example with species of *Porphyrobacter*, *Rhodobacter*, and *Roseococcus*, however all the overall 16S rRNA community profiles of the two ponds appear to be distinct. The extent to which the introduction of water from the auxiliary pond into the FGMSP affected the microbial community is debatable, for example *Legionella* species were detected in the FGMSP in September 2016, having only been observed in the auxiliary pond sample collected in August of the same year.

According to the data collected in this study, eukaryotic organisms were significantly less abundant in the FGMSP compared to that seen in the auxiliary pond. The higher levels of radioactivity, elevated pH, and continuous purge of the FGMSP with caustic dosed demineralised water are plausible explanations for the low abundance of eukaryotic organisms (Goldman *et al*., 1982).

Pseudanabaena species make up a group of small filamentous cyanobacteria, with simple morphology, and cells that are longer than wide and unable to differentiate (Acinas *et al*., 2009). Reports of *Pseudanabaena* in the scientific literature are limited, although they have previously been reported as part of cyanobacterial blooms (Bertos-Fortis *et al*., 2016; Bukowska *et al*., 2017) and have been found in some extreme environments (Zhu *et al*., 2015), such as in the closed cryoconite holes in the Antarctic (Webster-Brown *et al*., 2015). Whilst there are reports of *Pseudanabaena* species in cyanobacterial blooms, there is little information relating to their physiology or metabolic capabilities (Acinas *et al*., 2009). Some members of the *Pseudanabaena* genus are capable of complementary chromatic adaptation (CCA) (Acinas *et al*., 2009), in which the organism is able to adjust the structure of the phycobilisomes to optimize the transfer of light energy to the photosystem II reaction centres in response to different light conditions (Kehoe and Gutu, 2006). It is not known whether the *Pseudanabaena* species that colonise the pond have the capacity for CCA, however if they do this could provide them with a competitive advantage in varying light conditions.

The indigenous microbial communities of several other SNFPs have been studied recently, of which the most intensively studied pond is located in Confrentes, Spain. Here there have been several studies that have relied on culture-dependent assessments, on the native bacterial community to form biofilms on steel coupons in the pond. The biofilm forming organisms included the following genera; *Burkholderia*, *Bacillus*, *Nocardia, and Microbacterium* (Chicote *et al*., 2004; Chicote *et al*., 2005, Sarró *et a*l., 2003; Sarró *et al*., 2005, Sarró *et al*., 2007). Biofilm forming organisms not only present a biofouling problem but also the potential for microbial induced corrosion, which could result in damage fuel containers and other inventory in the pond, resulting in increased levels of radiation (Chicote *et al*., 2005; Diósi *et al*., 2003; Masurat *et al*., 2005). Interestingly several other genera were identified in the Confrentes SNFP that were also detected in the waters of the FGMSP at Sellafield, namely; *Stenotrophomonas*, *Pseudomonas*, and *Staphylococcus* (Chicote *et al*., 2005). Whether organisms such as these are forming biofilms in the Sellafield pond has yet to be determined, however it is

likely that a fraction of the microbial community in the pond exists as part of a biofilm. *Pseudanabaena* species have also been identified in biofilms and cyanobacterial mats in natural water bodies (Sorokovikova *et al*., 2008; Sorokovikova *et al*., 2013), and their presence in a biofilm e.g. on the pond walls, could help explain their persistence. Other studies looking at different SNFPs have identified a range of organisms for example, Bagwell *et al* (2018) determined the dominance of members of the families *Burkholderiaceae*, *Nitrospiraceae*, *Hyphomicrobiaceae* and *Comamonadaceae*.

Whilst most studies have identified prokaryotic organisms, there is evidence that eukaryotic organisms are prevalent, and in some cases dominant in SNFPs. The green microalga *Haematococcus pluvialis* has recently been identified as the dominant organism responsible for microbial blooms which occur in another SNFP on the Sellafield Ltd. site that is maintained at a neutral pH (MeGraw *et al*., 2018). The ability of *H. pluvialis* to colonise the pond was attributed to its ability to synthesise and accumulate the carotenoid astaxanthin, which is known to have antioxidant properties (Li *et al*., 2008; Wada *et al*., 2013; Wang *et al*., 2003; Wang *et al*., 2014). The adaptive processes that members of the *Pseudanabaena* genus utilise have yet to be determined, but clearly warrant investigation. Rivasseau *et al* (2010; 2013; 2016) showed further evidence of eukaryotic organisms present in a research SNFP in France, with the identification of the green microalgae species *Coccomyxa actinabiotis*. The organism was isolated and was found to be capable of accumulating large quantities of radionuclides and fission products intracellularly (Rivasseau *et al*., 2013). The ability to remove radionuclides and fission products from aquatic environments is of interest for remediation efforts both in engineered environments and at sites where radioactive contamination has occurred (Fukuda *et al*., 2014; Gadd, 1990). Members of the *Pseudanabaena* genus could be candidate organisms for the remediation of fission products and other radionuclides, since their presence in the pond suggests they are tolerant to highly radioactive environments. Further work investigating the interaction of this genus of cyanobacteria and radionuclides is ongoing.

4.6 Conclusion

The FGMSP is a unique environment with a combination of high background levels of radioactivity and high pH ~11.4, despite these conditions microorganisms are able to

thrive within the pond. Two microbial bloom samples photosynthetic component has been shown to be dominated by a single cyanobacterial genus, *Pseudanabaena*. The onset of the microbial bloom containing this cyanobacterium appears to be triggered by the reduction of the purge rate, allowing their growth to flourish and reduce the visibility within the pond. Once the purge rate is re-established, the abundance of the blooming microorganisms is managed and restored to background levels. Further work is required to determine the critical rates of the purge at which *Pseudanabaena* species are capable of forming a bloom and what adaptive processes these organisms utilise to withstand the inhospitable conditions within the pond. Further strategies to control the cyanobacterial growth in the pond can be trialled in the laboratory, with specific reference to *Pseudanabaena* species responses. The microbial communities of SNFPs appear to be unique to the site and conditions of the individual ponds. Comparisons between the 16S rRNA gene microbial community profile of the two ponds in this study showed limited similarities, although more frequent sampling and analysis is required to better determine the full extent of these observations. Here we present members of the genus *Pseudanabaena* as potential candidate for the remediation of radionuclides, however this needs to be studied to determine their suitability.

4.7 Acknowledgements

LF was supported by an EPSRC PhD CASE Studentship (Grant number EP/G037426/1) with Sellafield Ltd. We would also like to thank Sellafield Ltd. for providing the samples and detailed pond data. In addition we would like to thank staff at NNLs Central Laboratory for assistance with handling and transferring the samples.

4.8 References

Acinas, S.G., Haverkamp, T.H., Huisman, J., Stal, L.J., 2009. Phenotypic and genetic diversification of *Pseudanabaena* spp. (cyanobacteria). ISME J. 378, 31–46. https://doi.org/10.1038/ismej.2008.78

Amaral-Zettler, L.A., McCliment, E.A., Ducklow, H.W., Huse, S.M., 2009. A method for studying protistan diversity using massively parallel sequencing of V9 hypervariable regions of small-subunit ribosomal RNA Genes. PLoS One 4, 1–9. https://doi.org/10.1371/journal.pone.0006372

Andrews, S. FastQC. *Babraham Bioinformatics* (2018). Available at: https://www.bioinformatics.babraham.ac.uk/projects/fastqc/. (Accessed: 19th June 2018)

Ashworth, H., Abrahamsen-Mills, L., Bryan, N., Foster, L., Lloyd, J.R., Kellet, S., Heath, S.L., 2018. Effect of humic acid and bacterial exudates on sorption-desorption interactions of ^{90}Sr with brucite. Environ. Sci. Process. Impacts Accepted m. https://doi.org/10.1039/b816135f

Avery, S. V., Codd, G.A., Gadd, G.M., 1992. Caesium transport in the cyanobacterium *Anabaena variabilis*: Kinetics and evidence for uptake via ammonium transport system(s). FEMS Microbiol. Lett. 95, 253–258. https://doi.org/10.1016/0378-1097(92)90438-T

Avery, S. V, Codd, G., Gadd, M., 1992. Replacement of cellular potassium by caesium in *Chlorella emersonii*: differential sensitivity of photoautotrophic and chemoheterotrophic growth. J. Gen. Microbiol. 138, 69–76.

Badri, H., Monsieurs, P., Coninx, I., Wattiez, R., Leys, N., 2015. Molecular investigation of the radiation resistance of edible cyanobacterium *Arthrospira* sp. PCC 8005. Microbiologyopen 4, 187–207. https://doi.org/10.1002/mbo3.229

Bagwell, C.E., Noble, P.A., Milliken, C.E., Li, D., Kaplan, D.I., 2018. Amplicon sequencing reveals microbiological signatures in spent nuclear fuel storage basins. Front. Microbiol. 9, 1–12. https://doi.org/10.3389/fmicb.2018.00377

Bertos-Fortis, M., Farnelid, H.M., Lindh, M. V., Casini, M., Andersson, A., Pinhassi, J., Legrand, C., 2016. Unscrambling cyanobacteria community dynamics related to environmental factors. Front. Microbiol. 7, 1–13. https://doi.org/10.3389/fmicb.2016.00625

Billi, D., Friedmann, E.I., Hofer, K.G., Caiola, M.G., Ocampo-Friedmann, R., 2000. Ionizing-radiation resistance in the desiccation-tolerant cyanobacterium *Chroococcidiopsis*. Appl. Environ. Microbiol. 66, 1489–1492.

Billi, D., Potts, M., 2002. Life and death of dried prokaryotes. Res. Microbiol. 153, 7–12. https://doi.org/10.1016/S0923-2508(01)01279-7

Blanco-Rivero, A., Leganés, F., Fernández-Valiente, E., Calle, P., Fernández-Piñas, F., 2005. *mrpA*, a gene with roles in resistance to Na+ and adaptation to alkaline pH in the cyanobacterium *Anabaena* sp. PCC7120. Microbiology 151, 1671–1682. https://doi.org/10.1099/mic.0.27848-0

Boldareva, E.N., Tourova, T.P., Kolganova, T. V., Moskalenko, A.A., Makhneva, Z.K., Gorlenko, V.M., 2009. *Roseococcus suduntuyensis* sp. nov., a new aerobic bacteriochlorophyll a-containing bacterium isolated from a low-mineralized soda lake of Eastern Siberia. Microbiology 78, 92–101. https://doi.org/10.1134/S0026261709010123

Brankatschk, R., Bodenhausen, N., Zeyer, J., Burgmann, H., 2012. Simple absolute quantification method correcting for quantitative PCR efficiency variations for microbial community samples. Appl. Environ. Microbiol. 78, 4481–4489. https://doi.org/10.1128/AEM.07878-11

Bruhn, D.F., Frank, S.M., Roberto, F.F., Pinhero, P.J., Johnson, S.G., 2009. Microbial biofilm growth on irradiated, spent nuclear fuel cladding. J. Nucl. Mater. 384, 140–145. https://doi.org/10.1016/j.jnucmat.2008.11.008

Bukowska, A., Kaliński, T., Koper, M., Kostrzewska-Szlakowska, I., Kwiatowski, J., Mazur-Marzec, H., Jasser, I., 2017. Predicting blooms of toxic cyanobacteria in eutrophic lakes with diverse cyanobacterial communities. Sci. Rep. 7, 1–12. https://doi.org/10.1038/s41598-017-08701-8

Caporaso, J.G., Kuczynski, J., Stombaugh, J., Bittinger, K., Bushman, F.D., Costello, E.K., Fierer, N., Peña, A.G., Goodrich, J.K., Gordon, J.I., Huttley, G. a, Kelley, S.T., Knights, D., Koenig, J.E., Ley, R.E., Lozupone, C. a, Mcdonald, D., Muegge, B.D., Pirrung, M., Reeder, J., Sevinsky, J.R., Turnbaugh, P.J., Walters, W. a, Widmann, J., Yatsunenko, T., Zaneveld, J., Knight, R., 2010. correspondence QIIME allows analysis of high- throughput community sequencing data Intensity normalization improves color calling in SOLiD sequencing. Nat. Publ. Gr. 7, 335–336. https://doi.org/10.1038/nmeth0510-335

Caporaso, J.G., Lauber, C.L., Walters, W.A., Berg-Lyons, D., Huntley, J., Fierer, N., Owens, S.M., Betley, J., Fraser, L., Bauer, M., Gormley, N., Gilbert, J.A., Smith, G., Knight, R., 2012. Ultra-high-throughput microbial community analysis on the Illumina HiSeq and MiSeq platforms. ISME J. 6, 1621–1624. https://doi.org/10.1038/ismej.2012.8

Caporaso, J.G., Lauber, C.L., Walters, W.A., Berg-Lyons, D., Lozupone, C.A., Turnbaugh, P.J., Fierer, N., Knight, R., 2011. Global patterns of 16S rRNA diversity at a depth of millions of sequences per sample. Proc. Natl. Acad. Sci. 108, 4516–4522. https://doi.org/10.1073/pnas.1000080107

Chen, Y.C., 2011. The hormesis of the green macroalga *Ulva fasciata* with low-dose 60cobalt gamma radiation. J. Phycol. 47, 939–943. https://doi.org/10.1111/j.1529-8817.2011.01018.x

Chicote, E., García, A.M., Moreno, D.A., Sarró, M.I., Lorenzo, P.I., Montero, F., 2005. Isolation and identification of bacteria from spent nuclear fuel pools. J. Ind. Microbiol. Biotechnol. 32, 155–162. https://doi.org/10.1007/s10295-005-0216-3

Chicote, E., Moreno, D. a, García, A.M., Sarró, M.I., Lorenzo, P.I., Montero, F., 2004. Biofouling on the walls of a spent nuclear fuel pool with radioactive ultrapure water. Biofouling 20, 35–42. https://doi.org/10.1080/08927010410001662670

Cole, J.R., Wang, Q., Cardenas, E., Fish, J., Chai, B., Farris, R.J., Kulam-Syed-Mohideen, A.S., McGarrell, D.M., Marsh, T., Garrity, G.M., Tiedje, J.M., 2009. The Ribosomal Database Project: Improved alignments and new tools for rRNA

analysis. Nucleic Acids Res. 37, 141–145. https://doi.org/10.1093/nar/gkn879

Crossland, I., 2012. Nuclear fuel cycle science and engineering, 1st ed. Woodhead Publishing, Philadelphia.

Daly, M.J., 2009. A new perspective on radiation resistance based on *Deinococcus radiodurans*. Nat. Rev. Microbiol. 7, 237–245. https://doi.org/10.1038/nrmicro2073

Daly, M.J., Gaidamakova, E.K., Matrosova, V.Y., Vasilenko, A., Zhai, M., Venkateswaran, A., Hess, M., Omelchenko, M. V, Kostandarithes, H.M., Makarova, K.S., Wackett, L.P., Friedrickson, J.K., Ghosal, R., 2004. Accumulation of Mn (II) in *Deinococcus radiodurans* facilitates gamma-radiation resistance. Science 306, 1025–28. https://doi.org/10.1126/science.1103185

Dekker, L., Osborne, T.H., Santini, J.M., 2014. Isolation and identification of cobalt- and caesium-resistant bacteria from a nuclear fuel storage pond. FEMS Microbiol. Lett. 359, 81–84. https://doi.org/10.1111/1574-6968.12562

Diósi, G., Telegdi, J., Farkas, G., Gazsó, L.G., Bokori, E., 2003. Corrosion influenced by biofilms during wet nuclear waste storage. Int. Biodeterior. Biodegrad. 51, 151–156. https://doi.org/10.1016/S0964-8305(02)00138-5

Edgar, R.C., 2013. UPARSE: Highly accurate OTU sequences from microbial amplicon reads. Nat. Methods 10, 996–998. https://doi.org/10.1038/nmeth.2604

Edgar, R.C., 2010. Search and clustering orders of magnitude faster than BLAST. Bioinformatics 26, 2460–2461. https://doi.org/10.1093/bioinformatics/btq461

Edgar, R.C., Haas, B.J., Clemente, J.C., Quince, C., Knight, R., 2011. UCHIME improves sensitivity and speed of chimera detection. Bioinformatics 27, 2194–2200. https://doi.org/10.1093/bioinformatics/btr381

El-Fatah Abomohra, A., El-Shouny, W., Sharaf, M., Abo-Eleneen, M., 2016. Effect of gamma radiation on growth and metabolic activities of *Arthrospira platensis*. Brazilian Arch. Biol. Technol. 59, 1–12. https://doi.org/10.1590/1678-4324-2016150476

Fukuda, S. ya, Iwamoto, K., Atsumi, M., Yokoyama, A., Nakayama, T., Ishida, K. ichiro, Inouye, I., Shiraiwa, Y., 2014. Global searches for microalgae and aquatic plants that can eliminate radioactive cesium, iodine and strontium from the radio-polluted aquatic environment: A bioremediation strategy. J. Plant Res. 127, 79–89. https://doi.org/10.1007/s10265-013-0596-9

Gadd, G.M., 2004. Microbial influence on metal mobility and application for bioremediation. Geoderma 122, 109–119. https://doi.org/10.1016/j.geoderma.2004.01.002

Gadd, G.M., 1990. Heavy metal accumulation by bacteria and other microorganisms. Experientia 46, 834–840. https://doi.org/10.1007/BF01935534

Glaeser, J., Klug, G., 2005. Photo-oxidative stress in *Rhodobacter sphaeroides*: Protective role of carotenoids and expression of selected genes. Microbiology 151, 1927–1938. https://doi.org/10.1099/mic.0.027789-0

Goldman, J.C., Azov, Y., Riley, C.B., Dennett, M.R., 1982. The effect of pH in intensive microalgal cultures. I. Biomass regulation. J. Exp. Mar. Bio. Ecol. 57, 1–13. https://doi.org/10.1016/0022-0981(82)90140-X

Gregson, C.R., Goddard, D.T., Sarsfield, M.J., Taylor, R.J., 2011a. Combined electron microscopy and vibrational spectroscopy study of corroded Magnox sludge from a legacy spent nuclear fuel storage pond. J. Nucl. Mater. 412, 145–156. https://doi.org/10.1016/j.jnucmat.2011.02.046

Gregson, C.R., Hastings, J.J., Sims, H.E., Steele, H.M., Taylor, R.J., 2011b. Characterisation of plutonium species in alkaline liquors sampled from a UK legacy nuclear fuel storage pond. Anal. Methods 3, 1957. https://doi.org/10.1039/c1ay05313b

Gweon, H.S., Oliver, A., Taylor, J., Booth, T., Gibbs, M., Read, D.S., Griffiths, R.I., Schonrogge, K., 2015. PIPITS: An automated pipeline for analyses of fungal internal transcribed spacer sequences from the Illumina sequencing platform. Methods Ecol. Evol. 6, 973–980. https://doi.org/10.1111/2041-210X.12399

Haas, B.J., Gevers, D., Earl, A.M., Feldgarden, M., Ward, D. V, Giannoukos, G., Ciulla, D., Tabbaa, D., Highlander, S.K., Sodergren, E., Methé, B., DeSantis, T.Z., The Human Microbiome Consortium, Petrosino, J.F., Knight, R., Birren, B.W., 2011. Chimeric 16S rRNA sequence formation and detection in Sanger and 454-Pyrosequenced PCR amplicons. Genome Res. 21, 494–504. https://doi.org/10.1101/gr.112730.110.Freely

Hanada, S., Kawase, Y., Hiraishi, A., Takaichi, S., Matsuura, K., Shimada, K., Nagashima, K. V, 1997. *Porphyrobacter tepidarius* sp. nov., a moderately thermophilic aerobic photosynthetic bacterium isolated from a hot spring. Int. J. Syst. Bacteriol. 47, 408–413. https://doi.org/10.1099/00207713-47-2-408

Hiraishi, A., Yonemitsu, Y., Matsushita, M., Shin, Y., Kuraishi, H., Kawahara, K., 2002. Characterization of *Porphyrobacter sanguineus* sp. nov., an aerobic bacteriochlorophyll-containing bacterium capable of degrading biphenyl and dibenzofuran. Arch. Microbiol. 178, 45–52. https://doi.org/10.1007/s00203-002-0423-5

Jackson, S.F., Monk, S.D., Riaz, Z., 2014. An investigation towards real time dose rate monitoring, and fuel rod detection in a First Generation Magnox Storage Pond (FGMSP). Appl. Radiat. Isot. 94, 254–259. https://doi.org/10.1016/j.apradiso.2014.08.019

Jensen, S.E., Nønbel, E., 1999. Description of the Magnox Type of Gas Cooled Reactor (MAGNOX).

Jolivet, E., Matsunaga, F., Ishino, Y., Forterre, P., Prieur, D., Myllykallio, H., 2003. Physiological responses of the hyperthermophilic archaeon " *Pyrococcus abyssi* " to DNA Damage Caused by ionizing radiation. J. Bacteriol. 185, 3958–3961. https://doi.org/10.1128/JB.185.13.3958

Joshi, N.A., Fass, F.N., 2011. Sickle: a sliding-window, adaptive, quality-based trimming tool for FastQ files (version 1.33). [Software].

Karley, D., Shukla, S.K., Rao, T.S., 2017. Isolation and characterization of culturable bacteria present in the spent nuclear fuel pool water. Environ. Sci. Pollut. Res. 1–

9. https://doi.org/10.1007/s11356-017-0376-5

Kehoe, D.M., Gutu, A., 2006. Responding to color: the regulation of complementary chromatic adaptation. Annu. Rev. Plant Biol. 57, 127–150. https://doi.org/10.1146/annurev.arplant.57.032905.105215

Kozich, J.J., Westcott, S.L., Baxter, N.T., Highlander, S.K., Schloss, P.D., 2013. Development of a dual-index sequencing strategy and curation pipeline for analyzing amplicon sequence data on the MiSeq Illumina sequencing platform. Appl. Environ. Microbiol. 79, 5112–5120. https://doi.org/10.1128/AEM.01043-13

Lane, D.J., 1991. Nucleic acid techniques in bacterial systematics. John Wiley & Sons, Ltd, New York.

Li, Y., Sommerfeld, M., Chen, F., Hu, Q., 2008. Consumption of oxygen by astaxanthin biosynthesis: A protective mechanism against oxidative stress in *Haematococcus pluvialis* (Chlorophyceae). J. Plant Physiol. 165, 1783–1797. https://doi.org/10.1016/j.jplph.2007.12.007

Martin, M., 2011. Cutadapt removes adapter sequences from high-throughput sequencing reads. EMBnet.journal 17, 10. https://doi.org/10.14806/ej.17.1.200

Masella, A.P., Bartram, A.K., Truszkowski, J.M., Brown, D.G., Neufeld, J.D., 2012. PANDAseq: PAired-eND assembler for Illumina sequences. BMC Bioinformatics 13, 1–7. https://doi.org/10.1186/1471-2105-13-31

Masurat, P., Fru, E.C., Pedersen, K., 2005. Identification of *Meiothermus* as the dominant genus in a storage system for spent nuclear fuel. J. Appl. Microbiol. 98, 727–740. https://doi.org/10.1111/j.1365-2672.2004.02519.x

MeGraw, V.E., Brown, A.R., Boothman, C., Goodacre, R., Morris, K., Sigee, D., Anderson, L., Lloyd, J.R., 2018. A novel adaptation mechanism underpinning algal colonization of a nuclear fuel storage pond. MBio 9, 1–15. https://doi.org/10.1128/mBio.02395-17

Muyzer, G., Teske, A., Wirsen, C.O., Jannasch, H.W., 1995. Phylogenetic relationships of *Thiomicrospira* species and their identification in deep-sea hydrothermal vent samples by denaturing gradient gel-electrophoresis of 16S rDNA fragments. Arch. Microbiol. 164, 165–172. https://doi.org/10.1007/bf02529967

NDA, 2016. Nuclear Decommissioning Authority: Business plan 2017 to 2020 [WWW Document]. Gov.uk. URL https://www.gov.uk/government/consultations/nuclear-decommissioning-authority-business-plan-2017-to-2020 (accessed 5.4.18).

Nurk, S., Bankevich, A., Antipov, D., Gurevich, A., Korobeynikov, A., Lapidus, A., Prjibelsky, A., Pyshkin, A., Sirotkin, A., Sirotkin, Y., Stepanauskas, R., McLean, J., Lasken, R., Clingenpeel, S.R., Woyke, T., Tesler, G., Alekseyev, M.A., Pevzner, P.A., 2013. Assembling genomes and mini-metagenomes from highly chimeric reads, in: Conference: Proceedings of the 17th International Conference on Research in Computational Molecular Biology, RECOMB 2013. Bejing, China, pp. 158–170. https://doi.org/10.1007/978-3-642-37195-0_13

Pikuta, E. V., Hoover, R.B., Tang, J., 2007. Microbial extremophiles at the limits of life.

Crit. Rev. Microbiol. 33, 183–209. https://doi.org/10.1080/10408410701451948

Quast, C., Pruesse, E., Yilmaz, P., Gerken, J., Schweer, T., Yarza, P., Peplies, J., Glöckner, F.O., 2013. The SILVA ribosomal RNA gene database project: Improved data processing and web-based tools. Nucleic Acids Res. 41, 590–596. https://doi.org/10.1093/nar/gks1219

Rivasseau, C., Farhi, E., Atteia, A., Couté, A., Gromova, M., de Gouvion Saint Cyr, D., Boisson, A.-M.M., Féret, A.-S., Compagnon, E., Bligny, R., 2013. An extremely radioresistant green eukaryote for radionuclide bio-decontamination in the nuclear industry. Energy Environ. Sci. 6, 1230–1239. https://doi.org/Doi 10.1039/C2ee23129h

Rivasseau, C., Farhi, E., Compagnon, E., de Gouvion Saint Cyr, D., van Lis, R., Falconet, D., Kuntz, M., Atteia, A., Couté, A., 2016. *Coccomyxa actinabiotis* sp. nov. (Trebouxiophyceae, Chlorophyta), a new green microalga living in the spent fuel cooling pool of a nuclear reactor. J. Phycol. 52, 689–703. https://doi.org/10.1111/jpy.12442

Rivasseau, C., Farhi, E., Gromova, M., Ollivier, J., Bligny, R., 2010. Resistance to irradiation of micro-algae growing in the storage pools of a nuclear reactor investigated by NMR and neutron spectroscopies. Spectroscopy 24, 381–385. https://doi.org/10.3233/SPE-2010-0459

Rognes, T., Flouri, T., Nichols, B., Quince, C., Mahé, F., 2016. VSEARCH: a versatile open source tool for metagenomics. PeerJ 4, e2584. https://doi.org/10.7717/peerj.2584

Sarró, M.I., García, A.M., Moreno, D.A., 2005. Biofilm formation in spent nuclear fuel pools and bioremediation of radioactive water. Int. Microbiol. 8, 223–230. https://doi.org/im2305032 [pii]

Sarró, M.I., García, A.M., Moreno, D.A., Montero, F., 2007. Development and characterization of biofilms on stainless steel and titanium in spent nuclear fuel pools. J. Ind. Microbiol. Biotechnol. 34, 433–441. https://doi.org/10.1007/s10295-007-0215-7

Sarró, M.I., Moreno, D.A., Chicote, E., Lorenzo, P.I., García, A.M., Montero, F., 2003. Biofouling on austenitic stainless steels in spent nuclear fuel pools. Mater. Corros. Und Korrosion 54, 535–540. https://doi.org/DOI 10.1002/maco.200390117

Sellafield, 2014. Sellafield magazine [WWW Document]. URL https://www.gov.uk/government/publications/sellafield-magazine-issue-4 (accessed 5.30.18).

Singh, H., Anurag, K., Apte, S.K., 2013. High radiation and desiccation tolerance of nitrogen-fixing cultures of the cyanobacterium *Anabaena* sp. strain PCC 7120 emanates from genome/proteome repair capabilities. Photosynth. Res. 118, 71–81. https://doi.org/10.1007/s11120-013-9936-9

Sorokovikova, E.G., Belykh, O.I., Gladkikh, A.S., Kotsar, O. V., Tikhonova, I. V., Timoshkin, O.A., Parfenova, V. V., 2013. Diversity of cyanobacterial species and phylotypes in biofilms from the littoral zone of Lake Baikal. J. Microbiol. 51, 757–765. https://doi.org/10.1007/s12275-013-3240-4

Sorokovikova, E.G., Tikhonova, I. V., Belykh, O.I., Klimenkov, I. V., Likhoshwai, E. V., 2008. Identification of two cyanobacterial strains isolated from the Kotel'nikovskii hot spring of the Baikal rift. Microbiology 77, 365–372. https://doi.org/10.1134/S002626170803017X

Tanaka, R., Hino, A., Tsai, I.J., Palomares-Rius, J.E., Yoshida, A., Ogura, Y., Hayashi, T., Maruyama, H., Kikuchi, T., 2014. Assessment of helminth biodiversity in wild rats using 18S rDNA based metagenomics. PLoS One 9. https://doi.org/10.1371/journal.pone.0110769

Taylor, D.L., Walters, W.A., Lennon, N.J., Bochicchio, J., Krohn, A., Caporaso, J.G., Pennanen, T., 2016. Accurate estimation of fungal diversity and abundance through improved lineage-specific primers optimized for Illumina amplicon sequencing. Appl. Environ. Microbiol. 82, 7217–7226. https://doi.org/10.1128/AEM.02576-16.Editor

Wada, N., Sakamoto, T., Matsugo, S., 2013. Multiple roles of photosynthetic and sunscreen pigments in cyanobacteria focusing on the oxidative stress. Metabolites 3, 463–483. https://doi.org/10.3390/metabo3020463

Wang, B., Zarka, A., Trebst, A., Boussiba, S., 2003. Astaxanthin accumulation in *Haematococcus pluvialis* (Chlorophyceae) as an active photoprotective process under high irradiance. J. Phycol. 39, 1116–1124. https://doi.org/10.1111/j.0022-3646.2003.03-043.x

Wang, B., Zhang, Z., Hu, Q., Sommerfeld, M., Lu, Y., Han, D., 2014. Cellular capacities for high-light acclimation and changing lipid profiles across life cycle stages of the green alga *Haematococcus pluvialis*. PLoS One 9. https://doi.org/10.1371/journal.pone.0106679

Wang, Q., Garrity, G.M., Tiedje, J.M., Cole, J.R., 2007. Naïve Bayesian classifier for rapid assignment of rRNA sequences into the new bacterial taxonomy. Appl. Environ. Microbiol. 73, 5261–5267. https://doi.org/10.1128/AEM.00062-07

Webster-Brown, J.G., Hawes, I., Jungblut, A.D., Wood, S.A., Christenson, H.K., 2015. The effects of entombment on water chemistry and bacterial assemblages in closed cryoconite holes on Antarctic glaciers. FEMS Microbiol. Ecol. 91, 1–14. https://doi.org/10.1093/femsec/fiv144

Willett, J., Smart, J.L., Bauer, C.E., 2007. RegA control of bacteriochlorophyll and carotenoid synthesis in *Rhodobacter capsulatus*. J. Bacteriol. 189, 7765–7773. https://doi.org/10.1128/JB.00853-07

Wilson, P.D., 1996. The nuclear fuel cycle from ore to waste. Oxford University Press, Oxford.

Yurkov, V., Stackebrandt, E., Holmes, A., Fuerst, J.A., Hugenholtz, P., Golecki, J., Gad'on, N., Gorlenk, V.M., 1994. Phylogenetic positions of novel aerobic , bacteriochlorophyll a-containing bacteria and description of *Roseococcus thiosulfatophilus* gen . nov ., sp . nov ., *Erythromicrobium ramosum* gen . nov ., sp . nov ., and Erythrobacter litoralis. Int. J. Syst. Bacteriol. 427–434.

Zhu, M., Yu, G., Song, G., Chang, J., Wan, C., Li, R., 2015. Molecular specificity and detection for *Pseudanabaena* (cyanobacteria) species based on *rbcLX* sequences. Biochem. Syst. Ecol. 60, 110–115. https://doi.org/10.1016/j.bse.2015.04.009

4.9 Supplementary material:

Supplementary Table 4-1: Details of the fungal ITS2 region, and the 16S and 18S rRNA gene targets

Target	Read length	Forward primers	Reverse primers	PCR cycling conditions
16S rRNA V4 hyper variable region	2 × 250-bp paired-end sequencing (Illumina) (Caporaso et al., 2012, 2011)	515F, 5′-GTGYCAGCMGCCGCGGTAA-3′	806R, 5′-GGACTACHVGGGTWTCTAAT-3′	initial denaturation at 95°C for 2 min, followed by 36 cycles of 95 °C for 30 s, 55 °C for 30 s, 72 °C for 1 min, and a final extension step of 5 min at 72 °C
18S rRNA	2 × 250-bp paired-end sequencing (Illumina)(Amaral-Zettler et al., 2009)	forward primer, 1391F, 5′-GTACACACCGCCCGTC-3′	reverse primer, EukBR, 5′-TGATCCTTCTGCAGGTTCACCTAC-3′	initial denaturation at 95°C for 2 min, followed by 36 cycles of 95°C for 30 s, 57°C for 30 s, 72°C for 1 min, and a final extension step of 5 min at 72°C

Fungal ITS2 internal transcribed spacer region between the large subunit (LSU) and the 5.8S ribosomal genes	2 × 300-bp paired-end sequencing (Illumina)(Caporaso et al., 2011)	forward primer, ITS4F, 5′-AGCCTCCGCTTATTGATATGCTTAART-3′	reverse primer, 5.8SR, 5′-AACTTTYRRCAAYGGATCWCT-3′;)(Taylor et al., 2016)	initial denaturation at 95°C for 2 min, followed by 36 cycles of 95°C for 30 s, 56°C for 45 s, 72°C for 2 min, and a final extension step of 5 min at 72°C

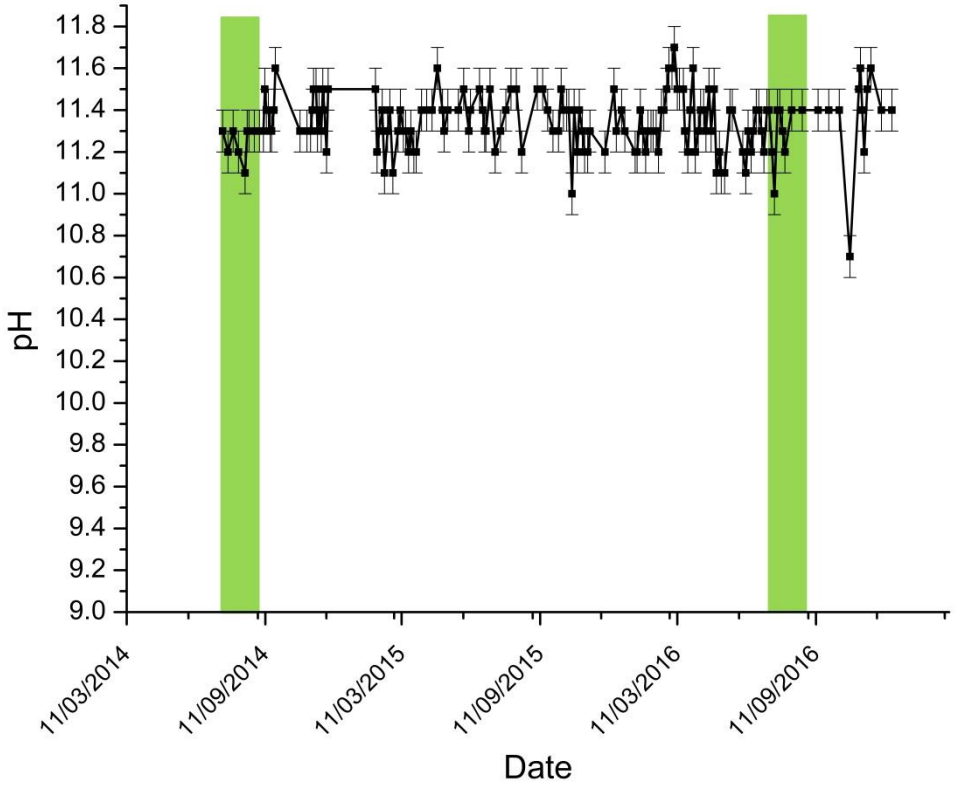

Supplementary Figure 4-1: The pH of the FGMSP between August 2014 and December 2016. Green panels indicate when the two microbial bloom events occurred. Green panels indicate the microbial bloom periods. Error bars indicate the standard deviation of multiple measurements throughout the day (>3).

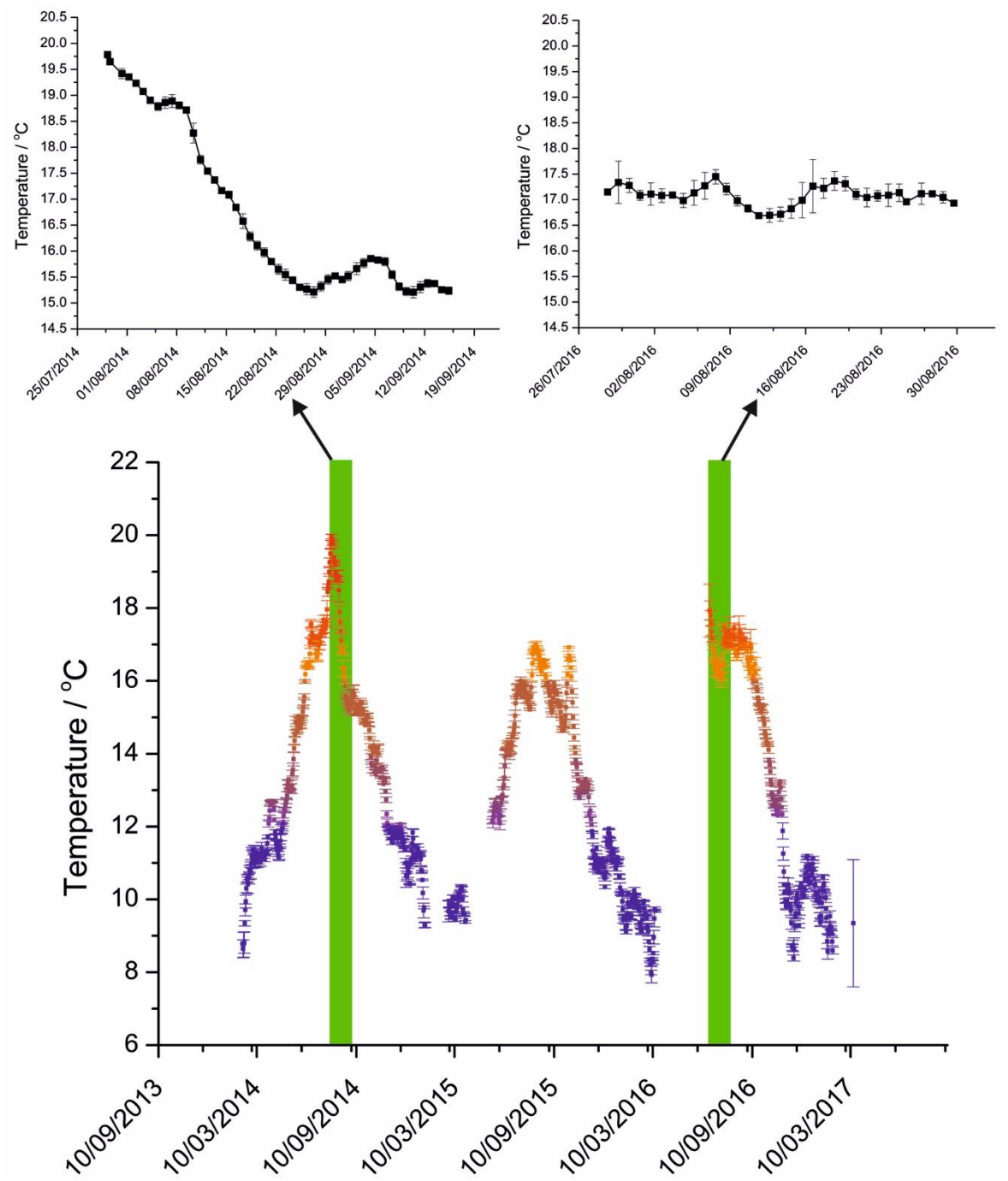

Supplementary Figure 4-2: Temperature of the FGMSP recorded between February 2014 and March 2017, showing seasonal variations. Green panels indicate the temperature of the pond during the two microbial bloom periods, with blown up regions of the recorded temperatures. Error bars indicate the standard deviation of multiple measurements throughout the day (>3).

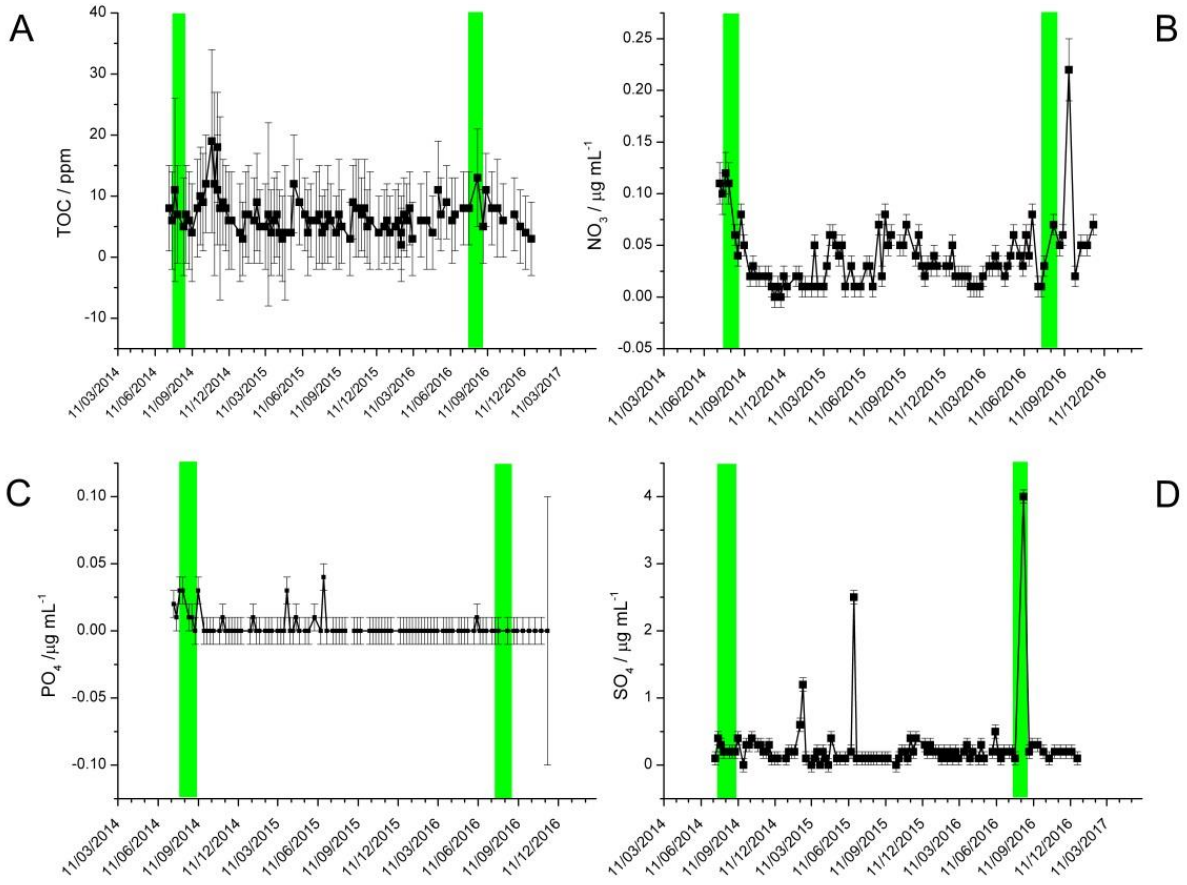

Supplementary Figure 4-3: The averaged measurements collected from the FGMSP throughout the sampling period for: a) Total organic carbon (TOC) in ppm; b) average NO_3^- concentrations (µg mL^{-1}); c) average PO_4^{3-} concentrations (µg mL^{-1}) ; and d) average SO_4^{2-} concentrations (µg mL^{-1}). Green panels indicate the two microbial bloom periods. Error bars indicate the standard deviation of multiple measurements throughout the day (>3).

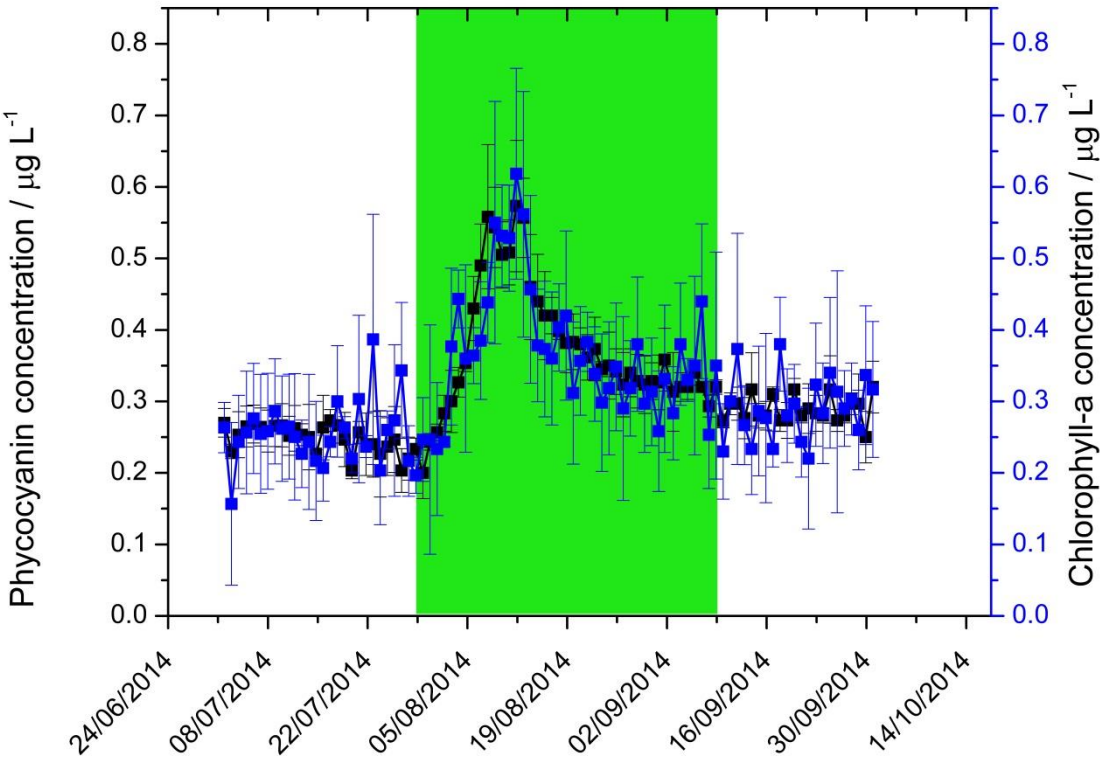

Supplementary Figure 4-4: Phycocyanin (black points) and chlorophyll-a (blue points) concentrations measured in the FGMSP from 1st July- 30th September 2014, including a microbial bloom period indicated by the green panel. Error bars denote the standard deviation of 3+ measurements collected each day.

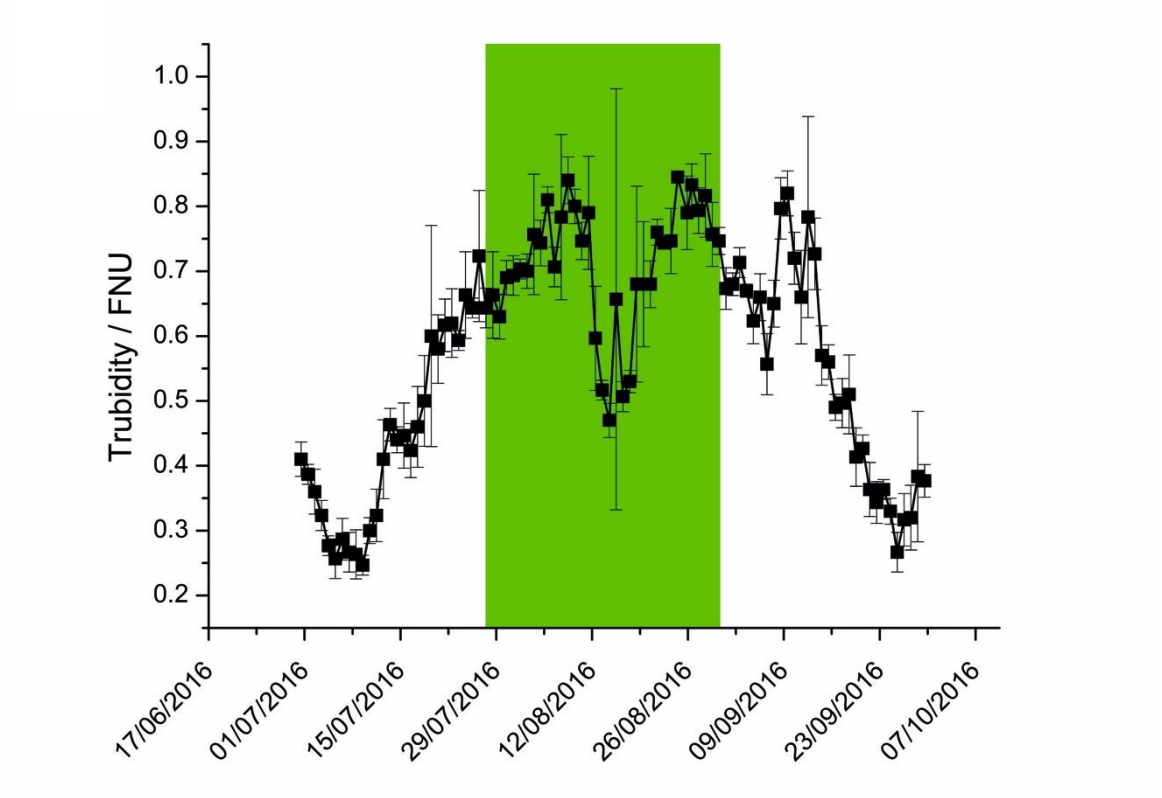

Supplementary Figure 4-5: Average turbidity measurements recorded in the FGMSP during the August 2016 microbial bloom period. Green panel indicate the microbial bloom period. Error bars indicate the standard deviation of multiple measurements throughout the day (>3).

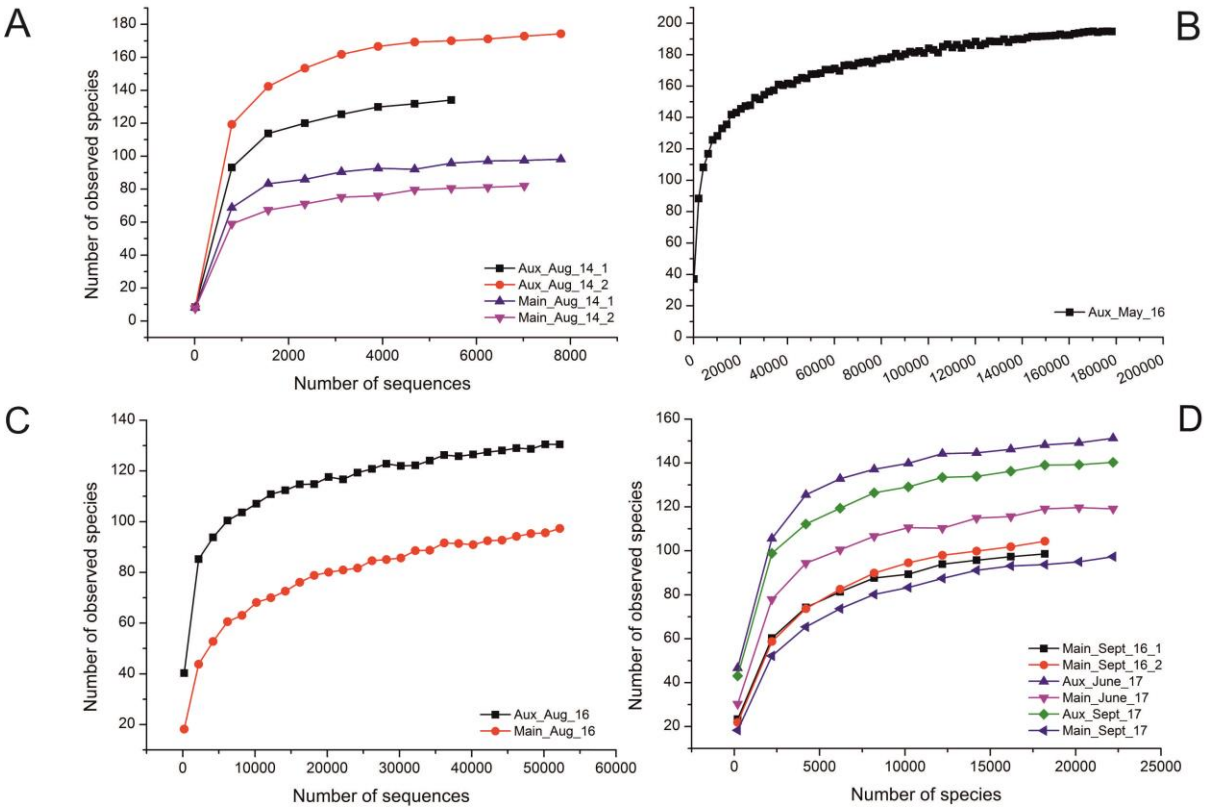

Supplementary Figure 4-6: Rarefaction curves for all sequencing runs; a) auxiliary pond and FGMSP samples collected in August 2014; b) auxiliary pond sample collected May 2016; c) auxiliary pond and FGMSP samples collected August 2016; and d) auxiliary pond and FGMSP samples collected in 2017.

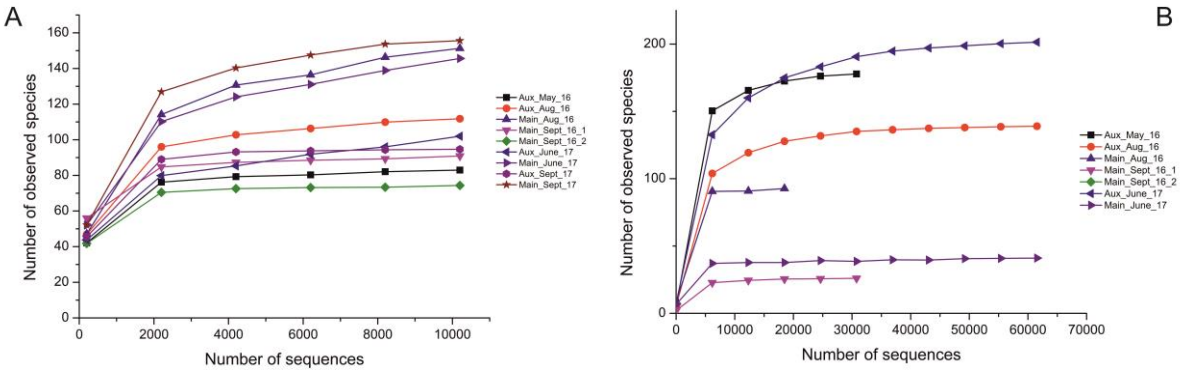

Supplementary Figure 4-7: Rarefaction curves for; a) all 18S rRNA sequencing runs for all auxiliary pond and FGMSP samples; and b) all fungal ITS2 sequencing runs for all auxiliary pond and FGMSP samples.

4.9.1 18S rRNA gene community analysis of the FGMSP

Since no eukaryotic DNA was detected in the August 2014 samples, only 5 samples from 2016 and 2017 were analysed. The results showed that each of the samples had different overall eukaryotic community profiles when compared at the class-level (Supplementary Figure 4-8). During the August 2016 bloom, the most abundant grouping was affiliated with the Chrysophyceae class (47.80 %), a group of golden algae commonly found in freshwater environments. Other relatively abundant groupings belonged to Bicosoecida (17.57 %), Heterolobosea (9.75 %) and Saccharomycetes (9.25 %). The samples taken in September 2016, showed almost identical 16S rRNA profiles, however the 18S rRNA sequences for the two samples were remarkably different to one another, suggesting that there is a varied eukaryotic community across the pond. The sample collected in June 2017 was broadly similar to the August 2016 sample with the same affiliations present, although differences in the relative abundances were observed. The most abundant grouping in June 2017 was affiliated with an unknown fungal species present at 43.06 % of the sample compared to just 3.27 % in August 2016. The September 2017 sample was distinct from the previous samples with the 4 groupings, previously not detected accounting for 94.25 %, namely; *Apiales* (33.55 %); Dothideomycetes (13.26 %); Eurotiomycetes (28.52 %); and Trebouxiophyceae (18.92 %).

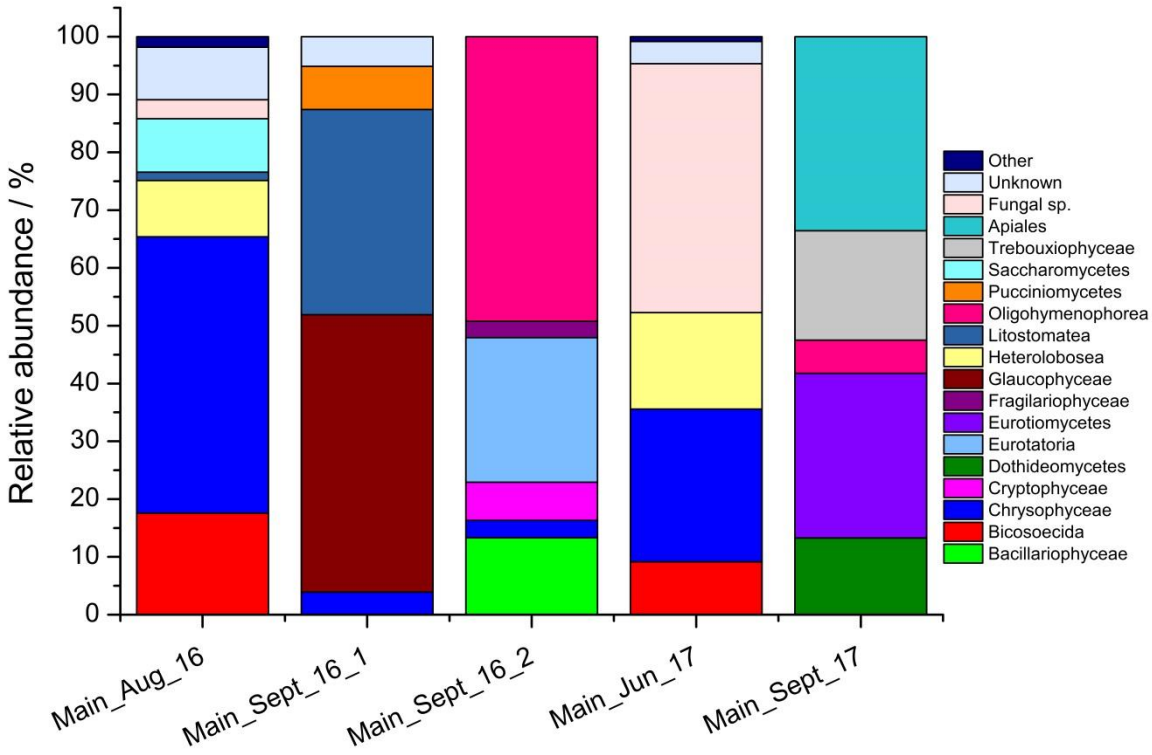

Supplementary Figure 4-8: Class-level microbial community comparison of FGMSP samples collected between August 2016 and September 2017, based of 18S rRNA gene sequences.

4.9.2 Fungal ITS2 region community analysis of the FGMSP

Four samples were analysed to determine the fungal community profile (Supplementary Figure 4-9). The results of the sequencing showed a high level of variation between the samples, with only one genus common across all samples, which was affiliated with the *Cladosporium* genus, albeit at different relative abundances. The sample collected in August 2016 was the most diverse with 38 groups that could be affiliated to genus-level from a total of 66 OTUs. Members belonging to the *Phoma* genus were the most abundant fungal sequences that could be identified to this taxonomic level, accounting for 12.54 % of the sample whilst a single OTU affiliated with the *Botrytis* genus accounted for 7.14 %. The samples collected in September 2016 consisted of 16 and 18 OTUs, with 9 and 11 genera able to be identified. Despite being collected at the same time these samples showed very little similarity as seen with the 18S rRNA sequencing, likely due to the different sampling locations. One of the September 2016 samples was

dominated by a single OTU that was affiliated with the genus *Leptobacillium*, accounting for 87.96 %, but this genus was not present in the second sample. The fungal community identified in the June 2017 sample was dominated by OTUs that could not be identified at any taxonomic level (43.51 %), with a further 24.17 % consisting of OTUs affiliated with the genus *Fusarium*.

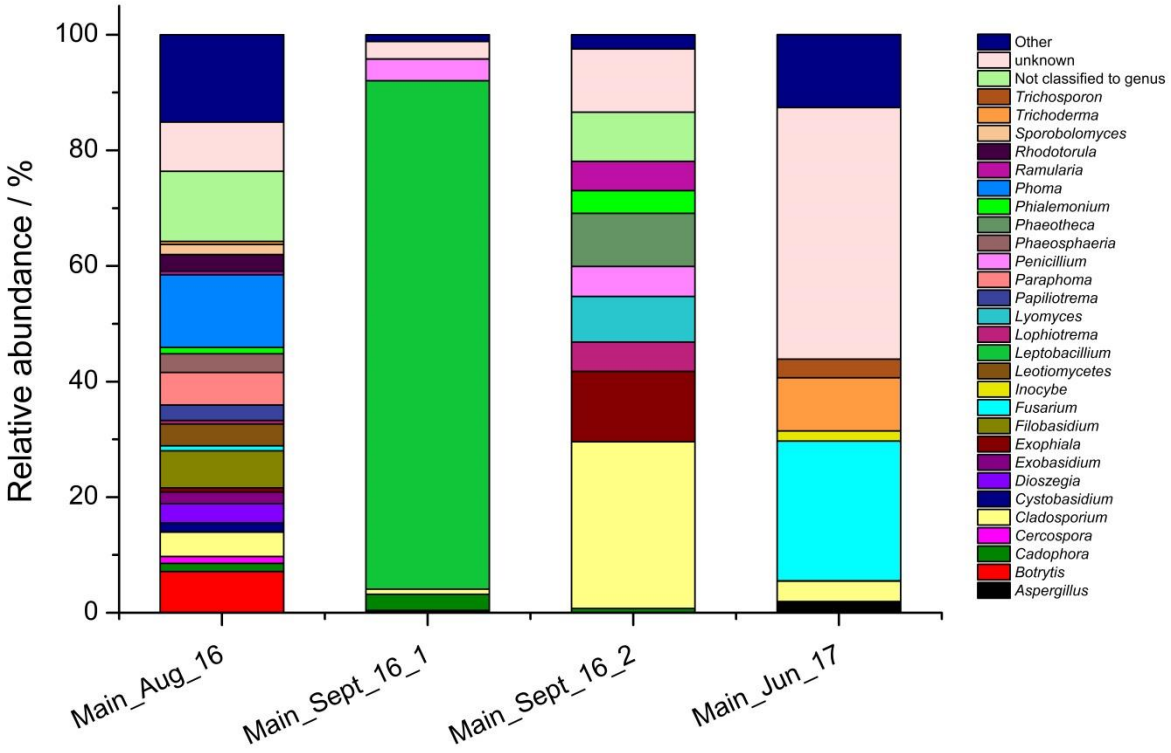

Supplementary Figure 4-9: Genus-level microbial community comparison of FGMSP samples collected between August 2016 and June 2017, based of fungal ITS2 region sequences. Genera that accounted for 1 % or less of the combined abundance were omitted.

4.9.3 18S rRNA gene community analysis of the auxiliary pond

The 18S rRNA gene community profile of 4-samples, collected between May 2016 and September 2017, were analysed at the class-level (Supplementary Figure 4-10). The sample collected in May 2016 was dominated by members of the Chrysophyceae class (30.06 %), with other abundant groups affiliated with member of Aphelidea (16.72 %), Dinophyceae (9.55 %), and Eustigmatophyceae (11.30%). The majority of the OTUs in the August 2016 sample could not be ascribed to any known eukaryotic organism (47.94 %). Of the OTUs that could be assigned to a class, the most abundant were as

follows; Chrysophyceae (11.88 %); Eurotiomycetes (10.13 %); Eustigmatophyceae (9.61 %); and Gleomeromycetes (11.56 %). The 18S rRNA community profile of the June 2017 auxiliary pond sample was very similar to the profile of the corresponding sample taken in from the FGMSP at the same time. The community profile of the June auxiliary pond included: Chrysophyceae 23.34 %, Heterobolosea comprised 15.19 %, and Bicosoecida 12.93 %. The most abundant grouping was affiliated with an unknown fungal species present at 45.17 %. Bicosoecida was the most dominant class of eukaryotic organisms in the September 2017 sample at 41.26 %, whilst 36.21 % of the sample was affiliated with an unknown fungal species. A further 16.86 % of the sample could be described by a further 8 class, the most abundant of which were Trebouxiophyceae (5.38 %); Discosea (4.11 %), and Heterolobosea (2.63 %).

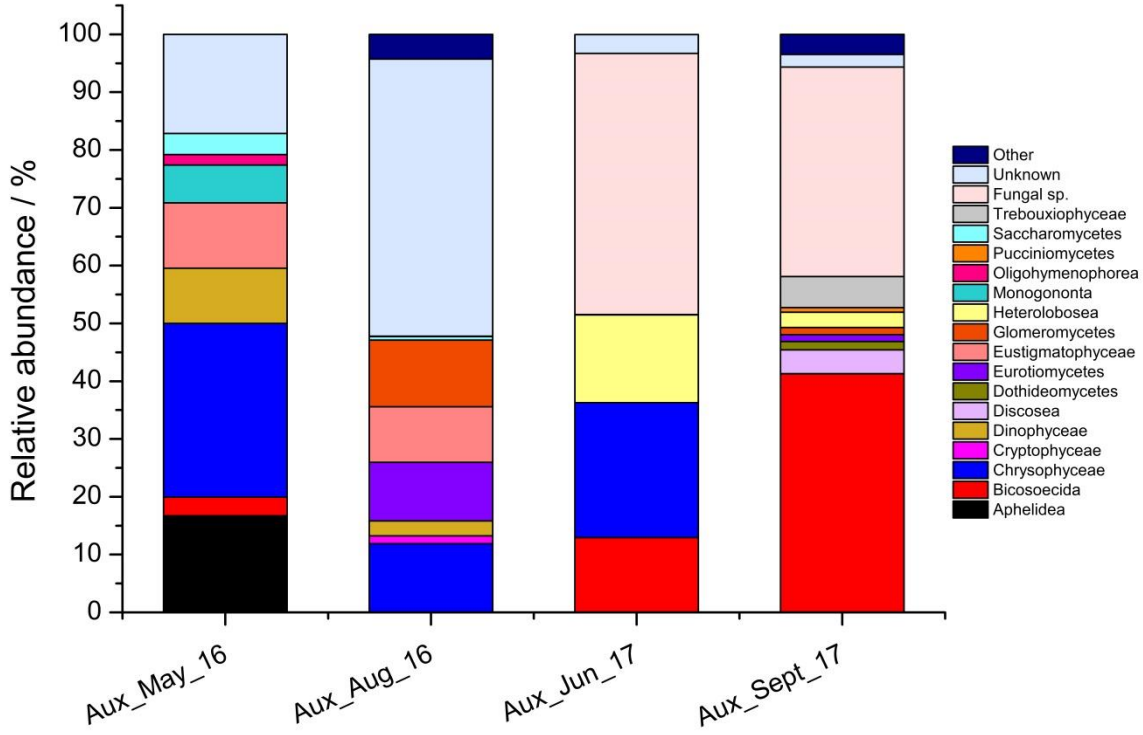

Supplementary Figure 4-10: Class-level microbial community comparison of the auxiliary pond samples collected between May 2016 and September 2017, based of 18S rRNA gene sequences.

4.9.4 Fungal ITS2 region community analysis of the auxiliary pond

Three samples collected from the auxiliary pond had the fungal community profile analysed following the amplification and sequencing of the ITS2 region (Supplementary figure 4-11). The May 2016 sample was dominated by a single OTU affiliated with the *Cladosporium* genus (43.29 %), a further 19.89 % could be accounted for by another single OTU affiliated with the *Botrytis* genus. The fungal community profile of the August 2016 sample was significantly different to that seen in the sample taken 3 months earlier. The majority of the OTUs present in the sample could not be identified at any taxonomic level (46.78 %), whilst the most abundant OTUs that could be identified at the genus-level were affiliated with *Cadophora* (33.46 %) and *Exophialia* (9.48 %). The fungal community present in the June 2017 sample was more diverse, although *Cadophora* and *Exophialia* remained the most abundant genera at 16.49 % and 11.01 %, respectively. A further 15 genera could explain 43.67 % of the samples diversity, the most abundant of which were: *Ramularia* (7.15 %); *Cordyceps* (6.43 %); *Cryptococcus* (5.09 %); *Hypocreales* (4.14 %); *Penicillium* (4.08 %); and *Phoma* (4.55 %).

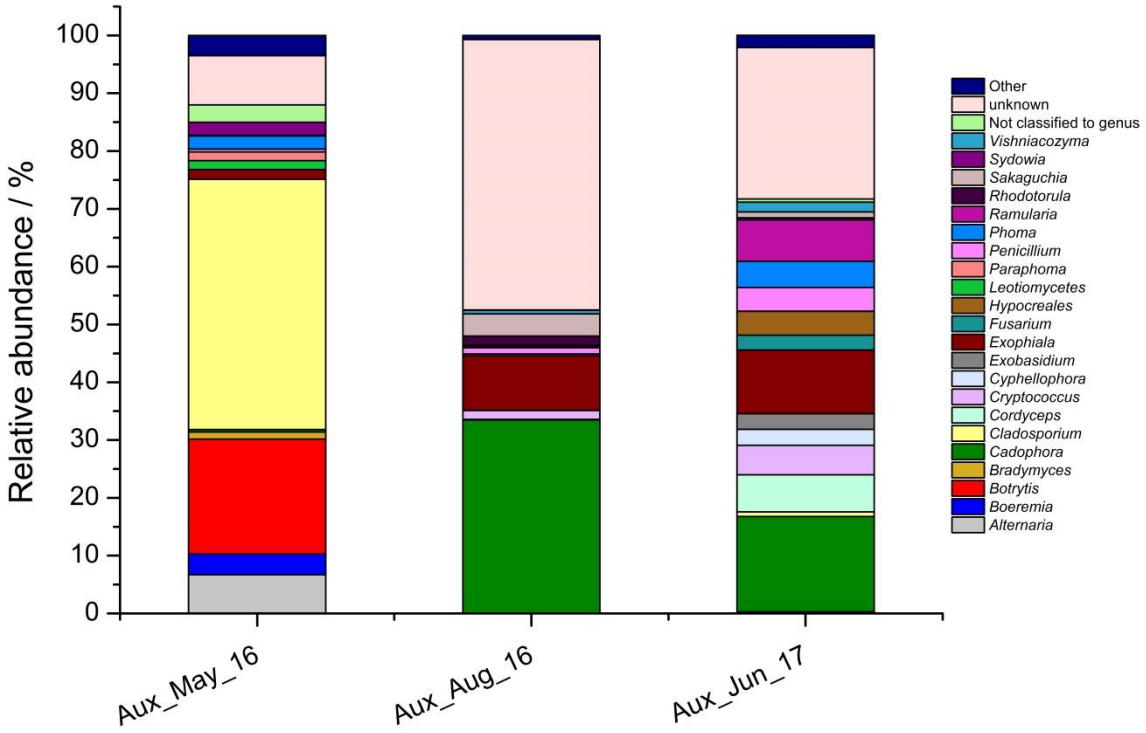

Supplementary figure 4-11: Genus-level microbial community comparison of auxiliary pond samples collected between May 2016 and June 2017, based of fungal ITS2 sequences. Genera that accounted for 1 % or less of the combined abundance were omitted.

Chapter 5

Research chapter 5: The effect of X-irradiation on the growth and metabolic status of *Pseudanabaena catenata*

5 Research Chapter 5: The effect of X-irradiation on the growth and metabolic status of *Pseudanabaena catenata*

Lynn Foster[1], Howbeer Muhamadali[2], Christopher Boothman[1], David Sigee[1], Jon K Pittman[1], Royston Goodacre[2], Katherine Morris[1], and Jonathan R Lloyd[1*]

[1] Research Centre for Radwaste Disposal and Williamson Research Centre for Molecular Environmental Science, School of Earth and Environmental Sciences, The University of Manchester, Oxford Road, Manchester M13 9PL, U.K.

[2] Manchester Institute of Biotechnology, School of Chemistry, The University of Manchester, Manchester M1 7DN, U.K.

Keywords: Cyanobacteria, FT-IR spectroscopy, metabolic fingerprint, radiation, polysaccharide, spent nuclear fuel pond

5.1 Abstract

Recently a species of *Pseudanabaena* was identified as the dominant organism during a bloom event in a high pH (pH ~11.4), radioactive spent nuclear fuel pond (SNFP) at the Sellafield Ltd. UK facility. The metabolic response of a laboratory culture containing the cyanobacterium *Pseudanabaena catenata,* representative of the major photosynthetic microorganism found in the SNFP, to X-irradiation was studied to identify potential survival strategies used to support colonisation of radioactive environments. Growth was monitored and the metabolic fingerprints of the cultures, during irradiation and throughout the post-irradiation recovery period, were determined using Fourier transform infrared (FT-IR) spectroscopy. A dose of 95 Gy delivered over 5 days did not significantly affect cell growth of *P. catenata*, as determined by turbidity measurements and cell counts. Multivariate statistical analysis of the FT-IR spectral data revealed metabolic variation during the post irradiation recovery period, within the polysaccharide and amide spectral regions. Increases in polysaccharides were confirmed by complementary analytical methods including total carbohydrate assays and calcofluor white staining. The results show that *P. catenata* is capable of tolerating an elevated dose of ionizing radiation. The observed increased production of polysaccharides is of significance, since this could have an impact on the fate of the radionuclide inventory in the pond via biosorption of cationic radionuclides, and may also impact on downstream processes through biofilm formation and biofouling.

5.2 Introduction

Microorganisms are ubiquitous and inhabit a wide range of environments including those with extremes of pH, temperature, pressure, availability of water, salinity and radiation (Billi and Potts, 2002; Blanco-Rivero *et al*., 2005; Katz *et al*., 2007; Pikuta *et al*., 2007). To colonise such environments, extremophiles are able to regulate their intracellular environment, whilst extracellular structures and enzymes in direct contact with the environment show specific adaptations and modifications e.g. in ion transport pathways (Pikuta *et al*., 2007). The presence of microorganisms in radioactive environments has been widely reported, for example in Spent Nuclear Fuel Ponds (SNFPs) (Chicote *et al*., 2004; Chicote *et al*., 2005; Dekker *et al*., 2014; Diósi *et al*., 2003; Karley *et al*., 2017; MeGraw *et al*., 2018; Rivasseau *et al*.,2010; Rivasseau *et al*., 201; Sarró *et al*., 2003; Sarró *et al*., 2005; Sarró *et al*., 2007), and in contaminated land surrounding the Chernobyl nuclear reactor (Dadachova *et al*., 2008). The ability of microorganisms to inhabit highly radioactive environments has been linked previously with their ability to survive other extreme environmental conditions such as desiccation (Billi *et al*., 2000; Billi and Potts, 2002; Jolivet *et al*., 2003).

Nuclear generated power accounts for just over 10 % of global electricity ("The nuclear fuel cycle," 2018). Since their development in the mid-1950s, nuclear power plants have undergone various improvements in terms of energy production and safety, leading to several generations of reactor types (Crossland, 2012). At the point where energy production is no longer efficient, the fuel rods are deemed "spent" and need to be replaced (Crossland, 2012; "The nuclear fuel cycle," 2018). As the spent fuel rods will continue to generate significant levels of radiation and heat, they are therefore stored in onsite pools containing water, which acts to shield against radiation and cool them (Wilson, 1996). Once the fuel rods have been stored for a suitable period of time, they are relocated to a separate facility to await long term storage, which in the UK is based at the Sellafield Ltd. facility (Cumbria, UK) (Crossland, 2012).

Studies investigating the presence of microorganisms in SNFPs across several sites, including in Spain, USA, France, India and the UK, have shown that each site exhibits a unique microbial community profile (Chicote *et al*., 2004; Chicote *et al*., 2005; Dekker *et al*., 2014; Diósi *et al*., 2003; Karley *et al*., 2017; MeGraw *et al*., 2018; Rivasseau *et al*., 2010; Rivasseau *et al*., 2016, Sarró *et al*., 2003; Sarró *et al*., 2005; Sarró *et al*., 2007). The majority of sites are dominated by Proteobacteria, although eukaryotic

microalgae have also been identified as being dominant at some sites (MeGraw *et* al., 2018; Rivasseau *et al*., 2010). The presence of microorganisms in SNFPs is problematic since high levels of biomass can result in reduced visibility (hampering pond management), may lead to microbiologically induced corrosion (MIC) and could lead to the formation of organic-rich radioactive waste. Bruhn *et al*. (2009) highlighted the potential for the formation of biofilms and MIC in the presence of high levels of radiation, which signals the possibility of MIC on waste storage containers and fuel cladding. Indeed, several studies investigating biofilm forming organisms in ponds at the Confrentes site (Valencia, Spain) have shown the occurrence of MIC on steel coupons (Chicote *et al*., 2004; Chicote *et al*., 2005; Sarró *et al*., 2003; Sarró *et al*., 2005; Sarró *et al*., 2007). The potential for MIC on waste storage containers and fuel cladding could have implications for the longevity of spent fuel storage. Biofilms are produced by bacteria to facilitate attachment to surfaces and to provide a barrier against adverse environmental conditions (Chicote *et al*., 2004). Biofilms largely consist of polymeric substance which, in addition to the microorganisms themselves, can interact with radionuclides and heavy metals (Tišáková *et al*., 2013). Biofilm interactions with radionuclides are mediated by mechanisms which include biosorption, bioaccumulation and biopreciptation. Such interactions have the potential to impact the radionuclide inventory in the system, resulting in controls on the speciation and solubility of priority radionuclides (Chicote *et al*., 2004; Sarró *et al*., 2003; Tišáková *et al*., 2013). Microorganisms have also been shown to accumulate fission products as shown with the free-living eukaryotic microalga *Coccomyxa actinabiotis*, isolated from a SNFP in research reactor in France, which has been shown to accumulate large quantities of ^{137}Cs (Rivasseau *et al*., 2013).

The conformation of fuel rods is dependent on the type of nuclear reactor they are used in. The early gas cooled reactors, commonly referred to as Magnox reactors, form part of the UK's legacy nuclear fleet, and the fuel rods used in these reactors were clad in a magnesium non oxide (Magnox) alloy (Gregson *et al*., 2011a; Gregson *et al*., 2011b; Jackson *et al*., 2014; Jensen and Nønbel, 1999). Spent fuel rods containing this cladding have been stored in an open air legacy storage ponds, including the First Generation Magnox Storage Pond (FGMSP) situated on the Sellafield site (Cumbria, UK), since the late 1950s (Jackson *et al*., 2014). Within the FGMSP, fuel storage times have been longer than anticipated and the Magnox spent fuel has been subject to extensive corrosion due to the Magnox cladding and metallic fuel having low chemical stability in

water. This corrosion has led to the formation of a hazardous radioactive environment with radioactive corroded spent nuclear fuel, radioactive pond effluent (NDA, 2016) and radioactive sludge (Gregson *et al*., 2011a; Gregson *et al*., 2011b; Jackson *et al*., 2014). Since the pond is open-aired, it is also subject to an influx of carbon, nitrogen and environmental debris, including seabird guano and other airborne particles. There is clear evidence for the presence of microorganisms in the pond, including events described as algal blooms (Gregson *et al*., 2011a; Gregson *et al*., 2011b). In order to provide thermal cooling and minimise further corrosion of the fuel rods and growth of microorganisms, the pond is continuously purged with alkaline dosed demineralised water (pH ~11.4) (Gregson *et al*., 2011a; Gregson *et al*., 2011b; Jackson *et al*., 2014).

The microbial community of the open-air legacy SNFP has recently been investigated over a three year period, including during a microbial bloom period in August 2016 (see Research chapter 4: The microbial ecology of a high pH spent nuclear fuel pond on the Sellafield site.). Over the course of the investigation, highly pigmented organisms with photosynthetic or hydrogen-metabolising capabilities were identified. Such organisms are likely to be pioneer species that facilitate the colonisation of the pond by heterotrophs. Background water samples indicated that Proteobacteria were the dominant microorganisms in the pond, whilst a single cyanobacterial species, *Pseudanabaena catenata*, was dominant during a significant bloom event (Research chapter 4: The microbial ecology of a high pH spent nuclear fuel pond on the Sellafield site.). *Pseudanabaena* spp. are filamentous cyanobacteria, displaying a simple morphology, and lack the ability to form branches or differentiate (Acinas *et al*., 2009; Zhu *et al*., 2015). Reports of *Pseudanabaena* spp.in the scientific literature are sporadic, with little known about their physiology or capabilities, and although they are associated with bloom events in a range of environments they are often overlooked (Acinas *et al*., 2009; Bukowska *et al*., 2017; Khan *et al*., 2018; Webster-Brown *et al*., 2015; Zhu *et al*., 2015).

The occurrence of cyanobacterial blooms in the legacy SNFP has the potential to disrupt waste retrieval operations and downstream processes. Although the microbial community structure of the legacy SNFP has been determined, nothing is known about how the microorganisms are able to colonise this radioactive and highly alkaline environment. The purpose of the present study is to determine the adaptive response of a *P. catenata* culture to ionizing radiation, to help inform control strategies employed onsite. It was not possible to source an axenic culture of *P. catenata* from any culture

collection for this study, therefore a non-axenic *P. catenata* culture was used for this work. The culture was characterised using 16S rRNA gene sequencing, which revealed that the culture contained multiple taxa in addition to *P. catenata* and was representative of the SNFP community, with 5 of the 9 operational taxanomic units (OTUs) in the culture also identified from SNFP community analysis (see Research chapter 4: The microbial ecology of a high pH spent nuclear fuel pond on the Sellafield site). To determine the physiological and metabolic fingerprint of the culture, Fourier transform infrared (FT-IR) spectroscopy and classical microbiological techniques were utilised. FT-IR spectroscopy is a metabolic fingerprinting technique that can be used to determine the intracellular metabolites in a given sample (Muhamadali *et al*., 2015a). Here, we demonstrate that a culture containing *P. catenata* as the sole cyanobacterial species is capable of surviving a significant dose of X-irradiation over a period of 5 days. When grown photosynthetically, the culture did not display any physiological differences to untreated cultures whilst receiving the irradiation treatment, however increases in polysaccharides and a reduction in chlorophyll-a (Chl-a) became more pronounced during the post-irradiation period. This study provides insight into the radiation resistance mechanisms employed by microorganisms representative of those colonising a high pH legacy SNFP. Understanding the behaviour of the microorganisms in response to radiation (and other stress responses) will help to provide fundamental information on adaptation mechanisms in extremophiles, and underpin more effective control strategies to minimize microbial growth and bloom formation.

5.3 Methods

5.3.1 Culturing and irradiation of *P. catenata*

It was not possible to culture organisms directly from water taken from the SNFP due to radiological safety limitations. A culture of the closest known relative to the *Pseudanabaena* species detected in the pond, *P. catenata* was obtained from the NIVA Culture Collection of Algae (NIVA-CYA 152), Norway. The *P. catenata* was inoculated in unbuffered BG11 media (Culture Collection of Algae and Protozoa) and incubated at 25 ± 1 °C, and shaken at 100 rpm in a light incubator with a photon flux density of 150 μmol m^{-2} s^{-1}, and a 16:8 h light–dark cycle (supplied by cool fluorescent daylight lamps). Biological triplicates were prepared by inoculating 20 mL BG11

medium with *P. catenata* to a starting optical density 0.2 (OD_{600nm}). The cultures were exposed to daily doses of ionising radiation using a Faxitron CP-160 Cabinet X-radiator (160 kV; 6 mA; tungsten target). A dose of 1 Gy min^{-1} for 19 min per day was administered to the cultures over five consecutive days to give a total dose of 95 Gy. A further triplicate set of "no dose" controls were placed inside the irradiator, shielded by an appropriate thickness of lead. All cultures were incubated following the treatment as previously described.

5.3.2 DNA extraction and 16S rRNA gene sequencing of the *P. catenata* culture

Since the *P. catenata* culture was not axenic, 16S rRNA gene sequencing was used to monitor the relative abundance of all the prokaryotic microorganisms present in the culture and quantify any differences in the cultures at the end of the experiment. Samples (1 mL) of irradiated and control cultures at day 16 were passed through a sterile 0.2 μm filter using a vacuum filtration technique. DNA was then extracted using the MoBio PowerWater DNA isolation kit (MoBio Laboratories, Inc., Carlsbad, CA, USA). The 16S rRNA gene was sequenced from PCR amplicons on the Illumina MiSeq platform (Illumina, San Diego, CA, USA) targeting the V4 hyper variable region (forward primer, 515F, 5′-GTGYCAGCMGCCGCGGTAA-3′; reverse primer, 806R, 5′-GGACTACHVGGGTWTCTAAT-3′) for 2×250-bp paired-end sequencing (Illumina) (Caporaso *et al*., 2011; Caporaso *et al*., 2012). The Roche FastStart High Fidelity PCR System (Roche Diagnostics Ltd, Burgess Hill, UK) was used to perform the PCR amplifications (50 μL reactions) under the following conditions; initial denaturation at 95 °C for 2 min, followed by 36 cycles of 95 °C for 30 s, 55 °C for 30 s, 72 °C for 1 min, and a final extension step of 5 min at 72 °C. The SequalPrep Normalization Kit (Fisher Scientific, Loughborough, UK) was used to purify and normalise the PCR products to ~20 ng each. The PCR amplicons from all samples were pooled in equimolar ratios. The run was performed using a 4 pM sample library spiked with 4 pM PhiX to a final concentration of 10 % following the method of Kozich (2013).

A sequencing pipeline was used to divide the raw sequences into samples by barcodes (up to one mismatch was permitted). Cutadapt (Martin, 2011), FastQC (Andrews, 2018), and Sickle (Joshi and Fass, 2011) were used to perform quality control and trimming,

whilst SPADes (Nurk *et al*., 2013) was used to carry out MiSeq error corrections. Forward and reverse reads were incorporated into full-length sequences with Pandaseq (Masella *et al*., 2012). ChimeraSlayer (Haas *et al*., 2011) was utilised to remove chimeras, and OTUs were generated UPARSE (Edgar, 2013) generated OTUs, that were classified by Usearch (Edgar, 2010) at the 97 % similarity level, and singletons were removed. Rarefaction analysis was conducted using the original detected OTUs in Qiime (Caporaso et al., 2010). The RDP classifier, version 2.2 (Wang *et al*., 2007) was used to perform the taxonomic assignment.

5.3.3 Growth, chlorophyll-*a* (Chl-a) concentration and pH measurements

To quantify the total biomass in cultures by turbidity, absorbance values at 600 nm (OD_{600nm}) were recorded for 1 mL aliquots of the *P. catenata* cultures using a Jenway 6700 UV/Vis spectrophotometer (Bibby Scientific Limited, Staffordshire).

The concentration of Chl-a was determined as follows: 1 mL samples were centrifuged at 14,000 *g* for 10 min to pellet the cells. The supernatant was then discarded and the cells re-suspended in 1 mL of 70 % ethanol and incubated at room temperature for 2 h. The samples were then centrifuged at 14,000 *g* for 10 min, the supernatant was then removed and analysed using the Jenway 6700 UV/Vis spectrophotometer (Bibby Scientific Limited, Staffordshire). The absorbance was measured at 665 nm (Chl-a) and at 750 nm to correct for turbidity (Bellinger and Sigee, 2010). The concentration of Chl-a was then calculated using the formula of Jespersen and Christoffersen (1987).

The pH of the cultures was measured using a FiveEasyPlus pH meter (Mettler Toledo Ltd, Leicestershire, UK).

5.3.4 Light microscopy

All light microscopy was carried out using a Zeiss Axio Imager A1 (Carl Zeiss Microimaging 234 GmbH, Germany) light microscope fitted with an Axiocam 506 mono camera using Zen2 imaging software.

5.3.4.1 Cell counts of *P. catenata*

Direct counts of *P. catenata* were carried out routinely throughout the experiment using a Sedgewick Rafter counting chamber. Ten images were taken of random sites across the samples. ImageJ was used to determine the length of filaments and individual cells. An average cell count was determined by dividing the total filament length by the average cell length. Samples were diluted with sterile BG11 medium to an appropriate concentration as required for analysis.

5.3.4.2 Calcofluor white staining of β-polysaccharides

Cells were washed twice and re-suspended in sterile normal saline (9 g L^{-1} NaCl), 5 μL of each sample was placed on a glass slide and 5 μL of calcofluor white stain (Sigma-Aldrich, Dorest, UK) was added and a cover slide placed over the sample. The samples were left to incubate for 10 min in the dark prior to being analysed.

The auto-fluorescence of the culture was observed using filter set 00 (530-585 nm excitation and 615-4095 nm emission). Calcofluor white stain fluorescence was observed using filter set 49 (335-383 nm excitation and 420-470 nm emission).

5.3.5 Assay to determine the total carbohydrate concentration

The total carbohydrate assay kit (Sigma-Aldrich, Dorset, UK) was used to determine carbohydrate concentrations. Prior to using the kit, the cells were prepared by washing twice with sterile normal saline solution (9 g L^{-1} NaCl), the cell pellets were flash frozen in liquid nitrogen and stored at -80 °C until they were analysed. All samples were normalised to an optical density of OD_{600nm} 15 (as per FT-IR preparation). Following this, a 200 μL aliquot was then centrifuged and re-suspended in the assay buffer, incubated for 10 min at room temperature. The samples were centrifuged at 14,000 *g* for 5 min and 15 μL aliquots from the samples were used for the assay reaction and made

up to 30 µL with Roche PCR grade water. The sample preparation was then carried out as detailed in the kit technical bulletin.

5.3.6 Metabolic profile of the cultures determined by FT-IR spectroscopy

Normalised samples were spotted as 20 µL aliquots onto a Bruker 96-well FT-IR silicon plate (Bruker Ltd., Coventry, United Kingdom) in triplicates, and heated to dryness (20-30 min) in an oven at 55 ˚C (Muhamadali *et al*., 2015b). All FT-IR spectra were recorded in the mid-infrared range (4000-600 cm^{-1}) with 4 cm^{-1} resolution and 64 spectral co-adds in absorbance mode using a HXT^{TM} module on a Bruker Equinox 55 infrared spectrometer (Muhamadali *et al*., 2015c).

5.3.6.1 Multivariate statistical analysis

The collected FT-IR spectra were analysed using MATLAB version 9 (The MathWorks Inc., Natick, MA). All spectra were scaled using the extended multiplicative signal correction (EMSC) method (Martens *et al*., 2003), followed by replacement of the CO_2 bands (2400 to 2275 cm^{-1}) with a linear trend. The pre-processed FT-IR spectral data were investigated by the unsupervised method of principal component analysis (PCA) to reduce the dimensionality of the data and determine any between group variations (Wold *et al*., 1986).

5.4 Results

5.4.1 Microbial community analysis of the *P. catenata* culture determined by 16S rRNA gene sequencing

Since the *P. catenata* culture was not axenic, 16S rRNA gene sequencing was carried out on the cultures to determine the community diversity of the culture. A comparison of the prokaryotic community at day 16 between the irradiated and control samples was made to determine what microorganisms were present and to see if the irradiation treatment resulted in shifts in the diversity of the culture with and without irradiation.

The culture consisted of 9 OTUs including *P. catenata* between the two sets of culture. This showed that the irradiation treatment did not result in a significant shift in phylogenetic diversity (Figure 5-1). As expected the most abundant OTU in both cultures was affiliated with a *Pseudanabaena* species, which comprised 30.7 % (control) and 32.7 % (irradiated) of the total community. The remainder of the OTUs were associated with the phyla Bacteriodetes (37.3 % control; 36.5 % irradiated; 2 OTUs) and Proteobacteria (32.0% control; 30.7% irradiated; 6 OTUs). A comparison of the microorganisms identified in the *P. catenata* culture showed strong similarities to those identified in legacy SNFP samples, particularly during the bloom. Of the 9 OTUs identified in the culture, 5 were affiliated with genera identified in the main pond namely: species of *Pseudanabaena*; *Flavobacterium*; *Porphyrobacter*; *Rhodobacter*; and *Hydrogenophaga* (see Research chapter 4: The microbial ecology of a high pH spent nuclear fuel pond on the Sellafield site). In addition, species of *Sediminibacterium* and *Lacibacterium* were observed in samples from an auxiliary pond (see Research chapter 4: The microbial ecology of a high pH spent nuclear fuel pond on the Sellafield site), which feeds into the high pH legacy SNFP on the Sellafield Ltd site, making this culture highly representative of the SNFP.

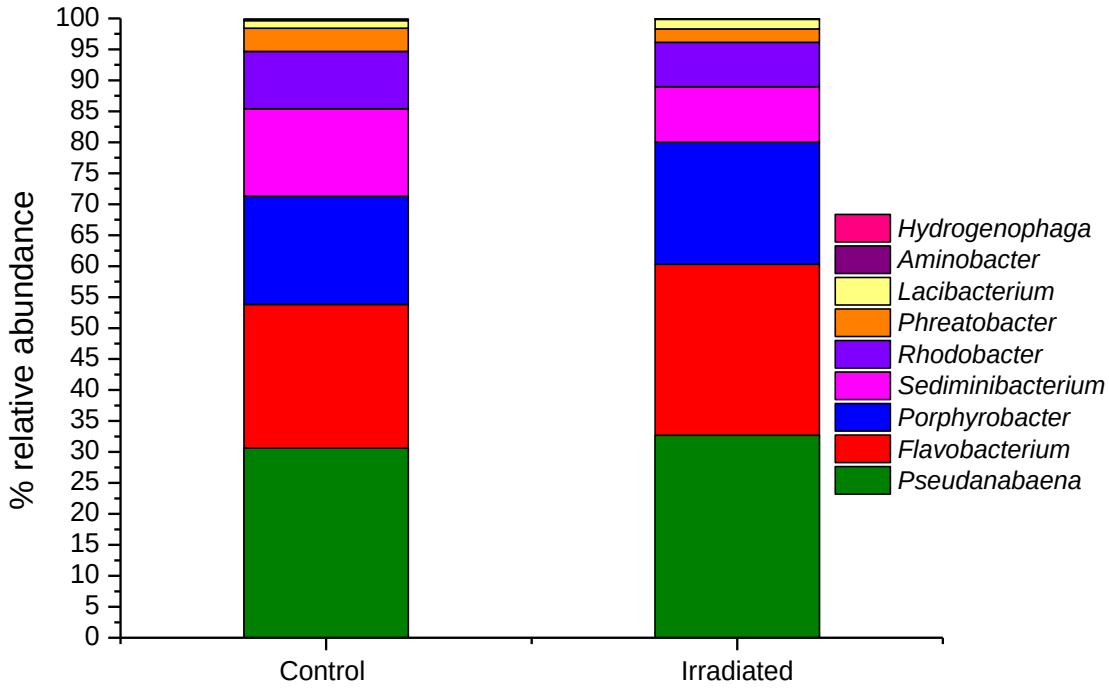

Figure 5-1: Genus-level microbial community analysis of the *P. catenata* culture at day 16, comparing the 16S rRNA gene irradiated community profile to that of the untreated control.

5.4.2 The effect of X-irradiation on the growth and chlorophyll concentration of the *P. catenata* culture

In order to determine the effect of ionising radiation on the growth and photosynthetic pigment characteristics of the *P. catenata* culture, the optical density at 600 nm (OD_{600nm}), cell counts and Chl-a concentration were monitored during and after the cultures were subjected to 95 Gy (1 Gy min^{-1}) of X-irradiation over a five day period (Figure 5-2). The absorbance of *P. catenata* cultures was measured at 600 nm over a period of 16 days (Figure 5-2a). There was a steady increase in the optical density recorded over time for both the irradiated culture and the control. The control culture started at an OD_{600nm} of 0.16 and reached 2.92 by day 16 whilst the irradiated culture started at a slightly lower OD_{600nm} of 0.13 and reached 2.79 by day 16. The overall absorbance measurements at 600 nm showed very similar trends indicating that the

amount of biomass in the cultures was not significantly different. Since the cultures contained other microorganisms in addition to *P. catenata*, direct cell counts were carried out using a light microscope to ensure the trends seen in the turbidity measurements reflected the proliferation of the cyanobacterium, with its characteristic chain morphology (see Figure 5-7 for representative morphology, and Figure 5-2c for cell counts). Observation of both irradiated and control cultures showed *P. catenata* dominated the field of view, which supports the sequencing data that shows it to be the most abundant organism in the culture. Both the irradiated and control cultures started with around $8x10^6$ cells mL^{-1} and showed an increase in cell numbers over time. By day 16 the average cell counts for the irradiated cultures were 31 % higher than those for the control at $2.8x10^8$ cells mL^{-1} and $2.2x10^8$ cells mL^{-1}, respectively. Interestingly the filament lengths were comparable between the irradiated and control cultures, and by day 16 the irradiated cells were more variable in their length compared to the controls. Both the turbidity measurements and the cell counts show the same overall trends in growth, with no significant difference between the two sets of cultures with either measurement. The concentration of Chl-a, (Figure 5-2b), did not follow the same trend as seen with the OD_{600nm} values and the cell counts. The initial Chl-a concentrations were 0.4 mg L^{-1} and 0.5 mg L^{-1} for the control and irradiated cultures, respectively. The cultures showed similar increases in the Chl-a concentration at day 4 and up to day 8, which was whilst the irradiation treatment was still being administered and the first 3 days post irradiation. The control cultures showed a continued increase in the Chl-a concentrations recorded, with 7.8 mg L^{-1} measured on day 16. The Chl-a levels in the irradiated cultures were lower, at day 16 a concentration of 2.6 mg L^{-1} was recorded, which is ~66 % less than the control value. Normalisation of the Chl-a concentration to cell number showed that by day 4, the concentration of Chl-a per cell increased in both treatments and reached the maximum of 1.1 $x10^{-4}$ μg L^{-1} $cell^{-1}$ and 1.0 $x10^{-4}$ μg L^{-1} $cell^{-1}$ for the control and irradiated cultures, respectively (Supplementary figure 5-1). Both sets of cultures showed a decline in the average Chl-a concentration per cell from day 8, which plateaued towards the end of the experiment, with the irradiated culture consistently showed significantly reduced concentrations of Chl-a per cell compared to the control. At day 16 the values were 9.4 $x10^{-6}$ μg L^{-1} $cell^{-1}$ compared to 3.7 $x10^{-5}$ μg L^{-1} $cell^{-1}$, for the irradiated and control cultures respectively. The pH of the unbuffered cultures was monitored over the course of sampling period, both cultures started off at a pH of 7.3 which increased to pH >10 by day 4. The pH of the irradiated culture (Figure 5-2d) started to decline after day 4 reaching pH 9.2 at day 16. The pH of the control

sample increased to 10.8 at day 8 and then gradually reduced to 9.8 at day 16. The pH of the irradiated culture is significantly lower than seen in the control culture.

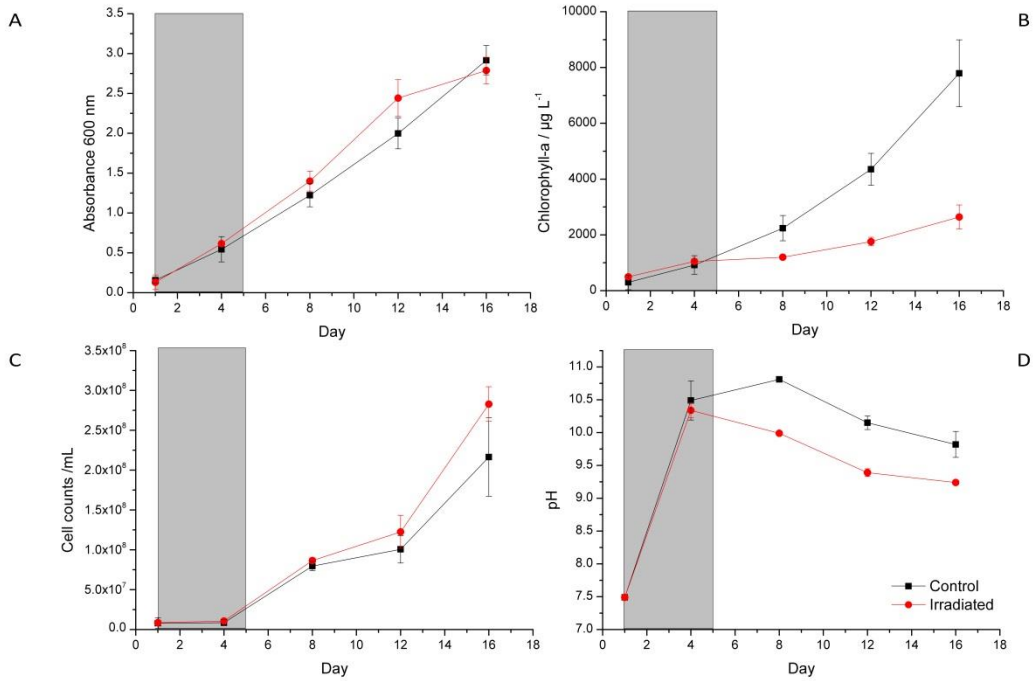

Figure 5-2: Growth of the *P. catenata* culture with and without radiation treatment: a) absorbance at 600 nm; b) chlorophyll concentration (µg L^{-1}); c) mean cell counts of *P. catenata*; d) pH. The grey panel indicated the period in which the irradiation treatment was being administered. Red lines are irradiated samples; black lines are control samples. Error bars are the standard deviation of three replicates.

5.4.3 Metabolic response of the *P. catenata* culture to X-irradiation determined by FT-IR spectroscopy

FT-IR spectroscopy was utilised to obtain a metabolic footprint of the cultures, and to determine if there were physiological changes associated with irradiation. A PCA score plot of the data (Figure 5-3) displayed clear separation of the samples according to PC1, which accounted for 88.6 % of the total explained variance (TEV). At day 4 both sets of samples clustered together, indicating that whilst receiving the treatment there was no significant difference between the cultures; by contrast, by day 8 there was clear separation of the samples according to the PC2 axis. The control samples from day 8 to 16 form a tight cluster (in top left part of the PCA scores plot) which was distinct from

the cluster at day 4. Interestingly the irradiated samples showed continued separation over time according to PC1 (from left to right) with each time point clustering closely.

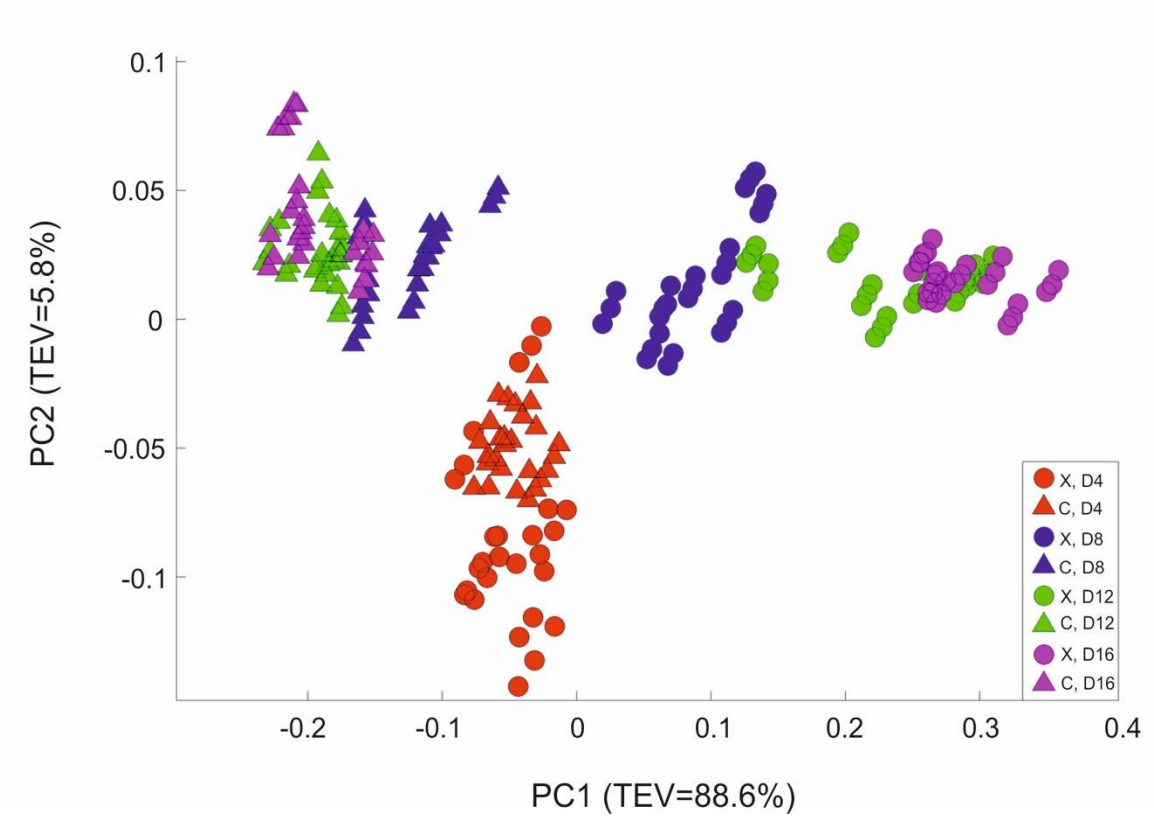

Figure 5-3: a) Principal component analysis scores plot of all the FT-IR spectroscopy data. Circles represent the irradiated samples; triangles are control samples. Colour code: Red- day 4; Blue- day 8; Green- day 12; and Purple day 16. TEV = Total Explained Variance

According to the PC1 loadings plot (Figure 5-4) the main vibrational regions that contribute toward the separation of the samples included: 1655 cm^{-1} (amide I, C=O of proteins and peptides) (Maquelin *et al*., 2002); 1545 cm^{-1} (amide II, combination of in-plane N-H bending and C-N stretching (40%) of proteins, secondary structure of protein) (Lu *et al*., 2010); 1153 cm^{-1} (stretching vibrations of hydrogen bonded C-O groups; carbohydrates) (Pop *et al*., 2013; Simonova and Karamancheva, 2013); 1080 cm^{-1} (carbonyl groups in cell wall, glycopeptides; P=O stretching, P-O-C (P-O-P) of phospholipids and esters) (Filip *et al*., 2008); 1024 cm^{-1} (C-O bending and stretching typical of glycogen) (Lewis *et al*., 2010). The FT-IR spectra confirmed the PCA findings, with clear variance in the baseline corrected spectra apparent, which became more pronounced in the irradiated samples taken at the later time points (Supplementary Figure 5-2). Over the course of the experiment the irradiated samples showed increased spectral intensities from 1200-900 cm^{-1}, which is indicative of an increase in total

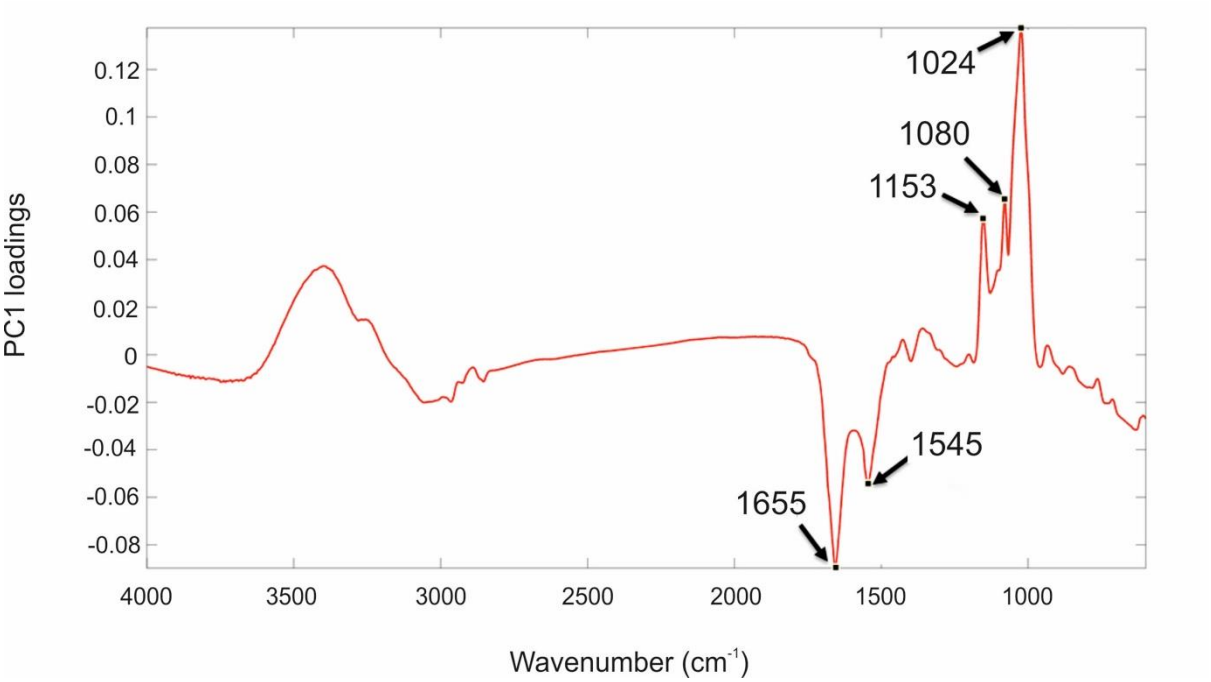

Figure 5-4: PC1 loading plot including the wavenumbers contributing to the shifts seen across PC1

polysaccharides (Ellis *et al*., 2012; Naumann, 2000). Conversely, reduced spectral intensities were apparent in the amide regions from 1750-1500 cm^{-1} which indicates that there was a reduction in the total peptide content as the irradiated cultures age (Ellis *et al*., 2012; Naumann, 2000). The total carbohydrate band heights at 1160, 1086, 1050, and 1036 cm^{-1} were quantified and normalised by expressing them as a ratio to the lipid band at 1740 cm^{-1}, since there was no significant differences observed in this region. At day 4, the ratio value at 1160 cm^{-1} (Figure 5-5) for the irradiated sample was 1.35 (s.d. 0.11) compared to 1.43 (s.d. 0.08) in the equivalent control sample, showing that there was very little difference in the polysaccharide levels during the irradiation treatment. The ratio value of the control samples did not vary much over the course of the sampling period, reducing slightly to 1.26 (s.d. 0.07) at day 16 (a 12 % reduction). The irradiated samples showed continued increases in the ratio value reaching 2.49 at day 16, which is a 1.85 fold increase from day 4. At day 16 there was a 1.97 fold increase in the polysaccharide content of the irradiated samples compared the control. The carbohydrate bands at 1086, 1050, and 1036 cm^{-1} all showed the same trend. The largest fold change between the day 16 samples was observed at the 1036 cm^{-1} band, which had a 2.69 fold increase in the irradiated samples.

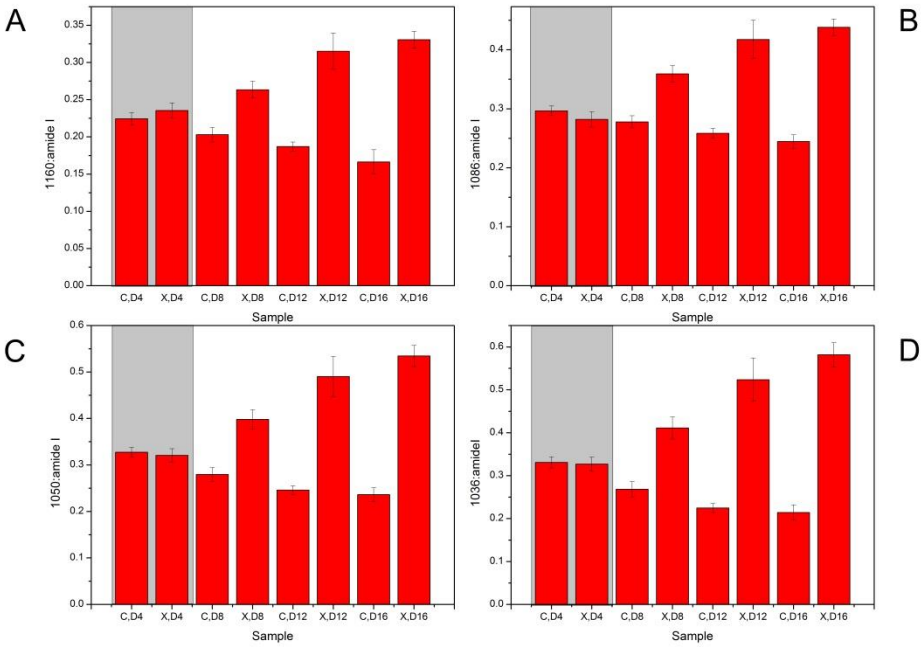

Figure 5-5: Ratio plot of carbohydrate absorbance peaks: a) 1036 cm^{-1}; b) 1050 cm^{-1}; c) 1086 cm^{-1}; and d) 1160 cm^{-1} normalised to the lipid peak at 1740 cm^{-1} taken from FT-IR data, grey boxes indicates samples taken whilst irradiation treatment was being administered, bars are the means from 3 FT-IR spectra and error bars denote standard deviation

5.4.4 Total carbohydrate concentrations

To investigate the FT-IR spectroscopy findings further, the total carbohydrate concentrations in the day 4 and day 16 samples (OD_{600nm} normalised to 15) were determined (

Figure 5-6). At day 4, the concentrations were 0.13 and 0.10 μg mL^{-1} for the control and irradiated samples, respectively. By day 16 the control sample had shown a slight reduction in carbohydrate levels to 0.09 μg mL^{-1}, which is in agreement with the ratio plots taken from the FT-IR spectroscopy data. The irradiated samples showed an increase to 0.26 μg mL^{-1} at day 16 (2.69 fold increase), which is also in agreement with the FT-IR ratio plots. A comparison of the carbohydrate concentrations at day 16 showed a 2.96 fold increase in the concentration of the irradiated samples compared to the control.

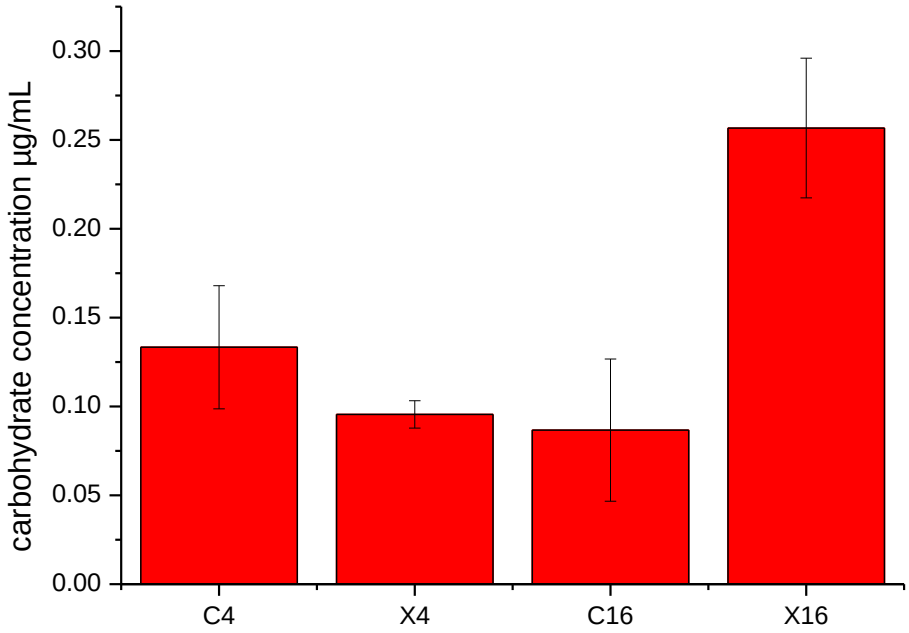

Figure 5-6: Total cell carbohydrate concentrations measured using Sigma-aldrich kit, samples include controls (C), and irradiated (X) at day 4 and 16, bars are mean from 3 measurements and error bars denote standard deviation

5.4.5 Fluorescent light microscopy determination of cell morphology and polysaccharide staining

Calcofluor white stain was used to label β-linked polysaccharides associated with cells in the culture, to determine if the changes seen in the FT-IR spectra and carbohydrate analyses were due to upregulation of polysaccharides associated with cells of *P. catenata*. The auto-fluorescence of *P. catenata* was also noted throughout the experiment, which gave a qualitative assessment of the levels of photosynthetic pigments in the cells/filaments. There was little difference in both the auto-fluorescence and the binding of the calcofluor white stain to the *P. catenata* filaments in either the control or the irradiated cultures whilst they were still receiving the treatment (day 4) (Supplementary Figure 5-3 a & c). However, by day 16 the auto-fluorescence seen across all of the *P. catenata* filaments in both treatments was more variable, with some cells lacking fluorescence altogether (Figure 5-7 a & c). Interestingly, the cells that had

been exposed to the irradiation treatment showed a greater degree of variability in the auto-fluorescence levels, with a higher proportion of the irradiated cells showing reduced fluorescence compared to the non-treated filaments. At day 4 the level of fluorescence with the calcofluor polysaccharide stain was comparable between the treated and non-treated cultures (Supplementary Figure 5-3 b & d). The non-irradiated controls showed the same level of fluorescence with the calcofluor white stain at day 4 and day 16, indicating that the levels of β-polysaccharides remained largely similar over time. The irradiated samples, however, showed increased levels of fluorescence of the calcofluor white stain at day 16 compared to the control cultures, providing evidence that *P. catenata* had higher levels of β-polysaccharides associated with the cell walls or extracellular mucilage (Figure 5-7 b & d). Unwashed samples were also inspected using the calcofluor white stain, and the non-irradiated cells showed low levels of binding and fluorescence (Figure 5-7e). The stain was concentrated at the poles of the unwashed non-irradiated cells where they were connected within the filament. The unwashed irradiated cells showed the same elevated levels of fluorescence with the calcofluor stain as the washed samples. The calcofluor stain was also bound to extracellular material apparently associated with the unwashed irradiated *P. catenata* filaments, localised at the points where the cells in the filaments were connected (Figure 5-7f). This suggests that the cells were potentially releasing materials into the supernatant that contain β-polysaccharides, which was removed upon washing.

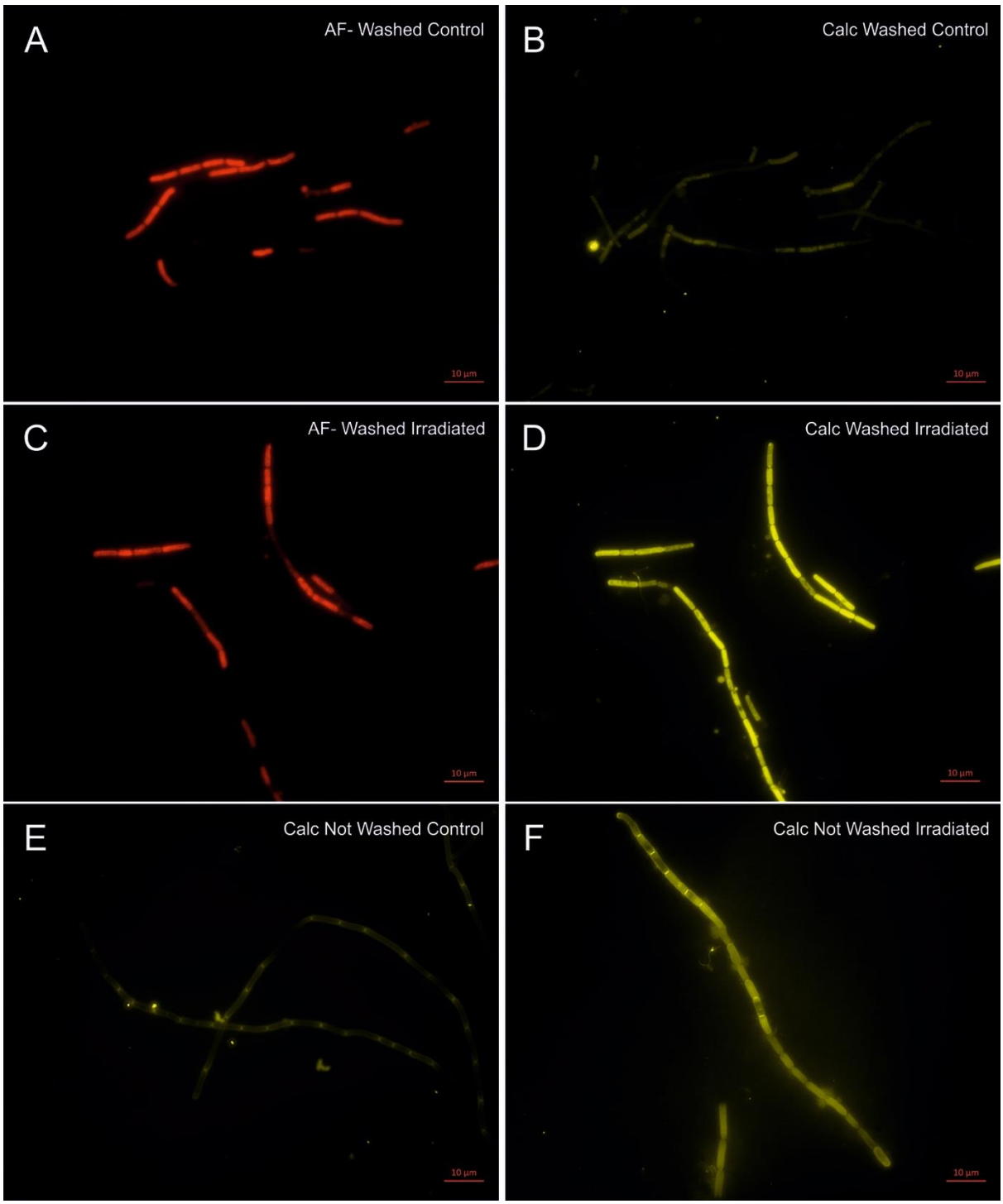

Figure 5-7: Light microscopy of *P. catenata* filaments at day 16: a-d were washed twice with normal saline [0.9 g L^{-1} NaCl] a) auto-fluorescence of control culture; b) calcofluor white stained control culture; c) auto-fluorescence of irradiated culture; d) calcofluor white stained irradiated culture; e) calcofluor white stained unwashed control culture; and f) calcofluor white stained unwashed irradiated culture. AF= autofluorescence; Calc= calcofluor white stain.

5.5 Discussion

The FGMSP spent nuclear fuel pond located on the Sellafield site is colonised by microorganisms that are diverse in their metabolic capabilities, including the potential to drive primary colonisation by photosynthesis. During a microbial bloom in August 2016, a cyanobacterium belonging to the genus *Pseudanabaena* was seen to dominate the community (Research chapter 4: The microbial ecology of a high pH spent nuclear fuel pond on the Sellafield site). This study investigated the effect of X-irradiation on the growth and metabolism of a non-axenic culture of *P. catenata.* 16S rRNA gene sequencing revealed the presence of five OTUs within the *P. catenata* culture, which were consistent with genera identified in the SNFP, making this culture an ideal representation of the pond community for use in laboratory studies. The levels of radiation associated with the legacy SNFP are significant, Jackson *et al*. (2014) reported doses of 5.65 Gy h^{-1} associated with sludge and 0.15 mGy h^{-1} with the pond liquor, but the activity is also dynamic, with the consistent purging of water and in pond activities changing the radiation flux that the microorganisms are likely to be in contact with. This is the first study to our knowledge assessing the effect of radiation on a mixed microbial culture representative of the microorganism community found in a high pH and significantly radioactive legacy SNFP and at relatively representative doses, over consecutive days.

Collectively the results of our experiments show that whilst the irradiation treatment was being administered to the culture there were no visible phenotypic differences observed when compared to the control cultures. This suggests that the entire culture, including all microorganisms present, was able to tolerate the dose of radiation administered. Differences between the two treatments only became apparent during the post-irradiation recovery period, and became more pronounced over time. The estimation of total biomass by the OD_{600nm} and cell counts were the only measurements that remained comparable between the two treatments. Perhaps surprisingly, although the cell counts of *P. catenata* increased over time, the recorded Chl-a concentrations did not increase in line with cell numbers. Inspection of the auto-fluorescence at day 16 when the differences were greatest showed varied levels of fluorescence across filaments. This suggests that within a filament of *P. catenata* cells were showing different levels of photosynthetic potential/activity. The differences between the Chl-a concentrations, the cell numbers and absorbance readings suggest that the proportion of

photosynthetically active *P. catenata* cells was much lower than those contributing to the total biomass data. A study by Sigee *et al.* (Sigee *et al*., 2007) highlighted that estimations of total abundance of cyanobacterial populations might be misleading as some organisms are at different stages of growth and may be in a senescent state. Thus, the increase in cell numbers predicted by the optical density measurements may be misleading, and do not match the number of viable and actively dividing cells.

Previous studies investigating the effect of ionizing radiation on axenic cultures of cyanobacteria have reported similar drops in chlorophyll concentrations but after much higher doses from a ^{60}Co-gamma radiation source. El-Fatah Abomohra *et al*. (2016) reported up to a 25 % reduction in the chlorophyll concentrations of *Arthrospira platensis* 15 days after exposure to 2.5 kGy of radiation. This coincided with a reduction in total biomass production by 34 %. At lower doses of 1 and 1.5 kGy no recorded drop in biomass was reported however chlorophyll concentrations were reduced by 8 and 12 % respectively. The effects of irradiation treatments on chlorophyll production is varied, however, as Badri *et al*. (2015) reported no significant impacts on chlorophyll when exposing *Arthrospira* cultures to similar doses used by El-Fatah Abomohra *et al*. (2016). The authors reported a reduction in the antenna pigments allophycocynanin and phycocynanin in addition to an increasing lag phase in growth as the dose of radiation increased. *Anabaena* cultures exposed to gamma irradiation showed bleaching of their pigments immediately after exposure to 6 kGy, with a 42.5 % reduction in Chl-a concentration. However, all cultures were able to recover following irradiation although longer lag phases were observed at higher doses (Singh *et al*., 2013). Several studies have reported that low doses of ionizing radiation can stimulate the growth of cyanobacteria, for example Wang *et al.* (1998) demonstrated this with an *Arthrospira* spp. at 500 kGy, whilst several studies report the enhanced growth of a *Synechococcus* spp. at dose rates of 20 mGy y^{-1} (Conter *et al*., 1984; Conter *et al*., 1986). The stimulatory effect of lower chronic doses of ionizing radiation could offer a plausible explanation for the continued increase in cell numbers despite the drop in Chl-a concentration and auto-fluorescence in *P. catenata*. These studies show that the effect of radiation can be varied and that photosynthetic pigments are affected but the dose at which this is observed is variable between species.

The collected FT-IR spectral data, ratio plots, total cell carbohydrate concentrations and calcofluor white staining all show an overall increase in carbohydrate production overtime in the irradiated cultures. From the FT-IR spectra it is not possible to

determine which organisms are responsible for the differences observed, as the interrogation beam has a diameter of ~1 mm and so measures the whole microbial community. The wavenumbers contributing to the shifts seen in the PCA scores and loadings plots indicate that there are potentially changes associated with intracellular and extracellular polysaccharides. The wavenumber 1024 cm^{-1} is indicative of glycogen which is a common storage molecule in cyanobacteria and some bacteria. Nutrient stress has been shown to result in increased storage of glycogen in *Synechococcus* species, however this coincides with a reduction of growth (Klotz *et al*., 2016), which is not observed in the current study. Calcofluor white stain is commonly used to identify the presence of chitin, a β-polysaccharide found in fungal cell walls, but it is also used to stain a variety of β-polysaccharides (Anderson *et al*., 2010; Dunker *et al*., 2017). In our study, the calcofluor white stain was associated with the outer surface of the *P. catenata* cells, suggesting that there is an increase in β-polysaccharides associated with either; the cell wall, membrane or extracellular polymeric substances (Singh *et al*., 2013). It should be noted that low doses of gamma irradiation (0.5-1.5 kGy) have been shown to result in the increased production of carbohydrates in *Arthrospira* spp. in another study (El-Fatah Abomohra *et al*., 2016). It is thought that the polymeric substances provide an array of functions including increasing cell buoyancy, binding metals, accumulating nutrients, aggregation of cells to one another, the formation of biofilms on surfaces and a barrier to protect against environmental stress (Gao *et al*., 2015; Nobles *et al*., 2001; Xu *et al*., 2013). It is not known whether the microorganisms in the legacy SNFP produce such polymeric substances; however the similarities between the community profile in the pond and the culture used in this study suggest that this is feasible and warrants further investigation. The increased production of polysaccharide/ polymeric substances by organisms in the pond could provide a mechanism to protect microorganisms from the damaging effects of reactive oxygen species (Gao *et al*., 2015).

The presence of polysaccharides or polymeric substances associated with the microorganisms could have implications for the fate of radionuclides in the pond and downstream processes. Cationic metals are able to adsorb to negatively charged functional groups on the surfaces of the microorganisms and polysaccharide containing mucilage of some cyanobacteria (Decho and Gutierrez, 2017; Gadd, 1990; Gadd, 2009; Javanbakht *et al*., 2014). Extracellular polymeric substances also have the ability to trap organic and inorganic colloids and nanoparticles, which are thought to be present in the

pond (Decho and Gutierrez, 2017; Maher *et al*., 2016; Neil *et al*., n.d.). The same experimental set-up described in this study was used recently to investigate the interaction of ^{90}Sr with the cell free medium from irradiated and control cultures (Ashworth *et al*., 2018). All of the ^{90}Sr remained in solution when it was added to the cell free medium from the control cultures, whilst the irradiated samples resulted in the removal of approximately 10 % of ^{90}Sr from solution. Analyses of the supernatants showed higher total carbon levels in the control cultures (324 mg L^{-1}) compared to the medium from the irradiated cultures (162 mg L^{-1}). The lower levels of TOC in the irradiated medium is surprising, particularly as the calcofluor staining presented in this study indicates the presence of extracellular material in unwashed samples which are not present following centrifugation and washing. The reduced TOC in the medium from the irradiated cultures suggests that irradiated medium either has modified functional groups which better facilitate interactions with ^{90}Sr or that the irradiation treatment has resulted in the secretion of additional metabolites not present in the control samples. As noted by Ashworth *et al*. (2018) the level of interaction although being low is worth exploring further, as is the interaction of Sr in the presence of the microorganisms in the culture.

This study provides an insight into broad scale changes in the metabolism of a microbial community dominated by *P. catenata* in response to doses of irradiation. The metabolic responses revealed by FT-IR are representative of a culture-wide response, and cannot be attributed to an individual organism. *P. catenata* specific responses were observed with the decline in photosynthetic pigments, whilst the calcofluor staining showed some of the changes observed in the polysaccharide levels could be attributed to this organism. Previous irradiation studies have looked at the effect of ionising radiation on axenic cultures of cyanobacteria at significantly higher doses. Whilst these are useful for understanding the specific responses of microorganisms to radiation treatment, they are not representative of this type of engineered system. The microorganisms in the pond exist as part of a community structure, and response of individual members is likely to influence the behaviour of others. Whilst it is not possible to know whether the responses of the microorganisms in the pond community are the same as seen in this experiment, the study does provide possible signatures to look for when further investigating the pond community. FT-IR spectroscopy would be a useful tool to investigate broad scale changes in the metabolic state of the pond community, as it is neither time nor labour intensive to generate results. Further work is required to better

understand the responses reported in this study. The utilisation of metabolomics techniques on cell extracts and spent medium could provide further information on the activity of different metabolic pathways and metabolite levels that support such resistant mechanisms. In addition transcriptomic or proteomic techniques could provide an insight into changes in gene expression, for example during the period of irradiation treatment where no perceivable differences were observed in this study. The reduced absorbance of the amide peaks in the FT-IR spectra have not been explored in this study, however, studies on the gene expression could provide insights into which proteins are responsible for the shifts seen. Additional work to characterise the culture medium and the polysaccharides using more in depth metabolomics methods based on LC-MS is required to determine more specifically what metabolic changes are occurring as part of the post-irradiation recovery process.

The legacy SNFP on the Sellafield site is currently being decommissioned, which involves amongst other things the removal of waste stored in the pond. In order to safely and efficiently carry out routine pond operations, visibility within the pond must be maintained. The presence of microorganisms in the pond has the potential to reduce visibility and cause delays in the on-site operations, particularly during microbial bloom events. Whilst the microbial community has been described recently (see Research chapter 4: The microbial ecology of a high pH spent nuclear fuel pond on the Sellafield site), little was known about the survival mechanisms the organisms used to colonise the pond. The results presented in this study provide clear insight into the adaptive response of a *P. catenata* dominated culture to doses of X-irradiation. The identification of increased cell polysaccharide levels is of importance since elevated polysaccharide levels could affect the behaviour and fate of key radionuclides present in the pond (Gadd, 1990). High levels of polysaccharide containing material could be supporting the growth of the heterotrophic microbial community whilst also providing the microorganisms with a protective barrier against the environment (Song *et al*., 2016). Analysis of microbial communities inhabiting SNFPs so far, indicate that the communities are specific to individual ponds. Recently the dominant algae species causing microbial blooms in a near neutral pH SNFP on the Sellafield Ltd. site, was shown to synthesize large quantities of the carotenoid astaxanthin, which is known to have antioxidant properties (MeGraw *et al*., 2018). The research carried out in this study and that of McGraw *et al*. (2018) indicate that the adaptive response of the microbial communities is unique to the specific microorganism and the SNFP that they have

colonised. A greater understanding of the microbial responses to the radiation they encounter in the legacy pond will help to optimise control strategies used on site to control the microbial load in the pond and prevent blooms occurring during the planned decommissioning of the FGMSP over the next 20+ years. This study also provides further information about the response of microorganisms to doses of ionizing radiation that have not previously been studied, but which are relevant to critical engineered environments, including a wider range of nuclear facilities worldwide.

5.6 Acknowledgements

LF was supported by an EPSRC PhD CASE Studentship (Grant number EP/G037426/1) with Sellafield Ltd. We would also like to thank Kaye Williams and Ayse Latif for allowing us the use of the Faxitron CP-160 Cabinet X-radiator.

5.7 References

Acinas, S.G., Haverkamp, T.H., Huisman, J., Stal, L.J., 2009. Phenotypic and genetic diversification of *Pseudanabaena* spp. (cyanobacteria). ISME J. 378, 31–46. https://doi.org/10.1038/ismej.2008.78

Anderson, C.T., Carroll, A., Akhmetova, L., Somerville, C., 2010. Real-Time Imaging of Cellulose Reorientation during Cell Wall Expansion in Arabidopsis Roots. Plant Physiol. 152, 787–796. https://doi.org/10.1104/pp.109.150128

Andrews, S. FastQC. *Babraham Bioinformatics* (2018). Available at: https://www.bioinformatics.babraham.ac.uk/projects/fastqc/. (Accessed: 19th June 2018)

Ashworth, H., Abrahamsen-Mills, L., Bryan, N., Foster, L., Lloyd, J.R., Kellet, S., Heath, S.L., 2018. Effect of Humic acid and bacterial exudates on sorption-desorption interactions of 90Sr with brucite. Environ. Sci. Process. Impacts Accepted m. https://doi.org/10.1039/b816135f

Badri, H., Monsieurs, P., Coninx, I., Wattiez, R., Leys, N., 2015. Molecular investigation of the radiation resistance of edible cyanobacterium *Arthrospira* sp. PCC 8005. Microbiologyopen 4, 187–207. https://doi.org/10.1002/mbo3.229

Bellinger, E.G., Sigee, D.C., 2010. Freshwater algae: Identification and use as bioindicators, 2010th ed. John Wiley & Sons, Ltd.

Billi, D., Friedmann, E.I., Hofer, K.G., Caiola, M.G., Ocampo-Friedmann, R., 2000. Ionizing-radiation resistance in the desiccation-tolerant cyanobacterium *Chroococcidiopsis*. Appl. Environ. Microbiol. 66, 1489–1492.

Billi, D., Potts, M., 2002. Life and death of dried prokaryotes. Res. Microbiol. 153, 7–12. https://doi.org/10.1016/S0923-2508(01)01279-7

Blanco-Rivero, A., Leganés, F., Fernández-Valiente, E., Calle, P., Fernández-Piñas, F., 2005. *mrpA*, a gene with roles in resistance to Na+ and adaptation to alkaline pH in the cyanobacterium *Anabaena* sp. PCC7120. Microbiology 151, 1671–1682. https://doi.org/10.1099/mic.0.27848-0

Bruhn, D.F., Frank, S.M., Roberto, F.F., Pinhero, P.J., Johnson, S.G., 2009. Microbial biofilm growth on irradiated, spent nuclear fuel cladding. J. Nucl. Mater. 384, 140–145. https://doi.org/10.1016/j.jnucmat.2008.11.008

Bukowska, A., Kaliński, T., Koper, M., Kostrzewska-Szlakowska, I., Kwiatowski, J., Mazur-Marzec, H., Jasser, I., 2017. Predicting blooms of toxic cyanobacteria in eutrophic lakes with diverse cyanobacterial communities. Sci. Rep. 7, 1–12. https://doi.org/10.1038/s41598-017-08701-8

Caporaso, J.G., Kuczynski, J., Stombaugh, J., Bittinger, K., Bushman, F.D., Costello, E.K., Fierer, N., Peña, A.G., Goodrich, J.K., Gordon, J.I., Huttley, G. a, Kelley, S.T., Knights, D., Koenig, J.E., Ley, R.E., Lozupone, C. a, Mcdonald, D., Muegge, B.D., Pirrung, M., Reeder, J., Sevinsky, J.R., Turnbaugh, P.J., Walters, W. a, Widmann, J., Yatsunenko, T., Zaneveld, J., Knight, R., 2010. correspondence QIIME allows analysis of high- throughput community sequencing data Intensity

normalization improves color calling in SOLiD sequencing. Nat. Publ. Gr. 7, 335–336. https://doi.org/10.1038/nmeth0510-335

Caporaso, J.G., Lauber, C.L., Walters, W.A., Berg-Lyons, D., Huntley, J., Fierer, N., Owens, S.M., Betley, J., Fraser, L., Bauer, M., Gormley, N., Gilbert, J.A., Smith, G., Knight, R., 2012. Ultra-high-throughput microbial community analysis on the Illumina HiSeq and MiSeq platforms. ISME J. 6, 1621–1624. https://doi.org/10.1038/ismej.2012.8

Caporaso, J.G., Lauber, C.L., Walters, W.A., Berg-Lyons, D., Lozupone, C.A., Turnbaugh, P.J., Fierer, N., Knight, R., 2011. Global patterns of 16S rRNA diversity at a depth of millions of sequences per sample. Proc. Natl. Acad. Sci. 108, 4516–4522. https://doi.org/10.1073/pnas.1000080107

Chicote, E., García, A.M., Moreno, D.A., Sarró, M.I., Lorenzo, P.I., Montero, F., 2005. Isolation and identification of bacteria from spent nuclear fuel pools. J. Ind. Microbiol. Biotechnol. 32, 155–162. https://doi.org/10.1007/s10295-005-0216-3

Chicote, E., Moreno, D. a, García, A.M., Sarró, M.I., Lorenzo, P.I., Montero, F., 2004. Biofouling on the walls of a spent nuclear fuel pool with radioactive ultrapure water. Biofouling 20, 35–42. https://doi.org/10.1080/08927010410001662670

Conter, A., Dupouy, D., Planel, H., 1986. Effects of dose rate on response of *Synechococcus lividus* to very low doses of chronic γ radiation : influence of enzymatic equipment of starting cells. Radiat. Res. 105, 379–386.

Conter, A., Dupouy, D., Planel, H., 1984. Light modulation of radiosensitivity of *Synechococcus lividus* to very low doses of ionizing radiation. Environ. Exp. Bot. 24, 229–237.

Crossland, I., 2012. Nuclear fuel cycle science and engineering, 1st ed. Woodhead Publishing, Philadelphia.

Dadachova, E., Bryan, R.A., Howell, R.C., Schweitzer, A.D., Aisen, P., Nosanchuk, J.D., Casadevall, A., 2008. The radioprotective properties of fungal melanin are a function of its chemical composition, stable radical presence and spatial arrangement. Pigment Cell Melanoma Res. 21, 192–199. https://doi.org/10.1111/j.1755-148X.2007.00430.x

Decho, A.W., Gutierrez, T., 2017. Microbial extracellular polymeric substances (EPSs) in ocean systems. Front. Microbiol. 8, 1–28. https://doi.org/10.3389/fmicb.2017.00922

Dekker, L., Osborne, T.H., Santini, J.M., 2014. Isolation and identification of cobalt- and caesium-resistant bacteria from a nuclear fuel storage pond. FEMS Microbiol. Lett. 359, 81–84. https://doi.org/10.1111/1574-6968.12562

Diósi, G., Telegdi, J., Farkas, G., Gazsó, L.G., Bokori, E., 2003. Corrosion influenced by biofilms during wet nuclear waste storage. Int. Biodeterior. Biodegrad. 51, 151–156. https://doi.org/10.1016/S0964-8305(02)00138-5

Dunker, S., Althammer, J., Pohnert, G., Wilhelm, C., 2017. A fateful meeting of two phytoplankton species—chemical vs. cell-cell-interactions in co-cultures of the green algae *Oocystis marsonii* and the cyanobacterium *Microcystis aeruginosa*. Microb. Ecol. 74, 22–32. https://doi.org/10.1007/s00248-016-0927-1

Edgar, R.C., 2013. UPARSE: Highly accurate OTU sequences from microbial amplicon reads. Nat. Methods 10, 996–998. https://doi.org/10.1038/nmeth.2604

Edgar, R.C., 2010. Search and clustering orders of magnitude faster than BLAST. Bioinformatics 26, 2460–2461. https://doi.org/10.1093/bioinformatics/btq461

El-Fatah Abomohra, A., El-Shouny, W., Sharaf, M., Abo-Eleneen, M., 2016. Effect of gamma radiation on growth and metabolic activities of *Arthrospira platensis*. Brazilian Arch. Biol. Technol. 59, 1–12. https://doi.org/10.1590/1678-4324-2016150476

Ellis, D.I., Brewster, V.L., Dunn, W.B., Allwood, J.W., Golovanov, A.P., Goodacre, R., 2012. Fingerprinting food: current technologies for the detection of food adulteration and contamination. Chem. Soc. Rev. 41, 5706. https://doi.org/10.1039/c2cs35138b

Filip, Z., Hermann, S., Demnerová, K., 2008. FT-IR spectroscopic characteristics of differently cultivated Escherichia coli. Czech J. Food Sci. 26, 458–463. https://doi.org/10.1016/j.micres.2004.05.002

Gadd, G.M., 2009. Biosorption: critical review of scientific rationale, environmental importance and significance for pollution treatment. J. Chem. Technol. Biotechnol. 84, 13–28. https://doi.org/10.1002/jctb.1999

Gadd, G.M., 1990. Heavy metal accumulation by bacteria and other microorganisms. Experientia 46, 834–840. https://doi.org/10.1007/BF01935534

Gao, L., Pan, X., Zhang, D., Mu, S., Lee, D.J., Halik, U., 2015. Extracellular polymeric substances buffer against the biocidal effect of H2O2 on the bloom-forming cyanobacterium *Microcystis aeruginosa*. Water Res. 69, 51–58. https://doi.org/10.1016/j.watres.2014.10.060

Gregson, C.R., Goddard, D.T., Sarsfield, M.J., Taylor, R.J., 2011a. Combined electron microscopy and vibrational spectroscopy study of corroded Magnox sludge from a legacy spent nuclear fuel storage pond. J. Nucl. Mater. 412, 145–156. https://doi.org/10.1016/j.jnucmat.2011.02.046

Gregson, C.R., Hastings, J.J., Sims, H.E., Steele, H.M., Taylor, R.J., 2011b. Characterisation of plutonium species in alkaline liquors sampled from a UK legacy nuclear fuel storage pond. Anal. Methods 3, 1957. https://doi.org/10.1039/c1ay05313b

Haas, B.J., Gevers, D., Earl, A.M., Feldgarden, M., Ward, D. V, Giannoukos, G., Ciulla, D., Tabbaa, D., Highlander, S.K., Sodergren, E., Methé, B., DeSantis, T.Z., The Human Microbiome Consortium, Petrosino, J.F., Knight, R., Birren, B.W., 2011. Chimeric 16S rRNA sequence formation and detection in Sanger and 454-Pyrosequenced PCR amplicons. Genome Res. 21, 494–504. https://doi.org/10.1101/gr.112730.110.Freely

Jackson, S.F., Monk, S.D., Riaz, Z., 2014. An investigation towards real time dose rate monitoring, and fuel rod detection in a First Generation Magnox Storage Pond (FGMSP). Appl. Radiat. Isot. 94, 254–259. https://doi.org/10.1016/j.apradiso.2014.08.019

Javanbakht, V., Alavi, S.A., Zilouei, H., 2014. Mechanisms of heavy metal removal

using microorganisms as biosorbent. Water Sci. Technol. 69, 1775–1787. https://doi.org/10.2166/wst.2013.718

Jensen, S.E., Nønbel, E., 1999. Description of the Magnox Type of Gas Cooled Reactor (MAGNOX).

Jespersen, A.-M., Christoffersen, K., 1987. Measurements of chlorophyll-a from phytoplankton using ethanol as extraction solvent. Arch. Hydrobiol. 109, 445–454.

Jolivet, E., Matsunaga, F., Ishino, Y., Forterre, P., Prieur, D., Myllykallio, H., 2003. Physiological responses of the hyperthermophilic archaeon " *Pyrococcus abyssi* " to DNA Damage Caused by ionizing radiation. J. Bacteriol. 185, 3958–3961. https://doi.org/10.1128/JB.185.13.3958

Joshi, N.A., Fass, F.N., 2011. Sickle: a sliding-window, adaptive, quality-based trimming tool for FastQ files (version 1.33). [Software].

Karley, D., Shukla, S.K., Rao, T.S., 2017. Isolation and characterization of culturable bacteria present in the spent nuclear fuel pool water. Environ. Sci. Pollut. Res. 1–9. https://doi.org/10.1007/s11356-017-0376-5

Katz, A., Waridel, P., Shevchenko, A., Pick, U., 2007. Salt-induced changes in the plasma membrane proteome of the halotolerant alga *Dunaliella salina* as revealed by blue native gel electrophoresis and nano-LC-MS/MS analysis. Mol. Cell. Proteomics 6, 1459–1472. https://doi.org/10.1074/mcp.M700002-MCP200

Khan, Z., Maznah, W., Omar, W., Merican, F., Sidik, M., Convey, P., 2018. Characterisation of *Pseudanabaena amphigranulata* (Synechococcales) isolated from a man-made pond , Malaysia : a polyphasic approach.

Klotz, A., Georg, J., Bučinská, L., Watanabe, S., Reimann, V., Januszewski, W., Sobotka, R., Jendrossek, D., Hess, W.R., Forchhammer, K., 2016. Awakening of a dormant cyanobacterium from nitrogen chlorosis reveals a genetically determined program. Curr. Biol. 26, 2862–2872. https://doi.org/10.1016/j.cub.2016.08.054

Kozich, J.J., Westcott, S.L., Baxter, N.T., Highlander, S.K., Schloss, P.D., 2013. Development of a dual-index sequencing strategy and curation pipeline for analyzing amplicon sequence data on the MiSeq Illumina sequencing platform. Appl. Environ. Microbiol. 79, 5112–5120. https://doi.org/10.1128/AEM.01043-13

Lewis, P.D., Lewis, K.E., Ghosal, R., Bayliss, S., Lloyd, A.J., Wills, J., Godfrey, R., Kloer, P., Mur, L. a J., 2010. Evaluation of FTIR spectroscopy as a diagnostic tool for lung cancer using sputum. BMC Cancer 10, 640. https://doi.org/10.1186/1471-2407-10-640

Maher, Z., Ivanov, P., O'Brien, L., Sims, H., Taylor, R.J., Heath, S.L., Livens, F.R., Goddard, D., Kellet, S., Rand, P., Bryan, N.D., 2016. Americium and plutonium association with magnesium hydroxide colloids in alkaline nuclear industry process environments. J. Nucl. Mater. 468, 84–96. https://doi.org/10.1016/j.jnucmat.2015.11.010

Maquelin, K., Kirschner, C., Choo-Smith, L.P., Van Den Braak, N., Endtz, H.P., Naumann, D., Puppels, G.J., 2002. Identification of medically relevant microorganisms by vibrational spectroscopy. J. Microbiol. Methods 51, 255–271. https://doi.org/10.1016/S0167-7012(02)00127-6

Martens, H., Nielsen, J.P., Engelsen, S.B., 2003. Light scattering and light absorbance separated by extended multiplicative signal correction. Application to near-infrared transmission analysis of powder mixtures. Anal. Chem. 75, 394–404. https://doi.org/10.1021/ac020194w

Martin, M., 2011. Cutadapt removes adapter sequences from high-throughput sequencing reads. EMBnet.journal 17, 10. https://doi.org/10.14806/ej.17.1.200

Masella, A.P., Bartram, A.K., Truszkowski, J.M., Brown, D.G., Neufeld, J.D., 2012. PANDAseq: PAired-eND assembler for Illumina sequences. BMC Bioinformatics 13, 1–7. https://doi.org/10.1186/1471-2105-13-31

MeGraw, V.E., Brown, A.R., Boothman, C., Goodacre, R., Morris, K., Sigee, D., Anderson, L., Lloyd, J.R., 2018. A novel adaptation mechanism underpinning algal colonization of a nuclear fuel storage pond. MBio 9, e02395-17. https://doi.org/DOI:10.1128/mBio.02395-17

Muhamadali, H., Weaver, D., Subaihi, A., AlMasoud, N., Trivedi, D.K., Ellis, D.I., Linton, D., Goodacre, R., 2015a. Chicken, beams, and *Campylobacter*: rapid differentiation of foodborne bacteria *via* vibrational spectroscopy and MALDI-mass spectrometry. Analyst 141, 111–122. https://doi.org/10.1039/c5an01945a

Muhamadali, H., Xu, Y., Ellis, D.I., Allwood, J.W., Rattray, N.J.W., Correa, E., Alrabiah, H., Lloyd, J.R., Goodacre, R., 2015b. Metabolic profiling of *Geobacter sulfurreducens* during industrial bioprocess scale-up. Appl. Environ. Microbiol. 81, 3288–3298. https://doi.org/10.1128/AEM.00294-15

Muhamadali, H., Xu, Y., Ellis, D.I., Trivedi, D.K., Rattray, N.J.W., Bernaerts, K., Goodacre, R., 2015c. Metabolomics investigation of recombinant mTNFα production in *Streptomyces lividans*. Microb. Cell Fact. 14, 1–12. https://doi.org/10.1186/s12934-015-0350-1

Naumann, D., 2000. Infrared spectroscopy in microbiology. Encycl. Anal. Chem. 102–131. https://doi.org/10.1002/9780470027318.a0117

NDA, 2016. Nuclear Decommissioning Authority: Business plan 2017 to 2020 [WWW Document]. Gov.uk. URL https://www.gov.uk/government/consultations/nuclear-decommissioning-authority-business-plan-2017-to-2020 (accessed 5.4.18).

Neil, T.S., Morris, K., Pearce, C.I., Sherriff, N.K., Burke, M.G., Chater, P.A., A, J., Natrajan, L., Shaw, S., n.d. Stability, composition and core-shell particle structure of uranium(IV)-silicate colloids. Environ. Sci. Technol.

Nobles, D.R., Romanovicz, D.K., Brown Jr, R.M., 2001. Cellulose in cyanobacteria. Origin of vascular plant cellulose synthase? Plant Physiol. 127, 529–542. https://doi.org/10.1104/pp.010557

Nurk, S., Bankevich, A., Antipov, D., Gurevich, A., Korobeynikov, A., Lapidus, A., Prjibelsky, A., Pyshkin, A., Sirotkin, A., Sirotkin, Y., Stepanauskas, R., McLean, J., Lasken, R., Clingenpeel, S.R., Woyke, T., Tesler, G., Alekseyev, M.A., Pevzner, P.A., 2013. Assembling genomes and mini-metagenomes from highly chimeric reads, in: Conference: Proceedings of the 17th International Conference on Research in Computational Molecular Biology, RECOMB 2013. Bejing, China, pp. 158–170. https://doi.org/10.1007/978-3-642-37195-0_13

Pikuta, E. V., Hoover, R.B., Tang, J., 2007. Microbial extremophiles at the limits of life. Crit. Rev. Microbiol. 33, 183–209. https://doi.org/10.1080/10408410701451948

Pop, C., Apostu, S., Rotar, A.M., Semeniuc, C.A., Sindic, M., Mabon, N., 2013. FTIR spectroscopic characterization of a new biofilm obtained from kefiran. J. Agroaliment. Process. Technol. 19, 157–159.

Rivasseau, C., Farhi, E., Atteia, A., Couté, A., Gromova, M., de Gouvion Saint Cyr, D., Boisson, A.-M.M., Féret, A.-S., Compagnon, E., Bligny, R., 2013. An extremely radioresistant green eukaryote for radionuclide bio-decontamination in the nuclear industry. Energy Environ. Sci. 6, 1230–1239. https://doi.org/Doi 10.1039/C2ee23129h

Rivasseau, C., Farhi, E., Compagnon, E., de Gouvion Saint Cyr, D., van Lis, R., Falconet, D., Kuntz, M., Atteia, A., Couté, A., 2016. *Coccomyxa actinabiotis* sp. nov. (Trebouxiophyceae, Chlorophyta), a new green microalga living in the spent fuel cooling pool of a nuclear reactor. J. Phycol. 52, 689–703. https://doi.org/10.1111/jpy.12442

Rivasseau, C., Farhi, E., Gromova, M., Ollivier, J., Bligny, R., 2010. Resistance to irradiation of micro-algae growing in the storage pools of a nuclear reactor investigated by NMR and neutron spectroscopies. Spectroscopy 24, 381–385. https://doi.org/10.3233/SPE-2010-0459

Sarró, M.I., García, A.M., Moreno, D.A., 2005. Biofilm formation in spent nuclear fuel pools and bioremediation of radioactive water. Int. Microbiol. 8, 223–230. https://doi.org/im2305032 [pii]

Sarró, M.I., García, A.M., Moreno, D.A., Montero, F., 2007. Development and characterization of biofilms on stainless steel and titanium in spent nuclear fuel pools. J. Ind. Microbiol. Biotechnol. 34, 433–441. https://doi.org/10.1007/s10295-007-0215-7

Sarró, M.I., Moreno, D.A., Chicote, E., Lorenzo, P.I., García, A.M., Montero, F., 2003. Biofouling on austenitic stainless steels in spent nuclear fuel pools. Mater. Corros. Und Korrosion 54, 535–540. https://doi.org/DOI 10.1002/maco.200390117

Sigee, D.C., Selwyn, A., Gallois, P., Dean, A.P., 2007. Patterns of cell death in freshwater colonial cyanobacteria during the late summer bloom. Phycologia 46, 284–292. https://doi.org/10.2216/06-69.1

Simonova, D., Karamancheva, I., 2013. Application of Fourier transform infrared spectroscopy for tumor diagnosis. Biotechnol. Biotechnol. Equip. 27, 4200–4207. https://doi.org/10.5504/BBEQ.2013.0106

Singh, H., Anurag, K., Apte, S.K., 2013. High radiation and desiccation tolerance of nitrogen-fixing cultures of the cyanobacterium *Anabaena* sp. strain PCC 7120 emanates from genome/proteome repair capabilities. Photosynth. Res. 118, 71–81. https://doi.org/10.1007/s11120-013-9936-9

Song, W., Zhao, C., Zhang, D., Mu, S., Pan, X., 2016. Different resistance to UV-B radiation of extracellular polymeric substances of two cyanobacteria from contrasting habitats. Front. Microbiol. 7, 1–8. https://doi.org/10.3389/fmicb.2016.01208

The nuclear fuel cycle [WWW Document], 2018. . World Nucl. Assoc. URL http://www.world-nuclear.org/information-library/nuclear-fuel-cycle/introduction/nuclear-fuel-cycle-overview.aspx (accessed 2.6.18).

Tišáková, L., Pipíška, M., Godány, A., Horník, M., Vidová, B., Augustín, J., 2013. Bioaccumulation of 137Cs and 60Co by bacteria isolated from spent nuclear fuel pools. J. Radioanal. Nucl. Chem. 295, 737–748. https://doi.org/10.1007/s10967-012-1932-6

Wang, Q., Garrity, G.M., Tiedje, J.M., Cole, J.R., 2007. Naïve Bayesian classifier for rapid assignment of rRNA sequences into the new bacterial taxonomy. Appl. Environ. Microbiol. 73, 5261–5267. https://doi.org/10.1128/AEM.00062-07

Wang, Z., Xu, B., Zhao, X., Jiang, J., Chen, S., 1998. The effect of gamma-irradiation on different strains and morphological filaments of *Spirulina*. Acta Agric. Univ. Zhejiangensis 24, 121–125.

Webster-Brown, J.G., Hawes, I., Jungblut, A.D., Wood, S.A., Christenson, H.K., 2015. The effects of entombment on water chemistry and bacterial assemblages in closed cryoconite holes on Antarctic glaciers. FEMS Microbiol. Ecol. 91, 1–14. https://doi.org/10.1093/femsec/fiv144

Wilson, P.D., 1996. The nuclear fuel cycle from ore to waste. Oxford University Press, Oxford.

Wold, S., Ebensen, K., Geladi, P., 1986. Principal component analysis. Chemom. Intell. Lab. Syst. 2, 37–52.

Xu, H., Yu, G., Jiang, H., 2013. Investigation on extracellular polymeric substances from mucilaginous cyanobacterial blooms in eutrophic freshwater lakes. Chemosphere 93, 75–81. https://doi.org/10.1016/j.chemosphere.2013.04.077

Zhu, M., Yu, G., Song, G., Chang, J., Wan, C., Li, R., 2015. Molecular specificity and detection for *Pseudanabaena* (cyanobacteria) species based on *rbcLX* sequences. Biochem. Syst. Ecol. 60, 110–115. https://doi.org/10.1016/j.bse.2015.04.009

5.8 Supplementary material

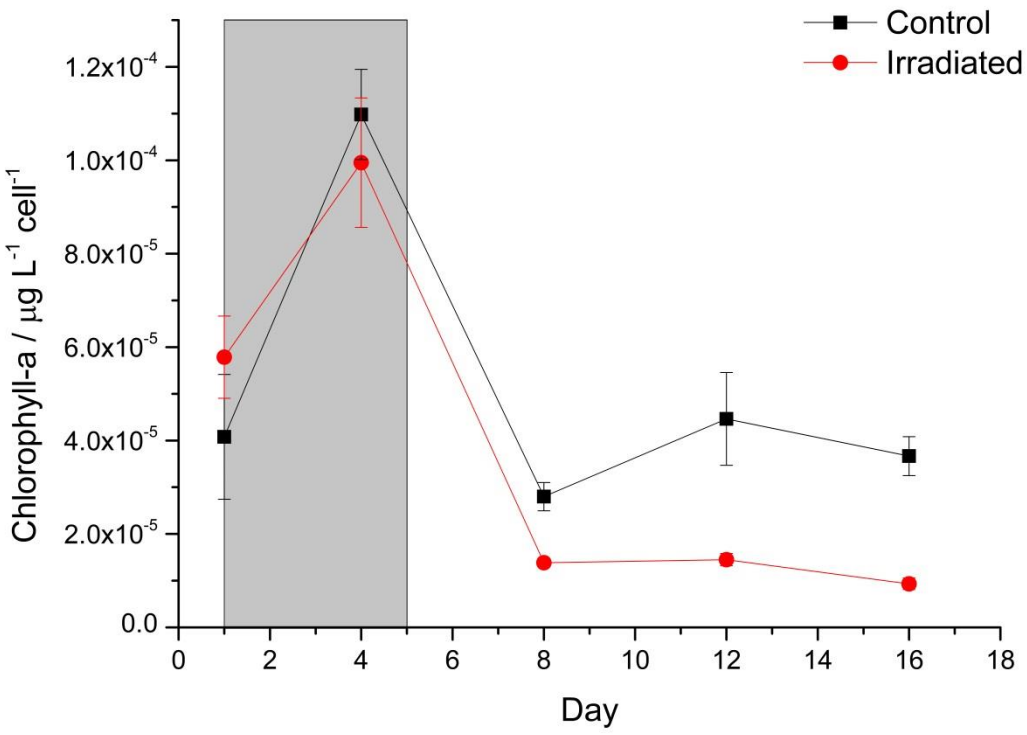

Supplementary figure 5-1: Chlorophyll-a concentration (µg L^{-1}) normalised to average cell number. Grey box indicated period where irradiation treatment was being administered. Error bars denote standard deviation of three replicates

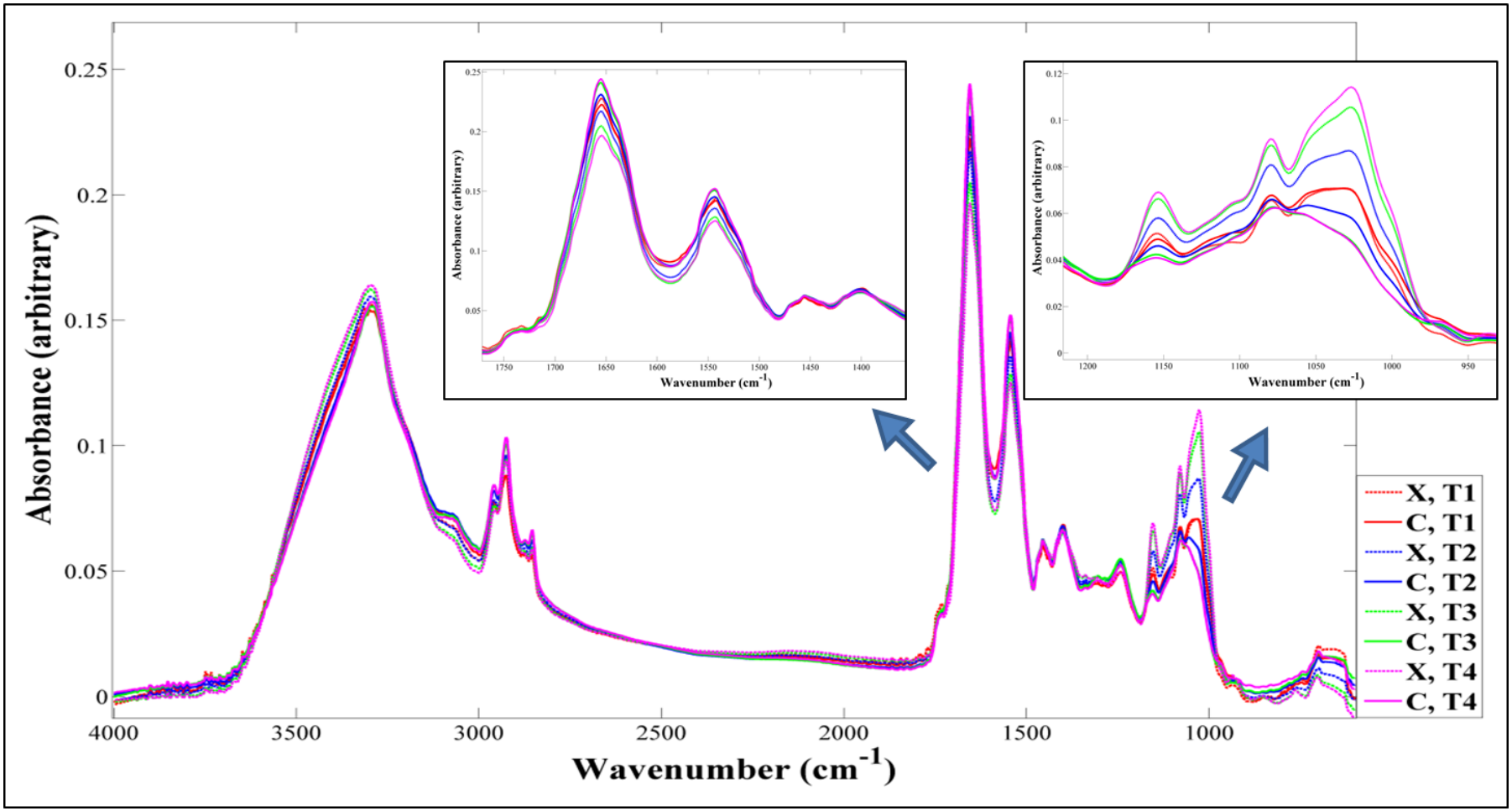

Supplementary Figure 5-2: Average absorbance FT-IR spectra, with zooms of important spectral features. X denotes irradiated samples and C denotes control samples. T1= day 4; T2= day 8; T3= day 12; and T4= day 16

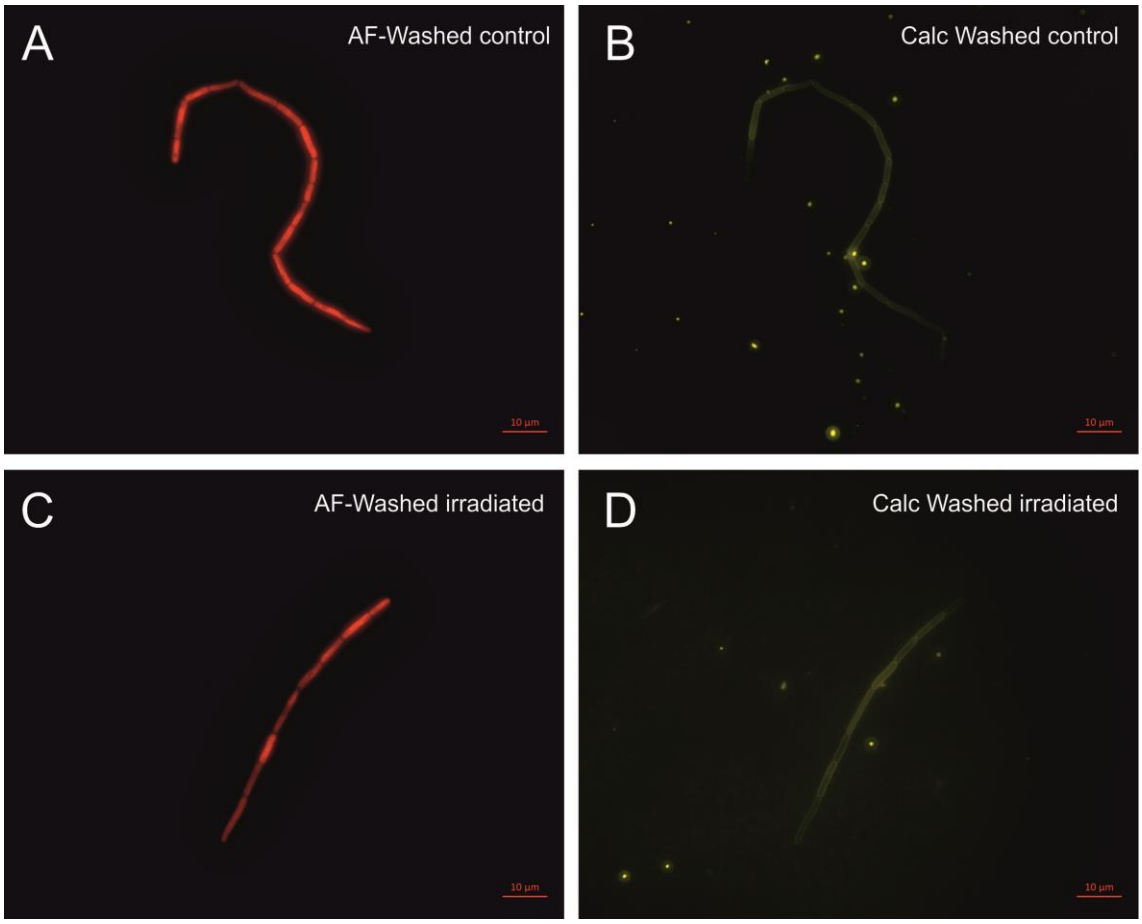

Supplementary Figure 5-3: Light microscopy of *P. catenata* filaments at day 4 after washing in normal saline: a) autofluorescence of control culture; b) calcofluor white stained control culture; c) autofluorescence of irradiated culture; and d) calcofluor white stained irradiated culture. AF= autofluorescence; Calc= calcofluor white stain.

Chapter 6

Research chapter 6: The fate of Sr in the presence of *Pseudanabaena catenata*

6 Research chapter 6: The fate of Sr in the presence of *Pseudanabaena catenata*

Lynn Foster, Adrian Cleary, Heath Bagshaw, David Sigee, Jon K Pittman, Katherine Morris, Kejing Zhang, Kurt F Smith, and Jonathan R Lloyd*

Research Centre for Radwaste Disposal and Williamson Research Centre for Molecular Environmental Science, School of Earth and Environmental Sciences, The University of Manchester, Oxford Road, Manchester M13 9PL, U.K.

KEYWORDS: Cyanobacteria, Sr behaviour, TEM, polyphosphate bodies, EXAFS

6.1 Abstract

A non-axenic culture of *Pseudanabaena catenata*, representative of the bloom-forming cyanobacterium found in a high pH legacy Spent Nuclear Fuel Pond (SNFP) at the Sellafield Nuclear Facility, was supplemented with 1 mM of $SrCl_2$, to determine its effect on the fate of Sr. The addition of Sr to the *P. catenata* culture resulted in ~16 % reduction in the overall growth of the culture (OD_{600nm}) and a 21 % reduction in the concentration of chlorophyll-a (Chl-a) compared to those without Sr. The fate of Sr was assessed using a multi-technique approach. Inductively coupled plasma atomic emission spectroscopy (ICP-AES) showed that virtually all of the Sr was removed from solution, while extracellular Sr-enriched biomineral precipitates were detected using transmission electron microscopy (TEM) analysis, which were shown to contain Sr, Ca and S using energy-dispersive X-ray spectroscopy (EDS) analysis. In addition, intracellular P-containing electron-dense features, likely to be polyphosphate (polyP) bodies, were associated with the *P. catenata* cells and contained low levels of Sr. Bulk analysis of the cultures by X-ray diffraction (XRD) showed the presence of Ca containing strontianite ($Sr(Ca)CO_3$), whilst extended X-ray absorption fine-structure spectroscopy (EXAFS) analysis showed the presence of $SrPO_4$ minerals. The presence of Sr associated with intracellular polyP was unexpected, and contrasts with other model photosynthetic systems in the literature that have highlighted carbonate biominerals as the dominant sink for Sr. Understanding the fate of freely available Sr within microorganisms associated with SNFPs is crucial to understanding the fate of radioactive ^{90}Sr in such

extreme environments, and could also suggest a potential remediation strategy for treatment of ^{90}Sr contaminated waters from SNFPs and also in contaminated aquatic systems.

6.2 Introduction

The generation of energy by the nuclear industry has resulted in the production of significant levels of radioactive spent fuel and other radioactive waste (Crossland, 2012; Wilson, 1996). Despite efforts to contain these radioactive materials, accidental releases have occurred, for example the accidents associated with the nuclear reactors at the Chernobyl (Ukraine) and Fukushima (Japan) sites (Fukuda *et al*., 2014; Krejci *et al*., 2011). The release of radionuclides into the environment requires effective remediation strategies to be employed to minimize their transport and any harmful effects. There has been a lot of interest in the potential use of microorganisms in cost-effective and efficient remediation strategies, since they are ubiquitous in the environment and have a diverse range of metabolic capabilities (Blanco-Rivero *et al*., 2005; Pikuta *et al*., 2007). A wide range of microorganisms, including bacteria, cyanobacteria, eukaryotic algae and fungi are known to influence the uptake of radionuclides by either metabolism-independent or dependent mechanisms (Gadd, 1990).

Of particular interest is the removal of fission products, such as ^{137}Cs and ^{90}Sr from aquatic environments, since they are not only radioactive but also bioavailable, as analogues for K^+ and Ca^{2+}, respectively (Brookshaw *et al*., 2012; Fukuda *et al*., 2014; Simonoff *et al*., 2007). The ability of microorganisms to influence the fate of these key fission products has been demonstrated, for example with high levels of ^{137}Cs uptake by the eukaryotic microalgal species *Coccomyxa actinabiotis* (Rivasseau *et al*., 2013). The fate of ^{90}Sr appears to be strongly linked to Ca behaviour with, for example, co-association with carbonate minerals that can precipitate out of solution or adsorb to surfaces (Fukuda *et al*., 2014; Kang *et al*., 2014; Lauchnor *et al*., 2013). In addition Sr is known to interact with phosphate, for example it can sorb to the surface of hydroxyapatite [$Ca_5(PO_4)_3(OH)$] and can be removed from solution in the presence of glycerol 2-phosphate (Handley-Sidhu *et*

al., 2014). The majority of carbonate mineral formation is thought to occur as extracellular precipitates that can adsorb to a variety of surfaces including clays and extracellular features of microorganisms (Chiang *et al*., 2010; Gadd, 1990; Schultze-Lam and Beveridge, 1994). Strontium carbonate formation has recently been shown to occur intracellularly in a small number of microorganisms including the desmid green algae *Closterium moniliferum*, and more recently some cyanobacteria species, e.g. *Candidatus Gleomargarita lithophora* (Cam *et al*., 2015; Cam *et al*., 2016; Krejci *et al*., 2011; Couradeau *et al*., 2012). Li *et al*., (2016) observed that traditional electron microscopy methods used to prepare microbial cells for examination of ultrastructure and sites of metal accumulation, can result in the removal or distortion of such features, and therefore give a false account of intracellular carbonate biomineralisation. It is therefore likely that the number of microbial species which are identified as being capable of forming such intracellular carbonate minerals will increase with improvements in preparation techniques.

In the UK, legacy waste from Magnox reactors, a type of gas-cooled nuclear reactor, has been stored in the First Generation Magnox Storage Pond (FGMSP). The FGMSP is an open air spent nuclear fuel pond (SNFP) on the Sellafield site (Cumbria, UK), since the late 1950s (Sellafield, 2014; Wilson, 1996). Magnox reactor fuel consisted of unenriched uranium metal clad in a magnesium non-oxidising (Magnox) alloy, which both have low chemical stabilities in water (Gregson *et al*., 2011a; Jackson *et al*., 2014). The Magnox fuel was originally intended for reprocessing, but in some cases has been stored in the Spent Nuclear Fuel Pond (SNFP) for considerably longer than anticipated, which has led to extensive corrosion of the MAGNOX cladding and fuel (Jackson *et al*., 2014). As a result of fuel corrosion, the pond has significant levels of radiation associated with the corroded spent nuclear fuel (NDA, 2016), pond effluent, and radioactive sludge (Gregson *et al*., 2011a; Gregson *et al*., 2011b; Jackson *et al*., 2014), of which a major constituent is brucite ($Mg(OH)_2$) (Ashworth *et al*., 2018). In addition to the radioactive inventory, the pond is open to the air and so it is subject to an influx of carbon, nitrogen and environmental debris (Gregson *et al*., 2011a; Gregson *et al*., 2011b; Jackson *et al*., 2014). The pond is continuously purged with alkaline dosed demineralised water at alkaline pH (~11.5), which provides thermal cooling whilst

minimizing any further corrosion to the fuel (Gregson *et al*., 2011a; Gregson *et al*., 2011b; Jackson *et al*., 2014).

Despite the extreme conditions of high pH and significant radioactivity, microorganisms are known to colonise the pond, with exponential growth periods observed and reported as algal blooms (Gregson *et al*., 2011a; Gregson *et al*., 2011b; see Research chapter 4: The microbial ecology of a high pH spent nuclear fuel pond on the Sellafield site). Recently the microbial community of the pond has been investigated over a three year period including during a bloom event in August 2016 (see Research chapter 4: The microbial ecology of a high pH spent nuclear fuel pond on the Sellafield site). The pond community of background water samples was shown to be dominated by Proteobacteria, with photosynthetic or hydrogen-metabolising capabilities present in abundant members of the population. During the August 2016 bloom event, the cyanobacterium, *Pseudanabaena catenata* (see Research chapter 4: The microbial ecology of a high pH spent nuclear fuel pond on the Sellafield site) was the most abundant organism detected, making up ~30 % of the 16S rRNA genes sequenced in water samples. Despite its presence in a range of other environments and in algal blooms (Acinas *et al*., 2009; Zhu *et al*., 2015), there is little information in the scientific literature about the ecology of this filamentous cyanobacterium, and its impact on radionuclide speciation.

The legacy SNFP is currently undergoing decommissioning as a high priority. This includes waste retrieval operations and more recently the removal of the radioactive sludge (Sellafield, 2014). It is important to understand the potential fate of key radionuclides in the pond during these plant operations, to ensure that they are safely managed and processed. ^{90}Sr is present at low but significant levels, and is both highly active and potentially very soluble, and thus needs to be considered carefully during effluent processing and discharge (Ashworth *et al*., 2018). The purpose of this investigation was to determine the fate of Sr in the presence of microorganisms representative of those in the FGMSP system, namely a mixed laboratory culture dominated by *P. catenata*, which is considered a good model for the pond community (Research Chapter 5: The effect of X-irradiation on the growth and metabolic status of *Pseudanabaena catenata*). This study also aimed to determine if intracellular Sr-containing minerals could be formed by this species of cyanobacterium. Here we demonstrate that in the presence of an actively growing *P.*

catenata culture, Sr forms both $(Sr,Ca)CO_3$ and $SrPO_4$ minerals. Interestingly, Sr could be observed by TEM and EDS analysis in association with the electron dense intracellular features containing P, thought to be polyphosphate (polyP) bodies. Understanding the interactions between Sr and the *P. catenata* culture provides an insight into the potential fate of Sr in the pond and may provide potential remediation strategies in other ^{90}Sr contaminated aquatic sites.

6.3 Methods

6.3.1 Culturing of *Pseudanabaena catenata* with Sr

Experiments were set up to investigate the interaction and fate of Sr with a cyanobacterium, *P. catenata,* which has been identified in a legacy SNFP on the Sellafield Ltd. site. Control measures in place at the Sellafield Ltd. site for the legacy SNFP prevented the isolation and culturing of microorganisms directly from pond water. A photosynthetic culture dominated by *P. catenata*, which is the closest match to the species identified in the pond, was obtained from the NIVA Culture Collection of Algae (NIVA-CYA 152), Norway. Whilst an axenic culture could not be sourced, previous 16S rRNA gene sequencing revealed that of the 9 operational taxonomic units (OTUs) identified in this culture, 5 were affiliated with genera identified in the legacy SNFP (Research Chapter 5: The effect of X-irradiation on the growth and metabolic status of *Pseudanabaena catenata*). The *P. catenata* culture used was therefore considered representative of the pond community.

Cultures were set up by inoculating *P. catenata* into 30 mL of unbuffered BG11 medium (Culture Collection of Algae and Protozoa) to a starting optical density (600 nm) of 0.2. Three biological replicates were spiked with $SrCl_2$ (Sigma-Aldrich) solution to a final concentration of 1 mM. The concentration of Sr used in this experiment is significantly higher than observed in the pond, the higher concentration was used to make the detection of any minerals easier. A further three identical cultures were set up with sterile deionised water used to adjust the total volume in line with the Sr-containing cultures, to assess the impact of Sr on the growth of the culture. All cultures were incubated at 25 ±1 °C, and shaken at 100

rpm in a light incubator with a photon flux density of 150 μmol m^{-2} s^{-1}, with a 16:8 h light-dark cycle (supplied by cool fluorescent daylight lamps). Sterile controls were also set up using 30 mL BG11 medium with 1 mM $SrCl_2$ to determine the effect of abiotic versus biotic processes.

6.3.2 Optical density, chlorophyll-a concentration, and pH measurements

In order to determine whether the addition of Sr affected the growth of *P. catenata*, optical density, chlorophyll-a (Chl-a) concentration and pH measurements were taken at selected time points throughout the experiment. All absorbance measurements were carried out on 1 mL samples using a Jenway 6700 UV/Vis spectrophotometer (Bibby Scientific Ltd, Staffordshire, UK). The growth of the *P. catenata* culture was assessed by measuring optical density at 600 nm (OD_{600nm}) to indicate the total biomass present in the cultures. The concentration of Chl-a was determined using the same samples as used for the OD_{600nm} measurements, as described in Research Chapter 5: The effect of X-irradiation on the growth and metabolic status of *Pseudanabaena catenata*. Briefly, the cells from a 1 mL sample were pelleted by centrifuging at 14,000 *g* for 10 min and the supernatant was discarded. The cells were re-suspended in 1 mL of 70 % ethanol and left in the dark at room temperature for 2 h. The samples were centrifuged for a further 10 min at 14,000 *g*, and the absorbance of the supernatant was recorded at 665 nm (Chl-a) and 750 nm (turbidity correction). The concentration of Chl-a was calculated using the formula as set out by Jespersen and Christoffersen (1987). pH measurements were made using a calibrated FiveEasyPlus pH Meter (Mettler Toledo Ltd, Leicestershire, UK).

6.3.3 Assessment of Sr behaviour

The fate of Sr in the presence of the *P. catenata* culture was determined using a range of analytical techniques.

6.3.3.1 Inductively coupled plasma atomic emission spectroscopy (ICP-AES)

The concentration of soluble Sr in the culture medium was measured by inductively coupled plasma atomic emission spectrometry (ICP-AES, Perkin-Elmer Optima 5300 dual view) using a matrix-matched serially diluted Specpure multielement plasma standard solution 4 (Alfa Aesar) for calibration. Briefly, a 600 μL sample was centrifuged at 14,000 *g* for 10 min, 500 μL of supernatant was added to 9.5 mL of 2 % nitric acid prior to analysis.

6.3.4 Electron Microscopy

In order to image any Sr minerals formed during the experiment and their potential interactions with *P. catenata* (and other associated microorganisms present in the culture), electron microscopy was carried out on non-fixed samples. Samples (1 mL) were taken after 20 days of incubation for analysis by transmission electron microscopy (TEM). The samples were washed twice in sterile demineralised water (centrifuged 10 min at 14,000 *g*). For TEM analysis, 2 μL of the washed cell suspension was dropped onto a copper TEM grid with a carbon film (Agar Scientific, Essex, UK) and allowed to dry at room temperature. The samples were assessed using a FEI Tecnai T20 LaB6 Transmission Electron Microscope operating at 200 kV equipped with an Oxford XMax EDS detector. The images were captured with Gatan Digital Micrograph whilst the EDS data analysis was performed using Oxford INCA software.

6.3.4.1 X-Ray Diffraction (XRD)

An aliquot of culture containing Sr was centrifuged to pellet the cells, the supernatant was discarded, and the cell pellet was spread evenly over a glass slide and allowed to dry. The sample was then analysed by XRD to identify any crystalline Sr-containing minerals present. Measurements were carried out on a Bruker D8 Advance diffractometer, equipped with a Göbel Mirror a Lynxeye detector. The X-ray tube had a Cu source, providing Cu $K_{\alpha 1}$ X-rays with a

wavelength of 1.540 Å. The sample was scanned from 5-70 ° 2θ, with a step size of 0.01 ° and a count time of 1.5 s per step. The resultant patterns were evaluated using EVA version 4, which compares experimental data to standards from the ICDD (International Centre for Diffraction Data) Database.

6.3.4.2 Extended X-ray absorption fine structure (EXAFS)

The coordination environment of Sr in the solid phase was analysed using X-ray absorption spectroscopy (XAS). Samples were prepared for XAS by removing the solid phase after 20 days from the culture media by vacuum filtration and then diluting with cellulose to form a pellet with approximately 1 % Sr loading. Sr K-edge spectra (16115.26 keV) were collected in transmission mode on Beamline B18 at the Diamond Light Source, Harwell, using a liquid nitrogen cooled cryostat. Multiple scans were averaged, calibrated, background subtracted and normalised using ATHENA (Ravel and Newville, 2005). ARTEMIS was then used to fit extended X-ray absorption fine structure (EXAFS) spectra to determine the coordination of Sr in the solid phase (Ravel and Newville, 2005). Shells were only included in the fit if they made a statistically significant improvement to the model fit as determined by the F-test (Downward *et al*., 2007).

6.3.5 PHREEQC modelling

All speciation and saturation thermodynamic calculations were performed using the United States Geological Survey thermodynamic speciation code PHREEQC Interactive (3.3.7) using the Andra Specific Interaction Theory (SIT)- database (ThermoChimie v.9.b0 August 2015version 3.4.0. The theoretical behaviour of Sr in BG11 medium was predicted at pH 7.2 and 10.

6.4 Results

6.4.1 The effect of Sr on the growth of the *P. catenata* culture

In order to determine whether the addition of Sr had any effect on the growth of the *P. catenata* culture, the optical density and the concentration of Chl-a of the cultures were measured. Measurements were taken over a period of 20 days. Both the control and Sr-containing cultures showed a steady increase in absorbance over the 20-day sampling period as expected, when inoculated with an actively growing culture (Figure 6-1a). The two sets of treatments started with approximately the same OD_{600nm} measurements of 0.21 for the Sr-containing cultures compared to 0.22 in the Sr-free controls. The culture containing Sr grew at the same rate as the control until day 12, indicating that the addition of the Sr did not inhibit growth during this period. The cultures reached their highest optical densities at day 20 at 2.49 and 2.10 for the control and Sr-containing cultures respectfully. Assessment of the OD_{600nm} measurements at day 20, using a one-way ANOVA test, shows that there was a significant difference between these measurements (P-value 0.01, F-ratio 15.3). This indicates that at the end of the sampling period the Sr had a measurable inhibitory effect on the final growth yields of the *P. catenata* culture compared to the control. In addition to the OD_{600nm} measurements, the concentration of Chl-a was measured to give an indication of the photosynthetic biomass of the cultures (Figure 6-1b). The cultures started off with Chl-a concentrations of 0.66 mg L^{-1} and 0.60 mg L^{-1} for the control and Sr-containing cultures respectfully. Both sets of cultures showed a continuous increase in the concentration of Chl-a, and were not significantly different for the first 12 days of the experiment. At day 20 the concentrations recorded were 8.0 mg L^{-1} in the control and 6.3 mg L^{-1} in the Sr-containing cultures, which represents a 21 % reduction in Chl-a levels between the two treatments. The differences seen between the two treatments at day 20 are significant according to a one-way ANOVA test (P-value 0.04, F-ratio 9.4). The reduction in the Chl-a concentrations are consistent with the reduction seen in the OD_{600nm} measurements indicating that this is likely to be a consequence of reduced biomass. The pH of the cultures was not controlled externally during the course of the experiment, allowing for natural shifts as a result of the photosynthetic activity of *P. catenata*. The pH

started at 7.5 and 7.6 in the control and Sr-containing cultures respectfully (Figure 6-1c). By day 5 the pH had risen to 9.3 (control) and 9.7 (Sr-containing) and remained relatively consistent over the remaining sampling period. The pH of sterile BG11 medium with Sr remained stable over the same experimental period (data not shown), which confirms that that the increase in the pH is driven by photosynthesis (Jin *et al*., 2005; López-Archilla *et al*., 2004).

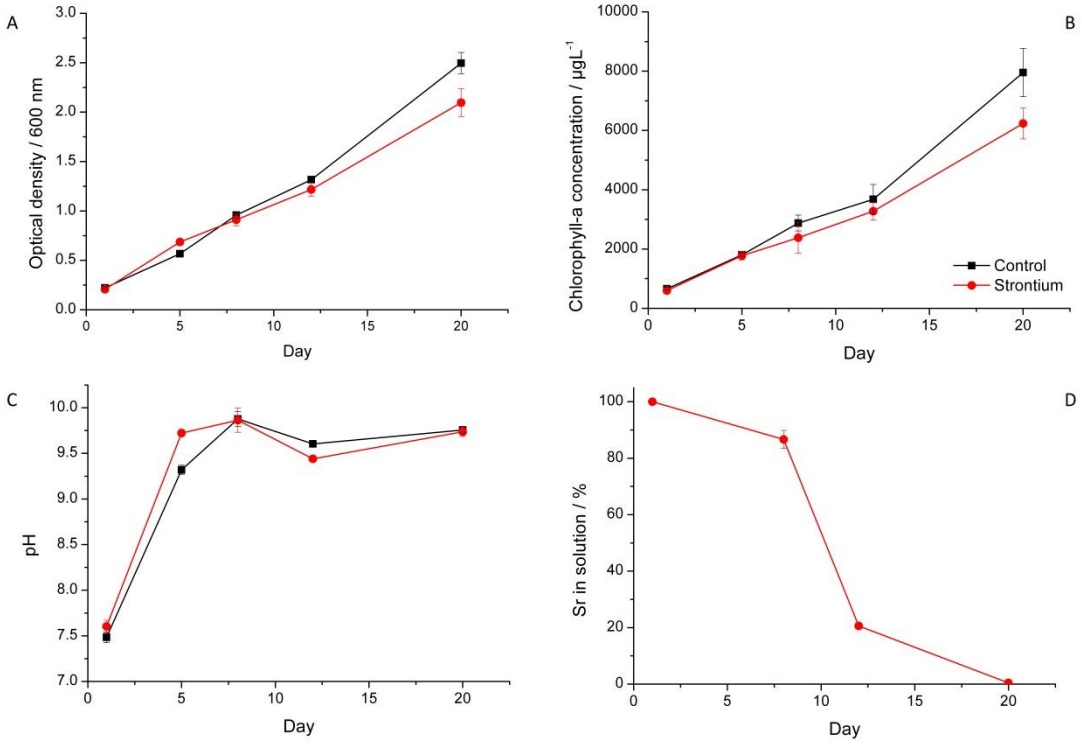

Figure 6-1: Growth curves of *P. catenata* with and without the addition of Sr: a) optical density at 600 nm; b) Chl-a concentrations (µgL^{-1}); c) pH; d) percentage of Sr in solution measured by ICP-AES. Error bars are the standard deviation of 3 replicates.

6.4.2 Sr removal from solution

In order to determine the amount of Sr in solution, ICP-AES was used to measure the concentration of Sr throughout the study (Figure 6-1d). At day 8, 13.5 % Sr was

removed from solution. In the next 4 days a further 65.3 % was removed from solution and by day 20 only 0.46 % of the total Sr added remained soluble. The largest reduction in soluble Sr concentrations coincided with the maximum pH measurements recorded. In contrast a maximum of 20 % of Sr was insoluble in sterile BG11 medium controls (Supplementary Figure 6-1), indicating the large-scale removal seen in this study was microbiologically driven.

6.4.3 Sr speciation and saturation calculations

Thermodynamic modelling of 1 mM Sr in BG11 medium was carried out to identify the products that could precipitate with Sr under our experimental conditions (Supplementary Table 6-1). The modelling indicated when the BG11 medium was held at a pH of 7.2, Ca and Sr metal phosphate phases were over saturated, suggesting precipitation was possible. When the modelling was repeated at pH 10, the saturation indices $\log_{10}$(ion activity/solubility product) for the metal phosphates phases increased, indicating that precipitation was more favourable. The thermodynamic calculations at the elevated pH (10) suggested that carbonates such as strontianite ($SrCO_3$) were oversaturated. The concentration of PO_4^{3-} and CO_3^{2-} in BG11 medium was 0.23 mM and 0.19 mM, respectively.

6.4.4 Determining the fate of Sr in the *P. catenata* culture

6.4.4.1 Electron Microscopy analysis

TEM was used to analyse samples from both the Sr-containing (and control cultures) to determine where the Sr was located and if it was associated with the microorganisms. The samples were washed twice with sterile demineralised water and air dried prior to analysis. Cells were clearly visible in both sets of samples, with the distinctive *P. catenata* filaments clearly visible (~ 1 μm x 5 μm). In both sets of samples *P. catenata* cells displayed circular electron dense features, which

frequently occurred centrally down the length of the filaments (Figure 6-2a and Supplementary Figure 6-2). EDS analysis of these features commonly identified the presence of phosphorus, suggested that these features could be polyP bodies. In addition low levels of calcium could be detected in association with these features. Sr could also be detected with phosphorus, indicating that the Sr detected could be intracellular (Figure 6-2). Sr could not be detected in other regions of the cells (Supplementary Figure 6-3), indicating that any Sr that is taken up by the cells was localised with the P-containing features. The micrographs also showed the

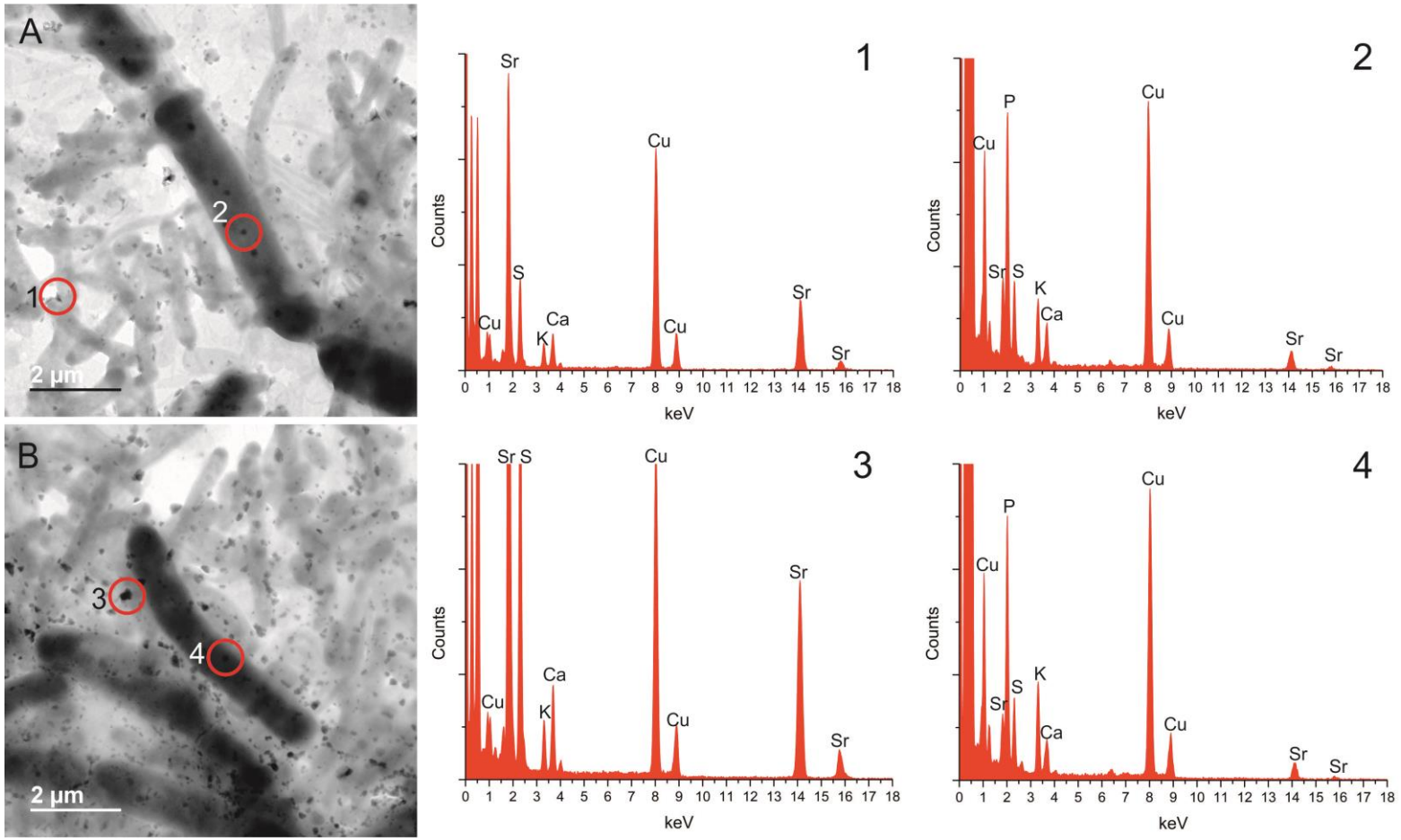

Figure 6-2: TEM images and EDS data taken from samples of *P. catenata* cultures incubated with $SrCl_2$ at day 20, washed twice. EDS data corresponds to the numbers on TEM images, site of scans indicated by red circle. All scale bars represent 2 µm.

presence of Sr-containing minerals which appeared to be extracellular but were still associated with the microorganisms (Figure 6-2: A1 and B3). EDS analysis of the extracellular minerals showed the presence of Sr, Ca and S in different proportions.

6.4.4.2 X-ray diffraction (XRD) characterisation of Sr biominerals

The remaining *P. catenata* culture that contained Sr was analysed using XRD to identify any crystalline minerals that had been formed during the course of the study. The results of the scan indicated the presence a carbonate mineral which was comprised of Sr and Ca in a ratio of 0.85 : 0.15 (Figure 6-3).

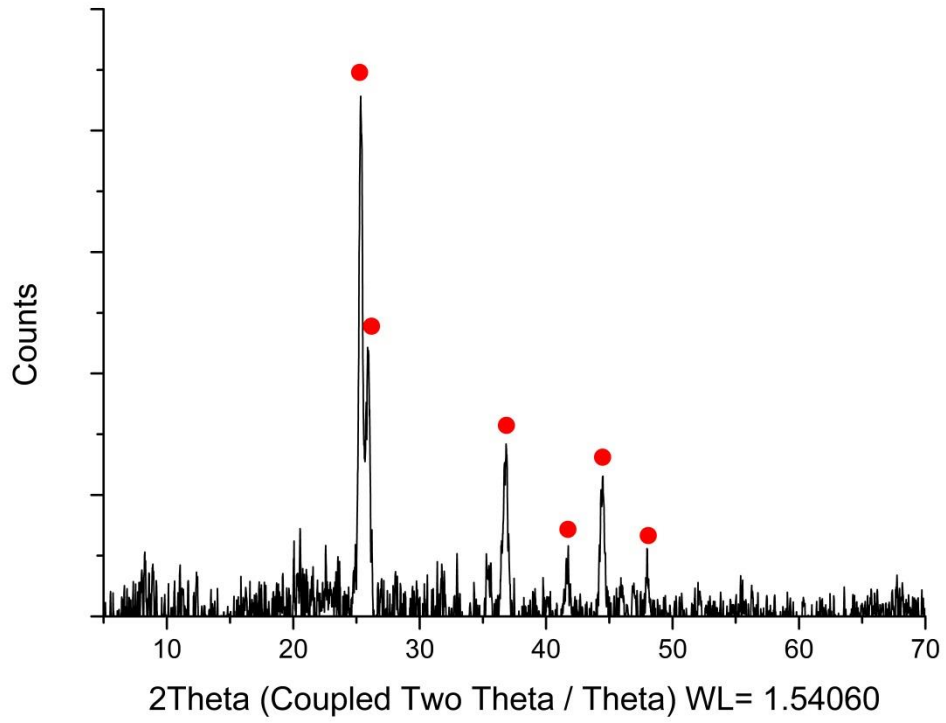

Figure 6-3: XRD analysis of a bulk sample of *P. catenata* culture incubated with Sr. Red dots indicate the presence of calcian strontianite [(Sr 0.85, Ca 0.15) (CO_3)]

6.4.4.3 EXAFS analysis of Sr minerals

The speciation and coordination environment of Sr in the biominerals was analysed using X-ray absorption spectroscopy. K-edge X-ray absorption near-edge spectroscopy (XANES) and EXAFS spectra were collected on Sr in the solid phase. XANES spectra for all samples showed a single peak consistent with a 9 fold coordination environment with no evidence for 6 fold coordination observed in Sr substituted calcite (Thorpe *et al*., 2012a; Thorpe *et al*., 2012b). Modelling of the EXAFS as outer sphere sorbed Sr with a single shell of 9 oxygen atoms at a distance of 2.6 Å provided a satisfactory first fit, however there were features between 3.2 and 3.6 Å in the Fourier Transform that were not resolved with this simple model (Figure 6-4). Further refinement of the the EXAFS modelling was informed by the relevant literature on Sr mineral formation (Bazin *et al*., 2014; Handley-Sidhu *et al*., 2014; Thorpe *et al.*, 2012b). The best fit was obtained when Sr was modelled to be incorporated into a phosphate mineral, with a shell of 1.8 P scattering paths at 3.2 Å and 1 Sr scattering path at 3.48 Å. These bond lengths are consistent with Sr substituted into hydroxyapatite-like nanoparticulate phases seen in previous literature (Bazin *et al*., 2014; Handley-Sidhu *et al*., 2014). Interestingly, as XRD data suggested some measurable fraction of the Sr was present in a crystalline strontianite phase, the EXAFS data were also modelled as $SrCO_3$, however this did not yield a realistic fit. This suggests the bulk of the Sr is associated with hydroxyapatite-like phases, consistent with observations from TEM that the polyP structures had Ca, Sr and P co-located.

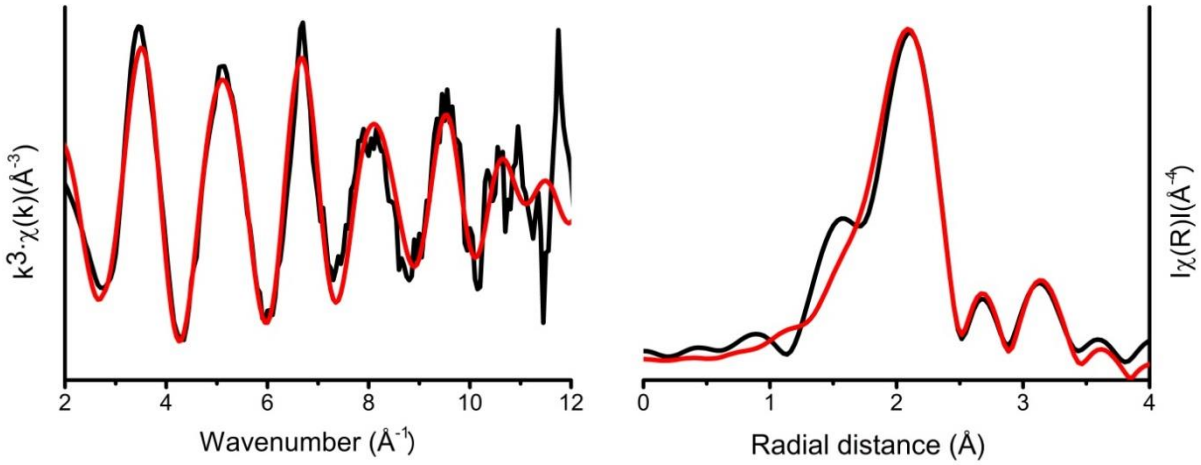

Figure 6-4: Sr K-edge EXAFS experimental data (black line). Theoretical best fit (red line) calculated using Artemis (Ravel and Newville, 2007)

6.5 Discussion

The First Generation Magnox Storage Pond (FGMSP) situated on the Sellafield site contains a significant inventory of fission products, including ^{90}Sr. This current study investigates the fate of Sr when incubated with non-axenic culture of *P. catenata*, representative of the microbial community detected in a microbial bloom in the pond on August 2016 (see Research chapter 4: The microbial ecology of a high pH spent nuclear fuel pond on the Sellafield site). This is the first study to our knowledge, which investigates the fate of Sr on a mixed microbial community relevant to the microbial ecology of a high pH legacy SNFP.

Collectively the results of our experiments show that the presence of Sr in the culture medium does not prevent the growth of the microorganisms in this mixed culture, although the total biomass at the end of the study period was lower when Sr was present, presumably due to toxicity of the added metal. Analysis of the Sr in the culture using EXAFS showed that Sr most likely formed Sr-Ca-PO_4 minerals, which is in agreement with the PHREEQC modelling. The TEM data provides evidence that *P. catenata* cells are capable of taking up a small proportion of the Sr in solution, which can become localised with polyP type features in the cells. Large quantities of small extracellular Sr-containing minerals were also visible using the TEM, which vary in their composition, with P not always present. The extracellular

minerals appeared to be associated with the outer surfaces of the microorganisms. The extracellular minerals lacking a P peak, are likely to be carbonate minerals, as indicated by XRD analysis. The XRD analysis was not able to confirm the presence of PO_4 minerals in the bulk sample, presumably due to the amorphous character of Sr-Ca-PO_4, hydroxyapatite-like phases implicated by EXAFS analyses.

PolyP bodies are made up of many orthophosphate residues that are linked by phosphoanhydride bonds to form linear polymers, and can be found in many organisms (Achbergerová and Nahálka, 2011; Albi and Serrano, 2016). Previous studies have shown that polyP bodies can have a variety of metals associated with them, with the most commonly studied metals including Cd, Pb, and Ca (Albi and Serrano, 2016; Baxter and Jensen, 1980; Jensen *et al*., 1982). Evidence for Sr interactions with polyP bodies is, however, extremely limited. A study by Baxter and Jensen (1980) showed variable uptake of Sr by the cyanobacterium *Plectonema boryanum*. Intracellular Sr, as shown by TEM analysis, was associated with two types of electron dense clusters, the first being polyP bodies whilst the second was devoid of any detectable P. The authors noted the presence of K in both of the Sr containing electron dense clusters, with the addition of S and Ca features when P was absent. Interestingly K, S, and Ca were also observed in the minerals formed in the *P. catenata* culture, including those associated with the polyP type bodies. The Sr containing electron dense bodies seen in *P. boryanum*, could potentially be carbonate minerals, incorporating both Sr and Ca. Such intracellular Sr carbonates have been the focus of more recent studies using *Candidatus Gleomargarita lithophora* and *Cyanothece* sp. PCC7425, which show selective uptake and carbonate mineral formation with Sr (Benzerara *et al*., 2014; Cam *et al*., 2015; Cam *et al*., 2016; Couradeau *et al*., 2012). The ability to form intracellular carbonate minerals does not appear to be ubiquitous, with *P. catenata* appearing to be incapable of such intracellular mineral formation.

The uptake of small amounts of Sr in *P. catenata*, which are localised at distinct features including polyP, is potentially significant, particularly during microbial bloom periods. There are multiple functions associated with polyP in organisms, including the detoxification of heavy metals (Albi and Serrano, 2016; Keasling, 1997). The level of polyP in microorganisms has been linked to metal tolerance, with higher levels resulting in increased tolerance (Albi and Serrano, 2016) and there is

evidence that polyP play a role in adaptation strategies in extreme environments (Achbergerová and Nahálka, 2011). In addition, efflux systems have been identified in other microorganisms that remove the metals as PO_4 minerals via the Pit transport system, following the enzymatic degradation of the polyP (Albi and Serrano, 2016; van Veen *et al*., 1994). Whilst this mechanism has not been observed previously with Sr systems, it is plausible that the microorganisms in the pond could utilise a similar mechanism to protect themselves against the toxicity of ^{90}Sr.

Interactions between the microorganisms in the pond and ^{90}Sr are as yet unknown, however this study provides information about the potential fate of ^{90}Sr in such systems. In pond effluents ^{90}Sr is present in the water column, suggesting that at least a proportion of the Sr is mobile in the pond. The levels of Sr in the pond water could be indicative of Sr-containing colloids (Mal'kovskii *et al*., 2014; Neill *et al*., n.d.). Whether such Sr-colloids can be influenced by microbial activity remains unknown and clearly requires further investigation. Given the low levels of PO_4 in the pond, it is more likely that the majority of microbial induced precipitation would be comprised of carbonate minerals in contrast to the observations in this laboratory study. The ability of microorganisms to adjust the pH of their surrounding environments and to influence the precipitation and the potential uptake of Sr is of interest in contaminated environments, such as the Fukushima site in Japan. Naturally occurring microbial populations could potentially provide a first step in the removal of fission products such as ^{90}Sr from aquatic systems.

6.6 Acknowledgements:

LF was supported by an EPSRC PhD CASE Studentship (Grant number EP/G037426/1) with Sellafield Ltd. Analysis of Sr samples was carried out at Diamond Light Source as part of the Nuclear Environment and Waste Block Allocation Grant, SP17270-1. We would also like to thank Paul Lythgoe for running the ICP-AES analysis and John Waters for carrying out the XRD analysis.

6.7 References

Achbergerová, L., Nahálka, J., 2011. Polyphosphate - an ancient energy source and active metabolic regulator. Microb. Cell Fact. 10, 1–14. https://doi.org/10.1186/1475-2859-10-63

Acinas, S.G., Haverkamp, T.H., Huisman, J., Stal, L.J., 2009. Phenotypic and genetic diversification of *Pseudanabaena* spp. (cyanobacteria). ISME J. 378, 31–46. https://doi.org/10.1038/ismej.2008.78

Albi, T., Serrano, A., 2016. Inorganic polyphosphate in the microbial world. Emerging roles for a multifaceted biopolymer. World J. Microbiol. Biotechnol. 32, 1–12. https://doi.org/10.1007/s11274-015-1983-2

Ashworth, H., Abrahamsen-Mills, L., Bryan, N., Foster, L., Lloyd, J.R., Kellet, S., Heath, S.L., 2018. Effect of Humic acid and bacterial exudates on sorption-desorption interactions of 90Sr with brucite. Environ. Sci. Process. Impacts Accepted m. https://doi.org/10.1039/b816135f

Baxter, M., Jensen, T., 1980. Uptake of magnesium, strontium, barium, and manganese by *Plectonema boryanum* (*Cyanophyceae*) with special reference to polyphosphate bodies. Protoplasma 104, 81–89. https://doi.org/10.1007/BF01279371

Bazin, D., Dessombz, A., Nguyen, C., Ea, K., Lioté, F., Rehr, J., Chappard, C., Rouzière, S., Thiaudière, D., Al, E., 2014. research papers The status of strontium in biological apatites : an XANES / EXAFS investigation research papers. J. Synchrotron Radiat. 21, 136–142. https://doi.org/10.1107/S1600577513023771

Benzerara, K., Skouri-Panet, F., Li, J., Férard, C., Gugger, M., Laurent, T., Couradeau, E., Ragon, M., Cosmidis, J., Menguy, N., Margaret-Oliver, I., Tavera, R., López-García, P., Moreira, D., 2014. Intracellular Ca-carbonate biomineralization is widespread in cyanobacteria. Proc. Natl. Acad. Sci. 1–6. https://doi.org/10.1073/pnas.1403510111

Blanco-Rivero, A., Leganés, F., Fernández-Valiente, E., Calle, P., Fernández-Piñas, F., 2005. *mrpA*, a gene with roles in resistance to Na+ and adaptation to alkaline pH in the cyanobacterium *Anabaena* sp. PCC7120. Microbiology 151, 1671–1682. https://doi.org/10.1099/mic.0.27848-0

Brookshaw, D.R., Pattrick, R.A.D., Lloyd, J.R., Vaughan, D.J., 2012. Microbial effects on mineral-radionuclide interactions and radionuclide solid-phase capture processes. Mineral. Mag. 76, 777–806. https://doi.org/10.1180/minmag.2012.076.3.25

Cam, N., Benzerara, K., Georgelin, T., Jaber, M., Lambert, J.F., Poinsot, M., Skouri-Panet, F., Cordier, L., 2016. Selective uptake of alkaline earth metals by cyanobacteria forming intracellular carbonates. Environ. Sci. Technol. 50, 11654–11662. https://doi.org/10.1021/acs.est.6b02872

Cam, N., Georgelin, T., Jaber, M., Lambert, J.F., Benzerara, K., 2015. In vitro synthesis of amorphous Mg-, Ca-, Sr- and Ba-carbonates: What do we learn about intracellular calcification by cyanobacteria? Geochim. Cosmochim. Acta 161, 36–49. https://doi.org/10.1016/j.gca.2015.04.003

Chiang, P.N., Wang, M.K., Huang, P.M., Wang, J.J., Chiu, C.Y., 2010. Cesium and strontium sorption by selected tropical and subtropical soils around nuclear facilities. J. Environ. Radioact. 101, 472–481. https://doi.org/10.1016/j.jenvrad.2008.10.013

Couradeau, E., Benzerara, K., Gérard, E., Moreira, D., Bernard, S., Brown, G.E., López-García, P., 2012. An early-branching microbialite cyanobacterium forms intracellular carbonates. Science (80-.). 336, 459–462. https://doi.org/10.1126/science.1216171

Crossland, I., 2012. Nuclear fuel cycle science and engineering, 1st ed. Woodhead Publishing, Philadelphia.

Downward, L., Booth, C.H., Lukens, W.W., Bridges, F., 2007. A variation of the F-test for determining statistical relevance of particular parameters in EXAFS fits. AIP Conf. Proc. 882, 129–131. https://doi.org/10.1063/1.2644450

Fukuda, S. ya, Iwamoto, K., Atsumi, M., Yokoyama, A., Nakayama, T., Ishida, K. ichiro, Inouye, I., Shiraiwa, Y., 2014. Global searches for microalgae and aquatic plants that can eliminate radioactive cesium, iodine and strontium from the radio-polluted aquatic environment: A bioremediation strategy. J. Plant Res. 127, 79–89. https://doi.org/10.1007/s10265-013-0596-9

Gadd, G.M., 1990. Heavy metal accumulation by bacteria and other microorganisms. Experientia 46, 834–840. https://doi.org/10.1007/BF01935534

Gregson, C.R., Goddard, D.T., Sarsfield, M.J., Taylor, R.J., 2011a. Combined electron microscopy and vibrational spectroscopy study of corroded Magnox sludge from a legacy spent nuclear fuel storage pond. J. Nucl. Mater. 412, 145–156. https://doi.org/10.1016/j.jnucmat.2011.02.046

Gregson, C.R., Hastings, J.J., Sims, H.E., Steele, H.M., Taylor, R.J., 2011b. Characterisation of plutonium species in alkaline liquors sampled from a UK legacy nuclear fuel storage pond. Anal. Methods 3, 1957. https://doi.org/10.1039/c1ay05313b

Handley-Sidhu, S., Hriljac, J.A., Cuthbert, M.O., Renshaw, J.C., Pattrick, R.A.D., Charnock, J.M., Stolpe, B., Lead, J.R., Baker, S., Macaskie, L.E., 2014. Bacterially produced calcium phosphate nanobiominerals: sorption capacity, site preferences, and stability of captured radionuclides. Environ. Sci. Technol. 48, 6891–6898. https://doi.org/10.1021/es500734n

Jackson, S.F., Monk, S.D., Riaz, Z., 2014. An investigation towards real time dose rate monitoring, and fuel rod detection in a First Generation Magnox Storage Pond (FGMSP). Appl. Radiat. Isot. 94, 254–259. https://doi.org/10.1016/j.apradiso.2014.08.019

Jensen, T.E., Baxter, M., Rachlin, J.W., Jani, V., 1982. Uptake of heavy metals by

Plectonema boryanum (Cyanophyceae) into cellular components, especially polyphosphate bodies: An X-ray energy dispersive study 27, 119–127.

Jespersen, A.-M., Christoffersen, K., 1987. Measurements of chlorophyll-a from phytoplankton using ethanol as extraction solvent. Arch. Hydrobiol. 109, 445–454.

Jin, X., Chu, Z., Yi, W., Hu, X., 2005. Influence of phosphorus on *Microcystis* growth and the changes of other environmental factors. J. Environ. Sci. 17, 937–941.

Kang, C.H., Choi, J.H., Noh, J.G., Kwak, D.Y., Han, S.H., So, J.S., 2014. Microbially induced calcite precipitation-based sequestration of strontium by *Sporosarcina pasteurii* WJ-2. Appl. Biochem. Biotechnol. 174, 2482–2491. https://doi.org/10.1007/s12010-014-1196-4

Keasling, J.D., 1997. Regulation of intracellular toxic metals and other cations by hydrolysis of polyphosphate. Ann. N. Y. Acad. Sci. 829, 242–249. https://doi.org/10.1111/j.1749-6632.1997.tb48579.x

Krejci, M.R., Finney, L., Vogt, S., Joester, D., 2011. Selective sequestration of strontium in desmid green algae by biogenic co-precipitation with barite. ChemSusChem 4, 470–473. https://doi.org/10.1002/cssc.201000448

Lauchnor, E.G., Schultz, L.N., Bugni, S., Mitchell, A.C., Cunningham, A.B., Gerlach, R., 2013. Bacterially induced calcium carbonate precipitation and strontium coprecipitation in a porous media flow system. Environ. Sci. Technol. 47, 1557–1564. https://doi.org/10.1021/es304240y

Li, J., Margaret Oliver, I., Cam, N., Boudier, T., Blondeau, M., Leroy, E., Cosmidis, J., Skouri-Panet, F., Guigner, J.-M., Férard, C., Poinsot, M., Moreira, D., Lopez-Garcia, P., Cassier-Chauvat, C., Chauvat, F., Benzerara, K., 2016. Biomineralization patterns of intracellular carbonatogenesis in cyanobacteria: Molecular hypotheses. Minerals 6, 10. https://doi.org/10.3390/min6010010

López-Archilla, A.I., Moreira, D., López-García, P., Guerrero, C., 2004. Phytoplankton diversity and cyanobacterial dominance in a hypereutrophic shallow lake with biologically produced alkaline pH. Extremophiles 8, 109–115. https://doi.org/10.1007/s00792-003-0369-9

Mal'kovskii, V.I., Dikov, Y.P., Latynova, N.E., Aleksandrova, E. V., 2014. Analysis of colloidal transfer of strontium-90 with groundwater. Dokl. Earth Sci. 458, 1104–1106. https://doi.org/10.1134/S1028334X14090104

NDA, 2016. Nuclear Decommissioning Authority: Business plan 2017 to 2020 [WWW Document]. Gov.uk. URL https://www.gov.uk/government/consultations/nuclear-decommissioning-authority-business-plan-2017-to-2020 (accessed 5.4.18).

Neill, T.S., Morris, K., Pearce, C.I., Sherriff, N.K., Shaw, S., n.d. Interactions of Sr with UO2 and U(IV)-silicate phases. unpublished.

Pikuta, E. V., Hoover, R.B., Tang, J., 2007. Microbial extremophiles at the limits of

life. Crit. Rev. Microbiol. 33, 183–209. https://doi.org/10.1080/10408410701451948

Ravel, B., Newville, M., 2005. *ATHENA, ARTEMIS, HEPHAESTUS*: Data analysis for X-ray absorption spectroscopy using *IFEFFIT*. J. Synchrotron Radiat. 12, 537–541. https://doi.org/10.1107/S0909049505012719

Rivasseau, C., Farhi, E., Atteia, A., Couté, A., Gromova, M., de Gouvion Saint Cyr, D., Boisson, A.-M.M., Féret, A.-S., Compagnon, E., Bligny, R., 2013. An extremely radioresistant green eukaryote for radionuclide bio-decontamination in the nuclear industry. Energy Environ. Sci. 6, 1230–1239. https://doi.org/Doi 10.1039/C2ee23129h

Schultze-Lam, S., Beveridge, T.J., 1994. Nucleation of celestite and strontianite on a cyanobacterial S-layer. Appl. Environ. Microbiol. 60, 447–453.

Sellafield, 2014. Sellafield magazine [WWW Document]. URL https://www.gov.uk/government/publications/sellafield-magazine-issue-4 (accessed 5.30.18).

Simonoff, M., Sergeant, C., Poulain, S., Pravikoff, M.S., 2007. Microorganisms and migration of radionuclides in environment. Comptes Rendus Chim. 10, 1092–1107. https://doi.org/10.1016/j.crci.2007.02.010

Thorpe, C.L., Lloyd, J.R., Law, G.T.W., Burke, I.T., Shaw, S., Bryan, N.D., Morris, K., 2012a. Strontium sorption and precipitation behaviour during bioreduction in nitrate impacted sediments. Chem. Geol. 306–307, 114–122. https://doi.org/10.1016/j.chemgeo.2012.03.001

Thorpe, C.L., Morris, K., Boothman, C., Lloyd, J.R., 2012b. Alkaline Fe(III) reduction by a novel alkali-tolerant *Serratia* sp. isolated from surface sediments close to Sellafield nuclear facility, UK. FEMS Microbiol. Lett. 327, 87–92. https://doi.org/10.1111/j.1574-6968.2011.02455.x

van Veen, H.W., Abee, T., Kortstee, G.J.J., Konings, W.N., Zehnder, A.J.B., 1994. Translocation of metal phosphate via the phosphate inorganic transport system of *Escherichia coli*. Biochemistry 33, 1766–1770. https://doi.org/10.1021/bi00173a020

Wilson, P.D., 1996. The nuclear fuel cycle from ore to waste. Oxford University Press, Oxford.

Zhu, M., Yu, G., Song, G., Chang, J., Wan, C., Li, R., 2015. Molecular specificity and detection for *Pseudanabaena* (cyanobacteria) species based on *rbcLX* sequences. Biochem. Syst. Ecol. 60, 110–115. https://doi.org/10.1016/j.bse.2015.04.009

6.8 Supplementary material

Supplementary Table 6-1: PHREEQC thermodynamic calculations of Sr (1 mM) saturation in BG11 medium at pH 7.2 and pH 10.

Complex	Saturation index / pH 7.2	Saturation index / pH 10.0
$Sr_5(PO_4)_3(OH)$ (s)	13.75	21.25
$Sr_5(PO_4)_3$ (s)	0.03	3.55
$MnPO_4$ (s)	3.32	0.84
Hydroxyapatite $[Ca_5(OH)(PO_4)_3]$	4.17	10.84
Chloroapatite $[Ca_5Cl(PO_4)_3]$	3.46	8.35
$Ca_3(PO4)_2$ (alpha)	-1.46	1.85
Strontianite $[SrCO_3]$	-1.06	2.42
Sphaerocobaltite $[CoCO_3]$	-2.73	0.17
Magnesite $[MgCO_3]$ (nat)	-2.00	1.47
Magnesite $[MgCO_3]$ (syn)	*2.82	0.64
Vaterite $[CaCO_3]$	-3.08	0.32
Dolomite $[CaMg(CO_3)_2]$	-4.76	2.11
$CaCO_3.H_2O$ (s)	-3.36	0.05
Calcite $[CaCO_3]$	-2.46	0.91
$CaMg_3(CO_3)_4$ (s)	-12.96	0.84
Argonite $[CaCO_3]$	-2.66	0.74

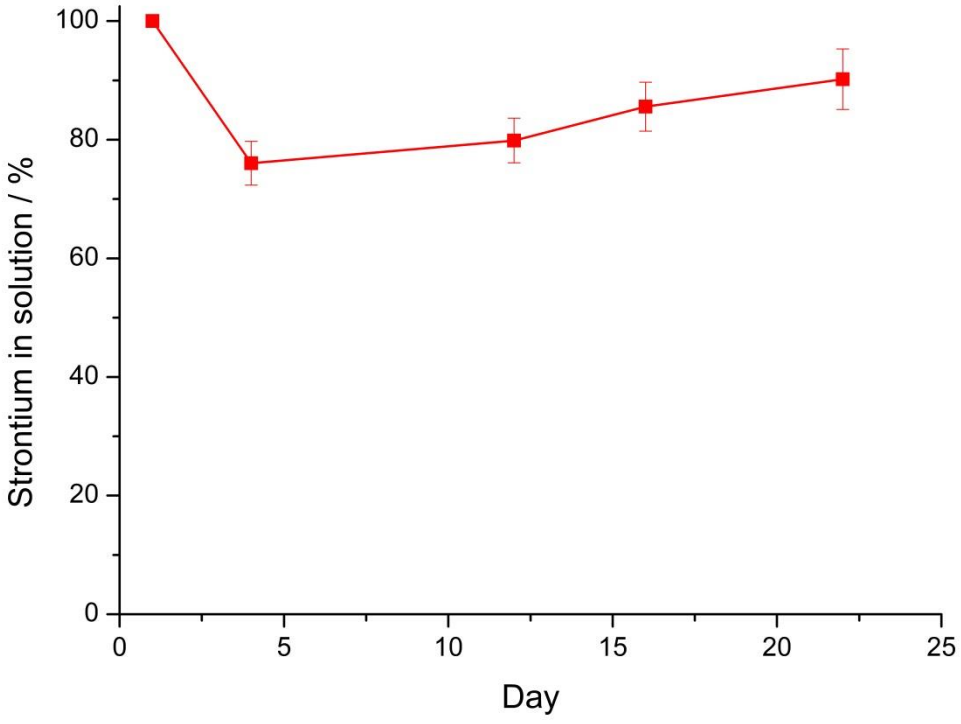

Supplementary Figure 6-1: Percentage of Sr in solution of sterile BG11 medium. Error bars denote standard deviation of three replicates.

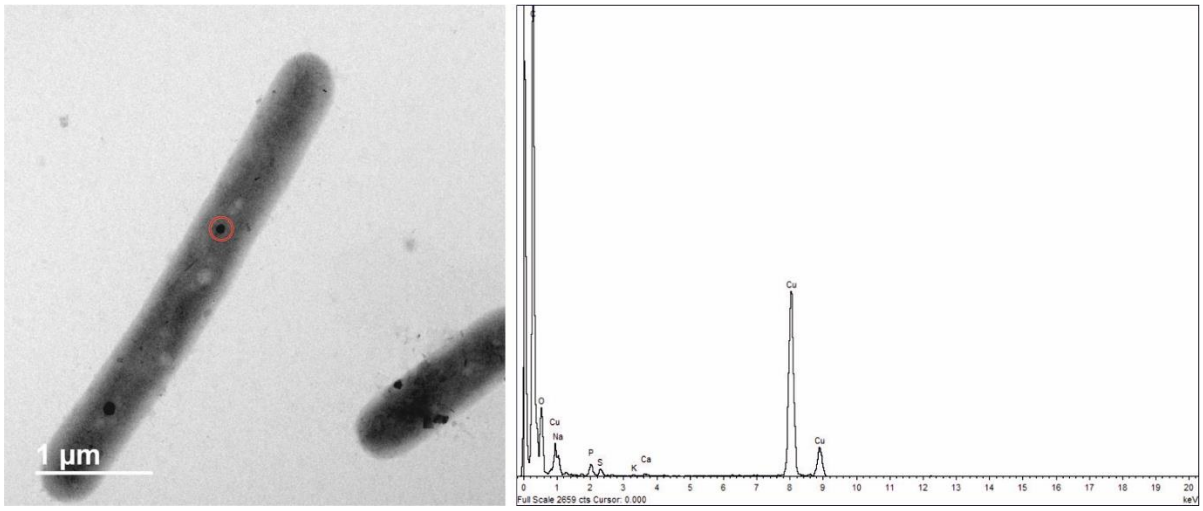

Supplementary Figure 6-2: TEM image and EDS data taken from a sample of *P. catenata* culture day 20, washed twice. EDS data taken from the electron dense feature of highlighted with the red circle.

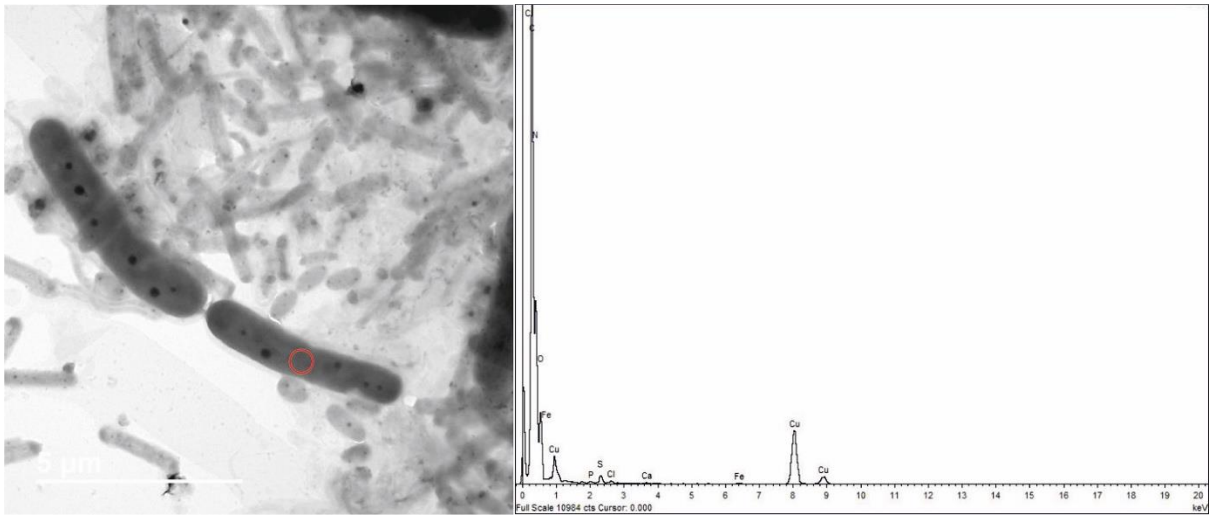

Supplementary Figure 6-3: TEM image and EDS data taken from a sample of *P. catenata* culture incubated with $SrCl_2$ at day 20, washed twice. EDS data collected from within the region indicated by red circle.

Chapter 7

Conclusions and Future Work

7 Conclusion and further work

7.1 Conclusion

The main aim of this project was to determine the microbial ecology of the First Generation Magnox Storage Pond (FGMSP) situated on the Sellafield Ltd. site. The facility is currently in the process of being decommissioned, as such microbial bloom episodes are inhibitory to the process since they restrict the visibility in the pond, resulting in delays to operations. Prior to this work the nature of the microorganisms that inhabit this extreme environment and indeed those responsible for the "bloom" events were not known. Information about the microorganisms present in the pond and a neighbouring auxiliary pond were gathered to determine possible sources for the microbial colonisation of the FGMSP. In addition to identifying the microbes, further efforts were made to determine possible adaptive mechanisms that key organisms use in response to ionizing radiation and how such organisms might influence the fate of radionuclides found in the pond. The hypotheses that were used as the basis for this research project and subsequently investigated in the research chapters 4-6 were:

- A mixed community of eukaryotic algae and cyanobacteria will contribute to the microbial blooms in the FGMSP
- Microorganisms, relevant to the FGMSP will be able to survive doses of ionizing radiation
- Microorganisms relevant to the FGMSP will influence the fate of radionuclides such as Sr, forming mineral precipitates

In **Chapter 4** the identity of microorganisms present in the FGMSP was determined over a 3-year period, including the fluctuations in the community profile over this period. Prokaryotic microorganism were found to be dominant in the pond, with two bloom samples providing evidence for a single cyanobacterium species dominating, namely *Pseudanabaena catenata*, which accounted for ~30 % in the August 2016 bloom sample. This cyanobacterium was the only one consistently identified throughout the 3-year period. Other microorganisms identified in the pond belonged to genera known to contain a variety of carotenoids and photosynthetic pigments.

Such photosynthetic pigments, particularly carotenoids, have been shown to be effective reactive oxygen species scavengers and therefore could provide an effective mechanism for surviving the doses of ionizing radiation experienced in the pond. Probe data, which estimates the concentration of chlorophyll-a (Chl-a) and phycocyanin, was useful in tracking the onset of the algal bloom and the progress. Upward trends in data such as this could provide an early warning sign of the onset of a bloom, and allow control mechanisms to be deployed. Increases in the residence time of the purge water in the pond coincided with the formation of the bloom events, and restoration of the purge rate to normal operational levels was seen to be effective at flushing the microorganisms out of the pond. Changes in the purge rate were the biggest contributor to the formation of blooms, with very little notable differences observed in other pond measurements such as PO_4^{3-} and NO_3^- concentrations. Efforts on site to plan necessary halts to the purge regime should be considered and scheduled away from the summer months, since the most recent bloom periods occurred during August when there were disruptions to the purge regime. Assessment of the microbial community of a hydraulically isolated auxiliary pond indicated a higher proportion of the community consisted of eukaryotic organisms, suggesting that when water is allowed to flow into the FGMSP the increased pH and radiation levels are sufficient to prevent colonisation. Comparison of the prokaryotic communities in the two ponds suggested that the two ponds had fairly discrete ecologies and that auxiliary pond does not significantly contribute to the microbial community in the FGMSP.

In **Chapter 5** the effect of ionizing radiation on the growth and metabolic state of microorganisms relevant to the FGMSP was assessed. Here *P. catenata* was selected as a model organism to study, since a non-axenic culture could not be obtained 16S rRNA gene sequencing was carried out on the culture. The results of the sequencing indicated that there was a high degree of similarity between the laboratory culture and the microorganisms present in the FGMSP. A total of 5 out of 9 OTUs could be affiliated to the genera found in the pond, making the culture used in the subsequent work highly representative of the microbial community of the FGMSP. The results from the FT-IR spectroscopy and other complementary techniques confirmed that upon receiving a total dose of 95 Gy of X-irradiation, the *P. catenata* culture produced elevated levels of polysaccharides. A proportion of the polysaccharides

produced could be seen to be associated with the *P. catenata* filaments. The production of polysaccharide materials is of interest for the FGMSP, since they are thought to have a wide array of functions such as; binding metals, accumulating nutrients, formation of biofilms and providing a protective barrier against environmental stress (Chicote et al., 2004; Diósi et al., 2003; Masurat et al., 2005). Increased levels of polysaccharides could have implications on the fate of radionuclides in the pond for example cationic metals are able to adsorb to some functional groups found on microbial cell surfaces and polysaccharide containing mucilage (Sorokovikova *et al*., 2008; Sorokovikova *et al*., 2013; Wada *et al*., 2013). This was demonstrated using the cell-free medium (collected from the same experimental set-up used in this chapter), to investigate the fate of ^{90}Sr and brucite (MgOH) in a related study. The cell-free medium from the irradiated cultures showed ~10 % removal of ^{90}Sr from solution, whilst the non-irradiated cell-free medium had no effect. The results suggest that organisms relevant to the pond community could produce compounds which are capable of influencing the fate of radionuclides such as ^{90}Sr in the pond (Ashworth *et al*., 2018). The results also showed a reduction in the concentration of Chl-a and auto-fluorescence of photosynthetic pigments in the irradiated *P. catenata* cells. These results suggest that the abundance of cyanobacterial cells might not be reflective of the proportion of cells that are photosynthetically active. The cyanobacteria in the pond have likely adapted to the doses of ionizing radiation in the pond and consequently photosynthetic pigments might not be affected. Other studies investigating chronic doses of ionizing radiation on *Synechococcus* spp. have suggested that the treatment can stimulate growth, whether this is the case for the *P. catenata* culture or occurs in the pond is unknown. Understanding the metabolic state of relevant microorganisms provides an insight into adaptive responses in the pond, which are unique to the organism(s) and the pond environment. The data are useful as they could help provide a more targeted approach for the assessment of the pond community. Increased understanding of the adaptive responses to ionizing radiation in such engineered systems will help to inform the control strategies employed for example the use of biocides or the purge rate utilised.

In **Chapter 6** the fate of Sr was determined when added to *P. catenata* cultures. In the presence of the actively growing culture, almost all the soluble Sr was removed

from solution according to ICP-AES measurements. The localisation of the Sr with respect to the *P. catenata* cells and other microorganisms was assessed using TEM, which indicated that a proportion of the Sr was localised at electron dense features, thought to be polyphosphate (polyP) bodies. Previous studies had shown the formation of intracellular carbonate mineral deposits consisting of Ca, Sr and Ba (Cam *et al*., 2015; Cam *et al*., 2016; Couradeau *et al*., 2012), however these were not observed in this study. Little work has been carried out looking at the interaction of Sr with polyP bodies, however other metal interactions have been well documented. Poly-P bodies have been shown to function as a detoxification system for heavy metals, whereby they are enzymatically cleaved from the polyP body as a metal phosphate and excreted from the cell via the Pit transport system (Albi and Serrano, 2016; van Veen *et al*., 1994). It is plausible that *P. catenata* is able to utilise similar pathways with Sr, resulting in the formation of $SrPO_4$ minerals, which were shown to be produced by EXAFS analysis of the solid phase from the cultures. In addition to the Sr that could be associated with the polyP bodies, minerals were observed that appeared to be extracellular and lacked P. Analysis of the solid phase by XRD identified the presence of calcian strontianite ($Sr(Ca)CO_3$), which is in agreement with the data collected by EDS on the TEM. Here we present plausible fates for Sr in the FGMSP, with $SrCO_3$ minerals likely to be more readily formed due to the low levels of PO_4^{3-} in the pond water. The ability of naturally occurring microbial populations to remove fission products e.g. Sr is of interest when considering the decommissioning of nuclear fuel ponds and the remediation of contaminated aquatic systems.

This project has demonstrated that there is a unique microbial community dominated by prokaryotic organisms residing in the FGMSP. It appears as though the community profile is not significantly influenced by the inflow of water from an auxiliary pond, and as such the elevated pH and radioactivity associated with the FGMSP is sufficient to limit the proliferation of eukaryotic organisms. *P. catenata* was present in all but one sample collected from the FGMSP, and was the most abundant cyanobacterium present in the bloom samples, indicating that it is able to persist in the pond despite the purge regime implemented to control its growth. The adaptive mechanisms utilised by *P. catenata* were predicted, using a representative culture, to involve the synthesis of elevated quantities of polysaccharides. Such a

strategy could potentially facilitate the colonisation of the pond by facilitating its attachment to pond surfaces, and the accumulation of nutrients, which enables other heterotrophic microorganisms to thrive in the pond. In addition the polysaccharide materials could directly influence the radionuclide inventory in the pond, such as adsorption to the negative functional groups thus removing them from the pond water, but creating hot spots of radioactivity. The activity of microorganisms relevant to those identified in the pond was shown to result in the removal of soluble Sr from solution. The potential involvement of polyP bodies to form $SrPO_4$ minerals, possibly as part of a detoxification mechanism could explain how microorganisms in the pond protect themselves from radionuclides in the pond. The Sr also formed calcian strontianite minerals, which are perhaps more likely to form in the pond as the levels of PO_4^{3-} are low in the pond. In summary, the work presented here highlights the benefit of investigating the capabilities of microorganisms that colonise spent nuclear fuel ponds. By investigating the adaptations and interactions of the microorganisms in the pond to relevant radionuclides, a clearer understanding of the processes that the organisms might influence can be gained, for example the fate of radionuclides. The more information about what such microorganisms are doing and how they are colonising the pond, will allow control strategies to be more specific for the system and therefore potentially more effective.

7.2 Further work

The assessment of the microbial community profile of the FGMSP was determined on a set of samples that were collected when possible from the site. Further assessment of the pond whilst it is undergoing decommissioning would provide information on if there are any significant changes to the microbial community which could be of concern e.g. the presence of sulphate-reducing bacteria, which could result in microbial induced corrosion (Hamilton, 1985). Any further assessments of the pond would benefit from a more structured sampling regime, to better observe any changes in the community structure. In addition regular monitoring of the microbial community of all water that enters the pond should be carried out to more thoroughly determine whether these influence the community in the FGMSP. Water samples collected from a variety of points across the pond would

determine whether the community is consistent throughout the pond or whether it varies. Variations in the microbial community could potentially identify areas in the pond where the water chemistry and/or radiation levels are not within the normal parameters of the general conditions. Safety limitations and the doses of radiation that workers are exposed to are obvious limiting factors on such proposals for more samples.

The experiments carried out in this thesis provide a detailed look at capabilities of *P. catenata* and the other microorganisms present in the culture. The experiments should be repeated in conditions more relevant to the pond such as lower nutrient concentrations particularly NO_3^- and PO_4^{3-} and maintaining the pH at around pH 11.4 using NaOH. Prior to subjecting the culture to ionizing radiation or the Sr-treatment, *P. catenata* and the other microorganisms should be allowed to adapt to the new conditions. Such experiments would help to determine whether the adaptive strategies observed in work carried out in this thesis are influenced by the culturing conditions. The fate of Sr in low nutrient conditions would be of particular interest since it is not known if *P. catenata* would form polyP bodies and whether the minerals formed would be the same. Additional analysis of the irradiation experiment using metatranscriptomics (see Appendix A1) and/ or metaproteomics would provide information about changes in gene expression, and give a clearer idea of what each of the organisms are doing individually. Further metabolic analysis of the culture such as liquid chromatography coupled with mass spectroscopy (LC-MS) and liquid chromatography (LC) analysis would characterise the changes in the metabolic state of the cells and identify the composition of the polysaccharides.

Similar experiments investigating the fate of a variety of radionuclides relevant to the pond, and of interest to Sellafield and the operation/decommissioning of the pond should be carried out. This would give a more complete picture of the capabilities of the microorganisms in the pond. Where possible non-active isotopes of radionuclides should be investigated first, only if the results could be of added value or interest and it is safe to do so should the radioactive isotopes be used. The use of radioactive isotopes would also subject the culture to different forms of ionizing radiation, which might elicit different adaptive responses from the organisms. The use of such radioactive isotopes could however restrict the analytical techniques that could be used on the system and therefore might not be as informative as non-active work. In

addition the fate of radionuclides with irradiated cultures of *P. catenata* should be investigated to see if this affects their behaviour. There is evidence that some of the radionuclides are in colloidal form in the pond (Javanbakht *et al*., 2014; Maher *et al*., 2016; Neill, 2018), it would therefore be of interest to determine if the microorganisms had any influence on these.

The development of "omic" techniques that could be used on pond samples would be of benefit to the future investigation of other SNFPs and other radioactive sites.

- Metagenomics: Here the entire genome of all the organisms present in a sample would be sequenced. The data can then be analysed and individual genomes can be drafted providing more information about what organisms are present in the pond. Since the data set contains all of the genetic information not just from a single region as with 16S rRNA gene sequencing, this would therefore provide more detailed information about the genes present in the community. The results of the sequencing could then be used to predict metabolic pathways that could be being utilised by the microorganisms. Such data could provide information on potential adaptive strategies the organisms are using, such as enzymes linked to combating reactive oxygen species or the synthesis of carotenoids. Such data would also provide a more detailed understanding of the possible physiology and phenotype of the microorganisms in the pond. It is important to understand these data would only be predictive and would show what genes are present, not what genes are being expressed.
- Transcriptomics/ proteomics/ metabolomics: Here the RNA, proteins and metabolites (respectively) are sequenced and characterised, the data produced provides detailed information about the genes that are being expressed and metabolites present either in the cells or excreted from them. These could be carried out on their own or combined to provide a more complete picture of which organisms are active in the pond and what their metabolic activities are. Trials on the extraction and preparation of pond water samples to check that the radioactivity is removed from the samples, or reduced to levels which are acceptable for transport and further analytical techniques, would need to be carried out. The results of such analyses would provide information that is specific to the time point when the samples were collected, and therefore the

interpretation would need to be carefully considered. Targeted sampling of the pond (and appropriate processing/analysis) during plant operation, or as the decommissioning efforts continue would provide information about changes in the activity of the microorganisms. Such information would identify the active organisms in the pond and potentially highlight specific metabolic pathways that could be targeted for control strategies.

7.3 References

Albi, T., Serrano, A., 2016. Inorganic polyphosphate in the microbial world. Emerging roles for a multifaceted biopolymer. World J. Microbiol. Biotechnol. 32, 1–12. https://doi.org/10.1007/s11274-015-1983-2

Ashworth, H., Abrahamsen-Mills, L., Bryan, N., Foster, L., Lloyd, J.R., Kellet, S., Heath, S.L., 2018. Effect of Humic acid and bacterial exudates on sorption-desorption interactions of 90Sr with brucite. Environ. Sci. Process. Impacts Accepted m. https://doi.org/10.1039/b816135f

Cam, N., Benzerara, K., Georgelin, T., Jaber, M., Lambert, J.F., Poinsot, M., Skouri-Panet, F., Cordier, L., 2016. Selective uptake of alkaline earth metals by cyanobacteria forming intracellular carbonates. Environ. Sci. Technol. 50, 11654–11662. https://doi.org/10.1021/acs.est.6b02872

Cam, N., Georgelin, T., Jaber, M., Lambert, J.F., Benzerara, K., 2015. In vitro synthesis of amorphous Mg-, Ca-, Sr- and Ba-carbonates: What do we learn about intracellular calcification by cyanobacteria? Geochim. Cosmochim. Acta 161, 36–49. https://doi.org/10.1016/j.gca.2015.04.003

Chicote, E., Moreno, D. a, García, A.M., Sarró, M.I., Lorenzo, P.I., Montero, F., 2004. Biofouling on the walls of a spent nuclear fuel pool with radioactive ultrapure water. Biofouling 20, 35–42. https://doi.org/10.1080/08927010410001662670

Couradeau, E., Benzerara, K., Gérard, E., Moreira, D., Bernard, S., Brown, G.E., López-García, P., 2012. An early-branching microbialite cyanobacterium forms intracellular carbonates. Science (80-.). 336, 459–462. https://doi.org/10.1126/science.1216171

Diósi, G., Telegdi, J., Farkas, G., Gazsó, L.G., Bokori, E., 2003. Corrosion influenced by biofilms during wet nuclear waste storage. Int. Biodeterior. Biodegrad. 51, 151–156. https://doi.org/10.1016/S0964-8305(02)00138-5

Hamilton, W.A., 1985. Sulphate-reducing bacteria and anaerobic corrosion. Annu. Rev. Microbiol. 39, 195–217. https://doi.org/10.1146/annurev.mi.39.100185.001211

Javanbakht, V., Alavi, S.A., Zilouei, H., 2014. Mechanisms of heavy metal removal using microorganisms as biosorbent. Water Sci. Technol. 69, 1775–1787. https://doi.org/10.2166/wst.2013.718

Maher, Z., Ivanov, P., O'Brien, L., Sims, H., Taylor, R.J., Heath, S.L., Livens, F.R., Goddard, D., Kellet, S., Rand, P., Bryan, N.D., 2016. Americium and plutonium association with magnesium hydroxide colloids in alkaline nuclear industry process environments. J. Nucl. Mater. 468, 84–96. https://doi.org/10.1016/j.jnucmat.2015.11.010

Masurat, P., Fru, E.C., Pedersen, K., 2005. Identification of *Meiothermus* as the dominant genus in a storage system for spent nuclear fuel. J. Appl. Microbiol. 98, 727–740. https://doi.org/10.1111/j.1365-2672.2004.02519.x

Neill, T.S., 2018. U(IV)-Silicate colloids and their interactions with Sr in natural and engineered alkaline environments. University of Manchester.

Sorokovikova, E.G., Belykh, O.I., Gladkikh, A.S., Kotsar, O. V., Tikhonova, I. V., Timoshkin, O.A., Parfenova, V. V., 2013. Diversity of cyanobacterial species and phylotypes in biofilms from the littoral zone of Lake Baikal. J. Microbiol. 51, 757–765. https://doi.org/10.1007/s12275-013-3240-4

Sorokovikova, E.G., Tikhonova, I. V., Belykh, O.I., Klimenkov, I. V., Likhoshwai, E. V., 2008. Identification of two cyanobacterial strains isolated from the Kotel'nikovskii hot spring of the Baikal rift. Microbiology 77, 365–372. https://doi.org/10.1134/S002626170803017X

van Veen, H.W., Abee, T., Kortstee, G.J.J., Konings, W.N., Zehnder, A.J.B., 1994. Translocation of metal phosphate via the phosphate inorganic transport system of *Escherichia coli*. Biochemistry 33, 1766–1770. https://doi.org/10.1021/bi00173a020

Wada, N., Sakamoto, T., Matsugo, S., 2013. Multiple roles of photosynthetic and sunscreen pigments in cyanobacteria focusing on the oxidative stress. Metabolites 3, 463–483. https://doi.org/10.3390/metabo3020463

Appendices

A1 The effect of X-irradiation on the gene expression of *Pseudanabeana catenata*

A1.1 Introduction

Work carried out in Chapter 5 aimed to determine the adaptive response of the *Pseudanabaena catenata* culture to doses of ionizing radiation. Fourier-transform infrared (FT-IR) spectroscopy assessment and subsequent principal component analysis (PCA) showed no significant difference in the metabolic state of the irradiated and control cultures at D4 (during the irradiation treatment). Differences in the metabolic state of the cultures could, however, be observed during the post irradiation recovery period, which became more pronounced over time. The irradiated cultures also displayed a reduction in the concentration of chlorophyll-a (Chl-a), whilst the growth rate of the irradiated and control cultures remained similar according to optical density measurements and direct cell counts of *P. catenata*.

The aim of the current work is to determine what changes in gene expression there are both during the irradiation treatment and in the subsequent recovery period. Changes in the expression of specific gene targets for example those associated with photosynthesis, stress response, and DNA repair, will be investigated. In addition, functional annotation will identify which metabolic pathways are involved in the stress response and which are activated or deactivated during the recovery period following the irradiation treatment.

This chapter highlights work that is ongoing, further data analysis will be carried out and used as the basis of a separate paper. Here, we provide a summary of the work that has been carried out to date and some of the data collected relating to the structural annotation of the differentially expressed genes (DEG), which is still undergoing further analysis. The work carried out in this chapter is in collaboration with Dr. Naji Bassil, who has supported the laboratory preparation of the metagenomic sample (DNA) and the metatranscriptomic samples (mRNA) and the bioinformatics and data handling of the metatranscriptomic data. The irradiation experiment was conducted solely by Lynn Foster. The metagenomic data analysis was initially conducted by Robert Danczak at the Ohio State University, including

quality checks, assembly, initial annotations and binning using MetaBAT and MaxBin. Additional support and guidance on manual binning and quality checks on the bins were provided by Dr. Sophie Nixon and Dr Edwin Gnanaprakasam.

A1.2 Methods

A1.2.1 Whole genome sequencing of the *P. catenata* culture

Sequencing and annotation of the entire metagenome of the *P. catenata* culture was carried out to provide a reference to align the metatranscriptomic data to. DNA was extracted from a sample taken from the culture using the MoBio PowerWater DNA isolation kit (MoBio Laboratories, Inc., Carlsbad, CA, USA) as described in Chapters 3.7, 4, and 5. The extracted DNA was then fragmented into approximately 200 bp lengths using the NEBNext dsDNA fragmentase (New England Biolabs, Ipswich, MA, USA). The concentration and purity of the fragmented DNA was checked using a Qubit 3.0 Fluorometer and the Qubit dsDNA HS Assay kit (Thermo Fisher Scientific, Waltham, MA, USA), and a Nanodrop^{TM} 2000 spectrophotometer (Thermo Fisher Scientific, Waltham, MA, USA). The fragmented DNA was then cleaned using the Beckman Coulter Agencourt AMPure XP beads (Fisher Scientific, Loughbourgh, UK). The library was prepared following the NEBNext Ultra DNA Library Prep Kit for Illumina instruction manual (New England Biolabs, Ipswich, MA, USA), selecting for a 200 bp size library, with 8 cycles of PCR used to amplify the sample with the NEBNext Mulitplex Oligos for Illumina (Index Primers Set 1), using the Index primer/ i7 (index 1), and the universal PCR primer /i5 primer. A final clean up step using the Beckman Coulter Agencourt AMPure XP beads was performed prior to sequencing. The DNA library was then prepared for sequencing following the Illumina manual (Illumina, San Diego, CA, USA), where it was diluted to 4 nM and denatured with freshly prepared 0.2 M NaOH, and then further diluted to 10 pM with solution HT1. A 1 % PhiX control DNA was added to the library before it was sequenced on the Illumina MiSeq platform using the MiSeq Reagent Kit v2.

The sequencing reads were sent to Ohio State University to carry out the initial data analyses, which consisted of quality trimming of the reads to ensure a Phred score of 30 or higher using Sickle (Joshi and Fass, 2011). Following this the reads were assembled using IDBA-UD v1.1.1 (Wrighton *et al*., 2012; Brown *et al*., 2015) which uses de Bruijn graphs for assembly. The coverage and GC of the scaffolds was determined using Bowtie 2 v2.2.9 (Wrighton *et al*., 2012). Scaffolds were annotated using Prodigal v2.2.6 (Hyatt *et al*., 2012). Binning was carried out using two binning tools, MetaBAT v0.32.4(Kang *et al*., 2015) and MaxBin v2.1.1 (Wu *et al*., 2014), and the resulting bins were assessed using DASTool to identify unique, non-redundant, high-scoring bins. The bins selected by DASTool v1 (Sieber *et al*., 2018) showed high levels of completion and low levels of contamination (i.e. scaffolds that have been mis-binned).

The Ohio State University pipeline uses an in house script to generate a Quicklooks file for all the data, which provides a basic annotation of all the scaffolds (> 5,000 bp). Each scaffold has the number of genes present, the GC content, probable affiliation to microorganisms (based on comparisons of gene sequences to the UniRef90 database (UniProt, 2018)), coverage and the percentage match. The Quicklooks file was used to manually bin the genomic data based on the coverage, GC content and affiliation.

The bins were assessed for completeness and redundancy by searching for the presence and number of single copy genes (SCGs), and the bins were reannotated using Prodigal v2.6 (Hyatt *et al*., 2012). The number of SCGs detected acts as a proxy for the completeness of the bin, whilst multiple copies should be checked to see if the gene is split across two scaffolds or whether the bin contains a scaffold that has been mis-binned. Bins with over 80 % completeness (i.e. 80 % of the SCGs searched for were present in the bin) were retained and deemed suitable for further analysis

A1.2.2 Metatranscriptomics

P. catenata cultures were subjected to doses of ionizing radiation, as previously described in Chapter 5. Briefly cultures of *P. catenata* (in triplicate) were irradiated

over five consecutive days, receiving a total dose of 95 Gy, using a Faxitron CP-160 Cabinet X-radiator (160 kV; 6 mA; tungsten target). A further set of biological triplicates were used as a "no-dose" control. Samples were collected at day 4 and day 8 (three days post irradiation), centrifuged at 14,000 *g* at 4 °C for 3 min, and the pellets were flash frozen in liquid nitrogen and stored at -80 °C. RNA (and protein) was extracted from the samples using the RNA/Protein Purification Plus Kit (Norgen Biotek Corp., Ontario, Canada). A DNase digestion (DNase, RNA-free, Thermo Fisher Scientific, Waltham, MA, USA) was carried out on the samples to ensure that no residual DNA remained in the samples that could interfere with rRNA removal and RNA sequencing. The concentration and purity of the RNA was checked using a Qubit 3.0 Fluorometer and the Qubit RNA BR Assay kit (Thermo Fisher Scientific, Waltham, MA, USA), and a Nanodrop™ 2000 spectrophotometer (Thermo Fisher Scientific, Waltham, MA, USA). The RNA integrity was checked by running the samples through a RNA ScreenTape on the TapeStation 4200 (Agilent, Santa Clara, CA, USA). The ribosomal RNA was then removed from the samples, leaving the mRNA which would then be sequenced. The rRNA was removed using the Ribo-Zero rRNA Removal Kit (Bacteria) (Illumina, San Diego, CA, USA). Following the removal of the rRNA the samples were run again through a RNA ScreenTape on the TapeStation 4200 (Agilent, Santa Clara, CA, USA) to ensure the rRNA had been removed. The concentration of rRNA depleated RNA was measured using a Qubit 3.0 Fluorometer and the Qubit RNA HS Assay kit (Thermo Fisher Scientific, Waltham, MA, USA) before sequencing. The samples were then prepared for sequencing by the University of Manchester Central Sequencing Facility using the Lexogen SENSE total RNA-Seq library prep kit (Lexogen GmbH, Vienna, Austria), and sequenced using the HiSeq 4000 (Illumina, San Diego, CA, USA). The principle of HiSeq sequencing is the same as the MiSeq, however shorter reads are sequenced, although more data are generated allowing for deeper sequencing.

The initial bioinformatics on the transcriptomic data were carried out by the University of Manchester core bioinformatics group. The sequences were aligned to the annotated metagenome (unbinned) using Bowtie 2 v2.1.0 (Wrighton *et al*., 2012) and the expressed gene counts were made using HTSeq v0.9.1 (Anders, 2018). Comparisons of differentially expressed genes (DEG) were made between the different treatments using DESeq2 v1.20.0 in R including;

- Irradiated day 4 v control day 4 (I4_C4)
- Irradiated day 8 v control day 8 (I8_C8)
- Control day 8 v Control day 4 (C8_C4)
- Irradiated day 8 v irradiated day 4 (I8_I4)

A1.3 Results

A1.3.1 Metagenomics

The whole genome sequencing of the *P. catenata* culture was carried out principally to provide a reference to align the metatranscriptomic data to. The metagenome was subsequently binned and checked with the aim of potentially being able to assign the metatranscriptome data to discrete genomes, and therefore identify organism specific responses to irradiation, in particular *P. catenata*. The bins generated through the Ohio State pipeline and manual binning were comparable, with similar completeness (based on SCGs), GC content and coverage observed (Table A 1-1). There are some differences between the two binning methods due to the difference in the cut-off length of the scaffolds used with each binning tool (MetaBAT >2,500 bp; MaxBin >1,000 bp; Quicklook/ manual binning >5,000 bp). Manual binning resulted in 11 bins (2 of which were below the 80 % threshold of completeness that would be used for further analysis if purely working on the metagenomic data), whilst DASTool selected 10 non-redundant bins. The taxonomic affiliations of the individual bins broadly matched those that were produced from the analysis of the PCR amplified 16S rRNA gene sequences (results from Chapter 5), with the *Pseudanabaena* genus showing the highest coverage.

A1.3.2 Metatranscriptomics

The raw data generated from the sequencing run is summarised in Table A 1-2; all but I_4.1 were sequenced at a sufficient depth for further analysis.

The number of differentially expressed genes (DEGs) for each comparison was variable with the highest number of DEGs observed in the I8_I4 comparison, whilst

the lowest number of DEGs was observed in the I8_C8 comparison, 1234 and 470 genes respectively (Table A 1-3). All comparisons apart from I8_C8 showed a higher proportion of significantly overexpressed genes. The total log_2 fold change for each of the comparisons also show a higher proportion of significantly overexpressed genes, with the exception of the I8_C8 comparison, where the levels of over and under expression are comparable (Figure A 1-1).

A list of genes of interest was generated relating to; photosynthesis, genes involved in stress responses, DNA repair, protein folding (chaperones), ATPases, and quinones. Checks were then made to determine whether the same genes (same locus tag) were differentially expressed in multiple comparisons, to determine whether the changes in gene expression were a result of time (C8_C4), stress (I4_C4), recovery response (I8_C8), or a combination of time and the recovery response (I8_I4). Table A 1-4 toTable A 1-8 show the DEGs which have been broadly grouped according their activity.

7.3.1 Stress (I4_C4)

A total of 16 genes associated with stress response showed significant levels of differential gene expression, 10 were over expressed whilst 6 were under expressed (Table A 1-4). There were 8 genes associated with photosynthesis that showed differential gene expression, 5 of which were under expressed in the irradiated samples compared to the control (Table A 1-6). All genes for chaperone proteins [11 genes] (Table A 1-5), cytochromes [10 genes] (Table A7), and ATP synthases [11 genes] (Table A 1-8) showed over expression.

7.3.2 Recovery (I8_C8)

There were 11 genes associated with stress response and cytochromes showed significant levels of differential gene expression, 3 was over expressed whilst 8 were under expressed (Table A 1-4 and Table A 1-7). There were 20 genes associated with photosynthesis that showed differential gene expression, 14 of which were

under expressed in the irradiated samples compared to the control (Table A 1-6). Chaperone protein genes only showed 5 DEGs, 4 were under expressed (Table A 1-5), whilst there were only 4 ATP synthase genes that showed significant differential expression, 3 of which were under expressed (Table A 1-8).

7.3.3 Time (C8_C4)

Photosynthetic genes showed the highest level of significant DEGs, 31 overall 29 of which were over expressed on day 8 compared to day 8 (Table A 1-6). Stress response genes also showed high levels of DEGs 13 over expressed and 4 under expressed (Table A 1-4). There were 9 genes that were over expressed associated with both chaperone (Table A 1-5) and cytochrome genes (Table A 1-7), with only 1 and 2 genes under expressed respectively. A total of 6 ATP synthase genes showed differential gene expression, 3 over and under expressed (Table A 1-8).

7.3.4 Recovery and time (I8_I4)

The comparison between day 8 and day 4 of the irradiated cultures showed the largest number of DEGs in each of the gene groupings. Genes associated with photosynthesis had the highest number of significant DEGs (46), with 35 genes over expressed and 11 under expressed (Table A 1-6). There were 24 stress response genes that were significantly differentially expressed, 15 of which were over expressed and 9 that were under expressed (Table A 1-4). Chaperone (Table A 1-5) and ATP synthase (Table A 1-8) genes both had 9 genes that were under expressed, whilst 6 and 2 genes were over expressed respectively. Differential gene expression of cytochromes was evenly split with 6 genes over and under expressed (Table A 1-7).

Further work is on-going to further understand the response of the *P. catenata* culture to both ionizing radiation and the recovery period.

Table A 1-1: Results of manual binning from the Quicklooks file (red) with the bins generated using the Ohio State University's pipeline which uses both MaxBin and MetaBAT to bin the metagenomics data and DASTool to identify the unique, non-redundant, high-scoring bins (green).

Predicted organism (Quicklooks)	Av. Coverage	Av. GC %	Completeness / %	Misbin / %	DASTool selected bins (coverage; GC %)	Completeness / %	Misbin / %
Pseudanabaena	538.21	42.21	81	0	Meta.1 (537.08; 42.22)	87	3
Porphoryrobacter	161.19	64.69	100	3	MaxBin.002 (163; 64.6)	100	3
Flavobacterium	145.71	33.28	100	0	MaxBin.003 (145.8_32.9)	100	0
Rhodobacteraceae	60.87	62.75	100	3	Meta.7 (61.97; 63.92)	100	0
Sphingomonadaceae	52.03	62.18	100	3	MaxBin.005 (51.59; 63.97)	100	3
Chitinophagaceae	48.45	39.98	100	0	MaxBin.006 (48.64; 38.96)	100	0
Comamonadaceae	37.97	65.10	100	0	Meta.10 (38.47; 65.07)	100	0
Rhizobiales	15.71	67.64	90	0	Meta.11 (15.80; 67.59)	94	0
Limnobacter	12.67	52.46	90	0	MaxBin.009 (12.78; 52.58)	100	6

Runella	9.07	45.35	48	3	MaxBin.010 (9.12; 45.14)	97	6
Hoeflea	6.57	63.53	13	0		0	0

Table A 1-2: Summary of the results collected from the HiSeq 4000 run on the 12 mRNA samples. Red highlighted sample showed insufficient sequencing depth and was therefore omitted from subsequent analysis.

Sample	Total reads	Filtered reads	Filtered %	Mapped reads	Mapped %	Pair	Pair %	Counts	Counts %
C_4.1	26105592	23526690	90	24126045	102	19993500	82	12032500	51
C_4.2	21310012	18268932	85	18667560	102	14671266	78	9451669	51
C_4.3	18527574	16020768	86	16409816	102	12493150	76	8306051	51
C_8.1	18990114	16866352	88	15855478	94	13750642	86	8914431	52
C_8.2	20885682	18041274	86	17926964	99	14517068	80	9884068	54
C_8.3	31543964	27556210	87	27818023	100	20482932	73	12922258	46
I_4.1	31600	25886	81	25734	99	22198	86	6135	23
I_4.2	27307638	23144464	84	22926937	99	17835796	77	11867181	51
I_4.3	16600702	14245374	85	14527717	101	11588052	79	7461434	52
I_8.1	23941794	20936806	87	20937998	100	14618794	69	9387520	44
I_8.2	17442426	14820260	84	10905176	73	7172326	65	4544197	30
I_8.3	10616544	9205866	86	9238300	100	6669752	72	4213580	45

Table A 1-3: Summary of number of differentially expressed genes (DEG) in each comparison between the I4 irradiated at D4, I8 irradiated D8, C4 control D4, and C8 control D8.

	I4_C4	I8_C8	C8_C4	I8_I4
Total number of DEG	691	470	915	1234
DEG (excluding ribosomal reads)	614	435	855	1146
Up regulated genes	497	219	631	735
Down regulated genes	194	251	284	499
Hypothetical proteins	150	138	264	345

Table A 1-4: The log_2 fold change of differentially expressed genes associated with the response to stress (for example reactive oxygen species), at a Padj<0.1. Comparisons are between the different treatments and time points; I4 is irradiated D4; I8 is irradiated D8; C4 is control D4; and C8 is control D8.

Product	Locus tag	log2FoldChange			
		I4_C4	I8_C8	C8_C4	I8_I4
Catalase C	ECKGJPBD_13290		8.115293		
Catalase-peroxidase	ECKGJPBD_06229	5.743753			
Catalase-peroxidase	ECKGJPBD_14160				2.480602
Catalase-peroxidase	ECKGJPBD_15297			1.592319	
Catalase-peroxidase	ECKGJPBD_16230			1.661126	
Ferredoxin	ECKGJPBD_29098		-0.65117		
Ferredoxin CarAc	ECKGJPBD_28843		-1.42584		
Ferredoxin-1	ECKGJPBD_29099		-0.88762		
Ferredoxin-6	ECKGJPBD_39416			7.465826	
Ferredoxin-dependent glutamate synthase 1	ECKGJPBD_05652		6.400769	-6.02682	
Ferredoxin-dependent glutamate synthase 1	ECKGJPBD_36887		0.52999	2.200815	

Ferredoxin--NADP reductase	ECKGJPBD_00482				8.450908
Ferredoxin--NADP reductase	ECKGJPBD_28734			0.860869	0.678882
Glutaredoxin arsenate reductase	ECKGJPBD_07623				7.819055
Glutathione import ATP-binding protein GsiA	ECKGJPBD_01426				5.079598
Glutathione transport system permease protein GsiC	ECKGJPBD_01424				10.08856
Glutathione transport system permease protein GsiD	ECKGJPBD_01425				3.503579
Glutathione-binding protein GsiB	ECKGJPBD_11092				7.795215
Glutathione-binding protein GsiB	ECKGJPBD_16557				6.732817
Glutathione-regulated potassium-efflux system protein KefC	ECKGJPBD_06380			4.833695	
LexA repressor	ECKGJPBD_00230	8.085158			-2.77555
LexA repressor	ECKGJPBD_11972	3.017348			-2.34608
Lon protease	ECKGJPBD_15437			1.523126	
Lon protease	ECKGJPBD_16288	9.026749			-9.65275

Lon protease 2	ECKGJPBD_22358		-6.5028		
Protein RecA	ECKGJPBD_06429	8.399741			-7.12525
Protein RecA	ECKGJPBD_12006	5.540286			
Putative peroxiredoxin	ECKGJPBD_04196				7.539139
putative peroxiredoxin	ECKGJPBD_22922			-0.65864	
Putative peroxiredoxin	ECKGJPBD_27247		-0.8683	0.63607	-1.67743
Putative peroxiredoxin bcp	ECKGJPBD_28684			0.765635	0.551343
Spermidine/putrescine-binding periplasmic protein	ECKGJPBD_01495	-8.46883			
Spermidine/putrescine-binding periplasmic protein	ECKGJPBD_08140	-5.58611			
Spermidine/putrescine-binding periplasmic protein	ECKGJPBD_23942	-0.70924			
Superoxide dismutase [Fe]	ECKGJPBD_09159				7.505788
Superoxide dismutase [Fe]	ECKGJPBD_14110		-5.53498		
Superoxide dismutase [Fe]	ECKGJPBD_35901		-0.66639		-0.85833
Thioredoxin	ECKGJPBD_04575	8.055419			
Thioredoxin	ECKGJPBD_38431			4.072216	8.799244

Thioredoxin 1	ECKGJPBD_17904	7.839502		6.883139	
Thioredoxin reductase	ECKGJPBD_27246	1.784892			-2.40163
Thioredoxin reductase	ECKGJPBD_33656	9.37163			-7.82006
Trehalose import ATP-binding protein SugC	ECKGJPBD_09798	-2.12624		-1.50692	
Trehalose transport system permease protein SugA	ECKGJPBD_01508	-5.93331		2.043996	7.575335
Trehalose transport system permease protein SugA	ECKGJPBD_09454	-8.10479			9.370231
Trehalose transport system permease protein SugB	ECKGJPBD_09795			-2.4901	-2.88998
Universal stress protein UP12	ECKGJPBD_24617		-4.99371	4.276654	

Table A 1-5: The log_2 fold change of differentially expressed genes associated with chaperone proteins, at a Padj<0.1. Comparisons are between the different treatments and time points; I4 is irradiated D4; I8 is irradiated D8; C4 is control D4; and C8 is control D8.

Product	Locus tag	Log_2 fold change			
		I4_C4	I8_C8	C8_C4	I8_I4
10 kDa chaperonin	ECKGJPBD_17678				-8.97297
10 kDa chaperonin	ECKGJPBD_33955	3.123051			-3.87024
10 kDa chaperonin	ECKGJPBD_35697	2.696437			-2.61423
60 kDa chaperonin	ECKGJPBD_27329	7.535438			-5.98956
60 kDa chaperonin 1	ECKGJPBD_03019	4.4237			
60 kDa chaperonin 1	ECKGJPBD_33954	3.021562	-0.82628		
60 kDa chaperonin 1	ECKGJPBD_33954				-3.63183
60 kDa chaperonin 2	ECKGJPBD_35696	2.532747			-3.399
60 kDa chaperonin 5	ECKGJPBD_17677	3.328477			
Chaperone protein ClpB 1	ECKGJPBD_04108		-7.73836		
Chaperone protein ClpB 1	ECKGJPBD_10119		-3.0223	6.208115	
Chaperone protein ClpB 1	ECKGJPBD_21027	1.14732			

Chaperone protein DnaJ	ECKGJPBD_12657				9.08567
Chaperone protein DnaK	ECKGJPBD_04707			1.822546	
Chaperone protein DnaK	ECKGJPBD_13026			1.878919	
Chaperone protein DnaK	ECKGJPBD_14965	8.330274			-9.00721
Chaperone protein DnaK	ECKGJPBD_24803				1.56888
Chaperone protein DnaK	ECKGJPBD_24805			1.316649	1.577116
Chaperone protein DnaK	ECKGJPBD_48847			-2.71632	
Chaperone protein dnaK2	ECKGJPBD_20227	2.593141		1.253876	
Chaperone protein dnaK2	ECKGJPBD_20227				-1.79077
Chaperone protein HtpG	ECKGJPBD_29910	2.075663			
Chaperone protein HtpG	ECKGJPBD_29910			1.227956	-1.22982
Chaperone SurA	ECKGJPBD_26329			6.249204	
Cold shock protein CspA	ECKGJPBD_06267				7.388759
Cold shock protein CspA	ECKGJPBD_16159		-1.36512	1.198707	
Heat shock protein HspQ	ECKGJPBD_15337				7.873936
Small heat shock protein IbpA	ECKGJPBD_00762		9.402129		5.589138

Small heat shock protein IbpA	ECKGJPBD_15948	1.931678	

Table A 1-6: The log_2 fold change of differentially expressed genes associated with photosynthesis, at a Padj<0.1. Comparisons are between the different treatments and time points; I4 is irradiated D4; I8 is irradiated D8; C4 is control D4; and C8 is control D8.

Product	Locus tag	log_2 fold change			
		I4_C4	I8_C8	C8_C4	I8_I4
Allophycocyanin alpha chain	ECKGJPBD_33685				7.718943
Allophycocyanin beta chain	ECKGJPBD_33684				6.06659
Carbon dioxide-concentrating mechanism protein CcmK	ECKGJPBD_32352				6.672542
Chlorophyllide reductase 52.5 kDa chain	ECKGJPBD_06245	5.433245			4.522592
Chlorophyllide reductase 52.5 kDa chain	ECKGJPBD_17135				6.628996
Chlorophyllide reductase subunit Z	ECKGJPBD_17136			6.984072	
C-phycocyanin alpha chain	ECKGJPBD_36210			8.227657	
C-phycocyanin-1 beta chain	ECKGJPBD_36209			5.508814	
C-phycocyanin-2 beta chain	ECKGJPBD_35335				
C-phycoerythrin beta chain	ECKGJPBD_37316				7.462897
Cytochrome b559 subunit beta	ECKGJPBD_20972		1.782904		3.78048

Cytochrome b6-f complex iron-sulfur subunit	ECKGJPBD_33945		1.327245	2.31559	5.670181
Cytochrome b6-f complex subunit 4	ECKGJPBD_35897				7.191599
Iron stress-induced chlorophyll-binding protein	ECKGJPBD_27462				4.305218
Light-harvesting protein B-800/850 beta 2 chain	ECKGJPBD_17137			2.197894	3.301984
Light-harvesting protein B-875 alpha chain	ECKGJPBD_01608	-6.55026			2.90888
Light-harvesting protein B-875 beta chain	ECKGJPBD_01609		2.680983		2.697982
Light-harvesting protein B-880 alpha chain	ECKGJPBD_17138			1.646631	2.314884
Light-independent protochlorophyllide reductase iron-sulfur ATP-binding protein	ECKGJPBD_17152	-7.3997			9.338372
Light-independent protochlorophyllide reductase iron-sulfur ATP-binding protein	ECKGJPBD_33612				0.494283
Light-independent protochlorophyllide reductase subunit B	ECKGJPBD_03196	8.360251	-0.61806		
Light-independent protochlorophyllide reductase subunit B	ECKGJPBD_17150		-1.07415		
Light-independent protochlorophyllide reductase subunit B	ECKGJPBD_33611			3.59213	5.947399

Light-independent protochlorophyllide reductase subunit N			ECKGJPBD_03195	7.132873			0.579375
Light-independent protochlorophyllide reductase subunit N			ECKGJPBD_17149		-1.45901		-1.26335
Light-independent protochlorophyllide reductase subunit N			ECKGJPBD_33610				0.395979
Photosynthetic reaction center cytochrome c subunit			ECKGJPBD_06239			5.508814	
Photosystem I assembly protein Ycf3			ECKGJPBD_41232				-0.46457
Photosystem I iron-sulfur center			ECKGJPBD_32523			2.803864	7.887966
Photosystem I P700 chlorophyll a apoprotein A1			ECKGJPBD_31679				0.323605
Photosystem I P700 chlorophyll a apoprotein A1			ECKGJPBD_56700		-1.21835		-0.89585
Photosystem I P700 chlorophyll a apoprotein A2			ECKGJPBD_31680		-1.52339	0.492591	-0.98066
Photosystem I reaction center subunit II			ECKGJPBD_29644				-3.81273
Photosystem I reaction center subunit III			ECKGJPBD_22919			0.914485	0.890766
Photosystem I reaction center subunit XI			ECKGJPBD_28092		-0.65765	0.540599	
Photosystem II CP43 reaction center protein			ECKGJPBD_30533		-1.22446	0.78724	-0.39209

Photosystem II CP47 reaction center protein	ECKGJPBD_38993		-1.0023	0.812303	
Photosystem II D2 protein	ECKGJPBD_30532		-1.52726		-1.61566
Photosystem II manganese-stabilizing polypeptide	ECKGJPBD_21407		-1.79802		-1.5441
Photosystem II protein D1	ECKGJPBD_27450		0.907376		1.077173
Photosystem II protein D1	ECKGJPBD_47506		0.899519		1.296158
Photosystem II reaction center protein H	ECKGJPBD_27315	-1.32339	0.788567		1.381368
Photosystem II reaction center protein K	ECKGJPBD_30133			0.800402	
Phycobiliprotein ApcE	ECKGJPBD_28090			0.657839	
Phycobiliprotein ApcE	ECKGJPBD_45805		-0.87039	0.661262	
Phycobiliprotein beta chain	ECKGJPBD_27251			1.976657	2.447824
Phycobilisome 27.9 kDa linker polypeptide, phycoerythrin-associated, rod	ECKGJPBD_34729			1.181464	0.799404
Phycobilisome 37.5 kDa linker polypeptide, phycocyanin-associated, rod	ECKGJPBD_34333		-0.9763	0.962069	
Phycobilisome 39 kDa linker polypeptide, phycocyanin-associated, rod	ECKGJPBD_34334				0.392014

Phycobilisome 8.9 kDa linker polypeptide, phycocyanin-associated, rod	ECKGJPBD_34335			1.434236	1.083207
Phycobilisome rod-core linker polypeptide CpcG	ECKGJPBD_20936		-0.95058	0.582847	
Phycobilisome rod-core linker polypeptide CpcG2	ECKGJPBD_36211			0.836388	0.790433
Phycocyanobilin lyase subunit alpha	ECKGJPBD_42190			1.128337	0.871881
Phycocyanobilin:ferredoxin oxidoreductase	ECKGJPBD_37313			1.111775	1.211397
Reaction center protein H chain	ECKGJPBD_01641	-6.30351		-1.95436	
Reaction center protein H chain	ECKGJPBD_11139			1.025796	0.706828
Reaction center protein H chain	ECKGJPBD_22070			0.507971	
Reaction center protein L chain	ECKGJPBD_01607	-6.3748			1.188023
Reaction center protein L chain	ECKGJPBD_17139				1.12189
Reaction center protein M chain	ECKGJPBD_01606			-1.12615	-0.9263
Reaction center protein M chain	ECKGJPBD_17140				-0.51525
R-phycocyanin-2 subunit alpha	ECKGJPBD_48242			1.326306	
Thylakoid-associated single-stranded DNA-binding protein	ECKGJPBD_22223		-1.5645	0.763241	-0.67576

Table A 1-7: The log_2 fold change of differentially expressed genes associated with cytochromes, at a Padj<0.1. Comparisons are between the different treatments and time points; I4 is irradiated D4; I8 is irradiated D8; C4 is control D4; and C8 is control D8.

Product	Locus tag	log_2 fold change			
		I4_C4	I8_C8	C8_C4	I8_I4
Cytochrome b	ECKGJPBD_17283		-2.36742	4.794867	
Cytochrome b	ECKGJPBD_37269	4.210853			
Cytochrome b561	ECKGJPBD_13131				8.349835
Cytochrome b6	ECKGJPBD_35898		-0.76527	0.819666	
Cytochrome c biogenesis protein CcsB	ECKGJPBD_05635		8.077725		
Cytochrome c oxidase subunit 1	ECKGJPBD_00664			3.925762	
Cytochrome c oxidase subunit 1	ECKGJPBD_02309	2.94194			-1.77549
Cytochrome c oxidase subunit 1	ECKGJPBD_10338		-1.62908	2.166059	
Cytochrome c oxidase subunit 1	ECKGJPBD_13324	2.67691		1.508796	-0.89365
Cytochrome c oxidase subunit 1	ECKGJPBD_19619	7.58008			-8.61835
Cytochrome c oxidase subunit 1 , bacteroid	ECKGJPBD_15583		-7.40457		
Cytochrome c oxidase subunit 2	ECKGJPBD_10337				-7.3917

Cytochrome c oxidase subunit 2	ECKGJPBD_27504		0.843425		1.654804
Cytochrome c oxidase subunit 3	ECKGJPBD_10342		-5.79914	4.728997	
Cytochrome c oxidase subunit 3	ECKGJPBD_22883			-5.22786	
Cytochrome c oxidase subunit 3	ECKGJPBD_27502		1.069507		1.663254
Cytochrome c1	ECKGJPBD_05685			-7.83893	
Cytochrome c1	ECKGJPBD_34349	8.507844			-8.66485
Cytochrome c2	ECKGJPBD_01648			1.677803	2.423345
Cytochrome c2	ECKGJPBD_03208	5.120065		4.774875	
Cytochrome c2	ECKGJPBD_06829	3.182057			
Cytochrome c2	ECKGJPBD_06897	3.449251		3.579519	
Cytochrome c4	ECKGJPBD_02339	4.109262			
Cytochrome c4	ECKGJPBD_05634	3.426098			
Cytochrome c-550	ECKGJPBD_37618		-1.44146		-0.84502
Cytochrome c-556	ECKGJPBD_08112				3.778401
Cytochrome c6	ECKGJPBD_28726		-3.68962		
Cytochrome f	ECKGJPBD_33946		-0.61457		

Cytochrome P450-terp	ECKGJPBD_11751	6.90818

Table A 1-8: The log_2 fold change of differentially expressed genes associated with ATP synthases, at a Padj<0.1. Comparisons are between the different treatments and time points; I4 is irradiated D4; I8 is irradiated D8; C4 is control D4; and C8 is control D8.

Product	Locus tag	log_2 fold change			
		I4_C4	I8_C8	C8_C4	I8_I4
ATP synthase epsilon chain	ECKGJPBD_11386	6.669715			-8.75809
ATP synthase gamma chain	ECKGJPBD_02826				7.346492
ATP synthase gamma chain	ECKGJPBD_11388	3.881848			
ATP synthase subunit a	ECKGJPBD_26220				-0.50917
ATP synthase subunit alpha	ECKGJPBD_03004	5.259723			
ATP synthase subunit alpha	ECKGJPBD_07997	3.776911			
ATP synthase subunit alpha	ECKGJPBD_11389	2.535455		-3.99764	
ATP synthase subunit alpha	ECKGJPBD_16782		-4.2705	1.787993	
ATP synthase subunit alpha	ECKGJPBD_21647	10.27056			-10.4099
ATP synthase subunit alpha	ECKGJPBD_26215				0.330018
ATP synthase subunit b	ECKGJPBD_11391			-7.82562	-3.41562
ATP synthase subunit b	ECKGJPBD_12045	5.996062			-6.88567

ATP synthase subunit beta	ECKGJPBD_16780	2.438865	-1.97222	1.751957	-2.58223
ATP synthase subunit beta	ECKGJPBD_40961	2.824625			
ATP synthase subunit beta 1	ECKGJPBD_11387	4.577366			-6.14497
ATP synthase subunit beta 1	ECKGJPBD_21645	10.52579			-9.75542
ATP synthase subunit c	ECKGJPBD_11392		8.217339		
ATP synthase subunit delta	ECKGJPBD_11390			-8.18281	-5.26242
ATP synthase subunit delta	ECKGJPBD_16783		-3.30893	2.865122	

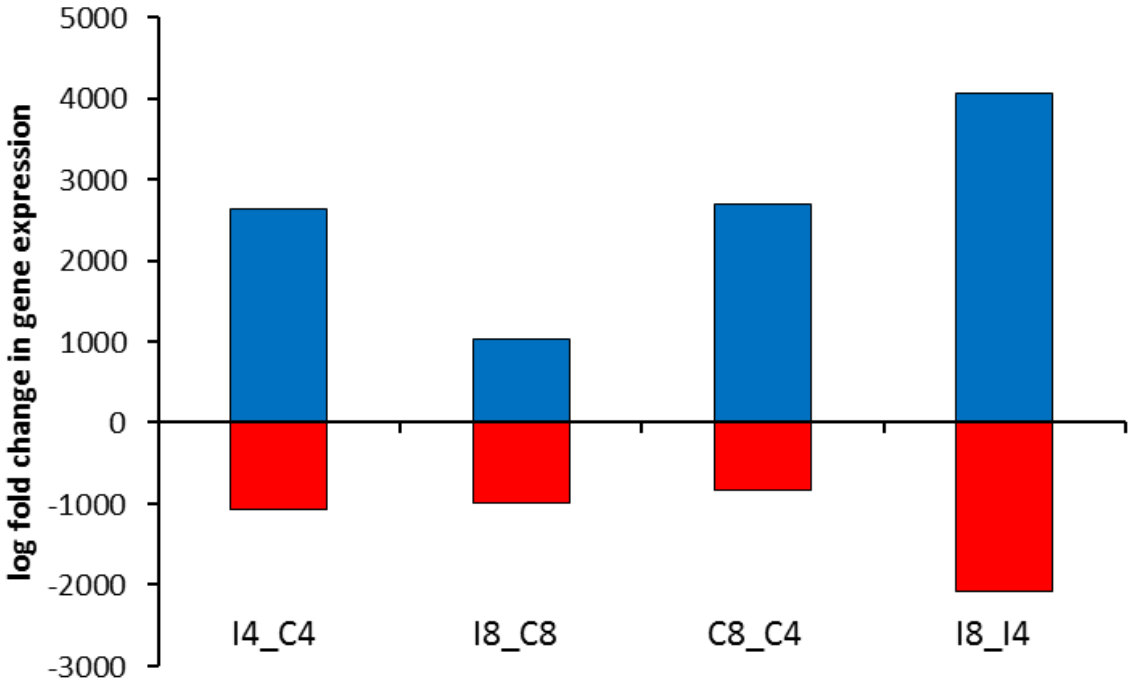

Figure A 1-1: The total log_2 fold change of the differentially expressed genes for each comparison, showing the up regulated and down regulated genes. Comparisons are between the different treatments and time points; I4 is irradiated D4; I8 is irradiated D8; C4 is control D4; and C8 is control D8.

A1.4 Future plans

- Functional annotation of the metatranscriptomic data set, to determine which metabolic pathways are most affected, using
  - COG
  - KEGG
  - GO
- Bin the metatranscriptomic data to try to determine the *P. catenata* specific response to ionizing radiation and recovery
- Draft manuscript for submission for publication

A1.5 References

Anders, S., 2010. Counting reads in features with htseq-count [WWW Document]. HTSeq 0.8.0 Doc. URL https://htseq.readthedocs.io/en/master/count.html (accessed 9.4.18).

Brown, C.T., Hug, L.A., Thomas, B.C., Sharon, I., Castelle, C.J., Singh, A., Wilkins, M.J., Wrighton, K.C., Williams, K.H., Banfield, J.F., 2015. Unusual biology across a group comprising more than 15% of domain Bacteria. Nature 523, 208–211. https://doi.org/10.1038/nature14486

Hyatt, D., Locascio, P.F., Hauser, L.J., Uberbacher, E.C., 2012. Gene and translation initiation site prediction in metagenomic sequences. Bioinformatics 28, 2223–2230. https://doi.org/10.1093/bioinformatics/bts429

Joshi, N.A., Fass, F.N., 2011. Sickle: a sliding-window, adaptive, quality-based trimming tool for FastQ files (version 1.33). [Software].

Kang, D.D., Froula, J., Egan, R., Wang, Z., 2015. MetaBAT, an efficient tool for accurately reconstructing single genomes from complex microbial communities. PeerJ 3, e1165. https://doi.org/10.7717/peerj.1165

Sieber, C.M.K., Probst, A.J., Sharrar, A., Thomas, B.C., Hess, M., Tringe, S.G., Banfield, J.F., 2018. Recovery of genomes from metagenomes via a dereplication, aggregation and scoring strategy. Nat. Microbiol. 3, 836–843. https://doi.org/10.1038/s41564-018-0171-1

Uniprot [WWW Document], 2018. . UniProt Consort. URL https://www.uniprot.org/help/uniref (accessed 9.13.18)

Wrighton, K.C., Thomas, B.C., Sharon, I., Miller, C.S., Castelle, C.J., VerBerkmoes, N.C., Wilkins, M.J., Hettich, R.L., Lipton, M.S., Williams, K.H., Long, P.E., Banfield, J.F., 2012. Fermentation, hydrogen, and sulfur metabolism in multiple uncultivated bacterial phyla. Science (80-.). 337, 1661–1665.

Wu, Y.W., Tang, Y.H., Tringe, S.G., Simmons, B.A., Singer, S.W., 2014. MaxBin: An automated binning method to recover individual genomes from metagenomes using an expectation-maximization algorithm. Microbiome 2, 1–18. https://doi.org/10.1186/2049-2618-2-26

A2 BG11 medium

Table A 2-1: Composition of BG11 media, including the concentration (M) of the final media and details of each stock solution.

Stock number		g L^{-1} of each stock	Concentration / M
1	$NaNO_3$	15.00	0.017648159
2	K_2HPO_4	4.00	0.000229621
3	$MgSO_4.7H_2O$	7.50	0.000304297
4	$CaCl_2.2H_2O$	3.60	0.000244881
5	Citric acid	0.60	3.12298E-05
6	Ammonium ferriccitrate green	0.60	7.76555E-06
7	$EDTANa_2$	0.10	2.68644E-06
8	Na_2CO_3	2.00	0.000188699
9 (trace metal solution)	H_3BO_3	2.86	4.62559E-05
	$MnCl_2.4H_20$	1.81	9.14557E-06
	$ZnSO_4.7H_2O$	0.22	7.65058E-07
	$Na_2MoO_4.2H_2O$	0.39	1.89394E-06
	$CuSO_4.5H_2O$	0.08	5.01225E-06
	$Co(NO_3)_2.6H_2O$	0.05	2.73309E-07

Each stock of BG11 media was made separately and was sterilised by autoclaving (gL^{-1} of each stock in Table A2-1). The stock solutions were diluted to the final concentrations shown in Table A2-1 by combining 100 mL of stock 1, 10 mL of stocks 2-8, and 1 mL of stock 9 (trace metal solution) and making up to 1 L with sterilised deionised water.

A3 List of courses and conferences attended

- "NERC funded Metagenomics workshop", University of Liverpool, 3 day workshop on practical metagenomics data handling, April 2018
- FEMS 7Th congress of European microbiologists , Valencia, Spain, July 2017
- Geomicrobiology research in progress meeting, University of Manchester, June 2017
- Microbiology society annual conference, Edinburgh, April 2017
- Leadership in action course, University of Manchester, January 2017
- Postgraduate research conference, University of Manchester, December 2016
- Dalton Symposium, University of Manchester, November 2016
- Geomicrobiology research in progress meeting, University of Bangor, June 2016